The Thesis Committee for Dean Alen Checkai
Certifies that this is the approved version of the following thesis:

Estimating Permeability Distribution of Leakage Pathways Along Existing Wellbores

APPROVED BY
SUPERVISING COMMITTEE:

Supervisor:

Steven L. Bryant

Paul M. Bommer

Estimating Permeability Distribution of Leakage Pathways Along Existing Wellbores

by

Dean Alen Checkai, B.S.

Thesis

Presented to the Faculty of the Graduate School of

The University of Texas at Austin

in Partial Fulfillment

of the Requirements

for the Degree of

Master of Science in Engineering

The University of Texas at Austin

August, 2012

Dedication

To my parents and Martha, thank you for your support and advice during graduate school. I could not have done this without you.

Acknowledgements

I would like to extend my gratitude to Dr. Bryant for having the patience to mentor me and for teaching me how to think as a petroleum engineer. I would like to thank Qing Tao for working with me on our research, and helping to summarize results for conferences and journal articles. I greatly appreciate that Dr. Bommer read my thesis and provided editing feedback. Thank you to Walter Crow, Charles Christopher, and Kevin Parsonage for their time answering questions about leaky wellbore dataset analysis. Teresa Watson provided valuable field data. Finally, I am grateful for the sponsorship of the Geological CO_2 Storage Joint Industry Project: BP, Chevron, ConocoPhillips, ExxonMobil, Foundation CMG, Halliburton/Landmark Graphics, Luminant, Shell, Statoil and the USGS. Without their generosity and commitment to funding research, this work would not have been possible.

Abstract

Estimating Permeability Distribution of Leakage Pathways Along Existing Wellbores

Dean Alen Checkai, M.S.E

The University of Texas at Austin, 2012

Supervisor: Steven L. Bryant

Increasing surface pressure buildup levels and surface venting flow rates on intermediate wellbore casing strings provided an opportunity to analyze wellbore field data to determine a distribution of leakage path permeability values. The gas leakage source in the leaky wellbore originated at depth, and formation gas/fluid traveled along defects in the cement to accumulate at the surface wellhead. The most likely pathway is the cement interface with casing or formation. Due to uncertainty about the location of the leak, and the different methods that were used for calculating leakage parameter values, a range of leakage path permeability values was produced. Most leakage pathway permeability values were greater than intact cement permeability (few microdarcies). This finding supports the practice of using cement filled annuli to provide a safe protective barrier against leakage and to prevent gas flow to surface. Proper cementing techniques are presented in order to identify possible reasons for cracks to form. It is hypothesized that the higher permeability values are a result of cracks in the cement interface with the casing or formation. These types of defects could also be found in

wellbores that are in communication with CO_2 sequestration reservoirs. The risk of leakage along such existing wellbores associated with CO_2 sequestration projects is quantified by the distribution of leakage path permeability. The gas migration path through existing leaky wellbores is an analog for wellbores that are in contact with migrating CO_2 plumes. Cracks in the leaky wellbores provide a highly permeable conduit for CO_2 to migrate out of the injection zone to the surface. By quantifying leakage path permeability, proper leakage risk assessment can be further developed.

Table of Contents

List of Tables

List of Figures

List of Illustrations

Chapter 1: Introduction to Leakage Path Permeability Research

1.1 Introduction Of Topics

The success of CO_2 storage reservoirs depends on the ability to store injected gas in the targeted formation and to prevent plume migration between geological intervals. Injection wellbores provide a means to inject CO_2 into the reservoir and are constructed by drilling a hole through the earth, supporting it with casing and re-establishing the geologic seal by placing cement between the casing and formation (Fig. 1.1.1). Storage reservoirs may have wellbores already drilled through them for other purposes such as oil and gas production from deeper formations. These wells will have been constructed analogously to Fig. 1.1.1, and the cement-filled annulus of these wells within the storage reservoir must prevent fluid migration out of the storage reservoir during and after storage operations.

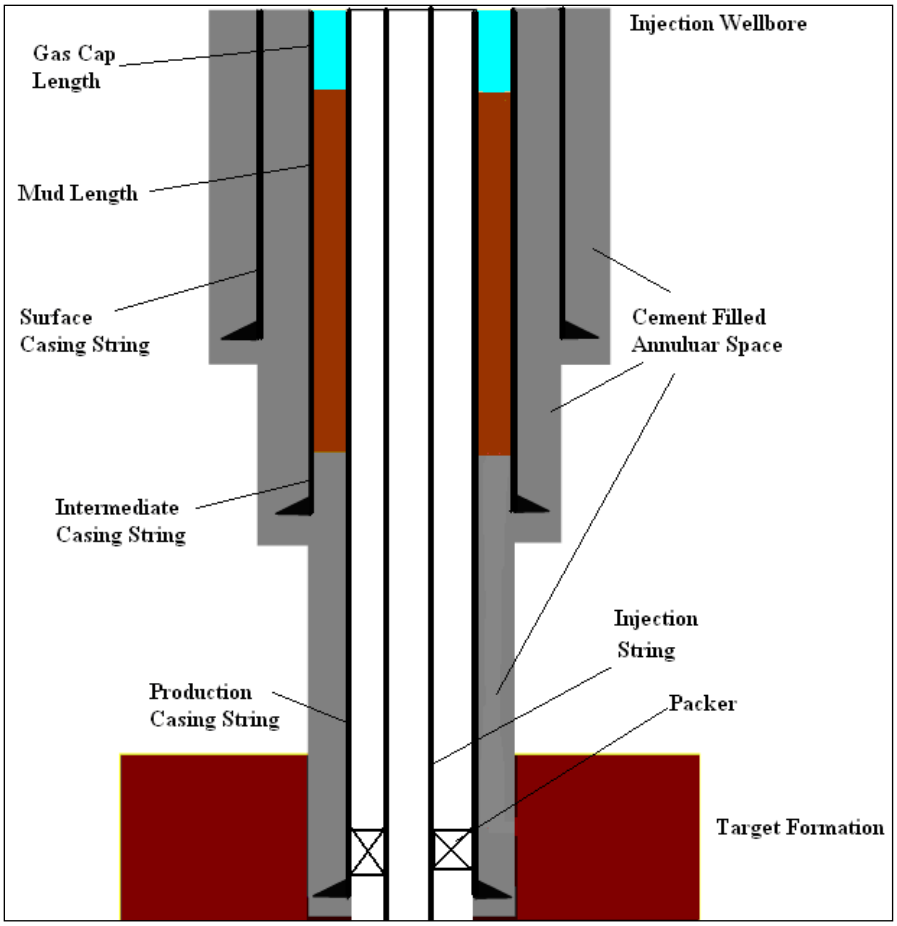

Figure 1.1.1 – Schematic of Injection Wellbore.

A constructed wellbore consists of several different annuli space between steel casing strings / formation that provide potential pathways to the surface. In the outermost annulus (between the surface steel casing and the rock formation) cement slurry is pumped and allowed to harden to create a seal. At deeper drilling depths, the inner steel casing strings are set in place and cement slurry volume is pumped into the intermediate annuli in order to create additional seals. Cement restores isolation between different formations at various depths that have been connected due to the penetration of the wellbore. Properly placed cement acts as a hydraulic seal and prevents formation fluids (gas, water, oil) from migrating to different zones along the path of the wellbore annulus.

The pressure must remain below the formation fracture pressure to avoid fluid loss. Different cementing techniques are applied, depending on the drilling conditions. During the cement pumping stages, the cement slurry increases in strength. It evolves with time, changing from liquid to gel to a permeable weak solid when setting, to a nearly impermeable solid after hardening (Nelson, 1990). After setting, the cement matrix has low permeability, on the order of less than 0.001 md (Nelson, 1990). At these permeability values, gas can no longer migrate through the cement pore space at any detectable rate (Nelson, 1990). The cement filled annulus space then acts as an effective seal, preventing formation fluids/gases from entering the space and migrating to surface.

For this research, the intermediate casing strings/annulus space was analyzed, rather than the production or innermost casing strings/annulus space contacting the production tubing. The degraded cement in these annular spaces were due to geo-mechanical forces, fluctuations in temperature, pressure within the steel casing, and the interaction between formation fluids and cement. Over time, the hardened cement can develop cracks that allow fluids/gas to flow between geological zones, defeating one of the main purposes of cement seals to provide isolation. The leakage conduits can be categorized as one of the following types: gas channel, micro-annulus, fracture aperture.

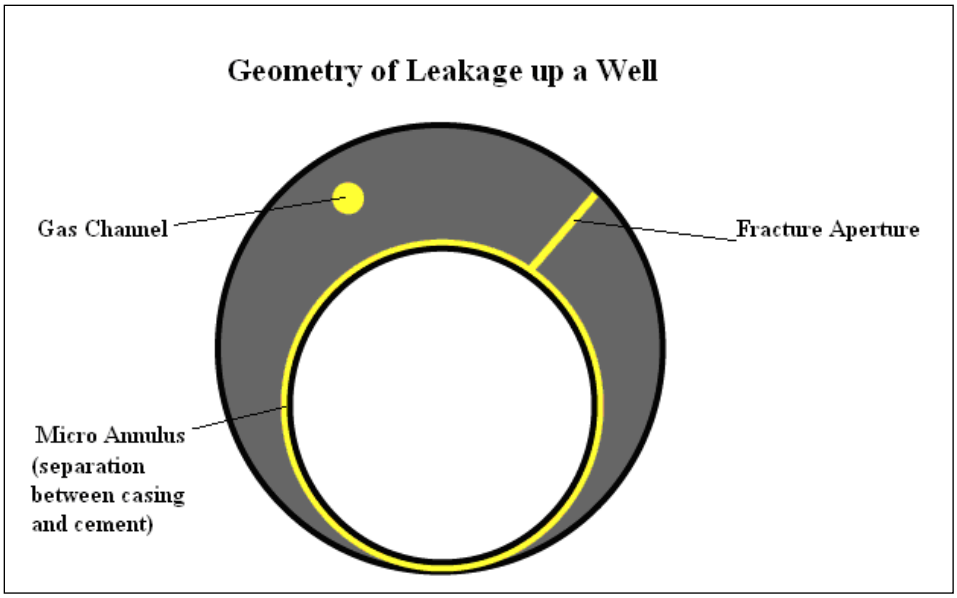

Figure 1.1.2 – Geometries of leakage pathways to surface (Huerta, 2009).

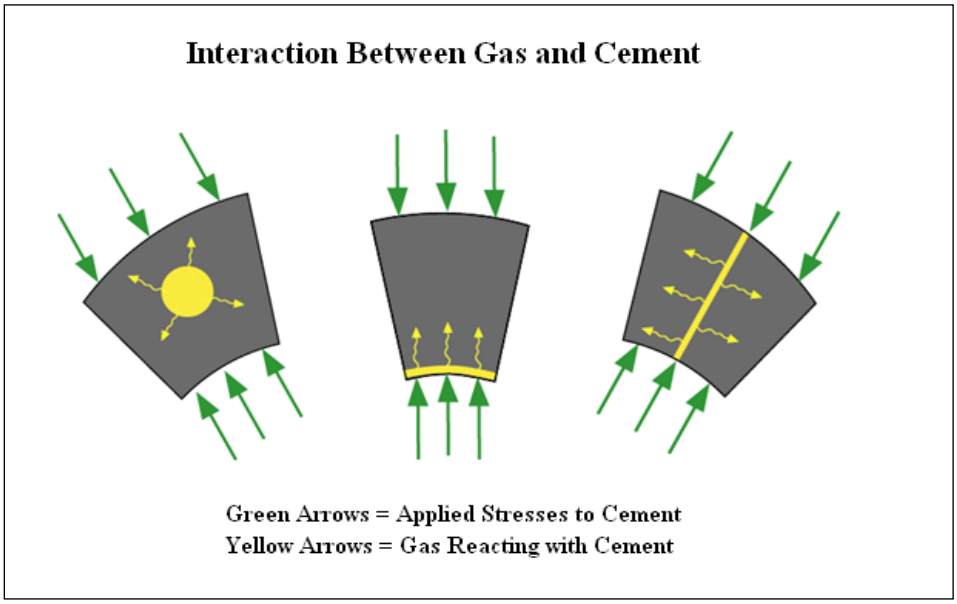

Figure 1.1.3 – Interaction between CO_2 gas and cement filled annulus space (Huerta, 2009).

The complete leaky wellbore dataset, used in this study, consisted of 238 wells from six different locations. Each dataset consisted of different levels of detailed information. In general, the datasets could be classified as either sustained casing pressure (SCP) wells or sustained casing vent flow (SCVF) wells. For SCP wells, a

pressure gauge recorded the increasing pressure levels in the corresponding surface annulus over time, thus indicating that fluid/gas migration occurred. For SCVF wells, the surface valve was opened to release the gas cap buildup, and the flow rate was recorded.

The invasion of formation fluid into the annular space was due to the pressure imbalance between the formation source and the top of cement. This pressure difference allowed formation fluid to flow from high to low pressure zones. The formation fluid migrated from deep depths, through a permeable conduit/crack, and accumulated near surface in the wellhead.

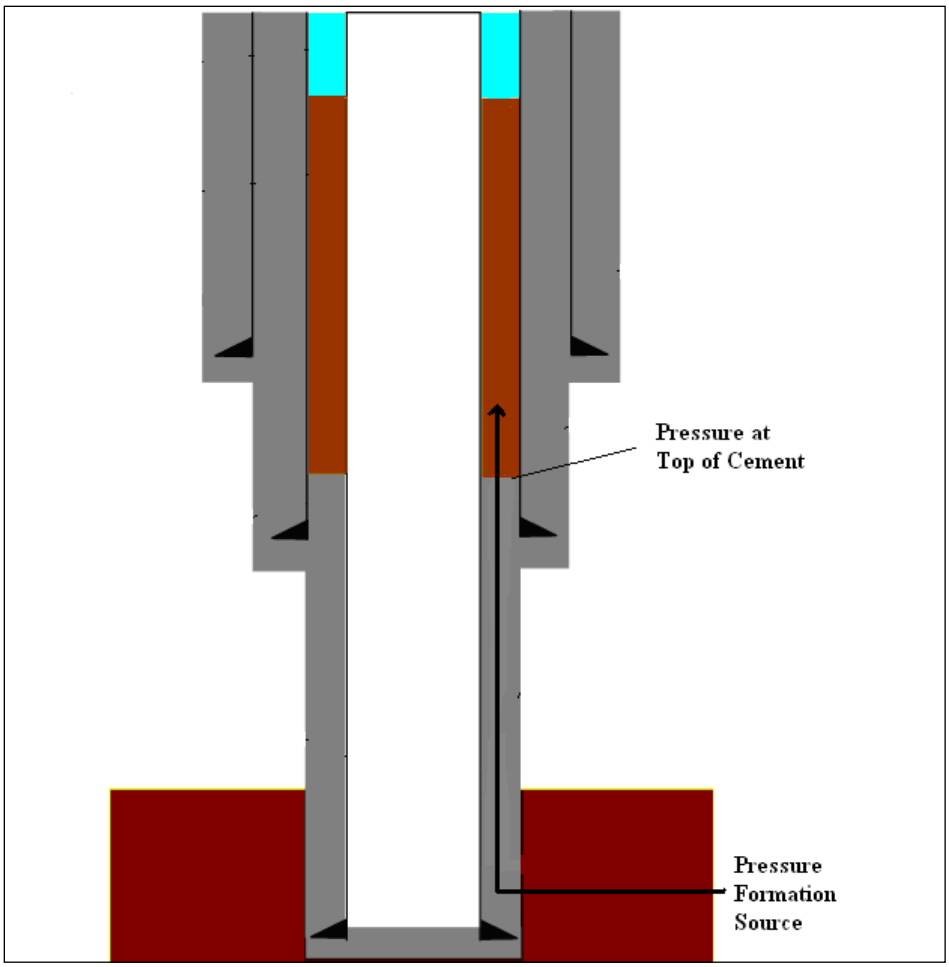

Figure 1.1.4 – Pressure imbalance between top of cement and formation source allows gas to flow and accumulate at surface.

The characteristics of this leakage path were determined for each of the 238 wellbores. Flow continued until there was zero pressure difference between the two zones. When the maximum surface pressure buildup plus the hydrostatic pressure due to completion mud equaled the leakage source pressure, then flow stopped.

During the gas pressure buildup period, the casing pressure was periodically bled down by the well operator in order to relieve the system. The pressure buildup data, bleed-down data, gas flow rates, and wellbore construction information were analyzed to determine the source depth of the leak and to generate an effective permeability of the leakage path.

As discussed further in Chapter 6, the range of leakage path permeability values was generally higher than that of intact cement permeability values (less than 0.001md). Therefore, the leakage conduits were the only means of gas migration/ travel, as opposed to migration through cement pore space.

Assuming SCP leakage paths are analogous to leakage paths outside the wellbore, (i.e: along the cement/earth interface) the range of permeability inferred from these SCP wells was extended to assess the risk of leakage through cement-sealed annuli space of existing wellbores that are in contact with CO_2 sequestration reservoirs. Further analysis provided plausible dimensions of CO_2 plumes that migrate from an injection well to an existing wellbore. The height of the plume was compared to the forces required to overcome capillary entry pressures so that gas would flow into the micro-annulus crack. The contact point between the CO_2 plume and the entry point into the annulus space was analyzed in detail. In addition, the given leakage scenarios provided a range of CO_2 fluxes migrating to the surface.

1.2 BACKGROUND INFORMATION

Field data leakage path permeability had never been quantified before, so researchers in previous work had to make assumptions about the distribution of permeability values (Celia and Nordbotten, 2008).

The importance of the accuracy of leakage path permeability value when simulating leakage models through existing wellbores cannot be understated. Results that are generated using leakage models depend on the assignment of the values of permeability along the well segments (Celia, *et al*., 2011). If no information is available to constrain wellbore parameters, then a random method (bi-modal distribution) can be used. For example, Celia and Nordbotten described regional wellbores in a field in Alberta, Canada as either having "good" or "bad" cement characteristics. "Good cement" was assigned an expected permeability value of 0.1 md. "Bad cement" was assigned an expected permeability value of 1 Darcy (Celia, *et al*., 2011).

Very few measurements of field data leakage path permeability along existing wellbore segments had been reported in the literature (Celia, *et al*., 2011). However, Watson and Bachu developed a "scoring system" which was based on assigning risk values for attributes of existing wellbores, such as well type, depth, time of drilling, etc (Watson and Bachu, 2008). The "score" was translated into an effective permeability by a random choice from the probability distribution (Celia, *et al.,* 2011). For example, a score range less than 2, resulted in a permeability range of 0.01 md to 0.02 md. A score range from 2 to 6, resulted in a permeability of 0.02 md to 0.5 md, etc (Celia, *et al.*, 2011). When modeling leakage scenarios, researchers had to assign such values for leakage path permeability. Changes to this parameter had significant effects on the output of the models that were run. Researchers recommended that an accurate

distribution of leakage path permeability based on field data measurements to be used in order to improve findings.

Leaky wellbore data were not easily accessible, as operators rarely published such information, making it available to the public. Most leaky wellbore data used in this thesis were obtained through state and federal regulatory agencies, contacts within the industry, and from wellbore examples in previously published research findings. Once the data was obtained, a careful analysis of the information provided individual case studies that were applied by using different versions of the SCP and SCVF leakage models (Xu, 2001). The Sustained Casing Pressure (SCP) Model and the Sustained Casing Vent Flow (SCVF) Model were modified over time, changing to fit the needs of research objectives for new datasets. The altered versions of the model provided more instructive techniques of analyzing the leaky wellbore data. As results were produced, the following questions were asked, "What these data mean, and how can the data be used to further advance research?"

1.3 RESEARCH OBJECTIVES

The research objectives were to generate a distribution of leakage path permeability by analyzing leaky wellbore field datasets. The goal was to provide these results for future research modeling of CO_2 migration and to quantify the risk of leakage through existing wellbores.

Therefore, the goal of this research was to "bridge the gap" between the assumptions being made, and the permeability results obtained from actual leaky field wellbore datasets. A secondary goal was to search for and obtain additional independent sources of leaky wellbore datasets with sustained casing pressure buildups.

Research was performed by making changes to the SCP and SCVF Models in order to generate a more robust set of results that could be interpreted. Some of the changes to the model include the following:

(1) Optimizing the pressure buildup curve to match the pressure field data by minimizing the sum of the errors (between actual data and model data) squared.

(2) Assigning weights to the asymptotic pressure to generate different permeability results.

(3) Changing parameter values to more closely match existing leakage conditions.

By analyzing the model results of the different leaky wellbore field datasets, a distribution of leakage path permeability values could then be compared with previous assumptions made. These ranges of leakage path permeability can quantify the leakage potential of cracks/ defects in the cement filled intermediate annular space. For an above zone leakage monitoring system, permeability values provide insight to the risk of gas migrating to the surface.

The arguments of the interpretation of the results were strengthened by performing data analysis on six different datasets, containing 238 wellbore construction details, pressure on annulus data, or surface gas flowing rates. Three systematic methods were established in order to reduce uncertainty. These three different methods (Cement Slurry Method, Maximum Pressure Method, and Monte Carlo Method) provided comparable leakage path permeability values for the same wellbore that had numerous pressure buildups.

For these methods, in order to calculate the maximum, minimum, and most probable leakage path permeability values, unknown parameter values had to be

constrained within a range of values. For the Monte Carlo Method, these unknown parameter ranges were assigned certain probability distributions. The goal of applying the different methods to the same wellbore was to generate more accurate leakage path permeability value ranges for each pressure buildup interval. In the future, additional permeability values can be generated by applying these methods, when wellbore construction information and pressure on annulus information are provided.

1.4 SUMMARY OF CHAPTERS

This thesis is organized into the following chapters. Chapter 2 is the literature review, which identifies significant achievements and discoveries in the CO_2 sequestration community that was used for a basis of this work. The importance and usefulness of CO_2 sequestration research is explained. Research findings by scientists and engineers have provided guidelines that provide platforms for future development of commercially sized CO_2 sequestration projects. Cementing techniques and best practices to prevent gas migration are discussed. The properties of intact cement are described. Reasons for gas flow and pressure buildups are described. Past modeling of leakage scenarios is explained.

Chapter 3 is the description of the leakage models (SCP and SCVF) and the input parameter values that are used. The possible leakage pathways are presented and the characteristics of the pathway are highlighted.

Chapter 4 is a full description of the pressure buildup information and wellbore construction details for each of the wellbores in all of the six datasets. Selection of the intermediate annulus space and pressure buildup data intervals are discussed. Each dataset provides sufficient information in order to run the model and highlights any

assumptions that were made for unknown parameter values. Unknown parameters are bounded by a range of plausible values.

Chapter 5 focuses on the three methods that are used to reduce uncertainty of the range of leakage path permeability values. Each method focuses on using different types of information provided, and re-creates plausible leakage scenarios (different leakage depths, length of mud, etc). The Maximum Pressure Method focuses on the pressure buildup data to solve for either unknown leakage depth or unknown mud length. The Cement Slurry Method fixes the length of mud, based on cement slurry volume information, while changing the leakage depths. The chapter concludes by describing the Monte Carlo Method, which is the most robust of all the methods presented.

Chapter 6 presents the results of modeling the wells using the different methods described in Chapter 5. First, there is a comparison of permeability values generated by the model between the Maximum Pressure Method and Cement Slurry Method for all datasets. The differences between the methods are highlighted in a detailed comparison. The results of the Monte Carlo Method SCP Model and SCVF Model results are then presented and compared. Wellbores that allowed for permeability results to be generated from both methods are used as comparisons between the SCP Model and SCVF Model Monte Carlo Method. Changes in permeability over time is then discussed. This is followed by a short discussion about results of a sensitivity analysis that was performed by changing different parameter values, while holding all other parameter values constant. These variables included gas cap length, mud density, leakage depth, mud length, and gas flow rate. Trends in permeability vs. parameter values are identified. Last, permeability values provided inputs to model case studies of CO_2 plume migration. The permeability was used to obtain aperture width, which was used to understand the

height of a plume required to overcome capillary entry pressures of cracks in cement. The distribution of CO_2 fluxes that migrate to surface for all the datasets is presented.

Chapter 7 is a conclusion of the final results for the SCP Model and the SCVF Model. The focus of the research findings is to compare the results with previously published permeability distributions by Celia *et al.*, 2008. The leakage path permeability distribution is obtained by applying the Monte Carlo Method (expected values) to the datasets. The permeability distributions are compared for each of the two models. The final comparison shows a reduction in the range of permeability, thus decreasing uncertainty. The combined SCP and SCVF results are recommended to be used as inputs to future CO_2 leakage models, because leakage path permeability has such a strong impact on determining CO_2 leakage fluxes. A discussion of future research work concludes this chapter.

Chapter 2: Literature Review

2.1 Importance of CO_2 Sequestration Research

It has been estimated that the combustion of oil, natural gas, and coal generates 27 billion tons of carbon dioxide (CO_2) each year (Reichle *et al.*, 1999). CO_2 is problematic to the atmosphere because it traps outgoing infrared and thermal radiation (Preuss, 2004). Scientists have documented increasing global temperatures (+0.3 C to 0.6 C) over the past 150 years. The debate of global warming caused by increased levels of CO_2 in the atmosphere has been on-going for several decades. The United States Environmental Protection Agency (EPA) estimates that fossil fuel power plants are responsible for over 40% of carbon emissions from fossil fuel combustion. Recently, The U.S. Congress unsuccessfully tried passing legislation to create carbon taxes that charge CO_2 producing industries per ton for their CO_2 output/ emissions. Having a price tag on the quantity of carbon emitted to the atmosphere would encourage alternative ways to dispose of CO_2.

One of the most promising techniques of reducing CO_2 emissions is the process of disposing CO_2 into deep storage reservoirs. For sequestration projects, CO_2 gas or brine is injected into the pore space of a target reservoir composed of sedimentary rock. The injected gas becomes trapped in the reservoir when there are low permeable rock layers that "trap" the migrating gas (de Figueiredo, 2004). For CO_2 sequestration projects to be successful, the following conditions must be met:

(1) There exists sufficient reservoir storage capacity (large pore volume) during the life of injection and storage of the project.

(2) Geological trapping reservoir characteristics prevent naturally occurring gas migration from the injected zone (Bachu and Bennion, 2009).

If the target sequestration reservoir meets the above criteria, then researchers must study the pore scale interaction between the injected CO_2 gas and the in-situ pore filling fluids. In order for the injected gas to enter the pore space, the pressure of the injected gas must be greater than the capillary entry pressure. However, it must not be at pressure large enough to fracture the rock (de Figueiredo, 2004). Vertical migration of the injected gas is a function of buoyancy driven flow. Buoyancy depends on the difference in density between the less dense injected gas and more dense formation fluids (de Figueiredo, 2004). This preliminary research is conducted before any gas injection can begin. During the planning stages, datasets are collected to provide supporting evidence that such a project will be successful.

For validation purposes, potential sequestration sites require small scale injection prototypes. During the prototype injection phases, plume monitoring and leakage detection technologies are used to identify possible leakage issues. Results from these prototypes are used to properly determine the feasibility of larger, industrial sized projects (Huerta, 2009). Researchers have estimated the global storage potential by analyzing reservoir data from different projects worldwide. Herzog and Golomb estimate that the global capacity estimates for CO_2 storage reservoirs in saline formations range from 100-10,000 GtC and in depleted oil and gas reservoirs range from 100-1000 GtC (Herzog and Golomb, 2004). If carbon dioxide production remained constant at 27 billion tons/year, it would take between 7000 years and 70,000 years to reach storage capacity.

The use of CO_2 for Enhanced Oil Recovery (EOR) projects have been conducted by the oil and gas industry for many decades, so the concept of pumping CO_2 into existing reservoirs is not an entirely new concept. For most CO_2 EOR projects, CO_2 that is produced from a natural source of CO_2 is pumped via pipeline to a producing oil field.

The gas is injected into the reservoir and then interacts with pore filled formation fluids as it migrates from the injection well. The produced gas that is extracted from the producing well contains different components. A surface separator is used to extract CO_2. This gas is then injected back into the subsurface for further oil recovery purposes. Operators follow strict federal and state guidelines for injection well design, construction, monitoring, and abandonment (de Figueiredo, 2004). The goal of the restrictions is to prevent the migration of injected fluids from the well. Proper well design includes the following (de Figueiredo, 2004):

(1) Packers that isolate different geological zones of interest.

(2) Injection tubing that can be pulled if problems occur.

(3) Long steel string casings that prevent interaction between formation fluids and injected fluids.

It has been shown that most of the gas leakage in EOR injection wells occurs through leaks in the well casing due to the following (de Figueiredo, 2004):

(1) Excessive injection pressures.

(2) Leaking packers.

(3) Tubing/casing corrosion.

Protective cement and steel casing strings should act as barriers between the injection gas and the formation fluids, but in many cases, they do not provide sufficient isolation. Therefore, operators must monitor the intermediate annulus to identify potential leakage from injected gas.

For EOR projects, the CO_2 interacts with the formation rock and fluids in the pore space of that rock. By injecting CO_2 gas, the reservoir pressure also increases. The CO_2 gas creates a “front” which displaces the formation fluids out of the pore space. There is an increase in production levels, since higher volumes of formation fluids are extracted

from the pore space. In addition to this, the formation fluids that interact with the CO_2 gas have smaller viscosity, which make it easier for the fluids to migrate through the rock.

The CO_2 injection wells are located a distance away from the producing wells. Since the CO_2 is miscible with the formation fluids, the producing wells extract formation fluid/gas containing various levels of CO_2 concentration. It is estimated that over 50% of the injected CO_2 gas returns to the surface through these production wells (Jessen, 2005). Surface separators are used to separate the produced gas into two streams, one composed of pure CO_2, and the other composed of sellable hydrocarbons. In some cases, the excess CO_2 stream is pumped back into the producing reservoir via an injection well (monitor injection pressure and flow rates), for further use in EOR. After the project is completed, the remaining CO_2 is allowed to be vented back into the atmosphere.

CO_2 sequestration projects are different from CO_2 EOR projects, in that the goal of a sequestration project is not to produce formation fluid/gas by injecting CO_2. Furthermore, there should not be measurable volumes of leaked CO_2 during the lifespan of the storage project. Two of the most widely suggested storage reservoirs for CO_2 sequestration projects include depleted oil and gas reservoirs and saline aquifers.

Results from large scale industrial sequestration projects have been published. The Norwegian government has imposed a tax on CO_2 emissions, making such projects economically feasible. Collaboration between industry and research institutions continues to aid in the technical development of such sequestration projects.

Statoil reported that their Sleipner Vest field sequestration operation is injecting 1 million tons of CO_2 (roughly one third of CO_2 output of a 300 MW coal fired power plant) each year. The Sleipner Vest field is located halfway between Norway and Scotland, in the North Sea, at a water depth of 2500 meters (Preuss, 2004). CO_2 storage

operations began there in 1996. The natural gas that is produced from the field has 9% CO_2 content which is separated at the surface, compressed, and then injected into a saline formation storage reservoir, located above the natural gas formation (de Figueiredo, 2004). A leakage monitoring system collects data on possible leakage information, but there has been no indication of CO_2 leakage into other geological formations (de Figueiredo, 2004).

A second carbon sequestration project under operation by Statoil is the Snohvit Sequestration Project in the Barents Sea. Natural gas production (at depths greater than 2300 meters) is transported by pipeline to an on-shore facility where CO_2 is captured from a liquefied natural gas facility. The CO_2 is then piped back to the field and injected into a saline formation (Tubaen formation at depth 2500 meters) located below the natural gas formation. An estimated 700,000 tons of CO_2 are injected into the formation each year (de Figueiredo, 2004).

For both of these projects, the CO_2 is sequestered in deep, offshore saline formations. However, the separation equipment used for the Sleipner Vest project is located offshore, while separation equipment used for the Snohvit project is onshore. Saline formations are composed of sedimentary rock saturated with water containing high concentrations of dissolved salts (de Figueiredo, 2004). According to some experts, these formations offer the largest potential storage volume among potential geological reservoirs (de Figueiredo, 2004). The estimated storage capacity depends on the accuracy of assigning values to reservoir characteristics. The injected CO_2 would dissolve in the aquifer brine and the resulting mixture would be denser than the original formation brine (Orr, 2004). The denser mixture would flow vertically downward and cause further dissolution, as fresh brine is brought into contact with the CO_2 brine mixture (Orr, 2004).

Due to the sensitivity of CO_2 storage projects, measurement, monitoring, and verification (MMV) devices would be used to monitor leakage Portable MMV devices should be installed at different surface locations to monitor and verify that CO_2 gas is not leaking from the target reservoir (de Figueiredo, 2004). This would validate that the injected quantities of CO_2 have been properly stored and sequestered in the target formation (de Figueiredo, 2004). The data collected from the sensors should also identify the movement of plumes, validating modeling forecasts of gas plume migration through porous media. The subsurface movement of CO_2 should not compromise the underwater drinking sources or other environmentally sensitive zones.

There are two potential leakage pathways for CO_2 to reach the underwater drinking sources near the surface. The first pathway is by travelling up existing wellbores. The second pathway is by traveling through a fracture. Determining the characteristics of the leaky wellbore pathway is a focal point of this research. Leakage risk assessments are a function of the leaky wellbore path characteristics. Leakage models use the characteristics of leakage pathways to run simulations and support conclusions made. Proper leakage risk assessment and prediction of leakage in carbon sequestration projects is further developed.

A major concern of regulators is that carbon capture and geological storage operations will cause significant damage to the environment. Proper risk assessment determines the extent to which injected gas or native brine in the storage reservoir will migrate into other geological formations (Celia, Nordbotten, *et al.*, 2010). In North America, there are millions of existing wellbores. In Texas, alone, more than 1 million wells have been drilled (Nordbotten, *et al.*, 2005). Properly abandoned wells have been plugged and sealed and are registered by the well owner with the state agency. There are also orphaned wells that are abandoned wells without proper ownership and are

considered higher leakage risk wells. If either abandoned or orphaned wells are located within close proximity to a CO_2 storage reservoir, there is an increased risk of leakage. The injected CO_2 is buoyant and can migrate through highly permeable conduits (cracks) in the cement. The cement that was used to seal the wellbore annulus can develop cracks which allow for communication between geologically sealed zones. Cracks defeat one of the purposes of cement, which was to act as an impermeable seal.

Clearly, there is a need for a comprehensive analysis of leakage pathways to contribute to leakage assessments of sequestration projects. Research findings from all areas of sequestration projects are used to develop proper procedures for future sequestration projects. Properly sequestering CO_2 will be an important contributing factor in reducing carbon emissions and helping to prevent global warming.

2.2 RESEARCH FINDINGS IN SUPPORT OF CO_2 SEQUESTRATION PROJECTS

Research findings cover many different technical aspects of a CO_2 sequestration project. Published results include proper CO_2 reservoir simulation, developing Equations of State (EOS) to describe properties of CO_2 under different conditions, determining leakage path permeability values of an existing wellbore, and analyzing large datasets of leaky wellbores that demonstrate sustained casing pressure buildups. These research findings test the technical feasibility of sequestration projects. This contributes to the successful advancement toward sequestration project approval and commissioning by providing supporting evidence that promotes safety.

To begin with, skeptics questioned whether CO_2 sequestration reservoirs provide sufficient reservoir volume capacity to store the large amounts of CO_2 that is being sequestered. Researchers at the National Energy Technology Laboratory (NETL) have presented results to show that this argument is without merit. In 2010, NETL published

version III of *The Carbon Sequestration Atlas of The United States and Canada*. In this report, NETL proposes several possible sequestration targets with estimated ranges of storage potential. For saline formations, storage resources range from 1,822 billion tons to more than 22,281 billion tons of CO_2. At current CO_2 emission rates, there would be more than 450 years of storage potential (NETL, 2010). For oil and gas reserves, there is 155 billion tons of CO_2 storage potential, allowing for more than 40 years of storage potential (NETL, 2010). For un-mineable coal areas, there are 65 billion tons to 128 billion tons of storage potential, indicating more than 15 years of storage potential (NETL, 2010).

Estimated storage capacity depends on the ability of the formation to "trap" the migrating gas in place. Research by Kumar has shown how saline aquifers can trap injected CO_2 gas in place and prevent migration. Results were generated by using a compositional reservoir simulation of a CO_2 sequestration project in a deep saline aquifer. The reservoir simulator (GEM) was used for modeling purposes (Kumar *et al.,* 2005). The characteristics of the aquifer were presented to provide accurate reservoir properties and realistic conductions. Plausible injection and storage estimates were based on this model, including leakage scenarios (Kumar *et al.,* 2005).

For their analysis, they assumed an injection period, lasting 10-50 years, and the monitoring period lasting 1000-100,000 years under a natural gradient flow. They showed that characteristics of the reservoir (permeability, residual gas saturation, brine salinity, temperatures, etc) had a large impact on the ability to keep CO_2 from migrating to the surface. Properly dissolved CO_2 in brine would also prevent buoyancy driven migration from occurring (Kumar *et al.,* 2005).

Due to changing pressures and temperatures of injected gas from surface to reservoir depths, research has focused on a more realistic CO_2 Equation of State (EOS).

Pruess performed simulations using a different EOS, describing the phase changes of CO_2 leaking from a target reservoir. His research findings provided a better understanding of the changing characteristics of CO_2, as described by the EOS.

The critical point of CO_2 is at a temperature of 31.04 C and a pressure of 73.82 bar (Preuss, 2004). At subcritical temperatures and pressures, CO_2 exists as a liquid or a gas. As the CO_2 migrates through the leakage pathway from subsurface reservoir conditions towards the surface, it encounters lower pressures and temperatures. This can cause the CO_2 to change phases. The EOS matches the observed properties of CO_2, thus leading to a more quantitative way of predicting how CO_2 will behave when migrating to the surface. The EOS can be used for the development of improved, more accurate leakage models (Pruess, 2004).

For CO_2 storage projects, regulatory agencies are concerned about the amount of CO_2 that would migrate back to surface. As discussed previously, one of the most likely pathways for gas to reach the surface is through existing wellbores with degraded cement filled intermediate annulus space. The permeability distribution of leakage conduits is an important factor in determining this rate of CO_2 that could leak. In order to determine the leakage path permeability range, collected field data provide insights (SCP buildup data or SCVF recorded over time). Research has used this type of data in order to determine the range of permeability.

For example, Crow *et al.,* 2008 analyzed the wellbore integrity of natural CO_2 wellbore producers. Field datasets were collected for a 30 year old well to determine the reaction/corrosion effects between CO_2 and cement. The data provided values for leakage pathway permeability of cracks in the cement seal that developed from contact with migrating CO_2. The well was in contact with a natural CO_2 reservoir that was composed of nearly pure CO_2 (96%, much higher than concentrations seen in CO_2 EOR

fields) (Crow *et al.*, 2008). A hydraulic isolation test (vertical integrity test) was performed to quantify the effective permeability range at 1-10 md. Since this is 3-4 orders of magnitude higher than intact cement (0.001 md), it suggested that the cement interfaces with casing or with earth formations were a potential migration pathway, as compared with the cement matrix. (Crow *et al.*, 2008).

Sustained casing pressure (SCP) is defined as "any measurable casing pressure that rebuilds after being bled down, attributable to causes other than artificially applied pressure or temperature fluctuations" (Xu, 2001). The Bureau of Ocean Energy Management, Regulation and Enforcement (BOEMRE), formerly the Minerals Management Service (MMS), requires that operators record the casing pressure on problematic wells once per hour. Data acquisition systems or chart recorders provide accurate information during a pressure bleed-down test. Pressure buildups on all the casing strings are recorded to provide evidence of cross flow or communication between casing strings.

Operators test for SCP by opening a surface wellhead 0.5 inch needle valve, allowing the gas cap to bleed down, then closing the valve and measuring pressure buildup for 24 hours. The liquid recovered is also measured and recorded. The gas inflow from a high pressure formation into the annulus migrates upward through the mud column and accumulates in a gas cap (Xu, 2001). Pressure bleed down data are collected from the surface annulus and provides information about the gas content, annular volume, and channel/micro-annulus flow capacity (Bourgoyne, 2000). When bleeding down dry gas, an orifice-type, gas-rate measurements device is used in series with the needle valve to accurately estimate gas bleed rate during the bleed-down period (Bourgoyne, 2000).

A mathematical model has been used to determine leakage path permeability by qualitatively analyzing intermediate annulus pressure buildup cases. Xu developed a

numerical model of wellbores exhibiting sustained casing pressure (SCP) buildups. Xu's mathematical model describes a gas leakage path in an annulus filled with a mud column above a cement top (Xu, 2001). The model assumed that the leakage path was one dimensional and that gas flowed along it according to Darcy's Law. The driving force for flow was the pressure difference between the leakage pressure and the pressure at the top of cement (Tao *et al.*, 2011). The gas migration process was described as steady state flow, composed of short time steps. In each time step, gas accumulated at the gas cap, and the pressure at the cement top increased.

Due to the complexity involved with modeling gas flow through a liquid, it was assumed that the gas instantaneously travelled from the top of cement to the wellhead surface. The gas that was released at the cement top completely accumulated in the casing gas cap during the next time step (Xu, 2001). Formation pressure was assumed constant, and the completion mud was assumed to be slightly compressible (Kutasov, 1988). The volume of mud therefore decreased as the pressure built up in the annulus. The pressure at the wellhead was provided. When the sum of casing and mud pressure at the top of cement was equal to the leakage formation pressure, gas flow stopped (Xu, 2001). The gas buildup was a function of cement properties. Bleed downs were classified as either instant bleed-downs or long bleed downs. Two examples of using the model to analyze actual SCP field data tests were published. Her analysis gave estimates of the depth of gas invasion zone, formation pressure, etc. (Xu, 2001). Xu developed the SCP model for testing and identification of the flow mechanisms of external leaks. She identified the controlling parameters of the SCP model, determined flow patterns of gas flow in the annulus, and assessed the severity of the gas flow problem (Xu, 2001).

Huerta *et al.*, 2009 applied a version of Xu's model to additional field measurements of leaky gas wells (buildup rates as large as several 1000s psi/day) that

demonstrated sustained casing pressure over time. Natural gas leakage occurred along the wellbore and the pressure buildup data were recorded. They treated the unknowns as effective permeability of the leakage path and the depth at which leakage into the wellbore is occurring (Huerta *et al.,* 2009). Results provided characteristics of the leakage pathway.

Huerta *et al.,* 2009 presented a summary of two case studies, although it was recommended that the SCP model be applied to a large number of wells to provide a probabilistic distribution of leakage pathway permeability (Huerta *et al.,* 2009). The work presented in this thesis has filled this gap in knowledge, by providing a robust leakage path permeability distribution for a large number of wells. As Huerta recommends, the leakage path permeability can provide input values to a leakage modeling tool in order to assess the risk associated with CO_2 migration along leaky wellbores. This would be necessary for site selection, permitting, and properly crediting sequestration operations (Huerta, 2009).

These are some of the examples of research findings that have contributed to continuing the effort of advancing technical knowledge and feasibility of CO_2 sequestration projects. The goal of this research was to use further advance the work by Huerta *et al.,* 2009 by improving the SCP Model and applying it to new leaky wellbore datasets. The generated distribution of leakage path permeability provided inputs to determine the characteristics of a migrating gas plume and to properly assess the risk of leakage.

2.3 CEMENTING TECHNIQUES TO PROPERLY SEAL THE INTERMEDIATE WELLBORE ANNULUS

The oil and gas industry published cementing “best practices” of intermediate annuli to create proper wellbore cement seals. Whenever pressure in the intermediate

annulus space is recorded, this indicates that gas migration has occurred, and that one objective of the cement has been compromised. There are many reasons why the cement seal can fail. By analyzing the cementing process, specific points of concern that can lead to gas flow issues were highlighted.

Drilling and completing wellbores required cement slurry to be pumped into the intermediate annulus space. The cement hardened to provide zonal isolation (Nelson, 1990). Cement prevented formation fluids or gases from migrating into other zones. Properly hardened cement acted as an impermeable seal between the steel casing and the rock formation (Nelson, 1990). There were different objectives when cementing various portions of the wellbore. For example, the following are the objectives of cementing certain casing strings (Nelson, 1990):

(1) Surface casing annulus space - To eliminate communication with ground water sources and to provide support to the remainder of the casing strings.

(2) Intermediate casing annulus space - To seal off abnormally high pressure formations and to eliminate formation fluid circulation between zones.

(3) Production casing annulus space - To prevent the migration of production fluids into the production annulus space.

For each casing string that was cemented, the objectives and conditions of cementing (pressure, depth, temperature, formation, etc) were different. Accordingly, the operator had to conduct proper calculations in order to ensure that the proper cement job was performed correctly.

During primary cementing jobs, the objective was to fill the intermediate annular space between the steel casing and the formation with cement slurry. This occurred after the drill bit reached its intended depth, and the drill pipe was removed from an open hole. A steel casing string that was slightly smaller than the drilled hole size was then run into

the well (Nelson, 1990). Completion mud was circulated through the U-tube annulus space, in preparation for the cementing job. The cement was then pumped down into the casing and it traveled upwards into the annular space, filling it from the bottom up (Nelson, 1990). Depending on the characteristics of the cement, the operator waited for a pre-determined amount of time for the cement slurry to cure. It was at this point that there was an increased risk of formation gas migrating into the cement slurry, as the hydrostatic pressure of the slurry was reduced during curing (Bachu and Bennion, 2009).

Surface casing strings were generally cemented back to surface, due to the possibility of contaminating surface fresh ground water sources. Many state oil and gas commissions required this practice in order to ensure that leakage does not occur. The cement also protected the steel casing from corrosion (Nelson, 1990). Cementing techniques have evolved over time, as operators developed the use of more effective cement additives to control fluid loss, alter the density of cement, and change the properties of cement slurry. Much research has been conducted to better understand the application and usefulness of cement additives. Changes to cement properties should reduce the problems of gas migration after cementing.

After cementing was completed, operators performed numerous tests to ensure that the cement job was completed properly. These tests included the following: hydraulic testing, pressure testing, dry testing, temperature logging, noise logging, nuclear logging, etc. A well log analysis can be conducted on cased holes that provide detailed data on gas or water flow behind casings (Bourgoyne, 2000).

One of the most widely used logging tools for used to determine the cement-formation bonding properties behind the pipe is called a sonic or ultrasonic bond log. Sonic bond logs emit acoustic waves that rely on acoustic impedance to determine the type of material in the annulus space (liquid, solid, void space). If there are liquids, then

there could be issues with zonal isolation and fluid flow through cracks or a micro-annulus. The logging tools use a series of transmitters and receivers, which send out signals though the casing steel, formation rock, and back to the tool. Depending on the material that the signal is traveling through, the time of travel varies. The cement quality is then determined by interpreting the logs, which identify derivations from normal homogenous, solid cement. Proper interpretation should always take into account the drilling and cementing reports which will include cement interpretation in context with the previous work performed.

Temperature logs provided data about fluid entry and exit points from the annulus space. An oxygen activation log can be used to detect a water flow channel by looking for oxygen in the water (Bourgoyne, 2000). A cement evaluation tool (CET) is a cement bond log that evaluates the quality of the cement bond in eight directions with a very fine vertical resolution (Bourgoyne, 2000). The CET can also be used to map the presence of gas channels (Bourgoyne, 2000). The top of cement can be identified by changes in temperature due to heat that was generated by the hydration of cement (Nelson, 1990). Additional testing can provide better decision making data in terms of remediation work needed to eliminate formation fluids from migrating behind the casing strings.

Cement can also be damaged during post-cementing operations from mechanical impacts that occur during tripping operations (Bourgoyne *et al.,* 1999). The term "tripping" is used in the oil industry to describe moving equipment (logging tools, drill pipe/collars, stabilizers, etc) down-hole. The mechanical impact of the tripping equipment with the steel casing can cause mechanical shocks that can weaken the casing cement bond behind the steel casing and cement filled annulus. Changes in pressure and temperature of the steel casing (during fracturing operations, etc) may also result in the separation of the casing from the cement (Bourgoyne *et al.,* 1999). Cement is a brittle

material and is susceptible to cracking when exposed to thermally-induced or pressure-induced tensile loads (Bourgoyne, *et al.*,1999). Huerta (2009) has conducted experiments to indicate such type of cracks under different conditions.

In summary, the cementing process was very complex and there were possibilities for errors, leading to gas migration. Although cementing is the best known practice of preventing gas migration under most conditions, there is no "special" cement that works every time for all conditions (Bourgoyne, 2000). Leakage problems (cracks in cement filled annulus space) develop due to many factors during different phases of the cementing process. Prevention of formation fluid flow behind casing strings required an integrated solution that incorporated the following processes (Bourgoyne, 2000):

(1) Proper properties of drilling mud.

(2) Increased bore-hole stability.

(3) Adequate hole pressure between pore pressure and fracture pressure.

(4) Changing cementing practices based on drilling conditions.

It is more difficult to fix a problem after leakage is detected, rather than to properly cement and seal annulus space. Therefore, it is recommended that drilling processes are followed to avoid conducting expensive remediation work. The state regulatory agencies require that the operator demonstrate that gas flow has been eliminated.

2.4 PREVENTION & REMEDIATION OF ANNULAR GAS MIGRATION

The risk of leakage can be mitigated through proper cementing procedures and post injection data collection. Wellbore characteristics are used to quantify wellbore leakage potential. Wellbores with a high likelihood of leakage can be fixed using

cementing remedial procedures. During sequestration injection periods, sensors can monitor leakage and provide validation to existing model forecasts.

Improper cementing can later lead to gas migration problems that require remediation work to fix the problem. Degraded cement is composed of highly permeable cracks. Research has been conducted to identify the risk of gas flow in existing wellbores and to conduct proper remediation to solve the problem.

The migration of formation fluids can lead to problems with different degrees of severity. For example, migrating gas flow problems range from the most hazardous situations (blowout) to marginal situations (rising wellhead gas pressure) (Nelson, 1990). The petroleum industry and regulatory agencies have long been concerned about recorded gas flow in wellbore locations that were supposed to be sealed. Gas flow and gas migration have been described by various terms, including the following:

(1) Gas communication

(2) Gas leakage

(3) Annular gas flow

(4) Gas channeling

(5) Flow after cementing

(6) Gas invasion

(7) Flow behind pipe

Operators use such descriptions when recording work done in a well's daily report. Many drilling reports or remediation reports were very useful for understanding the problems leading up to the gas migration problem. Most of the gas flow was a result of improper cementing procedures/techniques. Cementing service companies generally follow established cementing techniques to mitigate gas migration. After pumping, the cement hardens during a time period commonly called "Wait-On-Cement" or WOC time.

If the cement is not allowed to harden properly, gas migration may occur. The severity of gas flow depends on the properties of the cement (Nelson, 1990). For example, highly pressurized formation gases can invade cracks in the annular spaces that are filled with cured cement. The crack allows for communication between the formation gas source and a lower pressure zone. The formation gas invades the crack, as long as there is a pressure difference between the zones.

Researchers have conducted experiments on cemented annular space to show that mechanical defects, such as cracks in cement or gaps in bonding between the casing and the formation, allow for gas flow (Bachu and Bennion, 2008). The flow paths have significant permeability values, as opposed to intact cement, which has very low permeability. Thus, only sealed cement can provide an effective barrier to the upward flow of CO_2. However, when CO_2 mixes with water/ brine, carbonic acid forms which degrades the cement (de Figueiredo, 2004). The degradation of the cement over time increases the permeability of the crack, and increases the likelihood that CO_2 may leak from the subsurface.

Clearly, preventing gas migration by following proper cementing techniques is less expensive than performing remedial work to fix the problem. In order to quantify the risk for leakage, operators can assign values to characteristics of cement, which can then be used to predict the likelihood of gas flow occurring. For example, operators run logging tools to collect wellbore cement bonding information. The logged datasets are analyzed to assess the probability whether a well will leak and develop SCP problems.

Researchers have further quantified leakage assessments by developing a decision-tree type model to assess the risk potential of a well. Watson and Bachu published this model, quantifying the risks of CO_2 leakage from shallow and deep wellbore regions, based on the physical characteristics of the wellbore (Watson and

Bachu, 2008). They assigned risk factors for certain wellbore characteristics in order to quantify leakage potential. The extension of the findings was to include wellbores that would communicate with a CO_2 sequestration reservoir. A compilation of wellbore risk factors created a leakage potential score for each wellbore. For example, if a well was highly deviated from vertical and had low recorded Wait-on-Cementing (WOC) time, then the leakage potential score would be high. For each wellbore, the sum of the scores of the wellbore characteristics was a final leakage potential score. Generally, higher leakage scores had larger leakage path permeability values.

For wells that are leaking formation fluids, and buildup pressure is recorded at the surface, there are several remediation techniques that are used to fix the problem. The work performed depends on the severity of the gas flow. Remedial cementing jobs involve running logs down hole to locate potential leakage sources, perforating through casing steel/cement to reach the gas formation source, pumping in new cement to seal the hole, and allowing the cement to harden.

The petroleum industry refers to this as a “squeeze cement job”. Squeeze cementing is defined as the process of forcing cement slurry, under pressure, through holes in the casing/ wellbore annular space (Nelson, 1990). The slurry is injected at either low pressure (bottom-hole pressure below fracture pressure) or high pressure (bottom-hole pressure exceeds the formation fracturing pressure) (Nelson, 1990). High pressure injection is more complicated because it requires larger volumes of cement slurry to fill fractures that are located behind the casing string. The cement invades the formation rock and seals the formation source/hole. This procedure should repair the leak and eliminate zonal communication. Tests and logs can be run to evaluate the effectiveness of the squeeze job.

However, there are difficulties involved with such work. For example, the formation conduit may be difficult to locate behind the pipe. Also, the heightened pressures used to fracture the rock and pump in the cement may cause additional fractures to occur in different zones. Remedial cementing operations are expensive to conduct. Most regulatory agencies require that operators demonstrate that remedial work eliminated gas flow and that pressure buildups are negligible or below regulation limits.

2.5 PROPERTIES OF INTACT CEMENT PERMEABILITY

Due to the importance of using cement for sealing purposes when drilling and completing wellbores, research has focused on determining the micro-properties of intact cement. As a proven and established technique for proper wellbore construction, hardened intact cement provides an effective micro-Darcy permeable barrier that prevents gas migration through the seal. Nelson described gas migration through a cement filled annulus as “a complex problem that required considerable effort and techniques to prevent” (Nelson, 1990). The datasets that were used in this thesis contained limited information about the characteristics of the leakage pathway. However, pressure buildup or gas flow was measured at surface. Therefore, gas had to migrate through one of the following ways:

(1) Gas migration through pore structure of intact cement

(2) Gas migration through conduit/ crack in cement.

To answer this question, researchers first studied gas migration through cement slurry that was hardening into a solid. Cheung, 1987 showed through laboratory experiments that gas first invaded cement pore space when the cement was in a gelled state (Cheung, 1987). It was at this point that there was a higher potential for gas

migration within the gelling slurry, as compared to any other time during the hardening process.

Also, Cheung, 1987 showed that the cement slurry demonstrated hydrostatic pressure reduction. The cement slurry was pumped into the annulus space as a highly viscous liquid. Due to the weight of the liquid and the pump pressure, there was a hydrostatic pressure at the bottom of the cement length. During the Wait-On-Cement time, the cement begins to harden, and the solidification of the cement slurry reduces the hydrostatic pressure. During this hardening process, there is an increased risk that gas may enter into the annulus space. However, after the cement slurry has completely changed into a solid, gas can no longer migrate through the pore structure. The cement slurry permeability increased as the cement cured. During the early stages of cementing, the cement matrix permeability was measured to be as high as 300 md (Guyvoronsky and Frukshin, 1963). Parcevaux showed that pore size distribution decreased as cement slurry thickened (Parcevaux *et al.*, 1983).

Nelson,1990 demonstrated that cement slurries behaved as non-Newtonian fluids under high pumping pressures and flow rates (Nelson, 1990). Tinsley described the slurry during this solidification process as undergoing a "transition state," during which time the cement behaved neither as a fluid nor as a solid (Tinsley, 1979). During the "transition state", the cement slurry lost its ability to transmit hydrostatic pressure in the annulus. High pressured gas zones could then force gas through the cement slurry. To counter this problem, Tinsely, 1979 recommended using cement with higher gel strengths in order to prevent macroscopic gas bubbles from invading the slurry and rising through the cement due to buoyancy effects (Tinsely, 1979). Nelson recommended the use of different additives to cement to prevent such migration problems (Nelson, 1990).

Nelson further showed that after the cement hardened, normal density cement became a solid with very low permeability (microdarcy). As a result of these low permeability levels, gas were no longer able to migrate within the cement matrix pores (Nelson, 1990). Research findings on cement cores by Goode quantified the range of permeability in different types of intact cement ranging from 0.001 md to 0.10 md (Goode, 1968).

These findings provide evidence eliminating the possibility that gas can migrate through the cement matrix. Therefore, gas travelling through a conduit/crack in cement can be further described in detail by the following pathways:

(1) Gas flowing along the cement/pipe interface.

(2) Gas flowing along the cement/formation interface.

(3) Gas flowing through a crack in cement.

A combination of these pathways (i.e.: gas flowing through a crack in cement, then gas migrating through a channel between cement and formation) may also be used to describe the leakage gas pathway. In either of these cases, it is more likely that the pathway, not the intact cement contributes to gas migration and subsequent SCP buildup or SCVF. However Nelson does describe possible situations for which gas can migrate through cement, in section 8-3.6 of his book "*Well Cementing*",

> "After setting, during the hardening phase, a normal density cement becomes a solid of very low permeability, at the microdarcy level. As a result, gas can no longer migrate at any detectable rate within the partially water saturated pores of the cement matrix. It should be noted that low-density cement systems, with high water to cement ratios can exhibit fairly high permeability (0.5 md to 5.0 md). Therefore, it is possible for gas to flow, albeit at low rates, within the matrix of such cements, and to eventually reach the surface. Such events may take weeks or months to manifest themselves as measurable phenomena at the surface, where they usually appear as slow pressure buildups in the shut-in annulus."
>
> (Nelson, 1990).

The characteristics of the bond between the cement and formation or between the cement and steel casing were a function of proper cementing practices. Evans and Carter published research findings on cement-formation or cement-steel bonding properties. They showed that cement bond failure in the annulus was due to pipe expansion or contraction (Evans and Carter, 1962).

In addition to understanding the bond properties between substances, researchers studied how high flow rates of brine saturated with carbon dioxide gas would affect bonding. . For most sequestration projects, the injected gas would interact with formation brine. The brine saturated with CO_2 would contact concrete, causing an interaction between the fluid and the cement. Bachu and Bennion conducted two sets of experiments on class G cement in a laboratory to understand the process of well leakage in the presence of CO_2 (Bachu and Bennion, 2009). The cement core samples were subjected to 90 days of flow of CO_2 saturated brine at reservoir conditions of pressure, temperature, etc. Results suggested that proper cement bonding with the casing and the formation would provide a reliable barrier to upward flow of CO_2 (Bachu and Bennion, 2009). Research findings concluded that it is the presence of mechanical defects, (gaps or cracks in bonding between the casing and the formation), which would cause high permeability flow paths. Through these pathways, formation fluids would leak through cement filled wellbore annulus space (Bachu and Bennion, 2008).

It can be concluded that one of the most likely ways for gas to reach the surface is through existing leaky wellbore channels, and that such leaks are along defects like cracks within the cement or between cement and other wellbore materials. Therefore, a focal point of research in this thesis was to quantify permeability results of

cracks/pathways. These values can then be used as inputs to a leakage model, describing the gas flow channel through a leaky wellbore.

2.6 Determination of Wellbore Characteristics that lead to SCP Buildups

Researchers have investigated the correlation between wellbore characteristics and those that contribute to sustained casing pressure buildups. By analyzing a large number of leaky wellbores from a database, researchers determined the risk factors associated with certain types of wellbore designs. Researchers focused on the types of wells that were more prone to leakage problems over the lifecycle of the well.

For example, Bourgoyne *et al.,* 2000 analyzed a database of offshore leaky wellbores with SCP buildups from the now defunct federal agency, Mineral Management Service (MMS). Several case study wells were extracted from the database in order to highlight the analytical process used to dissect wellbore problems leading to SCP. Remediation techniques that were used to fix the problem were also discussed. Bourgoyne highlighted the severity and frequency of a large number of wellbores in offshore Gulf of Mexico that developed SCP buildup problems over time (Bourgoyne, *et al.,* 1999). These statistics were reported in aggregate.

Other researchers focused on the micro-details of a smaller database of leaky wells to draw conclusions. For example, Wojtanowicz studied the principles of gas flow/migration through wellbores after cementing. He obtained a small database of 16 leaky wellbores, located in the Gulf of Mexico from the MMS and focused on early annular gas flow data recorded after cementing (Wojtanowicz *et al.,* 2000). He also conducted field experiments to better understand the relationship between cement characteristics and SCP buildups.

Wojtanowicz *et al., (*2000) demonstrated that during the process of cement hardening (from slurry to solid), cement with high water loss reduced the hydrostatic pressure of the cement column. This pressure loss allowed gas to flow from the formation into the annulus space (especially in undetected gas pockets), eventually developing into a SCP buildup (Wojtanowicz *et al.,* 2000). It was recommended that operators use drilling technologies to diagnose zones of likely gas migration in order to use preventative technologies to reduce such issues. Proper diagnosis of leaky wellbores that demonstrated SCP buildups over time would lead to remediation efforts that were needed to fix the problem (Wojtanowicz *et al.,* 2000).

Bachu and Watson, (2008) further contributed to the determination of characteristics of leaky wellbores by publishing a series of papers in 2008. The first paper was, "Possible Indicators for CO_2 Leakage Along Wells" and their second paper was, "Identification of Wells with High CO_2 Leakage Potential in Mature Oil Fields Developed for CO_2 Enhanced Oil Recovery." Proper leakage assessment of CO_2 was determined by evaluating a large database of leakage wellbores (315,000 oil and gas wells and injection wells from the oil and gas regulatory agency in Alberta). They found that 4.6% of the wells had recorded surface casing vent flow (Bachu and Watson, 2008).

This database also provided detailed information about the cement types, cement volumes, casing strings, etc. Bachu and Watson, 2008 built a model to assess the risk of leakage in the shallow and deep wellbore regions. The potential for risk was quantified by assigning a leakage risk value to the wellbore (Watson and Bachu, 2008). This ranking system determined the potential for leakage, based on wellbore factors (Bachu and Watson, 2008). The risk analysis was applied to existing wells in two large Canadian fields, and the results populated a frequency distribution, ranging from most probable leakage to least probable leakage.

2.7 RESEARCH ON MODELING CO_2 LEAKAGE

Researchers have developed models to describe and predict the behavior of target reservoirs to be used for CO_2 sequestration purposes. Reservoir models have been developed to better understand the interaction between the reservoir formation fluid and injected CO_2. The injected CO_2 gas into the target reservoir causes significant changes to the properties of the reservoir fluid, pore space, and formation rock. For example, an accurately forecasting model predicts the migration of CO_2 plumes through highly permeable pathways. The heightened reservoir pressure levels create pressure "pulses" at the near wellbore surrounding area. These types of reactions should be captured by an accurate model.

At the XIX Conference on Computational Methods in Water Resources, several researchers provided details about their CO_2 sequestration modeling approaches. The presentations focused on the mathematical governing equations of the model, as well as inputs used for modeling purposes. Some provided examples of target sequestration reservoirs that were modeled. Researchers emphasized that the risk of leakage was one of the most important considerations when planning a sequestration project. Hence, leakage modeling quantified the leakage risk assessments and provided answers to practical questions about a specific CO_2 sequestration project. In order to reduce the risk of leakage, sequestration solutions required an enormous effort in the modeling community.

Most of the research presented was a follow-up to previously published work. For example, Nordbotten presented "Novel Approaches for Modeling Migration and Trapping at Geological Scale" (Nordbotten, 2012). He emphasized that modeling a target reservoir should be consistent with observations, provide useful suggestions for reservoir behavior, and be bounded by realistic parameter values. To properly model a CO_2 target

reservoir with a single injection well, the model inputs would be an appropriate CO_2 Equation of State (EOS), relative permeability curves, boundary conditions, and the dissolution rate of CO_2 into brine, formation fluids. Nordbotten also discussed how using the appropriate models for prototypes would need to be up-scaled to meet the needs of industrial sized projects, such as Statoil's Sleipner Field.

In general, when modeling sequestration reservoirs, the reservoir storage capacity is a function of the following reservoir characteristics:

(1) Geological rock properties (porosity and permeability).

(2) Formation fluid properties (oil, water, gas, etc).

(3) Pore space characteristics.

(4) Reservoir storage conditions (depths, pressures, temperatures).

Single phase flow models are less complex than multiphase flow models. However, researchers have attempted to model multiphase flow projects. For example, Martinez from Sandia National Labs presented "Coupled Multiphase Flow and Geo-Mechanics for Analysis of Caprock Damage during CO_2 Sequestration Operations" (Martinez, 2012). Martinez and Sandia National Labs identified specific pilot target reservoirs/sites used for sequestration purposes. In his presentation, Martinez described one particular site, a target reservoir that was intersected by abandoned wells and a geological fault. The heightened injection pressure near the wellbore caused damage to the cap rock seal. This allowed injected gas to reach the surface. Martinez developed a predictive leakage two phase model to describe two phase gas flow from the reservoir through the damaged cap rock and into formation zones above the target reservoir.

Since many targeted sequestration reservoirs were once oil and gas producing reservoirs, there exists large amounts of reservoir data that can be used as inputs to modeling CO_2 sequestration reservoirs. For example, an offshore CO_2 sequestration

project in Italy was based on two dry gas wells that were drilled by the Italian oil company, ENI. The target reservoir was then studied as a potential sequestration project.

Castelletto demonstrated the details of this project, in his presentation, "CO_2 Geological Sequestration: a Numerical Study in a Real Multi-Compartment Reservoir in the Northern Adriatic Sea, Italy" (Castelletto, 2012). This sequestration project was one of six large scaled projects in Europe aimed at exploring the potential application of CO_2 injection/ sequestration efforts in existing European target reservoirs. The source of CO_2 pumped into the target offshore reservoir would be from a local power plant. To better predict the behavior of CO_2 in the reservoir, Castelletto built a complex reservoir model composed of different reservoir characteristics (rock layers, faults, existing wellbores, etc). These parameter values were entered into the model to predict the interaction between formation fluids and injected CO_2. The two injection wells pumped CO_2 into the targeted reservoir where it was stored beneath an impermeable cap rock layer.

As CO_2 was pumped into the reservoir, the risk of leakage increased over time. In such reservoirs, the gas plume migrated through highly permeable layers, such as faults or existing wellbores. In order to develop a leakage forecast model to describe the gas pathway through wellbore, different assumptions were made about the frequency distribution of leakage pathway permeability. Assumptions of leakage path permeability may generate wide ranges of leakage flux. Therefore, field data generated leakage path permeability provided more accurate results.

Using assumed permeability values, Nordbotten published results of plume migration from an injection well of supercritical CO_2 that was pumped into a brine-saturated deep aquifer. The model predicted the extent of the plume and the leakage rates through an abandoned well, located a distance from the injection well (Nordbotten *et al.*, 2005).

Celia *et al.*, 2011 further applied this model to simulate leakage in an existing field of thousands of wells in Alberta in order to estimate CO_2 flux along existing wells (Celia, *et al.*, 2011). The model predicted the flux of injected gas that would migrate to different subsurface zones for a reservoir that was composed of multiple layers. The model simulated CO_2 injection, migration, and leakage over a 50 year time period in the existing field to quantify risk. In order to run the model, wellbore and reservoir parameter values were based on a distribution of possible values. The model results quantified leaky wellbore properties, and helped to determine the risk of leakage in a CO_2 injection project (Celia *et al.*, 2011).

Clearly, the need for proper data collection and useful models can provide researchers with a better understanding of the potential for leakage. Researchers can apply similar models to different potential projects, accounting for differences in rock and fluid properties. The characteristics of the target reservoir will have to be documented in order to produce accurate results.

Chapter 3: Description of Leakage Models and Wellbore Parameter Values

CHAPTER 3 OVERVIEW

In this chapter, the general issues of using a model to describe pressure buildup and vent flow will be discussed. The computed effective permeabilities for the wellbores are presented and compared. The description of the leakage pathway is characterized, using the SCP Model and the SCVF Model. Details about the selection of the inputs to the model are highlighted. In Chapter 4, the uncertainty of the parameters is presented for each leaky wellbore. In Chapter 5, methods used to reduce uncertainty are discussed.

3.1 INPUT PARAMETER VALUES AND LEAKAGE SCENARIOS

In order to run the SCP Model and the SCVF Model to generate leakage path permeability results, values must be assigned to a set of input parameters. These parameter values, plus the SCP or SCVF measurements were grouped within the following categories:

(1) Wellbore construction information. – Wellbores that contained information about casing sizes and casing depths, which were used as boundary conditions. The wellbore deviation from vertical, hole size, and cement slurry volume information were useful to describe gas leakage pathways.

(2) Pressure buildup data intervals. - For this category, there were 29 wellbores that contained pressure vs. time buildup information (SCP buildups) in the intermediate annulus space. The re-creation of the leakage scenarios, including wellbore diagrams and pressure buildup information is provided in Chapter 4 of this thesis.

(3) Gas flow information. - Over 210 wellbores provided surface gas flow datasets that were also used for re-creating leakage scenarios. The details of these

wellbores are provided in Chapter 4, and grouped by appropriate flow rates. The wellbore construction information for all 210 SCVF wellbores was provided in the appendix.

For each pressure buildup or flow rate recorded, the appropriate model (SCP or SCVF) was applied to generate corresponding effective permeability value. Changes in permeability were a result of changes to the input parameter values. Since all information required to run a model was not always properly recorded, estimates of certain input parameter values were used. The larger the range of values used to describe the parameter value, the greater the uncertainty of final results.

3.1.1 Selection of Model Input Parameter Values

The SCP Model and the SCVF Model are composed of a combination of interconnected parameter values. There can be a large degree of uncertainty when describing the characteristics of a leaky wellbore system because of limited information provided by the wellbore operator. For most cases, the leaky wellbore raw data (pressure vs. time, flow rates, and wellbore construction information) were sufficient to re-create a leakage scenario by limiting the values of unknown parameters within specific ranges. The targeted parameter value could vary between the upper and lower values, within a given range. For each new combination of leaky wellbore characteristics, pressure buildup, or flow rate, a range of permeability values were generated.

The importance of using consistent model parameter values when obtaining reasonable permeability outputs merits a complete description. The following parameter values that were used in the SCP and SCVF Model are described in detail:

(1) Outer diameter and inner diameter casing strings

(2) Gas constant

(3) Mud compressibility

(4) Gas cap length

(5) Bottom-hole pressure

(6) Bottom-hole temperature

(7) Wellhead temperature

(8) Temperature at standard conditions

(9) Pressure at standard conditions

(10) Gas law deviation factor

(11) Gas viscosity

(12) Mud density

If the original dataset did not provide detailed information about some of these parameters, then assumptions were made. Some of the parameter values that were entered into the leakage models were based on research findings by previously published authors. In other cases, unknown parameter values were assigned a range based on known boundaries from the original dataset. This reduced the uncertainty of these unknown parameter values.

(1) Outer Diameter and Inner Diameter Casing Strings

For the majority of the datasets, wellbore casing size information was provided. The outer and inner intermediate casing strings constitute two of the four boundaries of the wellbore annular space. These two boundary conditions were fixed when re-creating plausible leakage scenarios. For modeling purposes, the cross sectional area of the annular space was calculated using Eqn. 3.1.1.1

$$A = \frac{\pi}{4}\left(D_{outer}{}^{2} - D_{inner}{}^{2} \right) \tag{3.1.1.1}$$

where

D_{outer} = Outer diameter of the lower casing string [ft]

D_{inner} = Inner diameter of the upper casing string [ft]

(2) Gas Constant

The gas constant, R for an ideal gas is $8.314 \frac{J}{molK}$,based on the Ideal Gas Equation of State. However, for modeling purposes, the gas was not assumed to be ideal. A z-factor is used to quantify this change from the Ideal Gas Law.

(3) Mud Compressibility

Mud compressibility was a fixed, known value for water based mud (WBM) of 3.3 x 10^{-6} $psig^{-1}$. This value was provided by published research findings from I.M. Kutasov (1988). Kutasov described a procedure to quantify the changes in different fluid properties at subsurface (elevated temperature and pressure conditions). The change in drilling mud properties at depth were described by an empirical equation of state (EOS). The EOS for drilling mud and brine predicted the change in fluid density, compressibility, and other properties. Different fluids (WBM, OBM) were used to study the fluid property changes. Kutasov provided a range of different fluid compressibility, based on the type of fluid analyzed. For example, a light WBM with a density of 10.7 pounds per gallon (ppg) had a higher compressibility of 3.38 x 10^{-6} $psig^{-1}$. A heavy WBM fluid with a density of 18.1 ppg had a lower compressibility of 3.03 x 10^{-6} $psig^{-1}$. For OBM, the compressibility was generally greater. For example, a light OBM with a density of 11.0 ppg had a compressibility of 6.56 x 10^{-6} $psig^{-1}$. For a heavy OBM with a density of 18.0 ppg, the compressibility was 5.19 x 10^{-6} $psig^{-1}$.

Nelson stated that completion mud was mostly composed of WBM. Additional data provided in some of the datasets confirmed this. Therefore, the compressibility for WBM was assigned a value of 3.3 x 10^{-6} $psig^{-1}$, corresponding to the lighter density WBM described by Kutasov (Nelson, 1989).

(4) Initial Gas Cap Length (before bleed-down occurred)

In a closed boundary system (surface wellhead valve closed), the gas cap length is measured in the annular space as the distance from the surface wellhead to the depth at the top of completion fluid. The compressibility of the completion fluid is an important factor when determining the gas cap length. As the gas cap grows in size, the fluid compresses, creating more space. For larger mud compressibility, the mud compresses more and the gas cap size is larger. For smaller mud compressibility, the mud compresses less and the gas cap size is smaller.

Gas cap length was a difficult parameter value to obtain with a great deal of certainty. When an operator opens the surface annular valve to reduce pressure and to allow gas flow, the gas cap is reduced quickly without being recorded. The system changes from an "open" system to a "closed" system. Most of the data about the volume of gas volume was never collected. A leaky wellbore example in a report entitled, *"A Review of Sustained Casing Pressure Occurring on the OCS"* to the MMS (Bourgoyne, 2000) was used to determine a range and distribution of gas cap lengths. Bourgoyne described a remediation effort that was followed without the use of a work- over rig in order to reduce gas flow through cracks in the cement filled intermediate annulus space. The remediation procedure was designed to block the leakage path causing the problem. This involved removing mud and gas from an annular space by opening the surface valve and then replacing it by injecting weighted mud into the annular space and closing the valve. The high density mud that was pumped into the annular space increased the hydrostatic pressure of the column of mud. After each pumping cycle, the operators would wait 24 hours before they would measure the pressure and determine how much weighted mud to pump into the annular space. The operators used a "stair-step" procedure that entailed bleeding small amounts of light weight gas and fluid from the

annulus followed by injecting heavier mud into the annulus. This systematically increased the annular fluid density at each consecutive interval.

The amount of mud volume that was pumped into the annular space was compared to the amount of mud volume that bled off from the system. The difference in mud volume calculated was considered the gas cap volume. The length of the gas cap was calculated by dividing the gas cap volume by the annular area between the outer diameter casing string and the inner diameter casing string. For each 24 hour cycle, a gas cap length was calculated, providing a distribution of gas cap lengths. This recorded data was used to determine an original distribution of gas cap lengths (Fig. 3.1.1.1).

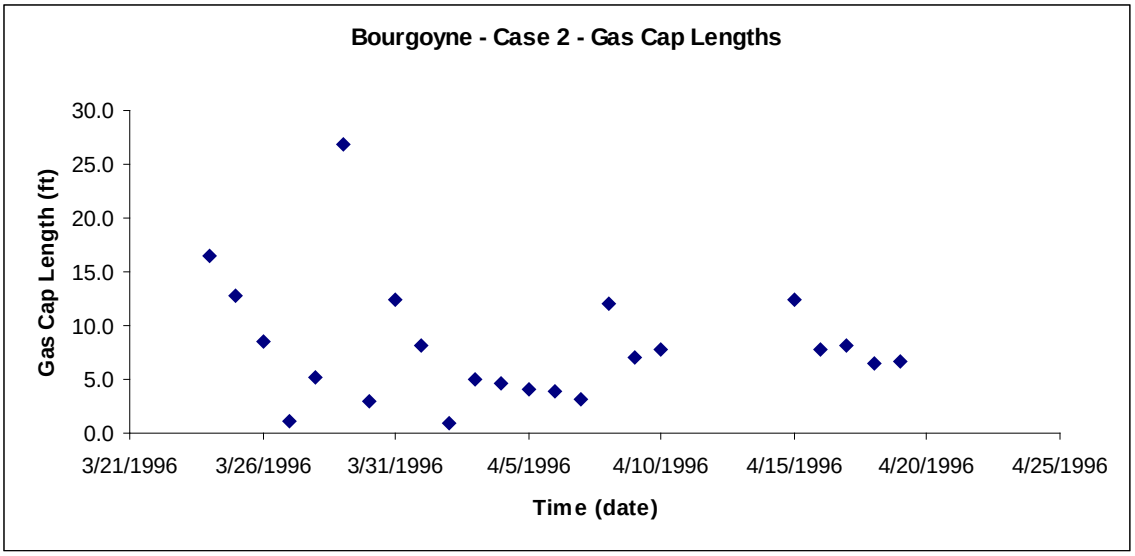

Figure 3.1.1.1 – Original gas cap length distribution from Bourgoyne Case History 2 wellbore.

The original gas cap distribution demonstrates a range of different gas cap lengths, with the average gas cap length of 6.7 ft. The gas cap lengths vary over time, thus indicating that the remediation efforts were unsuccessful. Bourgoyne provides detailed remediation information for one case study. For this wellbore, the monitoring

process started on March 24, 1996 and ended on April 19, 1996. This process occurred once, every 24 hour period.

A second approach to determine gas cap length distribution was to simply assume that the gas cap lengths could be described by a uniform distribution, ranging from 0 ft to 20 ft (gas cap length of any value in this range was equally probable of being selected). The leakage path permeability values that were generated were different, as can be observed in Fig. 3.1.2. The leakage path permeability outputs were generally higher values (magenta color) when using the uniform gas cap distribution, as opposed to permeability values (blue color) using Bourgoyne's gas cap distribution (Fig. 3.1.1.2).

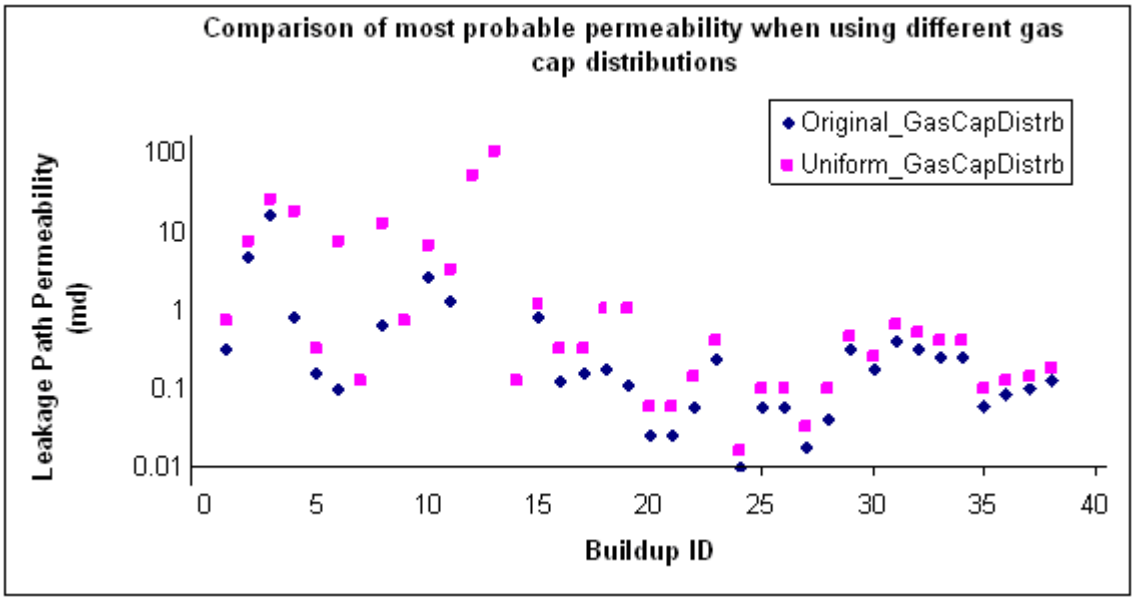

Figure 3.1.1.2 – Comparison of leakage path permeability between using uniform gas cap distribution and the original gas cap distribution.

These results confirm that the gas cap length had a significant effect on the permeability values that were originally generated. Overall, the leakage path permeability increased by less than one order of magnitude. It was recommended that

due to the sensitivity of gas cap with the results, it would not be prudent to apply the original gas cap length distribution to the analysis of all the wellbores. The finding from one wellbore would not be sufficient to apply to the other wellbore results. Therefore, a uniform gas cap length distribution was assigned for all other wellbores.

(5) Bottom Hole Pressure (Pressure at Leakage Depth)

Pressure increases with depth due to greater forces applied from the weight of the earth formation and filled pore space. The formation is composed of different types of rock and pore space is filled with different fluids. Rock has a higher density than liquids, so the pressure gradient is a composition of the different rock types and fluid types that composes the formation. The pressure gradient of 0.465 psi/ft was used. The pressure at the leakage depth was calculated by multiplying the pressure gradient of 0.465 psi/ft by the leakage depth. This pressure gradient is based on a normally pressurized formation zone.

(6) Bottom Hole Temperature (Reservoir Conditions)

Temperature increases with depth due to the geothermal sources which increase temperature at greater geological depths. The geothermal gradient used for this research was 1.5 F/100 ft.

(7) Wellhead Temperature

The flowing wellhead temperature is based on the flowing fluid/gas that travels through the production tubing from the leakage source to the wellhead surface. The wellhead temperature is assumed to be 120 F.

(8) Temperature at Standard Conditions

The temperature at standard conditions is assumed to be 60 F.

(9) Pressure at Standard Conditions

The pressure at standard conditions is 14.7 psi.

(10) Gas Law Deviation Factor

The gas law deviation factor (or z-factor) describes the departure of the gas behavior from that of the Ideal Gas Law, which does not account for variation in forces between molecules as a function of pressure (USGS, 2012). A z-factor less than 1 is introduced into the equation of state (Eqn. 3.1.1.2),

$$PV = ZnRT \qquad 3.1.1.2)$$

where $Z = 0.86$

(11) Gas Viscosity

The prediction of the behavior of gaseous viscosity can be described by the kinetic theory of gases (Bird, *et al.,* 2007). Viscosity in gases arises principally from the molecular diffusion that transports momentum between layers of flow (Elert, 2009). Viscosity is dependent on pressure and temperature. Staying consistent with previous research (Xu, 2001), and for modeling purposes, a constant gas viscosity value of 0.02 cp was used.

(12) Mud Density

The completion fluid density (mud density) was provided for most datasets. However, in a few cases where the density was not provided, a range from 8.8 ppg to 14.0 ppg was used.

In the intermediate annulus, the completion mud plays an important part in the determination of leakage path permeability. The mud density provides the necessary force to counteract the gas migration force into the mud column. The mud column starts at the wellbore surface and ends at the top of cement depth. In some cases, the mud length reaches depths that are shallower than the depth of the upper casing string. The remainder of the annulus space is then filled with cement.

Nelson describes the use of spacers and displacement fluid used to eliminate the WBM or OBM drilling fluid that occupied the annular space. The use of pre-flush fluids improves the cement bonding process by eliminating the interaction between drilling mud and cement slurry and creates a better bonding environment for the cement/steel/formation interface. The pre-flush eliminated the drilling mud from the annular space and remains after the cement solidify in the annular space. Nelson states that, "pre-flushes have density and viscosity close to that of water or oil. They have much higher solid particle content than washes and are more effective buffers for avoiding contact between the cement slurry and the drilling mud. The density of the spacer is higher than the density of the drilling mud, but lower than that of the cement slurry" (Nelson, 1989). For modeling purposes, the density of the pre-flush completion mud was assumed to be the same for WBM.

3.1.2 Example Model Inputs

The permeability values that were generated from the SCP and SCVF Model were based on the selection of the most likely input values within a range. A gas leakage scenario was composed of input parameter values that had been selected. The input parameter value with the largest degree of uncertainty was the leakage source depth. Accurate leakage depths (location at which gas enters into the cement filled annulus space) require the use of down-hole logging tools or gas analysis that can identify problematic zones of interest. These tools/procedures, as discussed in detail in Chapter 5, provide useful input data that can be used in order to reduce uncertainty. For a majority of the datasets, the operator did not disclose details about the location of the

leakage depth. Thus, the models were run with a range of leakage depths, varied along the cemented/open-hole section between the upper and lower casing shoes (Fig. 3.1.2.1).

Changing different input parameter values (formation pressure, mud length, mud density, mud compressibility, etc) had different degrees of magnitude on the effects of the model outputs (leakage path permeability.)

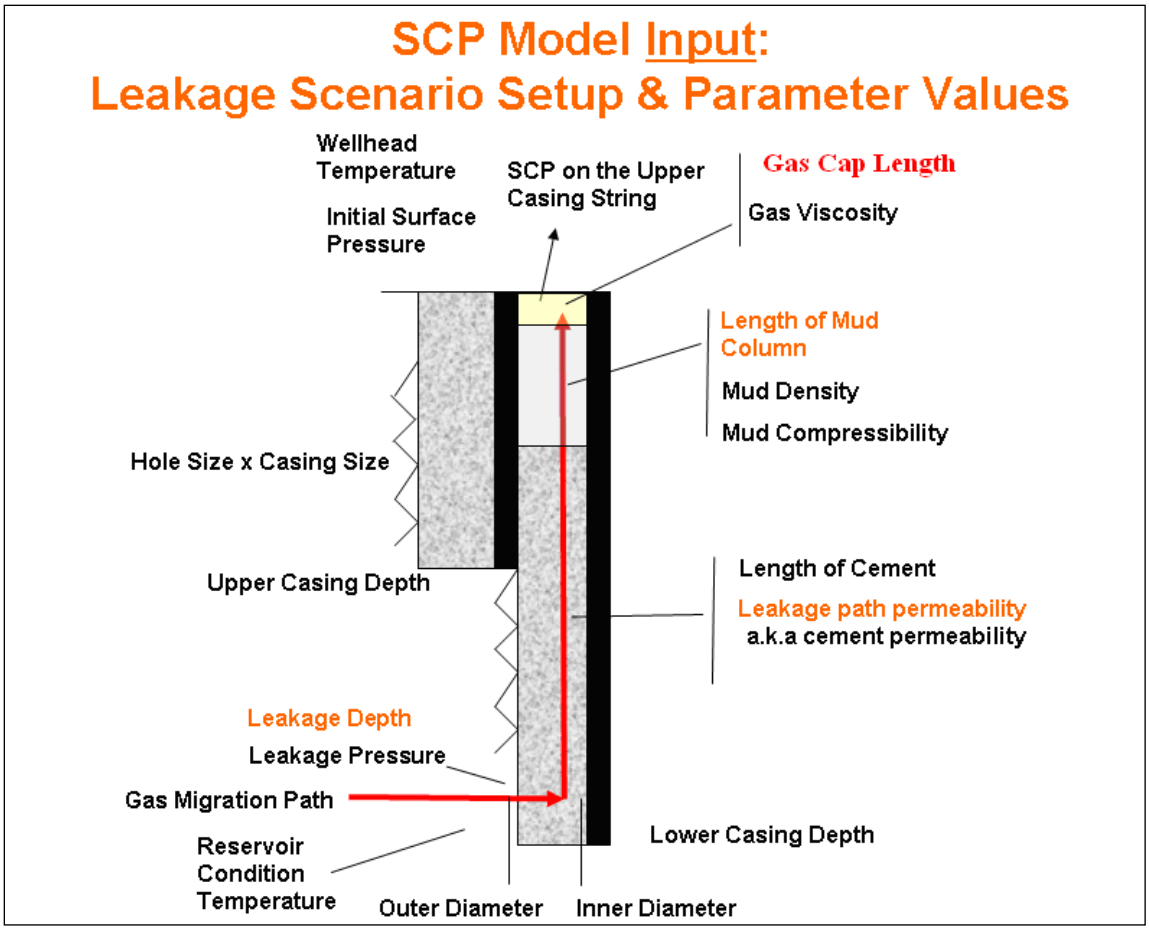

Figure 3.1.2.1 – Input parameters for the SCP Model (highlighted parameters have large impact on the model).

The leaky wellbore datasets provided different types of information, categorized under one of three groups. For example, one of the wellbores contained, to various

degrees of detail, discrete values of pressure buildup data over time, gas flow rates (m^3/day), and wellbore construction information (casing sizes, depths, cement slurry volume, etc). A range of plausible values was generally used to describe the unknown parameters. In order to obtain maximum and minimum permeability values, different combinations of input parameters were used. These detailed leakage scenarios generated a suitable range of leakage path permeability results used for comparison purposes.

Wellbores with pressure buildup data in the intermediate annulus space were chosen and used for separate case studies with the SCP Model. These wellbores are discussed in Chapter 4 (Sections 4.1 through 4.5). Wellbores with flow rate information were used for separate case studies with the SCVF Model. The majority of these wellbores are discussed in Chapter 4 (Section 4.6). Leakage path permeability results from both the SCP and the SCVF Models were compared for the same wellbore.

The pressure data sets provided different types of pressure buildup levels and rates of pressure buildup that were recorded over a period of hours, days, months, or several years. The gas continued migrating until there was zero pressure difference between the leakage source and the pressure at the top of cement. For safety reasons, pressure bleed-offs were conducted by the operator to release the pressure at the surface and to eliminate the gas cap. These bleed-offs may have contributed to changes in the characteristics of the gas migration pathway.

Over time, the pressure levels in some wellbore annuli fluctuated from low pressures (post bleed-down) to high pressures. The different asymptotic pressure levels that were recorded may have been a result of changes to the leakage system over time. For example, the characteristics of the crack/leakage conduit could have been altered by the fluctuating pressures in the annulus and the amount of gas flowing through the pathway. The gas formation source would continue to supply a highly pressurized gas to

migrate through a leakage conduit, but the crack may have closed with time, lowering the permeability values, and reducing the ability of the gas to flow. The asymptotic pressure level would be constant, but the rate at which the pressure built up would be lower. This is because less gas volume could migrate through a lower permeability pathway for a given time period.

Another example is the change in completion mud length or lower amounts of formation fluids in the annulus space over time. The change in the length of mud would lower the mud's hydrostatic pressure at the top of the cement. In order to equalize the pressure levels between the top of cement and the gas formation entry point, the asymptotic pressure levels would need to be higher in order to compensate for this pressure reduction. For example, if the leakage pressure source was 900 psi and the hydrostatic pressure at the top of cement was 700 psi, then the asymptotic pressure level would be 200 psi. However, if the hydrostatic pressure at the top of cement was reduced to 600 psi, and the leakage pressure source remained constant, then the asymptotic pressure level would be 300 psi.

In addition to changes in liquid annulus levels, another factor that would have a significant impact on asymptotic pressure levels would be the reduction of formation pressures over time. This would only occur if the reservoir had no communication with a secondary pressure source, such as a high pressure aquifer. As gas production continues from this reservoir, the gas source is depleted and pressures decrease over time. For example, if the leakage source was reduced from 900 psi to 800 psi, and the pressure at the top of cement was still 700 psi, the asymptotic pressure would be 100 psi. Since this type of depletion is common with gas producing reservoirs, it is common to observe such decreasing asymptotic pressure levels over time (Fig. 3.1.2.2).

At later points in the time interval, the pressure built up to smaller and smaller asymptotic pressure values. For example, in September-1998, the pressure level was at its highest value of 750 psi. By March 2000, the pressure level had dropped to 550 psi. In June 2001, the pressure level was 450 psi. By December 2002, the pressure level was 300 psi. This was a reduction of nearly 450 psi over 4 years (113 psi/year). This type of pressure reduction may be an indication of a declining reservoir pressure source over the life of the production well.

With a single wellbore containing multiple pressure buildups that reach different asymptotic pressure levels, it becomes important to discuss why certain buildups were selected, but other buildup intervals were not. The reasoning for this selection process was that there was a difference between "actual" asymptotic pressure intervals that demonstrate "leveling off plateaus" and "hypothetical" asymptotic pressure intervals that were bled down to low pressures before reaching pressure plateaus.

This comparison can be seen by studying the pressure buildups in Fig. 3.1.2.2. The first three pressure buildups were bled down to near zero, low pressures. The fourth pressure buildup interval (highlighted in yellow) was never bled down and reached an asymptotic pressure level of 300 psi. Therefore, the most accurate buildup interval used for modeling purposes would be this last one.

In addition to these observations, other types of inferences can be made. For example, the rate at which the pressure built up in each of the first three buildup intervals is greater than the rate of pressure buildup demonstrated in the last buildup interval. This may also be a result of declining reservoir pressure, which would reduce the gas driving force into the cement filled annulus space.

Another interesting time interval to study lasts from June 2001 to March 2002. The pressure levels during this time period are at or near 0psi. Since there was limited

access to remediation records for this example wellbore, it was difficult to determine with a great degree of certainty that remediation had been working for a short time period, before gas flow began to occur. However, this does appear to be plausible, since none of the other time buildup intervals demonstrate an extended period of time of constantly low pressure values. For the other buildup intervals, the wellbore surface valve was opened, allowing for the pressure to bleed down, only to be followed by a pressure buildup.

Remediation work aimed at fixing the problem may have occurred in June 2001, and seemed to work for short time period. The reduced pressure buildup rate may indicate a lower permeability pathway. Therefore, the leakage pathway permeability range that was generated corresponds to the characteristics of the pathway at this time period only (from June 2001 to March 2002). Had permeability been generated for the other time periods, each would be considered a unique and original case study used to describe a different leakage pathway. A single wellbore with multiple pressure buildups generates a range of permeability, suggesting that the leakage path characteristics changed with time.

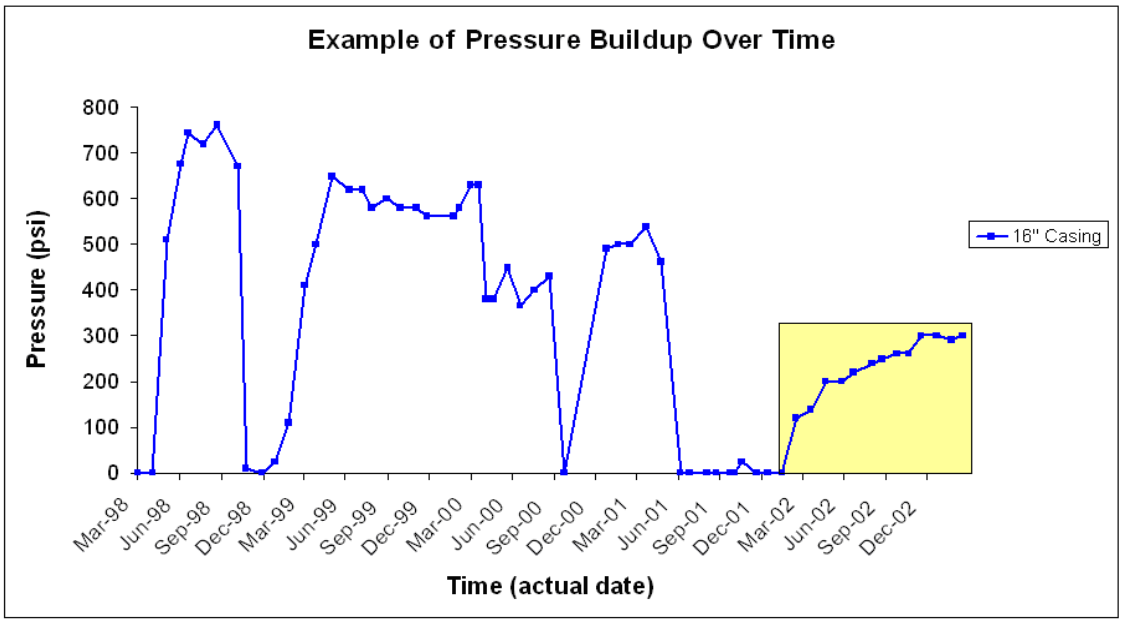

Figure 3.1.2.2 – Example pressure buildup dataset for one wellbore. The surface pressure gauge records pressure (psi) vs. time (raw data) on an intermediate casing (16'') annulus. The pressure build-up period (highlighted in yellow) is used as a constraint when estimating wellbore permeability.

In this example wellbore, no surface wellbore flow rate information was provided. Therefore, there was no use of the SCVF Model. The SCP Model was solely used instead. However, there are other cases of wellbores that contained both pressure buildup measurements and surface wellhead flow rates. In these cases, the wellbore construction information remained constant. Using the wellbore information, pressure data, and flow rates, the data was entered into either the SCP Model or the SCVF Model to generate different leakage pathway permeability values. The permeability results from both models were compared to demonstrate differences between the model outputs. The details of the SCP Model will be discussed in Section 3.3 and the details of the SCVF Model will be discussed in Section 3.4 of this chapter.

3.2 LEAKAGE PATHWAY DESCRIPTIONS

The datasets did not provide logging results to identify gas migration pathways. Therefore, assumptions had to be made regarding leakage pathways. Four possible gas migration pathways have been identified (Duguid, 2006). In Fig. 3.2.1, these locations are highlighted in detail. The figure is a close-up of plugged and abandoned wellbore with a cement sealed intermediate annulus space. Part (A) shows the migration through pores of a cement matrix. Part (B) shows gas migration through a defect between the steel casing and cement. Part (C) shows gas traveling through the interface between the formation and the cement. Part (D) shows gas entering the producing tubing through a faulty, damaged steel casing string.

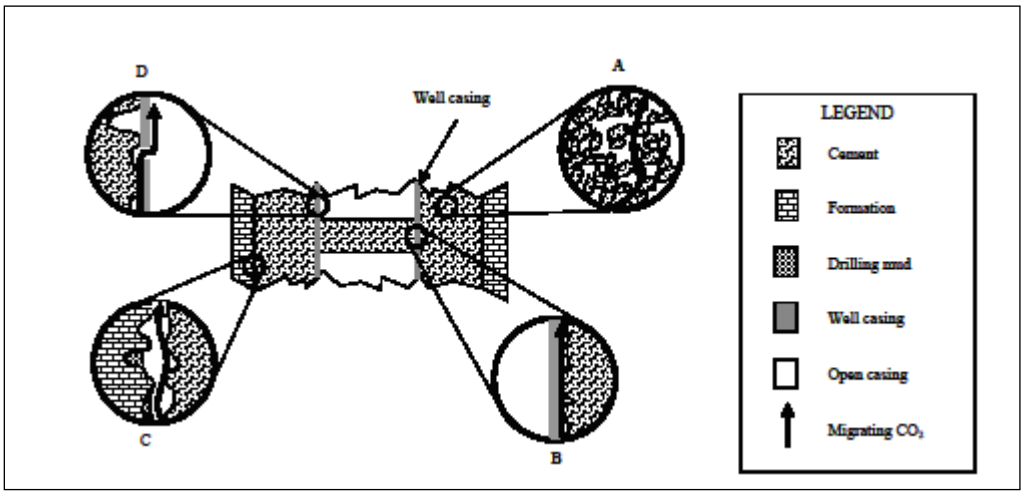

Figure 3.2.1 – Different source/explanation of leakage pathways (Duguid, 2006).

For this thesis, the leakage pathways used for modeling purposes are one or more of Parts (A), (B) and (C). There was no evidence or data to support which one of these three were the most appropriate pathway to select. The governing equation of Xu's leakage model describes such pathways as equivalent permeable media. Part (D) would

not be an option because the leakage model cannot describe this type of pathway. Moreover such a leak is not relevant to the risk of CO_2 leakage along existing wellbores.

When the results from the SCP Model and SCVF Model were generated, there was no distinction between pathways described in Part (A), (B) or (C). The leakage pathway permeability describes an effective permeability of the entire cement filled annulus space between the casing string boundaries. Therefore, the results do not explicitly describe a leakage pathway; rather the results describe the permeability of an equivalent continuum material.

Gas flow normally occurs at the interface between the steel casing and the formation due to improper cementing techniques. The leakage source fluid/gas enters a crack in the cement. The driving force of the fluid is the hydrostatic pressure of the formation fluid at leakage depth. The crack in cement is in communication with the formation gas source. As was previously discussed in chapter 2, section 2.3 of this thesis, there were many factors that could have contributed to the crack forming in the cement filled annulus space.

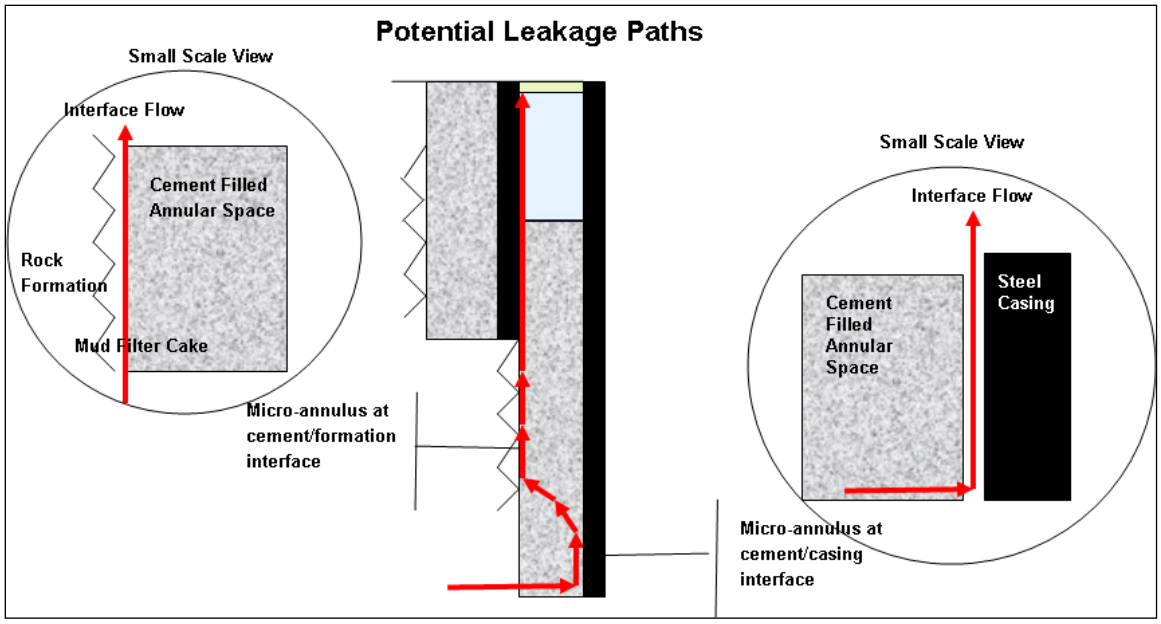

Figure 3.2.2 – Detailed focus area of study of two possible gas migration paths. Left: Possible Interface1 - Cement and rock formation. Right: Possible Interface 2 – Cement and the steel casing.

The leakage pathway entry depths were generally constrained to be located between an upper bound of the surface casing string seat depth and the lower bound of the intermediate casing seat depth. These boundaries constituted the intermediate annulus (Fig. 3.2.3). Upper and lower permeability values were generated by setting the leakage depths to these points of entry into the intermediate annulus space.

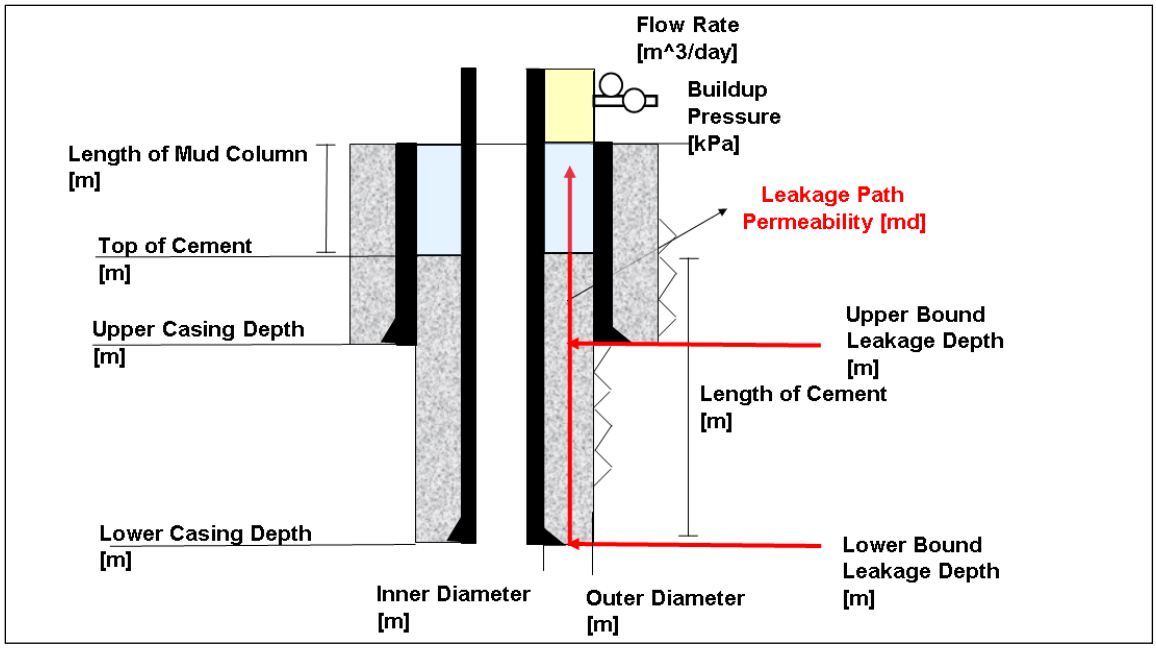

Figure 3.2.3 – Schematic of SCP, SCVF Model leakage boundaries and parameter values used. The SCP and SCVF Model output is leakage path permeability (highlighted in red).

3.3 SUSTAINED CASING PRESSURE (SCP) MODEL

When the surface casing valve was closed, the pressure buildup at the surface wellhead depended on the inflow of gas to the system. The gas migration pathway had a closed system boundary at the surface, but an open system boundary at the leakage source. The gas migration created a gradual pressure increase over time, which was recorded. As long as the pressure built up, this indicated that the formation pressure was greater than the pressure in the annulus at the base of the hydrostatic column (top of cement).

The gas accumulated at the surface during pressure buildup and then was reduced during pressure bleed-downs. The gas cap size increased, depending on the gas expansion and mud compression in the annulus (Xu, 2001). The purpose of the SCP Model is to model the migration of gas through the annulus space mathematically. The

Sustained Casing Pressure (SCP) Model used in this research is a simple mathematical model, based on previously published findings and development by past researchers (Wojtanowicz *et al*., 2001; Xu and Wojtanowicz, 2001; Xu, 2002; Huerta *et al*., 2009). The following nomenclature was used for deriving governing equations describing the SCP Model and SCVF Model.

Nomenclature (variable, description, units).

A = area of annulus, L^2, ft^2
c_m = mud compressibility, Lt^2/m, psi^{-1}
k = cement permeability to gas, L^2, md
L_c = length of cement column, L, ft
L_t = length of gas chamber, L, ft
L_f = length of mud column, L, ft
p_c = pressure at the top of cement, m/Lt^2, psia
p_f = gas-source formation pressure, m/Lt^2, psia
p_t = pressure on surface (wellhead), m/Lt^2, psia
q_c = flow rate at the top of the cement, SCF/D
T = reservoir condition temperature, K
T_{wb} = average wellbore temperature, K
T_{wh} = wellhead temperature, K
V_m = volume of mud column, L^3, ft^3
V_t = volume of gas chamber, L^3, ft^3
Z = gas-law deviation factor
μ_g = gas viscosity, m/Lt, cp
ρ_m = density of mud in wellbore, m/L^3, ppg
Δt = time step, t, day

Xu developed a mathematical model to describe the buildup of pressure p_t in the annulus, described by Eqn. 3.3.1. As seen in Fig. 3.3.1, the intermediate annulus was filled with a mud column L_f that was located above a top of a column of cement of length

L_c. The pressure buildup is not steady state, since the pressures increase and decrease over time. Xu used Eqn. 3.3.3 to compute gas flow at the top of cement, q_c from the gas source formation pressure, p_f and the pressure on the surface (wellhead), p_t. She assumed there was steady-state gas flow along the annulus between these two pressure boundaries. The new surface pressure p_t^n at time level *n* depends on the surface pressure at the end of the previous time step p_t^{n-1}. In a step-wise manner, casing pressure was computed as a function of time (Xu, 2001). The pressure at the top of cement p_c remained constant during each time step, thus resulting in the constant flow rate q_c for this step. The wellhead pressure, p_t in the annulus at *n*-th time step is described by Eqn. 3.1.1.

$$P_t{}^n = \frac{1}{2}\left(P_t{}^{n-1} - \frac{V_t^{n-1}}{c_m V_m^{n-1}} + \sqrt{\left(P_t^{n-1} - \frac{V_t^{n-1}}{c_m V_m^{n-1}} \right)^2 + \frac{4T_{wh}\sum_{k=1}^{n} p_c^k q_c^k \Delta t}{c_m V_m^{n-1} T_{wb}}} \right) \quad (3.3.1)$$

The wellhead pressure buildup, p_t is computed by assuming steady state flow for a series of short time steps over the duration of the buildup. Between steps, gas accumulates at surface, and pressure at the top of cement, p_c increases (Eqn. 3.3.2), reducing the driving force for leakage, q_c (Eqn. 3.3.3). Flow through the mud filled portion of the annulus is assumed instantaneous. Completion mud is assumed to be slightly compressible WBM and its properties are based on experiments by Kutasov, 1988. The annular space is bounded by boundary conditions consisting of inner and outer steel casing strings.

Xu assumed that the gas migration process was composed of numbers of short time steps. In each time step, the gas flow q_c is steady state in the cement. The pressure at the top of cement p_c remains constant during each time step, thus resulting in the constant flow rate q_c for this step. At the beginning of each time step, a new value of pressure at the top of cement is computed. The pressure at the top of cement, p_c is related to the casing pressure by using Eqn. 3.3.2.

$$p_c^n = p_t^{n-1} + 0.052\rho_m L_f^{n-1} \tag{3.3.2}$$

This equation is different than the equation in Fig.3.3.1. The equation used in this figure referred to the pressure balance equation that was developed for the Offshore wellbores dataset only. This dataset contained detailed drilling reports, which included the mud densities used for drilling different sections of the wellbore.

In Fig. 3.3.1, the left-hand side of the pressure balance equation is equivalent to the pressure at the top of cement, p_c, as seen in Eqn. 3.3.2. In Fig. 3.3.1, on the right-hand side of the equation, the pressure was equal to the water density, the density of the drilling mud used for the surface casing string, ρ_{mud1} and the density of the drilling mud used for the intermediate casing strings ρ_{mud2}. Drilling mud densities acted as proxies for pore pressure estimation at specific depth intervals.

When the pressure at the top of the cement (sum of casing and mud pressure) was equal to leakage formation pressures, gas flow ceased. In most scenarios, the leakage depth was unknown, but could be solved for if it was the only unknown variable in the equation.

The steady-state flow rate at the top of cement is calculated by Eqn. 3.3.3

$$q_c^n = \frac{0.00316kT_{sc}A}{p_{sc}TL_c\mu\, Z}\left[\, p_f^2 - \left(p_c^n\right)^2 \,\right] \tag{3.3.3}$$

where the constant 0.00316 is used as a unit conversion to convert the input units in Eqn. 3.3.3 to the appropriate output unit, flow rate, $\frac{SCF}{day}$.

The gas released at the cement top over one time step migrates through the mud and completely accumulates in the casing gas cap during the next time step. The gas migration time (controlled by gas rising velocity) is assumed to be shorter than the time step. For a low-viscosity and short mud column, it takes a very short time for gas to reach the top (Xu, 2001).

Formation pressure, and therefore the pressure at the leakage source p_f, is assumed constant due to the high formation permeability to gas compared with that of cement. The mud is assumed a slightly compressible fluid. The temperatures at the top of cement and the top of mud are different and known (Xu, 2001).

The SCP Model applies Darcy's Law flow for single phase methane gas through a conduit/crack in the cement, traveling from depth, upwards to the surface. The gas accumulates in the gas chamber at the top of the liquid filled annular space, and increases in size when the valve is closed. As demonstrated in Eqn. 3.3.3, the gas flow rate is related to the properties of the conduit/crack (effective permeability, length of cement), the gas formation pressure, the pressure at the top of cement, the viscosity of the gas/liquid, the temperature at the leakage source, and the boundary area between casing strings. The gas driving force is a result of the pressure difference between the pressure at the top of cement, and the pressure at the formation leakage depth source.

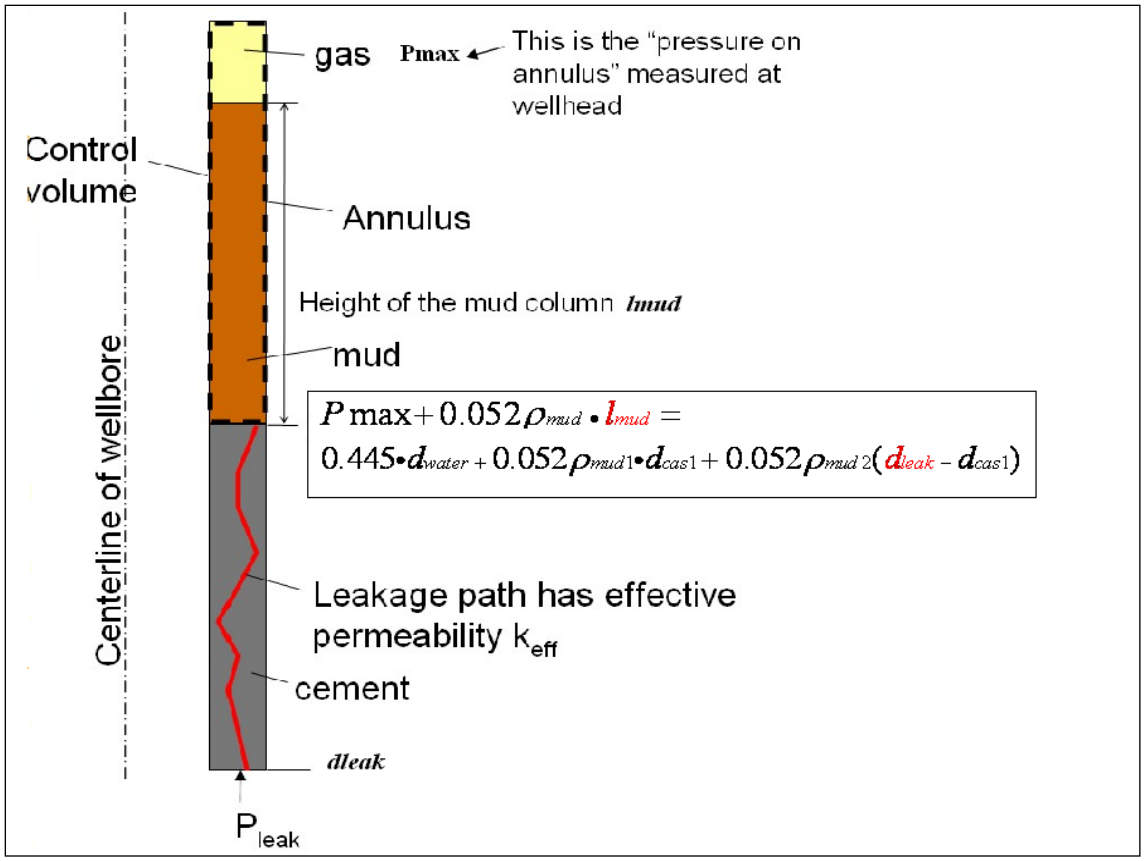

Fig. 3.3.1. The schematic of an annular leakage system with parameter values defined. The pressure balance equation for the Offshore dataset is described in the box and used to solve for unknown parameter values highlighted in red.

3.3.1 Using the SCP Model

The leakage driving force was highly pressurized methane located at the formation/cement interface. Poor cement bonding created a crack in the cement filled annulus space. The difference between capillary entry pressure of the crack and the buoyancy force between methane and brine dictated whether the gas would enter the pathway. The leakage pathway permeability values were generated for each individual wellbore and pressure buildup by using the SCP Model. Complete results are presented in Chapter 4.

The SCP Model outputs were a result of matching the field pressure buildup data over time. The fit of the model to the field pressure data was greatly affected by changing leakage pathway permeability values. For example, the pressure buildup data in Fig.3.3.2 demonstrated actual increasing asymptotic pressure buildup data (red dots) that were compared to the SCP Model generated results (blue curve).

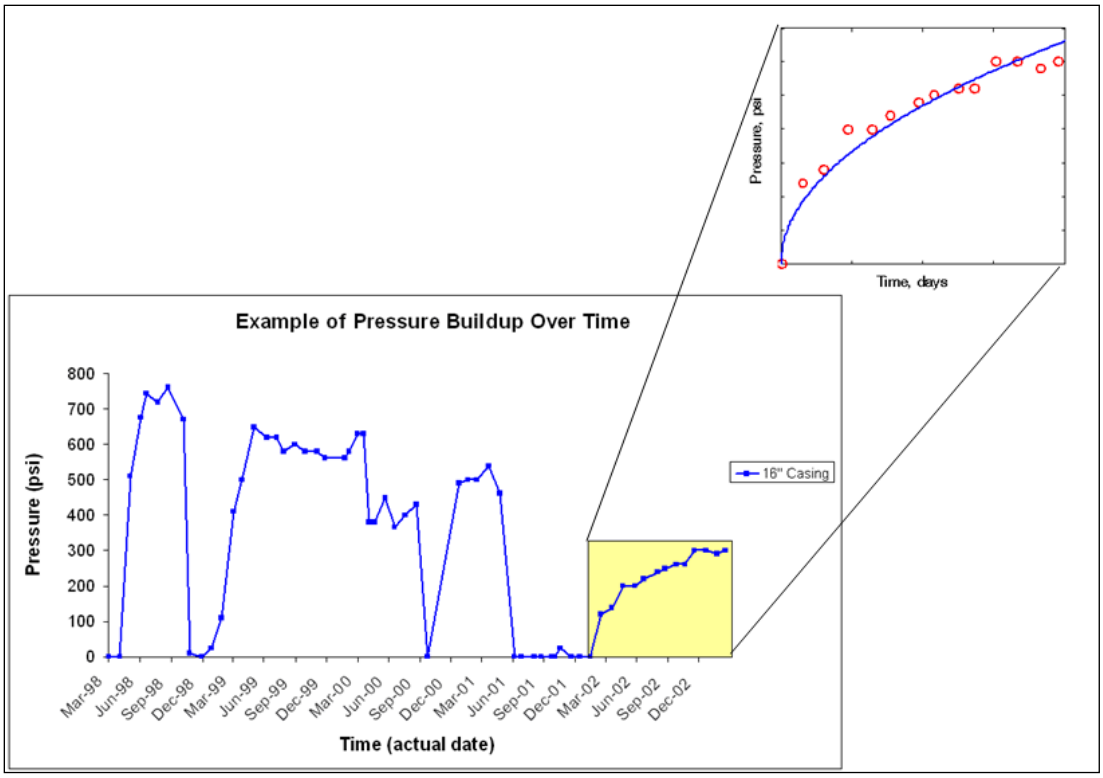

Figure 3.3.2 – Example of model matching actual field pressure buildup data.

In this example, the leakage path permeability was adjusted until the SCP Model buildup curve (blue) was a close fit to the observed pressure buildup data (red dots). The SCP Model was run within an outer loop that optimized the fit, minimizing the sum of the squared errors between the actual field data and model generated results. .

For each leaky wellbore and pressure buildup interval, a unique leakage scenario was re-created. Each wellbore parameter that described a wellbore characteristic was assigned a value (if known) or a range of values (if unknown). For different wellbores, the entire pressure buildup dataset contained multiple buildups and bleed downs over time. Much of the use of the SCP Model was based on changing parameter values within a known range, thus changing the leakage path frequency distribution.

3.4 SUSTAINED CASING VENT FLOW (SCVF) MODEL

When the surface casing wellbore valve is opened, gas is allowed to exit the intermediate annulus. During testing, the gas flow rate and the pressure at the surface is recorded by a monitoring device. The surface wellhead pressure depends on the outflow of gas from the system. The purpose of the Sustained Casing Vent Flow (SCVF) Model is to model the migration of gas through the annulus space mathematically. The SCVF Model used in this research is a simple mathematical model, based on slight changes to the Sustained Casing Pressure (SCP) Model. The following nomenclature is used for deriving governing equations used to describe the SCVF Model.

Nomenclature (variable, description, units).

A = area of annulus, L^2, ft^2
c_m = mud compressibility, L t^2/m, psi^{-1}
k = cement permeability to gas, L^2, md
L_c = length of cement column, L, ft
p_f = gas-source formation pressure, m/L t^2, psia
p_t = pressure on surface (wellhead), m/L t^2, psia
p_{sc} = pressure at standard conditions, m/L t^2, psia
q_t = flow rate at the top of the cement, SCF/D
T = reservoir condition temperature, K
T_{sc} = temperature at standard conditions, K
μ_i = gas viscosity, m/Lt, cp

The following equation describes SCVF at the surface.

$$q_t^n = \frac{0.00316kT_{sc}A}{p_{sc}TL_c\mu\, Z}\left[\, p_f^2 - \left(p_t^n\right)^2 \,\right] \tag{3.4.1}$$

The SCVF Model assumes that the gas passes instantaneously through the column of completion mud, and flows through the open surface wellhead valve. Therefore, the flow rate at the top of cement, q_t can be considered the same as the flow rate at the surface at time step *n*. At the surface, the operators are required to conduct surface casing vent flow tests in order to determine if gas, liquid, or any combination of substances is escaping from the casing vent assembly (ERCB Directive 020, 2010). For the SCVF Model, this surface flow rate is equivalent to the flow rate at the top of cement, q_t .

For properly sealed wellbores, there should be zero surface casing vent flow when the wellbore intermediate annulus surface valve is open. However, for improperly cemented intermediate annulus spaces, there are leaky wellbore issues. When the leaky

wellbores surface valve is opened, gas flows out of the system, exiting at a measurable rate through a surface orifice. For sustained casing vent flow (SCVF), the stabilized flow rate at the top of cement at time *n*, q_t^n and stabilized surface pressure at the surface at time *n*, p_t^n are described by Eqn. 3.4.1.

The inputs to the SCVF Model include known wellbore characteristics (casing sizes, casing depths, cement slurry volume information, etc), flow rates, and pressure levels. The outputs to the SCVF Model include a range of leakage path permeability for gas traveling through a crack defect in the cement filled annulus space.

There was limited cement logging information to help identify the proper location of the leakage depth. To generate a range of permeability values, the leakage depth was located at either the upper or lower casing string depth. The recorded gas flow rates were only available for a few wellbores in the Bourgoyne dataset and the Watson dataset. However, the flow rates were provided for 210 wellbores in the British Columbia Oil and Gas Commission.

To record surface casing vent flow, the surface wellhead that was connected the intermediate annulus space was opened with a valve to allow measurements of a steady gas flow rates/pressure buildup level in the wellhead annular space. For SCVF, the gas flow from the surface annular valve was due from communication with a high pressure formation leakage source. The gas entry point along the annulus was unknown, but was constrained between the upper and lower intermediate casing seats. For the British Columbia Oil and Gas Commission dataset, the measured flow rates ranged from 0.1 m^3/day to 1500 m^3/day.

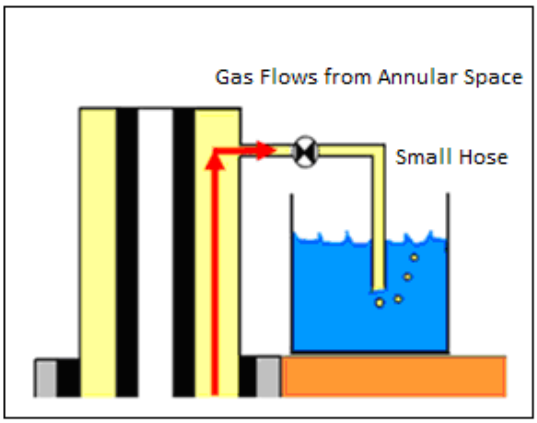

Fig. 3.4.1 – Testing apparatus for SCVF. A measurable flow at the surface casing annular space in the wellhead. 10 minute gas bubble test.

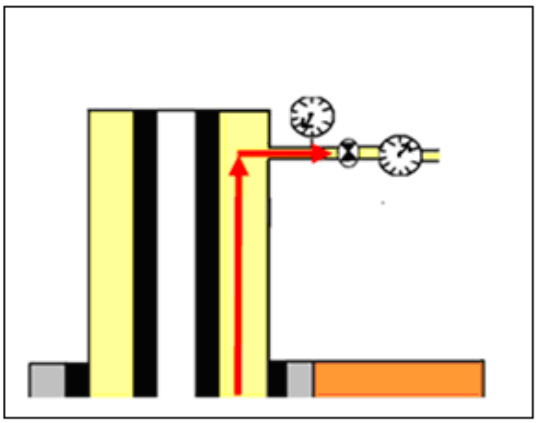

Fig. 3.4.2 – SCVF testing apparatus monitors and records shut-in casing pressure and vent flow rates.

The SCVF Model used a script that imported individual wellbore characteristics, pressure recordings, and vent flow data from a spreadsheet containing the following information: buildup pressure, gas flow rate, upper casing shoe depth, lower casing shoe depth, casing diameter sizes, casing depths, top of cement depth, and leakage depth. For minimum permeability values, the gas leakage depth into the annular space was set at the upper casing shoe depth. For maximum permeability values, the gas leakage depth was set at the lower casing shoe depth.

Using Eqn. (3.4.2), the length of cement, L_c was calculated by dividing the cement slurry volume, V_{cem}, by the area between the casing strings.

$$L_c = \frac{V_{cem}}{\frac{\pi}{4}\left(D_{outer}{}^2 - D_{inner}{}^2\right)} \tag{3.4.2}$$

where

L_c = Length of cement

V_{cem} = Cement slurry volume

D_{outer} = Casing outer diameter size

D_{inner} = Casing inner diameter size

3.4.1 Using the SCVF Model

The SCVF Model describes a leakage system with different boundary conditions than the SCP Model. There is an open upper boundary condition at the surface, as gas escapes from the annular system. There is an open lower boundary condition at the leakage source depth, as gas enters the annular system. There are closed boundary conditions on either side of the cement leakage path from the intermediate casing strings. The SCVF Model is only used for wellbores with recorded vent flow rate information. The leakage path permeability values are strongly correlated with gas flow; since the model describes gas flow through an intermediate annulus space. The complete results of the SCVF Model will be discussed in detail in Chapter 4.

Chapter 4: Selection of Leaky Wellbore Datasets, Casing Strings, and Pressure Buildups

CHAPTER 4 OVERVIEW

One of the goals of the research was to extend the results from a small sample size of leaky wells taken from one location to an overall analysis of leaky wells taken from many different locations. The findings from analyzing several different datasets bolstered the conclusions of the analysis. The results from the six datasets gathered for this research provided the ability to make robust arguments from existing data analysis. This also eliminated any communication/interference between the datasets, creating independent datasets that provided unique results.

4.0.1 Selection of Casing Strings & Intermediate Annulus Space

The raw data was formatted as a case study that was edited and used for analysis with the models described in Chapter 3. The selection- editing criteria were applied to the data to choose appropriate casing strings to use for pressure buildup analysis. It was determined that the intermediate casing strings should be used for modeling the leakage gas flow from the formation into the annulus, rather than using other casing strings.

,The inner-most production annulus (between production tubing and casing string) could have been affected by the flow of gas from production tubing leaks, rather than from a formation pressure source.

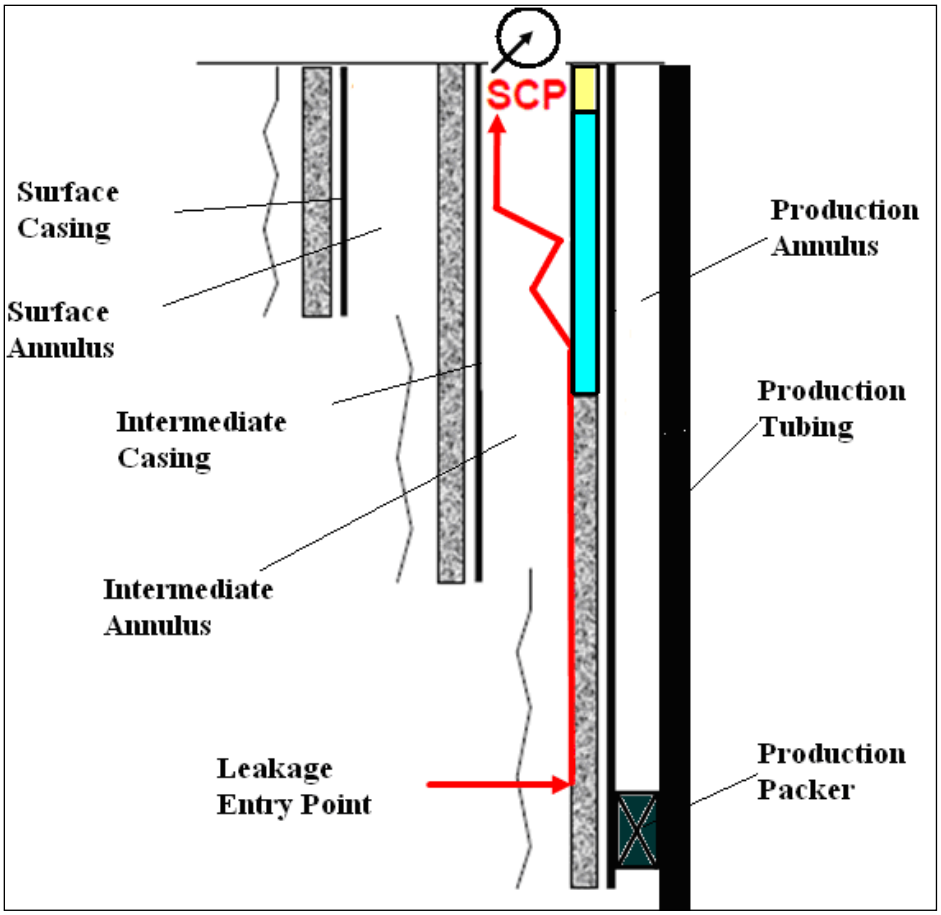

Figure 4.0.1 – Schematic of gas flow in the intermediate annulus, not the production annulus. SCP measured at the surface of the intermediate annulus.

The intermediate annulus space was selected because the leakage path to this annulus is believed to be most analogous to the likely leakage path for CO_2 storage reservoirs, i.e. between steel casing, cement and earth formations. To increase confidence that this was the leakage path, only buildups that showed limited communication with the other casing strings and producing gas zones were considered. The lack of communication was demonstrated when pressure in the other annuli remained constant or negligible, as pressure in the intermediate annulus built up or bled down.

For example, in wellbore 1, there is recorded pressure buildup in the intermediate annulus space (Fig. 4.1.2) bordered by the lower intermediate casing (10.75’’), and the upper intermediate casing (16’’). For the production casing (7.625’’) (blue) and lower intermediate casing (10.75’’) (magenta) casing string, the pressures remained constant from May 24, 2002 thru June 28, 2003. However, for the upper intermediate (red) casing string, the pressure built up from 300 psi to 420 psi. The pressure buildup on the upper intermediate annulus (16’’) was selected to evaluate migration along a defect at the cement barrier independent of possible influence from the production tubing connections. As seen in Figure 4.1.1, the gas migration path of an intermediate annulus ranged in depths between the upper 16’’ intermediate casing seat (X000 ft) and the 7.625’’ lower intermediate casing seat (X202 ft).

4.0.2 Selection of Pressure Buildup Data Intervals

The pressure buildup data intervals were classified by buildup rate and maximum pressure value. Buildup rates were calculated by dividing the change in pressure by the change in time. For example, in Figure 4.0.2, the wellbore demonstrated two pressure buildup intervals (highlighted in yellow). Buildup #1 lasted for a duration of 230 days. The starting pressure level was 550 psi and the ending pressure level was 1000 psi, before bleed down occurred. Buildup rate #1 was calculated as 1.96 psi/day. Buildup #2 lasted for duration of 285 days. The starting pressure level was 200psi and the ending pressure level was 500 psi. Buildup rate #2 was calculated as 1.05 psi/day.

There was no discernible relationship between increasing buildup rates vs. time. After bleed down occurred, the pressures increased at various pressure rates. There was no relationship between the number of pressure buildups for each wellbore and other

wellbore parameters. Wellbores demonstrated one to several different pressure buildups that were recorded after bleed off on the same intermediate casing string. Each pressure buildup interval was evaluated independently and wellbore construction information provided boundary conditions for leakage depths. The highlighted pressure buildups (Fig. 4.0.2) were used as raw pressure data inputs to the SCP Model. Other wellbore construction inputs were entered separately to the model. These inputs changed the pressure buildup curve fitting to the raw data. The model changed permeability in order to generate a "best-fit".

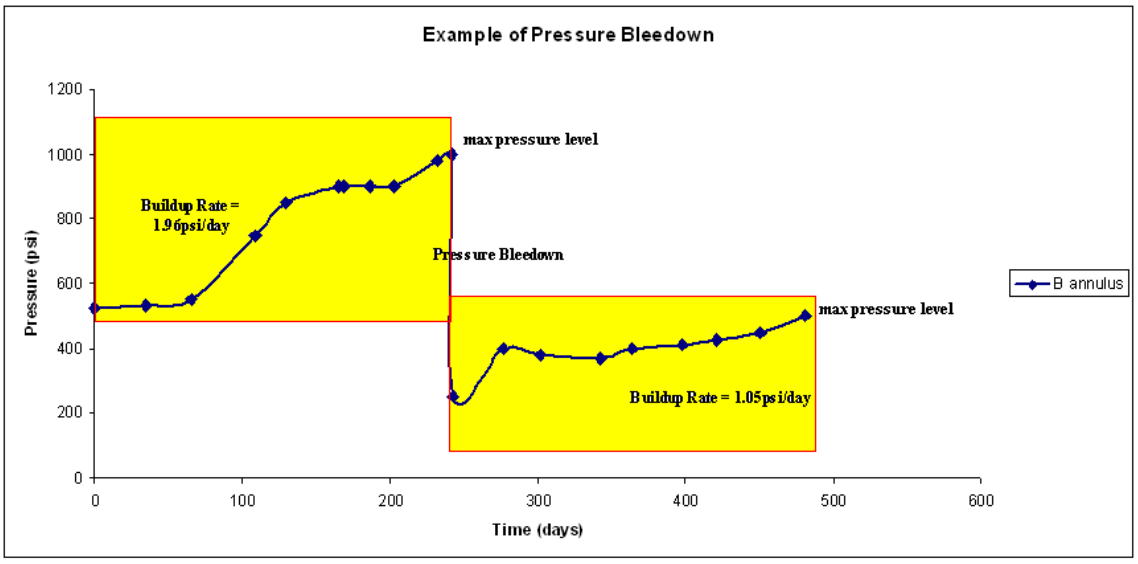

Figure 4.0.2 – Maximum Pressure Method applied to raw data set. Intermediate casing string, B annulus, that demonstrated an initial 1.96 psi/day pressure buildups, followed by a pressure bleed down, and then a secondary pressure buildup of 1.05 psi/day buildup.

For this example wellbore, two different pressure buildup intervals were used. This provided two separate ranges of leakage path permeability values. Each pressure buildup interval was used to generate a unique range of leakage path permeability values,

using three different methods, as described in Chapter 6 (Section 6.1 - Cement Slurry Method, Sec 6.1 - Maximum Pressure Method, Sec 6.2 - Monte Carlo Method). In order to be selected, the pressure buildup interval had to be increasing over time and had to include several pressure data points (two or more).

4.1 OFFSHORE WELLBORE DATASET

The Offshore wellbore dataset contained 17 individual raw wellbore construction information and raw pressure buildup datasets. It was the most comprehensive, detailed dataset of all those obtained for analysis purposes. This data was compiled and evaluated in order to be used as leakage scenario inputs to the SCP Model. Of these 17 wellbores, 12 wellbores passed the selection criteria for useful pressure data and sufficient wellbore casing/ cementing information. These 12 wellbores contained at least one, and in some cases, several pressure buildups on the intermediate annulus. For each pressure buildup, a leakage path permeability was calculated using the following methods:

1) Cement Slurry Method

2) Maximum Pressure Method

3) Monte Carlo Method

A schematic of the wellbore construction information provides a visual display of the gas leakage path scenario for each wellbore. The raw pressure buildup information displays the pressure vs. time data for the casing strings analyzed. The following are descriptions of leaky wellbores that demonstrated pressure buildups over time.

Wellbore 1

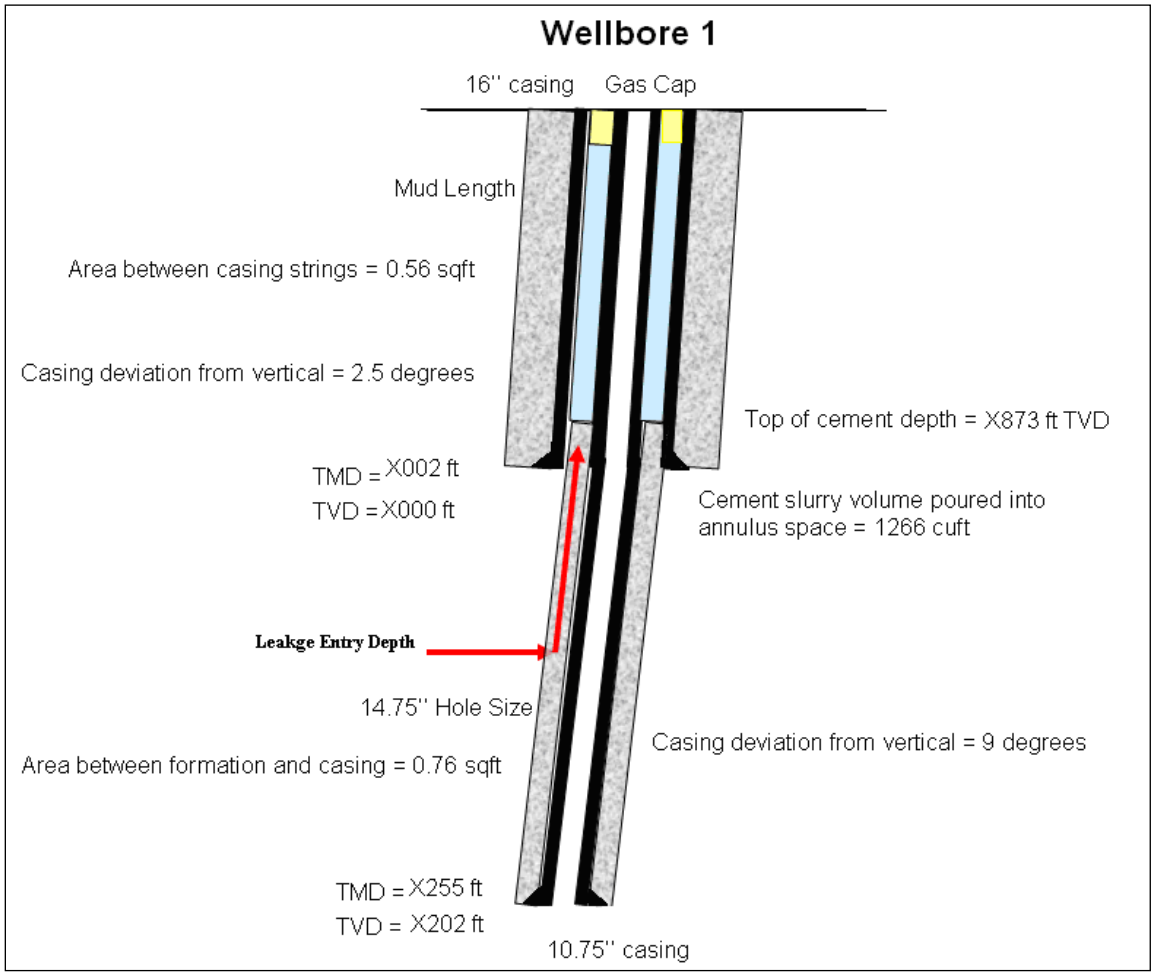

Figure 4.1.1 – Wellbore construction information for wellbore 1. The 16'' casing string is deviated from vertical by 2.5 degrees and the 10.75'' casing string is deviated from vertical by 9 degrees.

For this wellbore example, the top of cement reached a depth of X873 ft TVD. The amount of cement slurry that was pumped into the annulus space was compared to the volume of the hole-casing annulus. The TVD of the top of cement, D_{TVD} was calculated by using the deviated hole angle from vertical and the length of the TMD of the casing string, D_{TMD}. The cosine relationship, Eqn. 4.1.1 was used to solve for the D_{TVD} (vertical) of the top of cement (X873 ft).

$$\cos\theta = \frac{D_{TVD}}{D_{TMD}} \qquad (4.1.1)$$

Once the TVD of the top of cement, D_{TVD} was calculated, then the length of mud was determined by subtracting D_{TVD} from the surface depth of 0 ft. Since the annulus space is only composed of mud and cement, the gas cap length was not accounted for. The maximum and minimum permeability values were calculated by changing the leakage depths from the D_{TVD} (vertical) of the upper 16'' casing seat (X000 ft) to the D_{TVD} (vertical) of the lower 10.75'' casing seat (X202 ft).

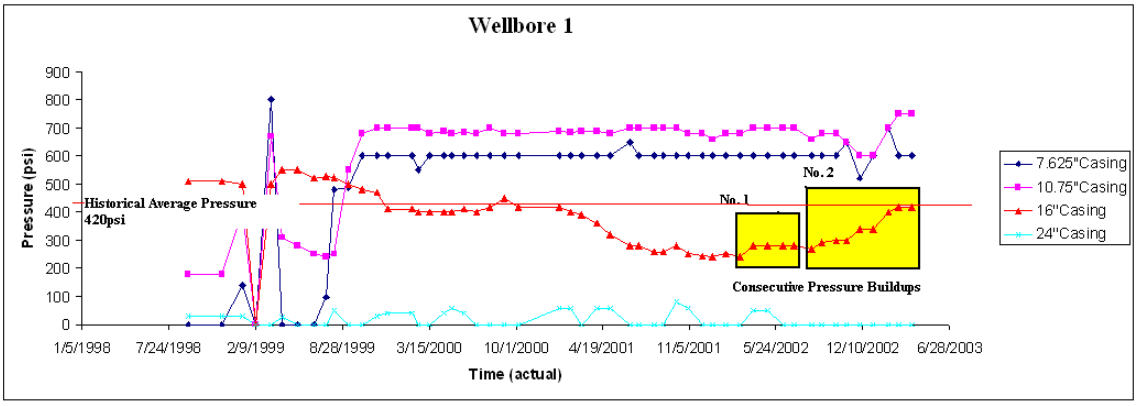

Figure 4.1.2 – Raw pressure buildup #1 (0.60 psi/day) and buildup #2 (0.64 psi/day) for wellbore 1.

Buildup No.1 and buildup No.2 were consecutive pressure buildups over time. However, buildup No.1 did not reach the historic average pressure level of 420 psi. Using the actual pressure data in the model provided inconsistent permeability results between these two buildups. Therefore, the final pressure value of buildup #1 (300 psi) was replaced with a final pressure value of 420 psi. The maximum pressure level of 420 psi would occur for buildup #1 if the wellbore was left undisturbed. Using the pressure buildup rate (0.64 psi/day), of buildup #2, it would take (420-290 psi) / 0.64 psi/day = 203 days to reach the final pressure of 420 psi.

Wellbore 2

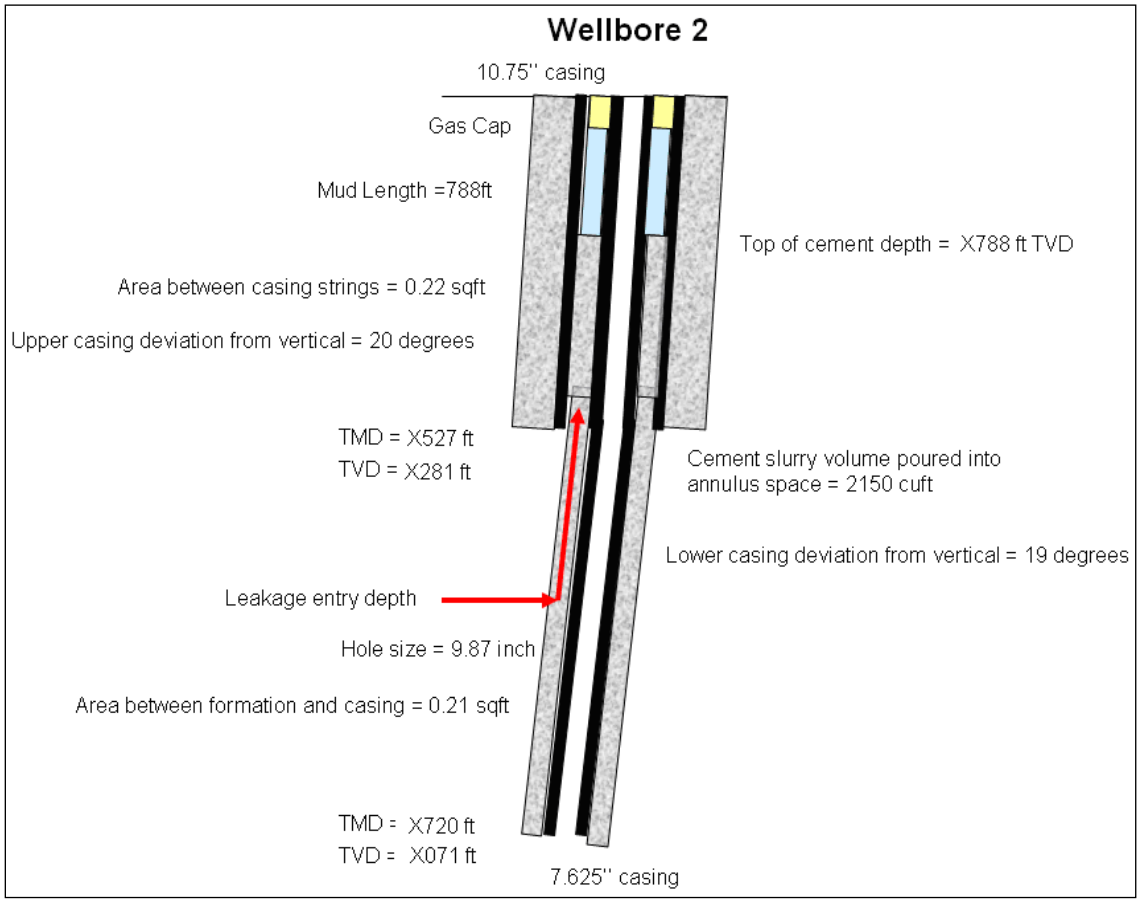

Figure 4.1.3 – Wellbore construction information for wellbore 2 – Upper casing string is deviated from vertical by 20 degrees. The lower casing string is deviated from vertical by 19 degrees. This results in a difference in depth of the 7.625'' lower casing string TMD (X720 ft), TVD (X071 ft).

In the original raw pressure buildup dataset of wellbore 2, there were three unique pressure buildup intervals that occurred at different points over time (Fig. 4.1.4). Thus, a historical asymptotic pressure level was not used, as was demonstrated with wellbore 1. For wellbore 2, each unique pressure buildup data interval was not altered, and the pressures reached different maximum levels. In order to generate maximum and minimum permeability values, different leakage scenarios were created by applying the

Maximum Pressure Method and the Cement Slurry Method to the data. Each data interval produced a unique set of maximum and minimum permeability.

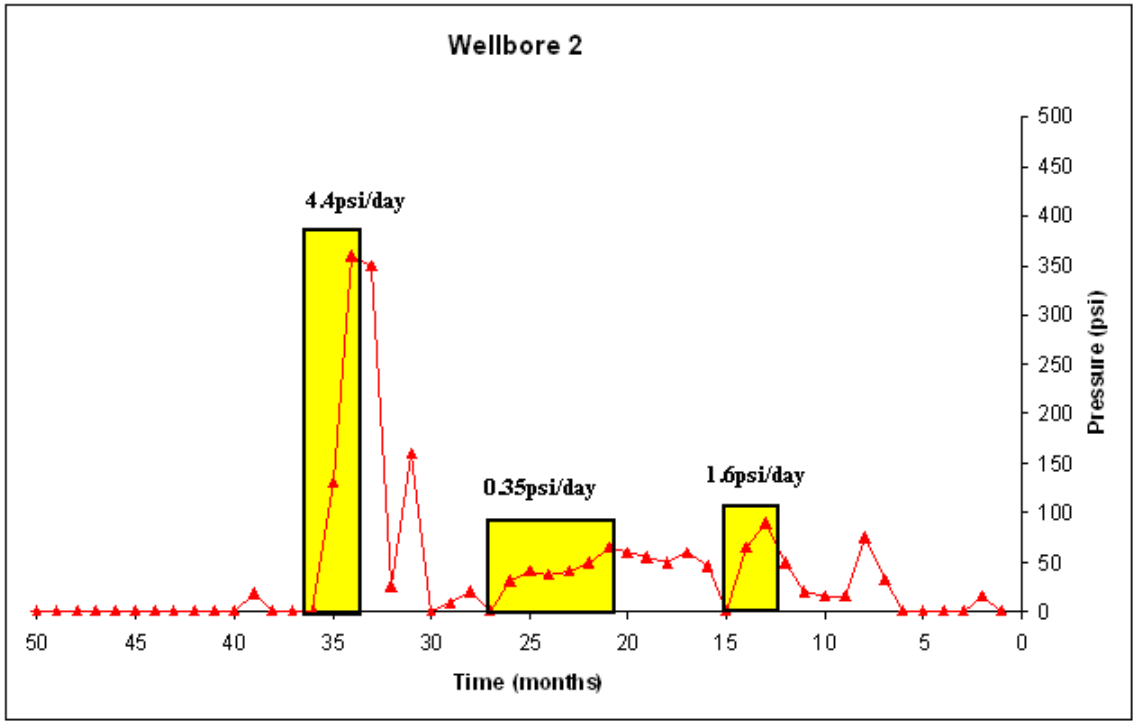

Figure 4.1.4 – Wellbore 2, raw pressure buildup intervals and rates (4.4 psi/day, 0.35 psi/day, 1.6 psi/day).

Wellbore 3

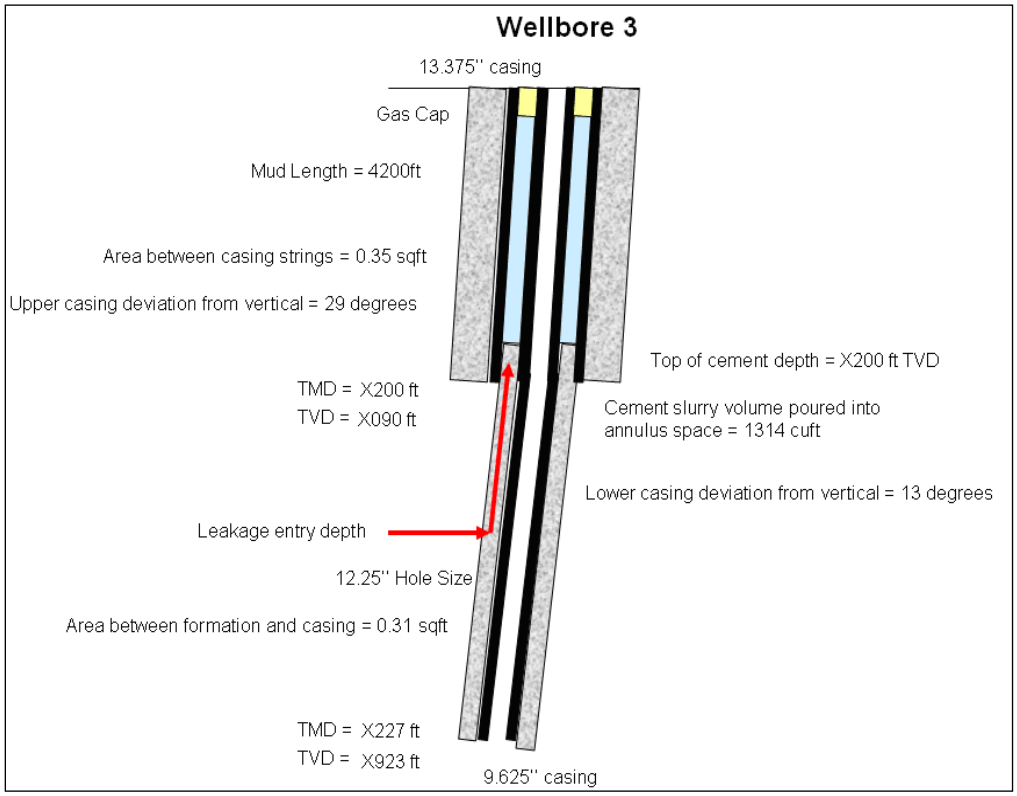

Figure 4.1.5 – Wellbore construction information for wellbore 3. The upper casing string is 29 degrees angle of deviation from vertical. The lower casing string is 13 degrees angle of deviation from vertical. This wellbore is highly deviated and there is significant difference between the TVD (X227 ft) and TMD (X923 ft) depths of the 9.625'' casing string.

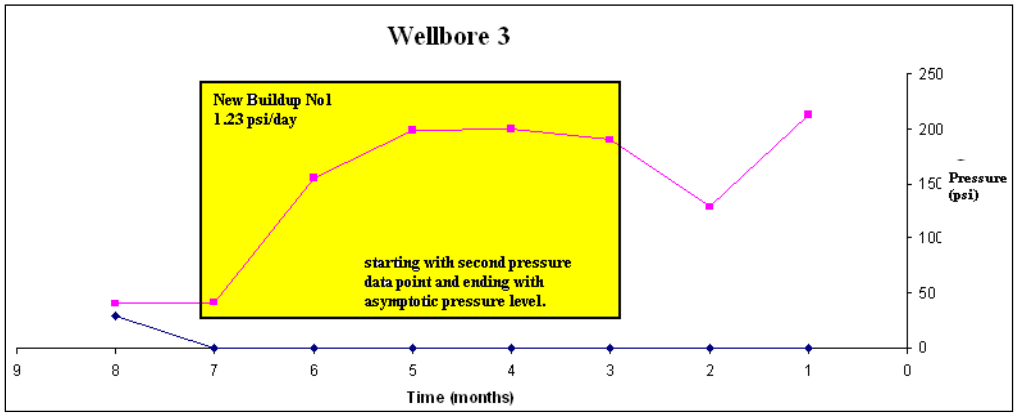

Figure 4.1.6 – Wellbore 3 - Raw pressure buildup data interval (1.23 psi/day).

Wellbore 4

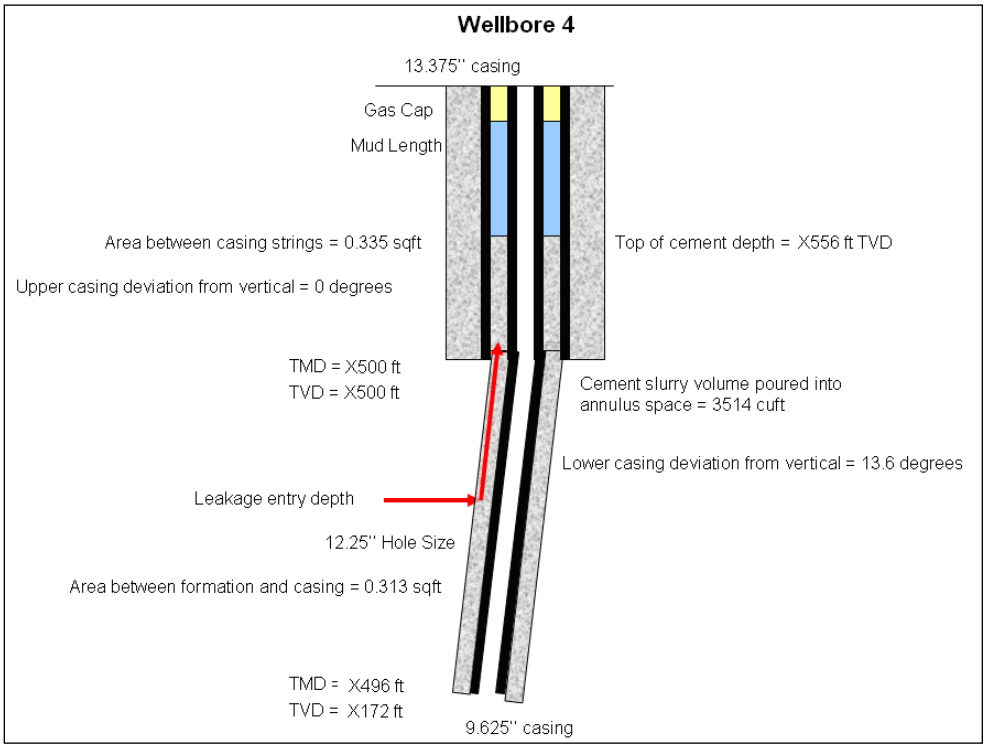

Figure 4.1.7 – Wellbore construction information for wellbore 4. The 13.375'' upper casing string was set straight vertical to a depth of X500 ft. The 9.625'' lower casing string was deviated 13.6 degrees from vertical to a TVD of X172 ft, TMD of X496 ft.

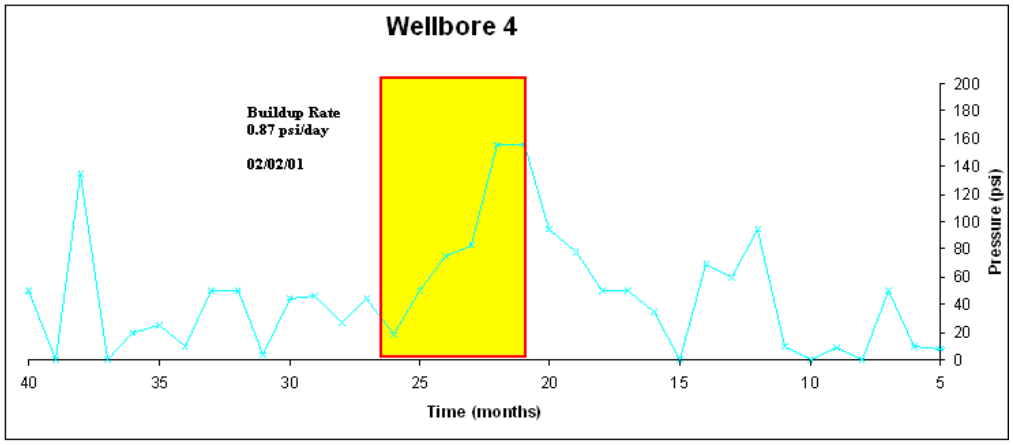

Figure 4.1.8 – Wellbore 4 - Raw pressure buildup data interval (buildup rate of 0.87 psi/day)

Wellbore 5

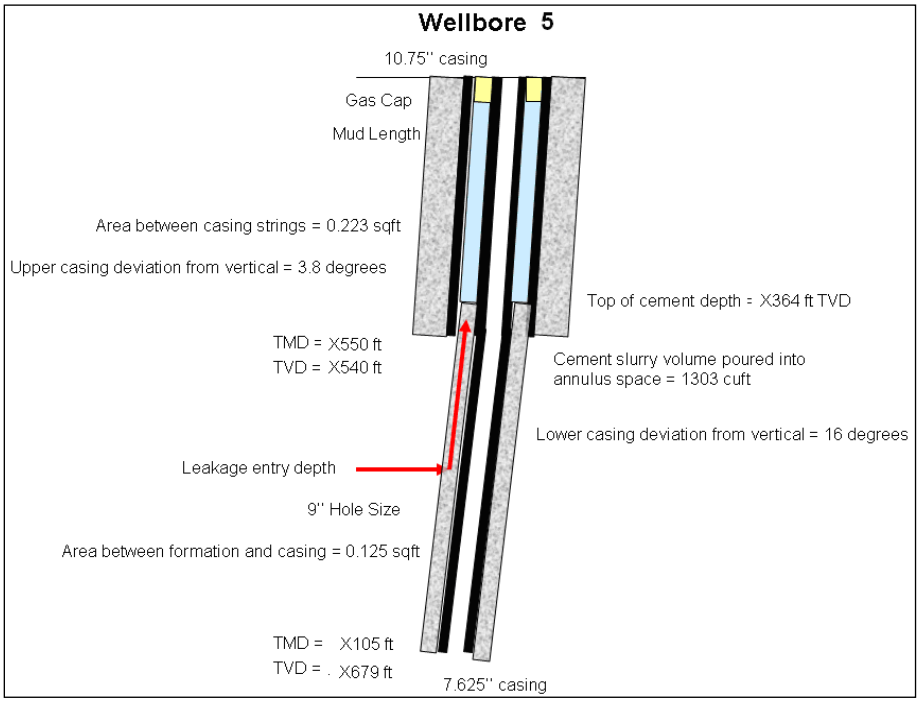

Figure 4.1.9 – Wellbore construction information for wellbore 5. The 10.75'' upper casing string deviates 3.8 degrees from vertical to a TVD of X540 ft, and TMD of X550 ft. The 7.625'' lower casing string deviates 16 degrees from vertical to a TVD of X679 ft, and TMD of X105 ft.

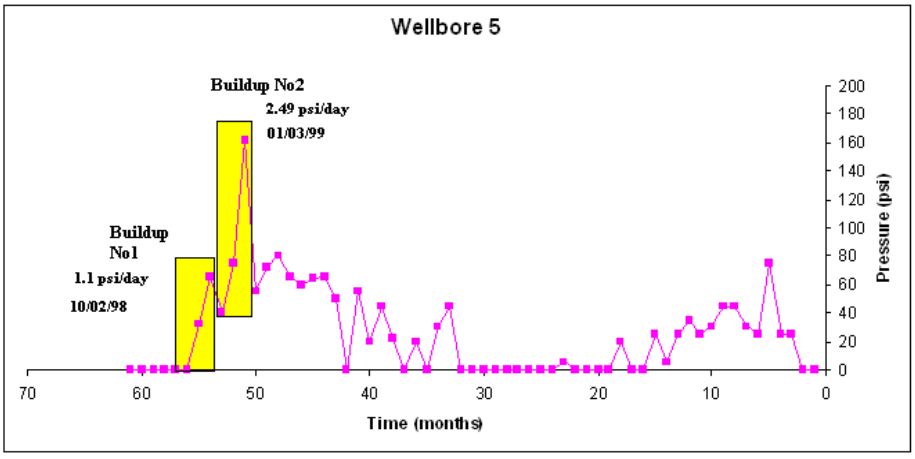

Figure 4.1.10 – Wellbore 5 - Raw pressure buildup data set with 2 pressure buildups (1.10 psi/day, 2.49 psi/day).

Wellbore 6

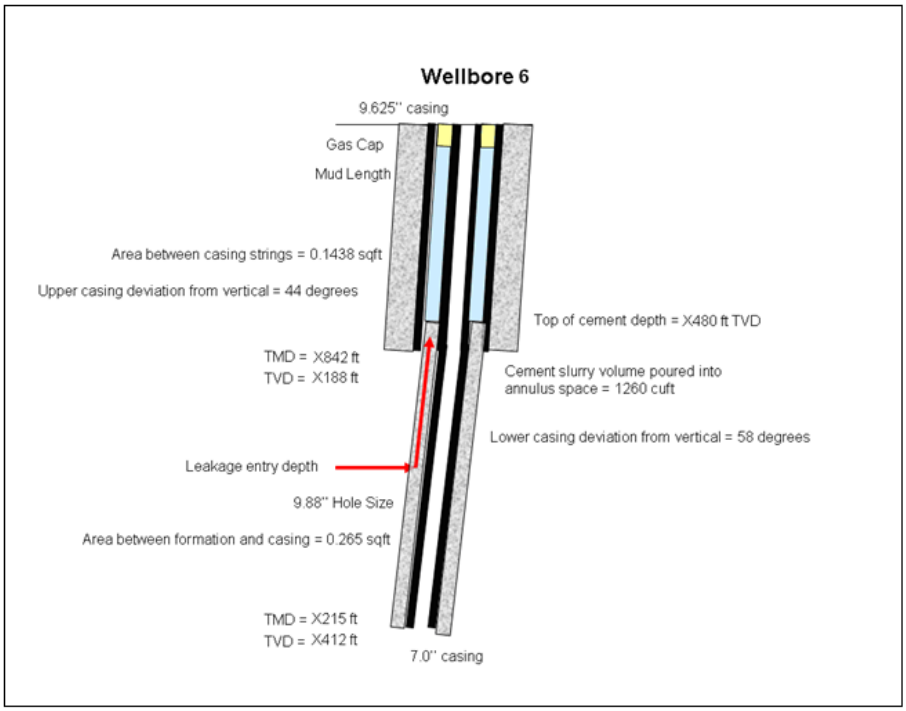

Figure 4.1.11 – Wellbore construction schematic for wellbore 6 – The 9.625'' upper casing string deviated from vertical by 44 degrees to a TMD of X842 ft, TVD of X188 ft. The 7.0'' lower casing string deviated from vertical by 58 degrees to a TMD of X215 ft, TVD of X412 ft.

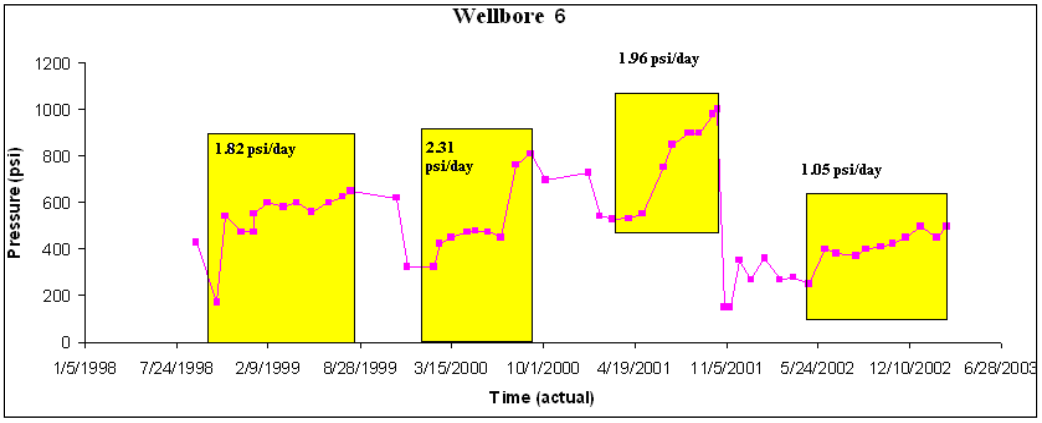

Figure 4.1.12 – Wellbore 6 - Raw pressure buildup data with 4 pressure buildups.

Wellbore 6 provided four different pressure buildups with similar pressure buildup rates. Buildup #1 (1.82 psi/day) began on October 22, 1998. Buildup #2 (2.31 psi/day) began on February 06, 2000. Buildup #3 (1.96 psi/day) began on March 1, 2001. Buildup #4 (1.05 psi/day) began on May 4, 2002.

Due to short distance between the top of cement (X480 ft) and the depth of the upper casing string (X188 ft), there were modeling problems. Therefore, an additional X00 ft of cement was added to the top of cement.

Wellbore 7

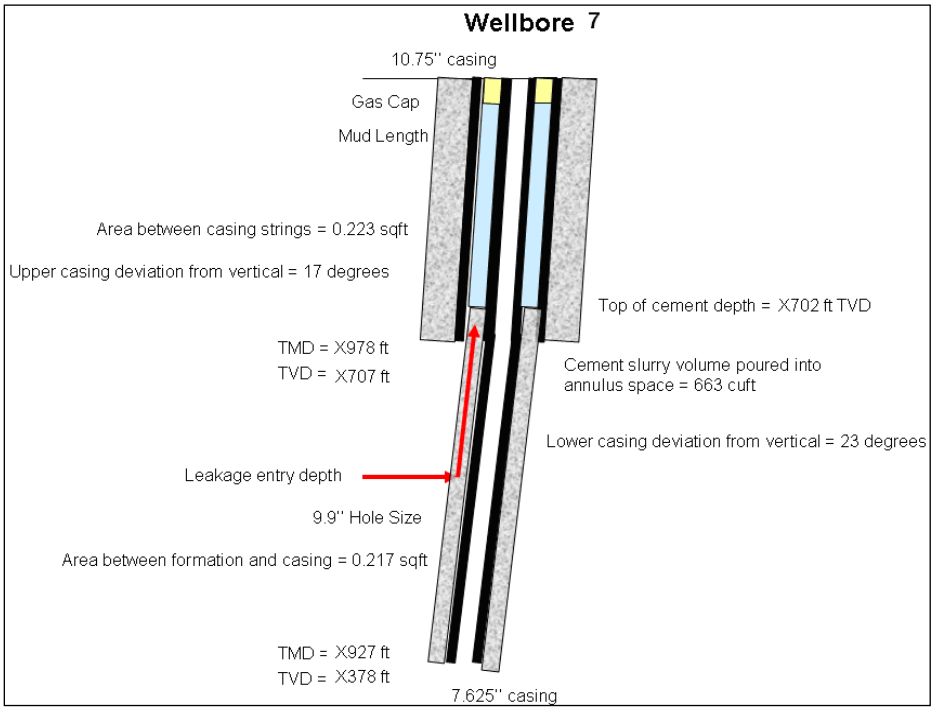

Figure 4.1.13 – Wellbore construction information for wellbore 7 – The 10.75'' upper casing string is deviated 17 degrees from vertical to a TMD of X978 ft, TVD of X707 ft. The 7.625'' bottom casing string is deviated 23 degrees from vertical to a TMD of X927 ft, TVD of X378 ft.

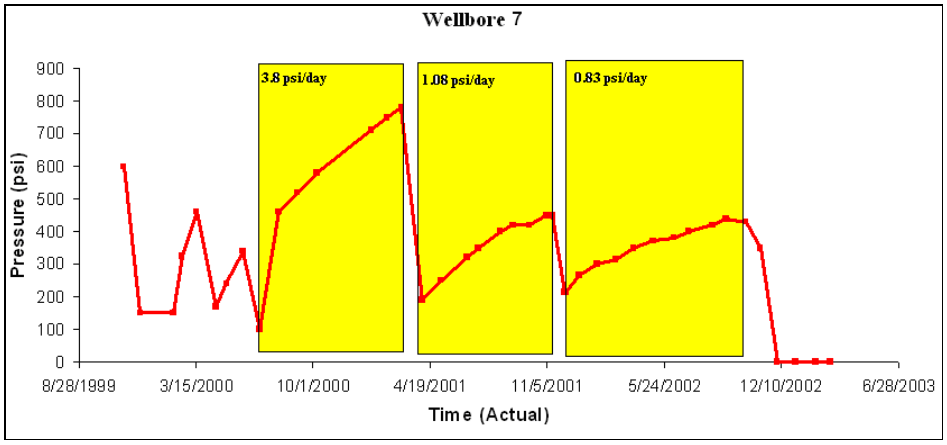

Figure 4.1.14 – Wellbore 7 - Raw pressure buildups. Three consecutive pressure buildup intervals.

Wellbore 8

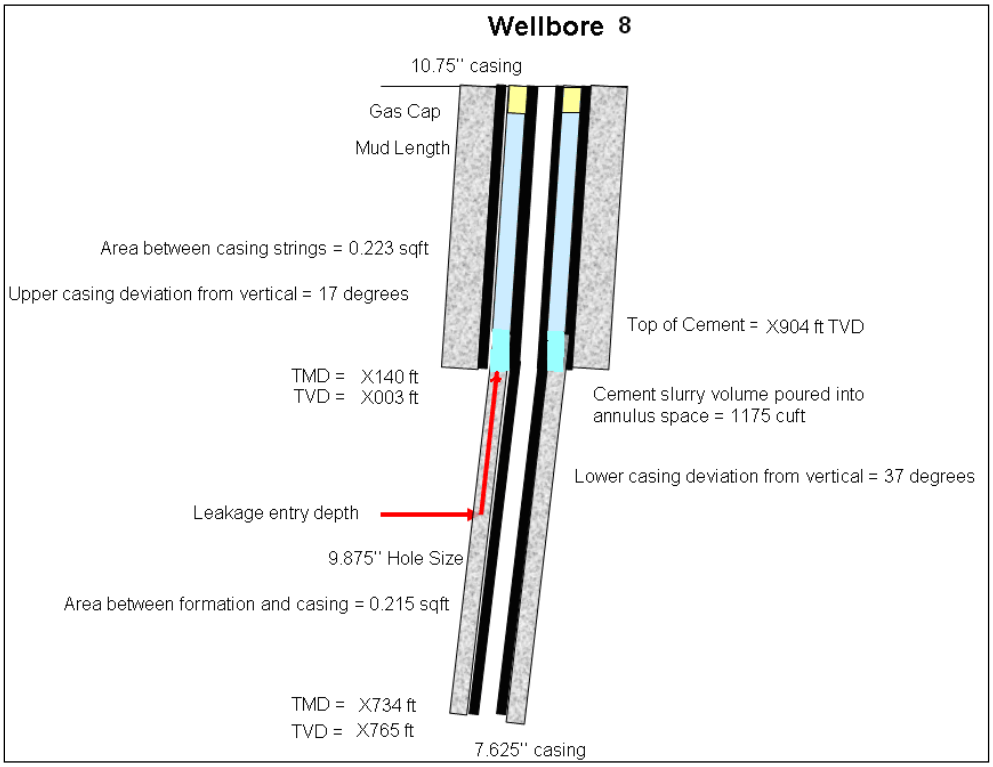

Figure 4.1.15 -Wellbore construction information for wellbore 8. Upper 10.75'' casing string is deviated by 17 degrees from vertical to TVD of X003 ft. Lower 7.625'' casing string is deviated by 37 degrees from vertical to TVD of X765 ft.

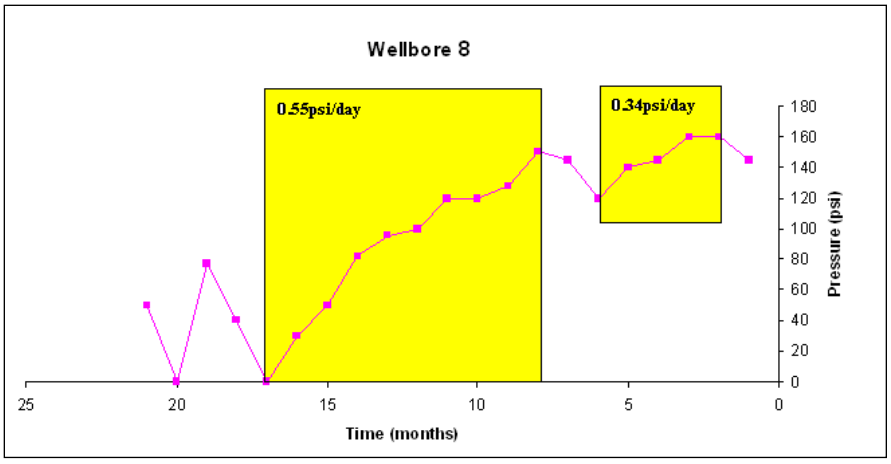

Figure 4.1.16 – Wellbore 8 - Raw pressure buildups (0.55 psi/day, 0.34 psi/day)

Wellbore 9

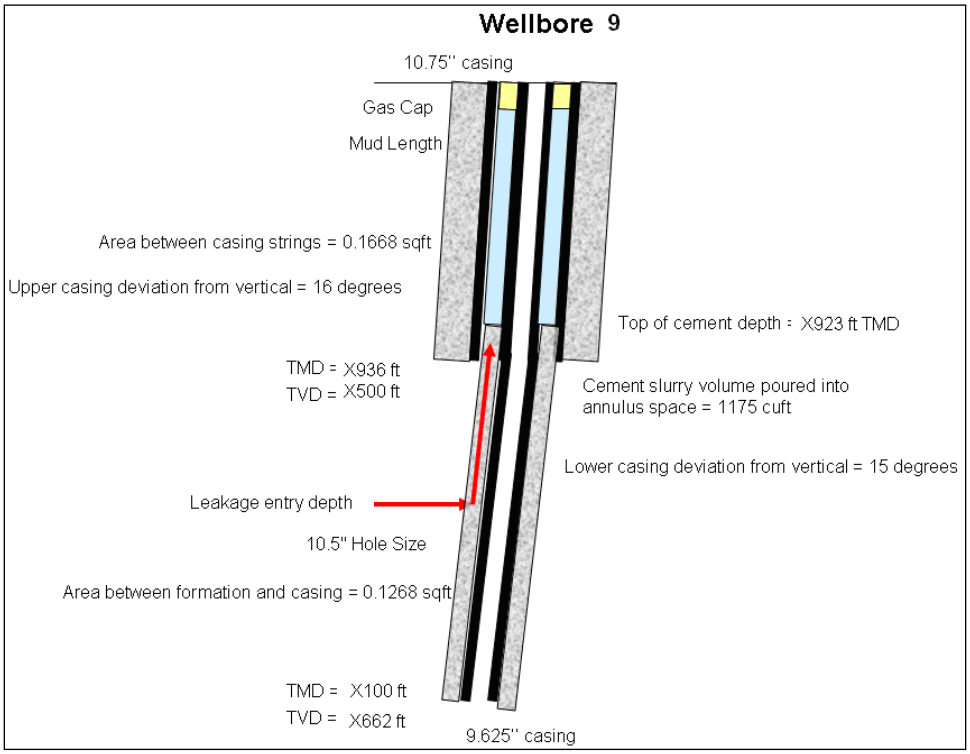

Figure 4.1.17 -Wellbore construction information for wellbore 9. Upper 10.75'' casing string is deviated by 16 degrees from vertical to TVD of X500 ft. Lower 9.625'' casing string is deviated by 37 degrees from vertical to TVD of X662 ft.

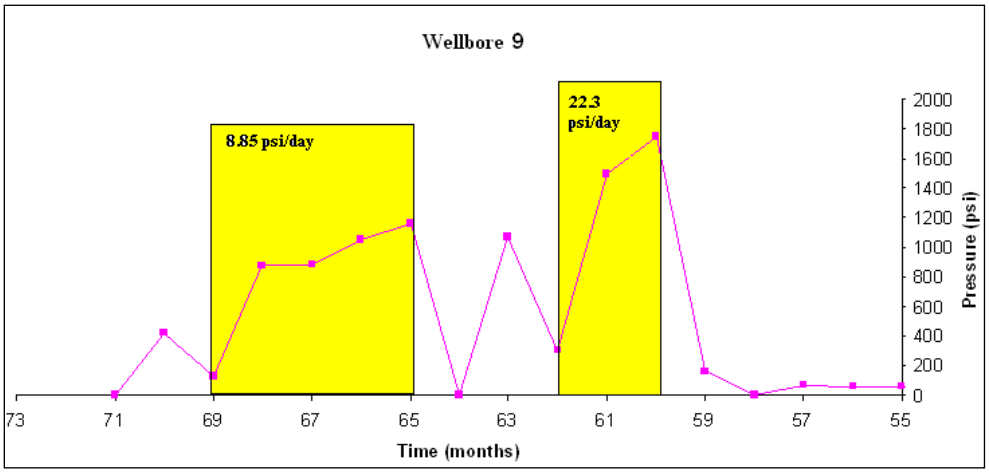

Figure 4.1.18 – Wellbore 9 - Raw pressure buildups (8.85 psi/day, 22.3 psi/day.

This concludes the section about the wellbore construction and pressure buildup details of the Offshore wellbore dataset. Information about wellbores 10, 11, 12 are not included in this section.

4.2 BOURGOYNE WELLBORE DATASET

The Bourgoyne wellbore dataset was obtained by extracting leaky wellbore information from a previously published research paper. Bourgoyne submitted a report to the Mineral Management Services (MMS) in 2000 entitled, *"A Review of Sustained Casing Pressure Occurring on the OCS"*. The report focused on the problem of sustained pressure buildups on producing wellbore casing strings located in the Gulf of Mexico. Bourgoyne compiled information from a MMS database of thousand of offshore wells that demonstrated SCP buildups in order to report on the magnitude of the problem and to analyze remediation work performed to fix such problems. In the report, three example case studies were explained in detail, and this information provided an additional dataset of leaky wellbores that was used for SCP modeling purposes. The results from the Bourgoyne dataset were compared to previous dataset results.

Three wellbore examples (Case History 1,2,3) were analyzed and the data were entered as inputs to the SCP Model in order to generate a range of leakage path permeability values. The wellbore construction information was very detailed, but the pressure buildup data had to be taken manually from a pressure vs. time chart, covering a time span of several years (no detailed pressure buildup data was included in the appendix). As was observed in Fig. 4.2.5, the pressure data was affected by a remediation effort (lubricated, weighted mud) that was pumped into the annular space in order to reduce pressure buildups.

For wellbore Case History 1, periodic pressure bleed downs temporarily reduced the pressure levels in the intermediate annulus space. The operator opened a wellbore surface valve in order to bleed down the gas to a near zero level. The volume of gas that collected near the surface was very small (Bourgoyne, 2000). In Fig. 4.2.2, the pressure

buildup data recorded three different pressure buildup intervals for wellbore Case History 1. Through use of temperature and noise logs, a leaky packer located at the top of the 7'' liner (9670ft), allowed gas to enter into the intermediate annulus space. The gas reached this packer from the intermediate cement filled annulus space between the upper 9 5/8'' casing and lower 7'' liner (Fig. 4.2.1).

The characteristics of the leakage path were unknown, so "effective permeability" was used to describe this leakage conduit within the cemented annulus. The range of the leakage depth was between an upper 9 5/8'' casing string, set to a depth of 10081 ft and a lower 7'' casing liner, set to a depth of 12886 ft. The annulus space was cemented above

the set packer, to a depth of 2986ft. Above the top of cement is completion mud.

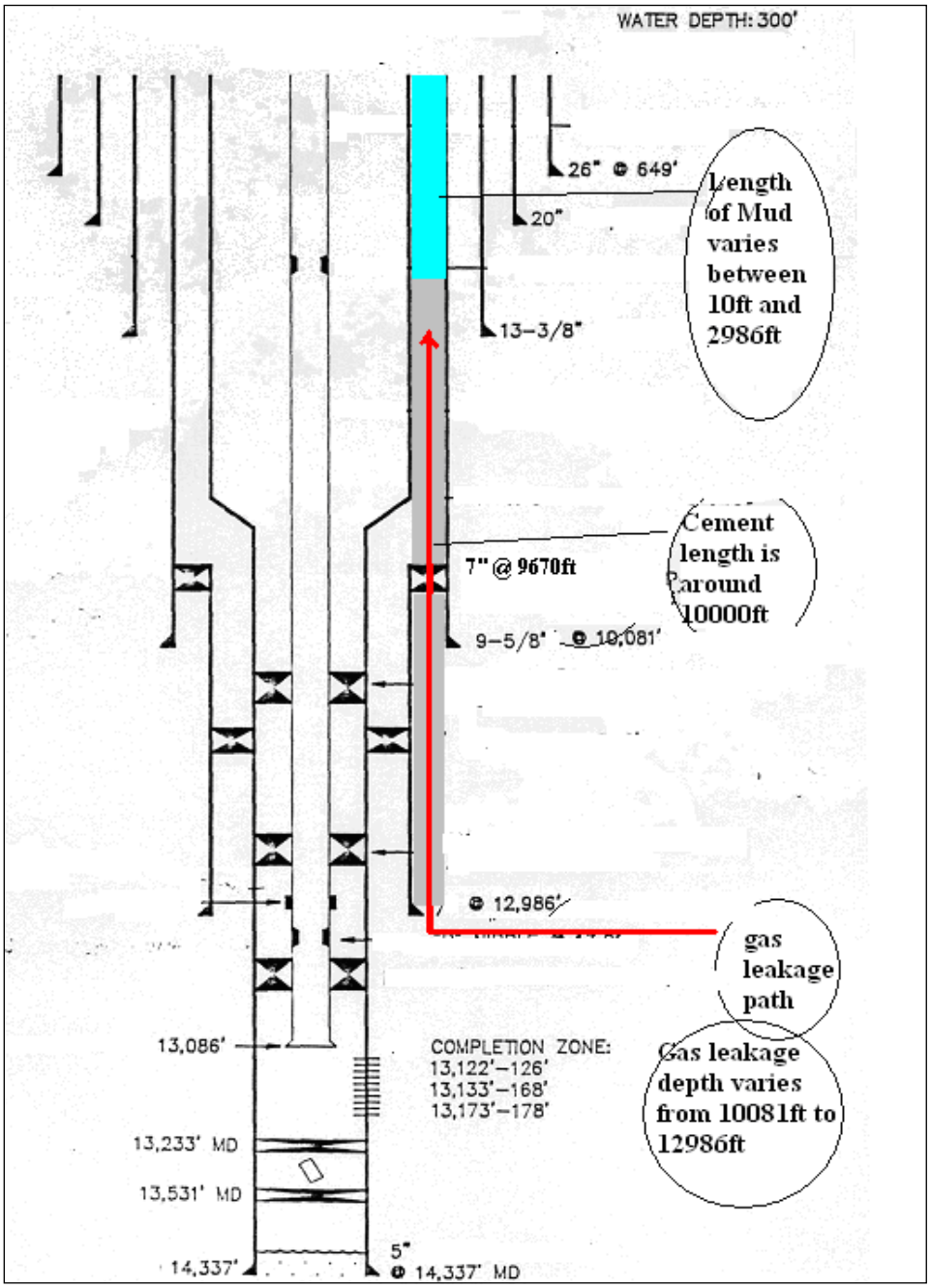

Picture 4.2.1 – Wellbore construction information - Case History 1 (Bourgoyne, 2000).

As can be observed in Fig. 4.2.2, the pressure buildup data for wellbore Case History 1 demonstrated three pressure buildup intervals with different buildup rates (5.0

psi/day, 20.7 psi/day, and 11.0 psi/day). The first pressure interval in the intermediate annulus space built up to 3500 psi. The second pressure interval built up to 4000 psi. The third pressure interval built up to 1700 psi. Each buildup interval was used as inputs to the SCP Model when generating different permeability values.

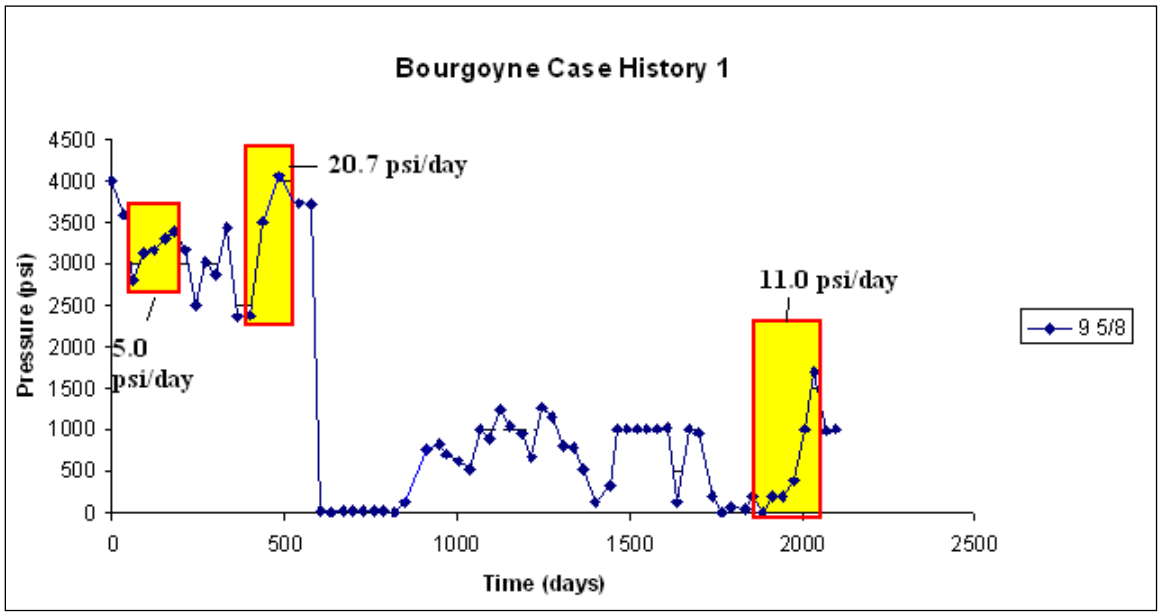

Figure 4.2.2 – Pressure buildup for Case History 1 (Bourgoyne, 2000).

At the end of each pressure buildup interval, the pressures were bled down to zero through a ½ inch needle valve in a 24 hour period. The flow rate decreased over time, reaching a constant flow rate of 5 m^3/day after 12 hours of continuous bleeding. This flow information was used in the SCVF Model, described in Chapter 3.

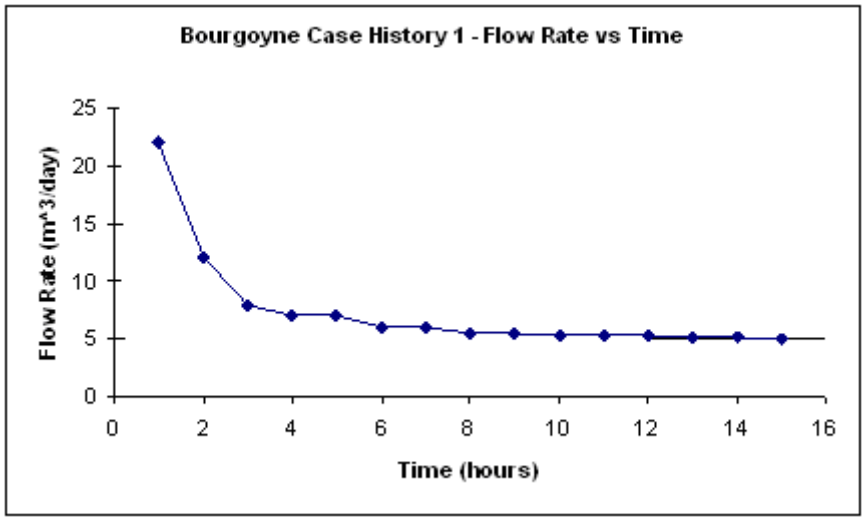

Figure 4.2.3 – Flow rate vs. time example for Case History 1 – (Bourgoyne, 2000).

For the other two wellbores (Case History 2 and Case History 3), Bourgoyne suggested that the wellbore construction information should be the same for both these wells since they were drilled with the same offshore rig to the same target reservoir depth. Therefore, only wellbore Case History 2 is described in detail.

For wellbore Case History 2, a lower casing string of 7.625'' diameter size is set to a depth of 9444 ft. An upper casing string of 10.75'' diameter size is set to a depth of 5489 ft. The gas leakage depth ranges from these upper and lower casing seat depths. The length of mud is unknown, but it is assumed to vary between 10 ft and 4989 ft (500 ft above the upper casing seat depth). The total cement length is 3955 ft (cement filled annulus space from the upper casing string to the lower casing string). The mud density of the completion mud above the top of cement is 15 ppg.

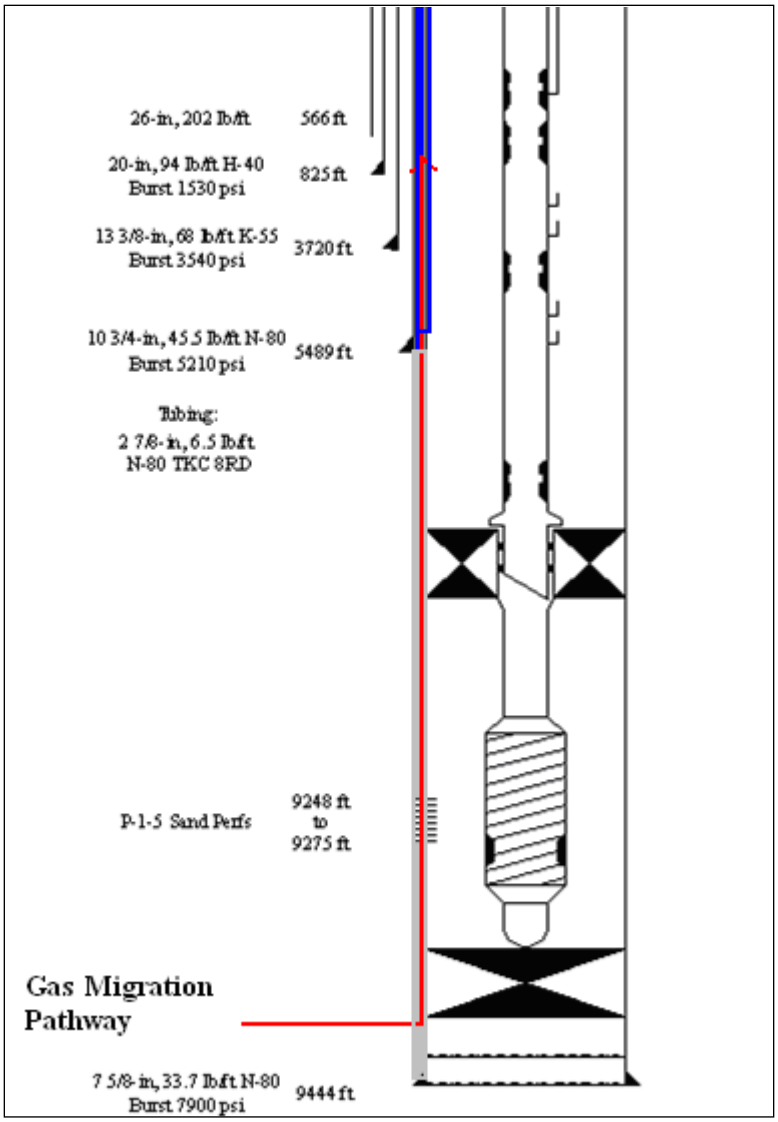

Figure 4.2.4 - Wellbore construction information - Case History 2,3 (Bourgoyne, 2000).

Since the pressure buildup data was recorded during remedial work, it was collected under different conditions/ circumstances than what was recorded for wellbore Case History 1. For example, the pressure buildup data was recorded during a process of pumping heavy completion mud into the annular space in order to remediate the leakage problem (lubricate in weighted brine or mud). The operator replaced formation gas and liquids that migrated to the surface cap, by opening the valve and allowing gas to escape.

A heavy, weighted up completion mud was pumped into the annular space in order to apply greater pressure down hole (this information was also used to determine a distribution of gas cap length). By injecting heavy mud into the annulus space, the operator was trying to eliminate the entry of formation fluids into the system by increasing the fluid hydrostatic pressure at the top of the cement, thus balancing the leakage pressure and reducing or eliminating sustained casing pressure buildups (Bourgoyne, 2000).

The intermediate annulus pressure buildup data was recorded at the surface wellhead each day after the bleed down, and after the heavy mud was injected into the annular space. The amount of mud pumped and the amount of mud bled off were recorded so that the new amount of mud being introduced into the casing could be measured (Bourgoyne, 2000). The operator shut in the valve, and returned 24 hours later to measure the sealed pressure buildup after pumping. The different between these two recordings provide a value for change in pressure over time.

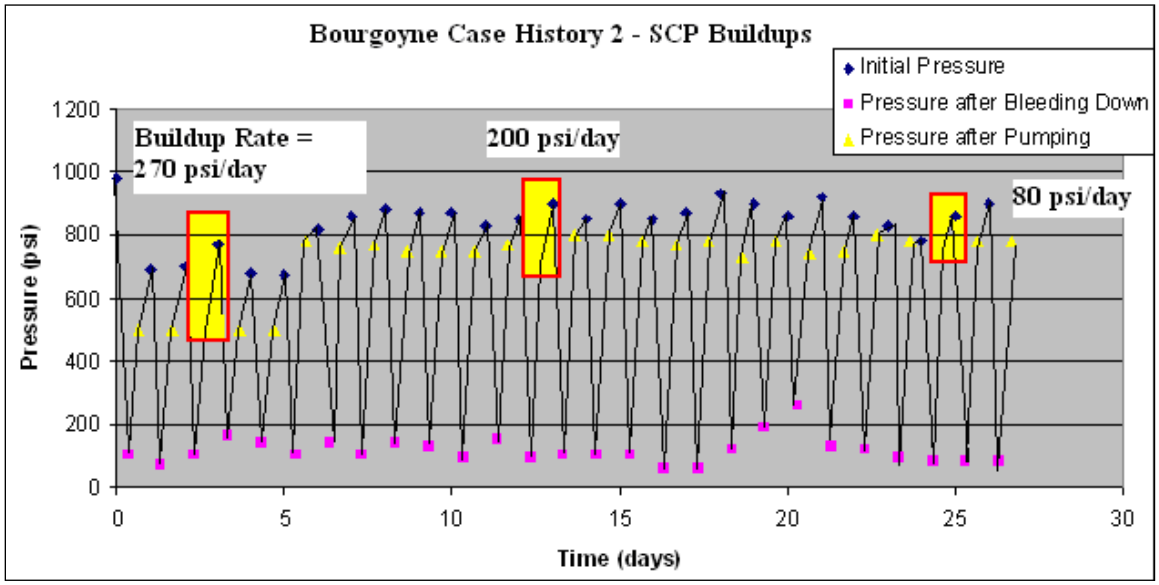

Figure 4.2.5 - Pressure buildups and bleed downs for Bourgoyne Case History 2 during the weighted mud remediation effort.

For wellbore Case History 2, three pressure buildup intervals (270 psi/day, 200 psi/day, 80 psi/day) are highlighted and used as examples for SCP modeling purposes. The weighted mud remediation work continued for a one month period, where a total of 15,000 lbs of mud was pumped into the intermediate annular space. The pressure levels were not reduced by a noticeable amount, so the remediation effort stopped at the end of the month. A sample size of three pressure buildup intervals was selected as inputs to the SCP model in order to generate permeability results.

For wellbore Case History 3, both the surface casing and the intermediate casing had sustained casing pressure buildups, and heavier mud was injected in the annular space in order to reduce pressure levels (Bourgoyne, 2000). The pressure buildups and injection data were provided. Initially, the pressure was started at 500 psi, and began building back up to a final pressure of 700 psi. The wellbore construction information and pressure data interval were used as inputs to the SCP Model.

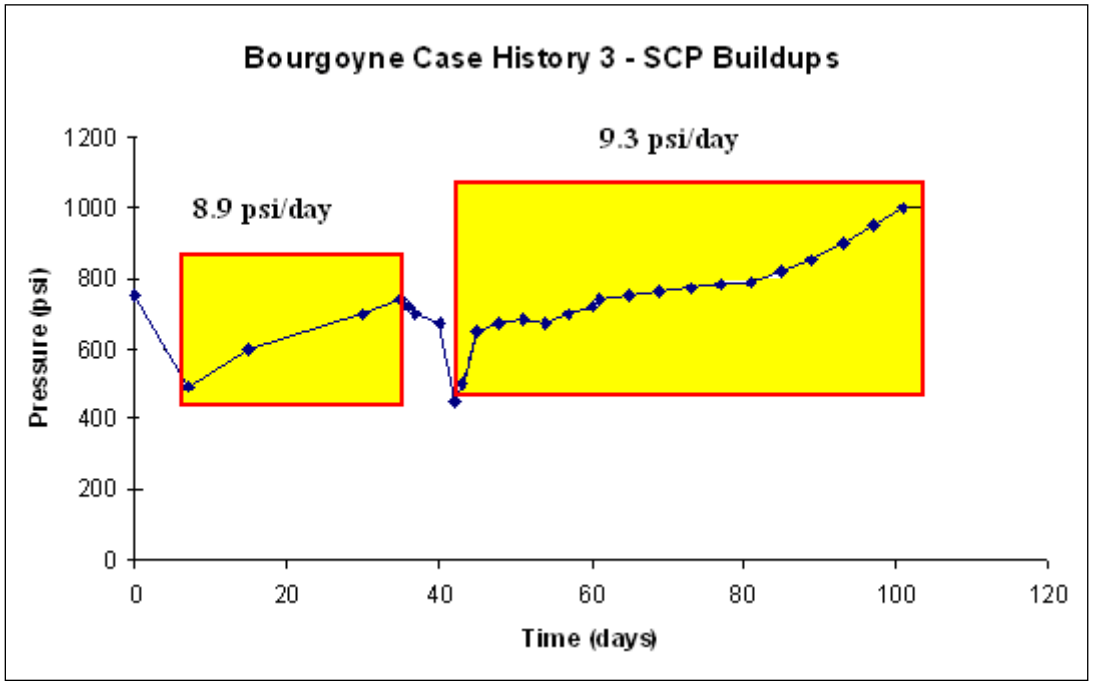

Figure 4.2.6 Pressure buildup intervals for Bourgoyne Case History 3.

4.3 XU WELLBORE DATASET

Xu validated the SCP Model by using 26 leaky wellbore field data sets. However, only 4 complete wellbore datasets that demonstrated sustained casing pressure buildups (wellbore 19, 25, 23, 24) were described in detail in her dissertation and published papers. Xu effectively matched the calculated pressure buildup curve to the monitored SCP buildup data by changing model parameter values. For these wellbores the detailed wellbore construction information and pressure buildup data was extracted and used for this research.

The annular system for Wellbore 19 was the same as what was used for Wellbore 25 because of missing data (Xu, 2001). The annulus selected had an inner diameter of 7.625'' and an outer diameter of 10.75''. The 7.625'' lower casing string was set to a depth of 8635 ft. The 10.75'' upper casing string was set to a depth of 5447 ft. The mud density of the completion mud sitting above the top of cement was 11 ppg. The length of mud was unknown, but assumed to vary between 10 ft and 5447 ft. The top of cement is located at 5447 ft. The length of cement used in the SCP model varies by changing the leakage depth. Wellbore 19 was bled down (eliminated dry gas from the system) for 12 minutes before the needle valve was closed. The pressure built up for 24 hours, following the bleed down. The recorded pressure data was matched to the model generated pressure buildup by changing the gas cap size, mud compressibility, and formation pressure (Xu, 2001).

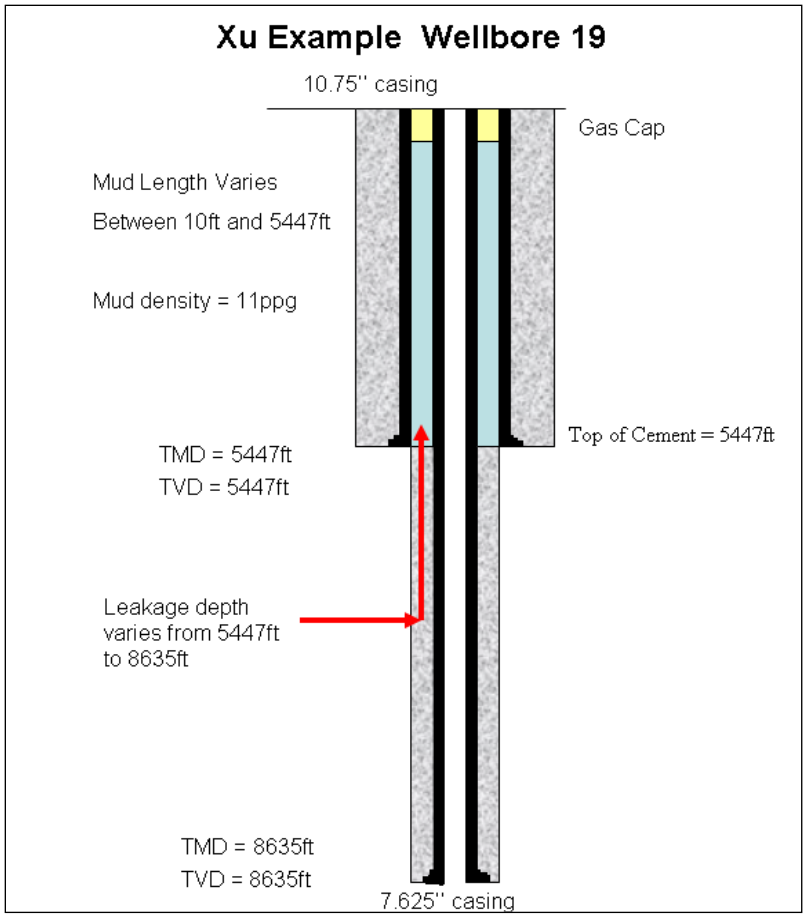

Figure 4.3.1 – Schematic of wellbore 19 leakage scenario.

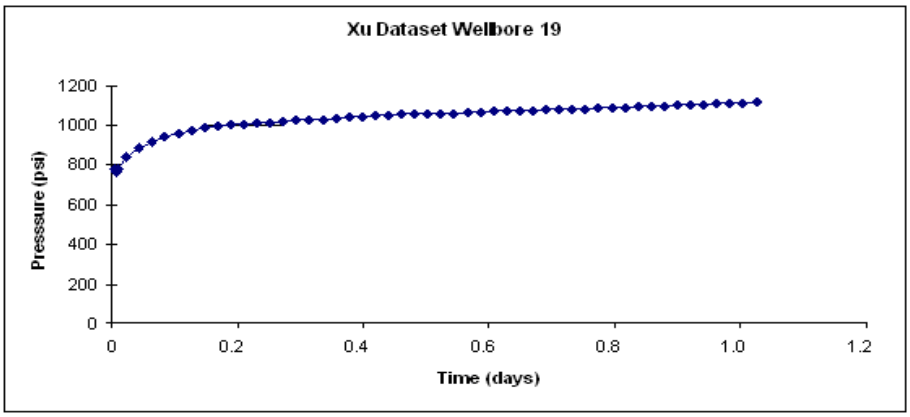

Figure 4.3.2 – Pressure buildup of wellbore 19.

The wellbore construction information for wellbore 25 was identical to that of wellbore 19, except that the mud density of the completion mud above the top of cement was 15 ppg, rather than 11 ppg. Xu had hypothesized that the leakage source was at the depth of the upper casing string at 5447 ft. Pressure buildup data was recorded daily. Xu found that some of the early buildup data was missing. Nevertheless, results show that the model matched the pressure buildup dataset, while providing a leakage path permeability range.

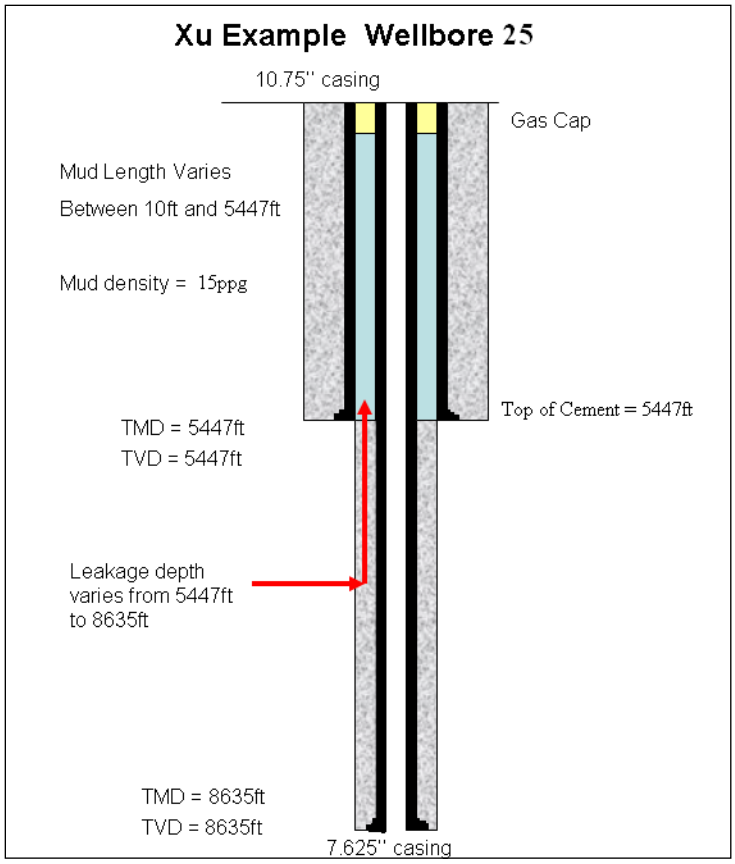

Figure 4.3.3 – Schematic of wellbore 25 leakage scenario (completion mud density is 15 ppg).

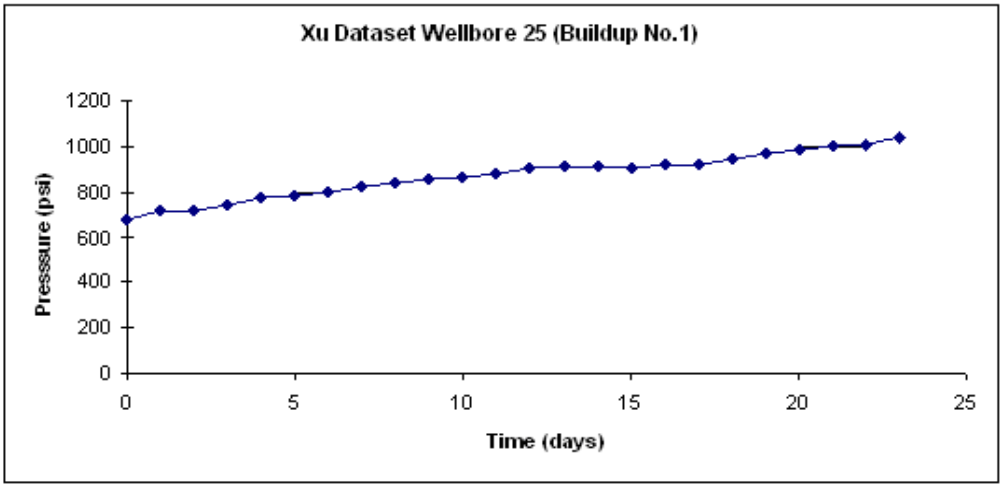

Figure 4.3.4 – Pressure buildup no. 1 for wellbore 25

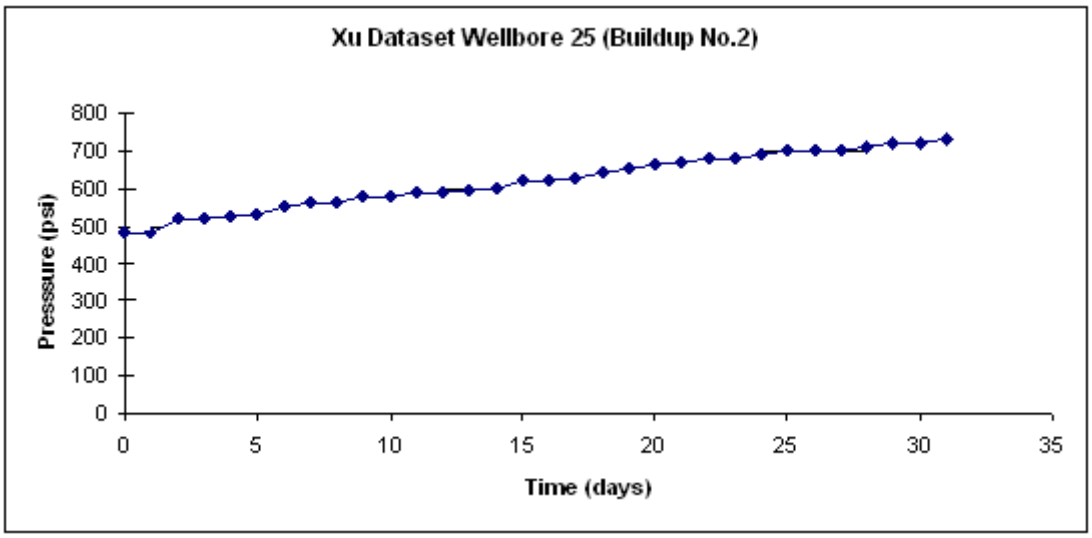

Figure 4.3.5 – Pressure buildup no. 2 for wellbore 25

For wellbore 23, the 7.0'' lower casing reached a depth of 11196 ft. The 9.95'' upper casing reached a depth of 4310 ft. The mud density was 10 ppg. The leakage depth was unknown, but was assigned values between the upper and lower casing depths, 4310 ft and 11196 ft. The pressure buildup data was recorded and used an input to the SCP Model. The intermediate casing annulus space demonstrated increasing pressure levels, reaching 1600 psi after 8 months.

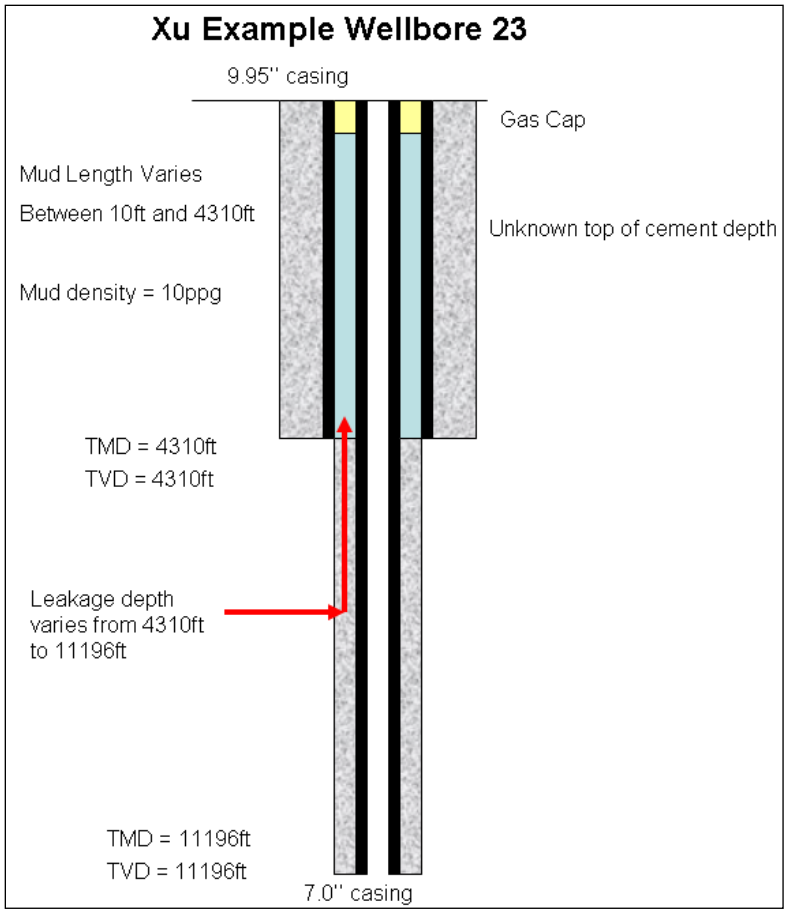

Figure 4.3.6 - Schematic of wellbore 23 leakage scenario.

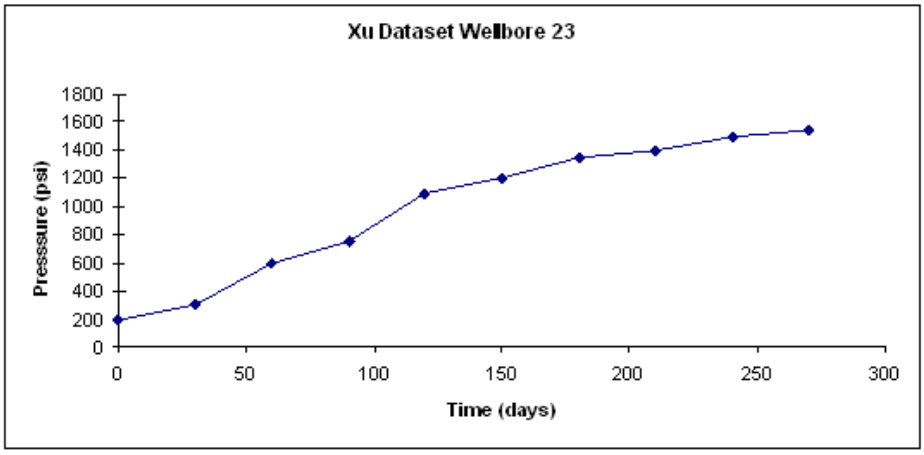

Figure 4.3.7 – Pressure buildup interval (5.0 psi/day) for Wellbore 23

For wellbore 24, the lower 7.625'' casing string was set to a depth of 9804 ft. The upper 9.95'' casing string was set to a depth of 6433 ft. The leakage depth was unknown, but was assumed to vary between 6433 ft and 9804 ft. The mud density was 16 ppg. The pressure buildup data was used as an input to the SCP model. Xu reported that this intermediate casing was bled down frequently, before the pressure buildup occurred. After each bleed-down, heavier mud was pumped back into the annulus. The operators recorded the volume and the weight of the mud that was pumped into the system. The pressure continued to increase, reaching an asymptotic level of 1000psi in one month (Xu, 2001).

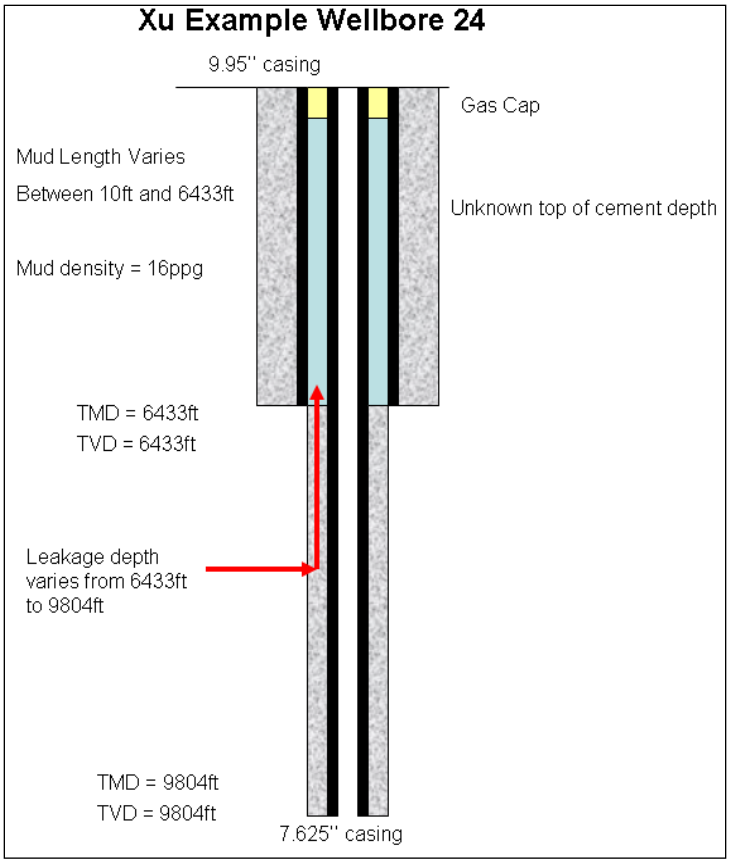

Figure 4.3.8 - Schematic of wellbore 24 leakage scenario.

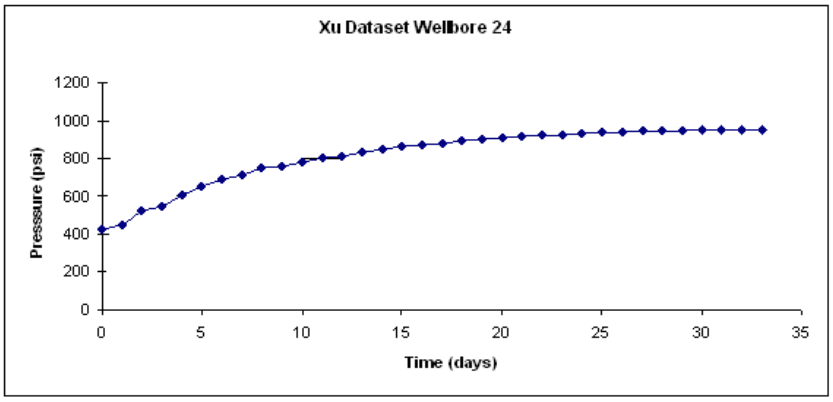

Figure 4.3.9 – Pressure buildup interval (16.0 psi/day) for Wellbore 24.

4.4 WATSON WELLBORE DATASET

In summer/fall of 2004, Watson performed a study to obtain findings of a site investigation/pad evaluation for gas migration and surface casing vent flow. Prior to Watson's study, many unsuccessful attempts were made to shut off the gas that was leaking to surface (Watson, 2004). The purpose of the study was to determine the gas source location in order to conduct remedial work to fix the problem.

In the field under investigation, there were 12 deviated wellbores (slant angle from vertical to 45 degrees) that demonstrated sustained casing pressure buildups. Watson obtained the wellbore construction information and recorded the sustained casing pressure buildup data over time using installed data loggers. Tests were performed to check for interference or cross flow between wells. Results showed that several of the wells were in communication with each other. It was concluded that the site could have been influenced by gas migration associated with another pad located in close proximity to the pad under study (Watson, 2004).

During flow testing, samples of the gas were taken in order to determine the weight and composition of the fluid flowing during pressure bleed down. Gas analysis results provided information about the density of the fluid and the possible location of the gas source. Soil samples located around the wellheads at the surface of each wellhead were also taken and analyzed. A chemical analysis provided the gas components and characteristics. The compositional, isomer, and carbon isotope analysis were performed on samples collected. The analysis was performed to match the gas collected to the location of source gases at different potential leakage zones. The results were compared to known formation gas analysis results, which identified the location of the gas source at depth locations. Therefore, it was possible to provide a range of leakage depth values, based on the matching of the components of the gas analysis.

In other cases where the maximum pressure level did not correspond with such shallow leakage sources, a leakage depth was calculated using a normal pressure gradient of 0.465 psi/ft. The leakage depth was then located at an appropriate depth (beneath the upper casing seat depth). Details from Watson's work provided upper and lower bounds for the leakage depth range.

For each leaky wellbore, the data log recorded the pressure build up and bled off. Following the bleed down, the pressure would build up again, for most of these wells. Watson (2009) provided detailed information for the following 10 wellbores: K10, M8, P9, J9, J10, N8, N9, O8, Q7, Q9. For this thesis, the data for each wellbore was compiled and analyzed, using the SCP Model.

4.4.1 Watson Dataset - Pressure Buildups and Wellbore Construction

Wellbore K10

For wellbore K10, the chemical gas analysis indicated that a possible leakage depth was located at 623 ft. This is located between the upper and lower casing strings. The lower 7.0'' intermediate casing was set to a depth of 1450 ft for a hole-size of 9.9''. The upper 10.75'' surface casing string was set to a depth of 380 ft. The mud length was 301 ft and the total length of cement was 1149 ft. The mud density was unknown, but assumed to range between 8.8 ppg and 14.3 ppg. When the valve was opened, a flow rate of 0.23 m^3/day was recorded. Wellbore K10 had recorded 4 separate pressure buildups (Fig 4.4.1 a,b,c) from years 2004, 2005, and 2006. The pressure buildups reached different asymptotic pressure values.

Picture 4.4.1 - Surface wellhead of Wellbore K10 (Watson, 2006).

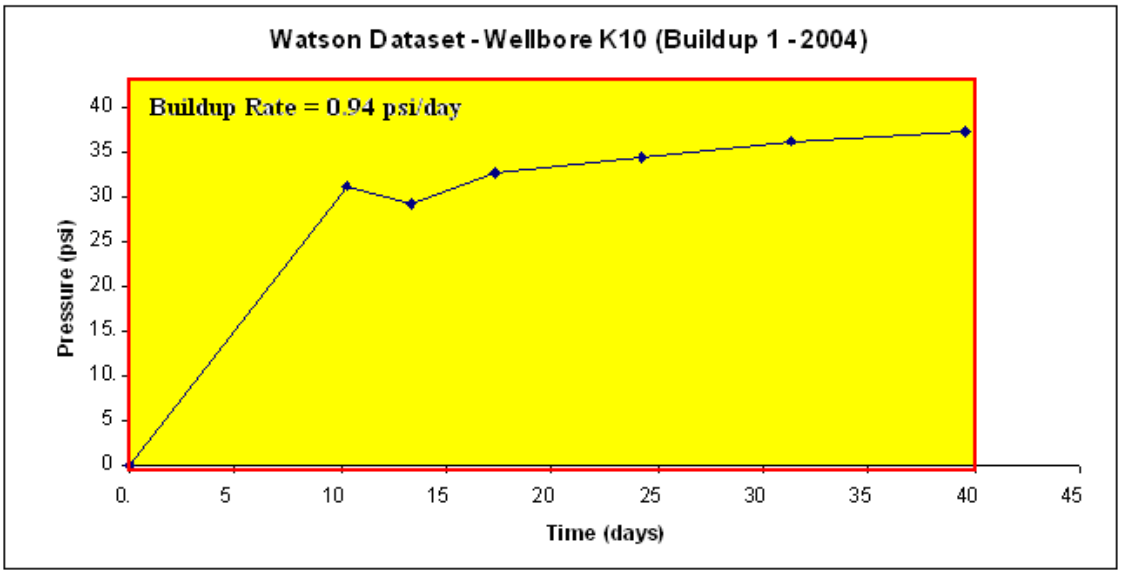

Figure 4.4.1a - Pressure buildup no.1 of Wellbore K10.

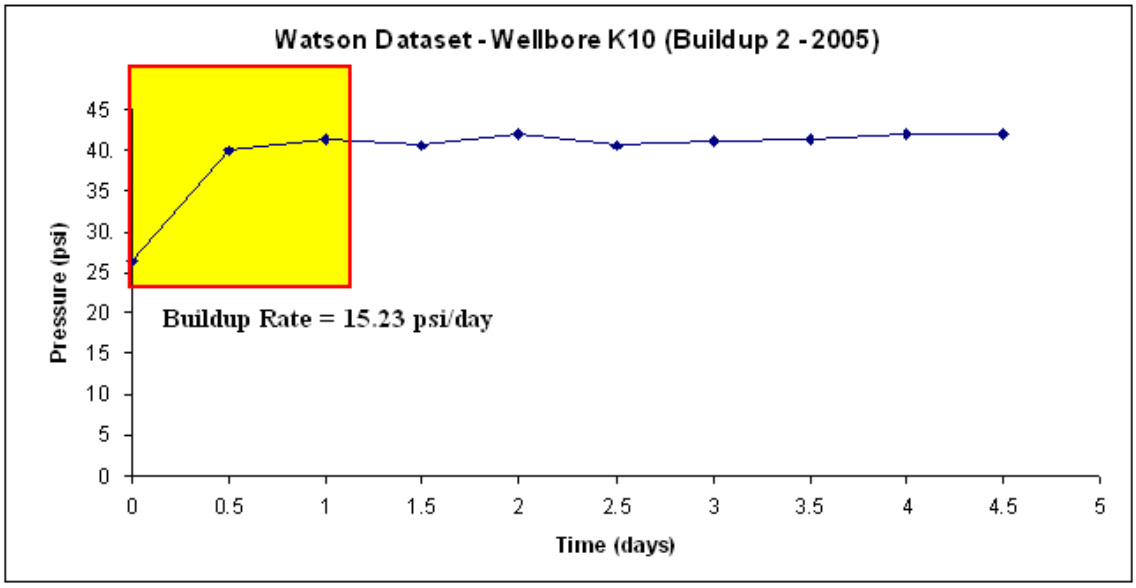

Figure 4.4.1b – Pressure buildup no.2 of Wellbore K10.

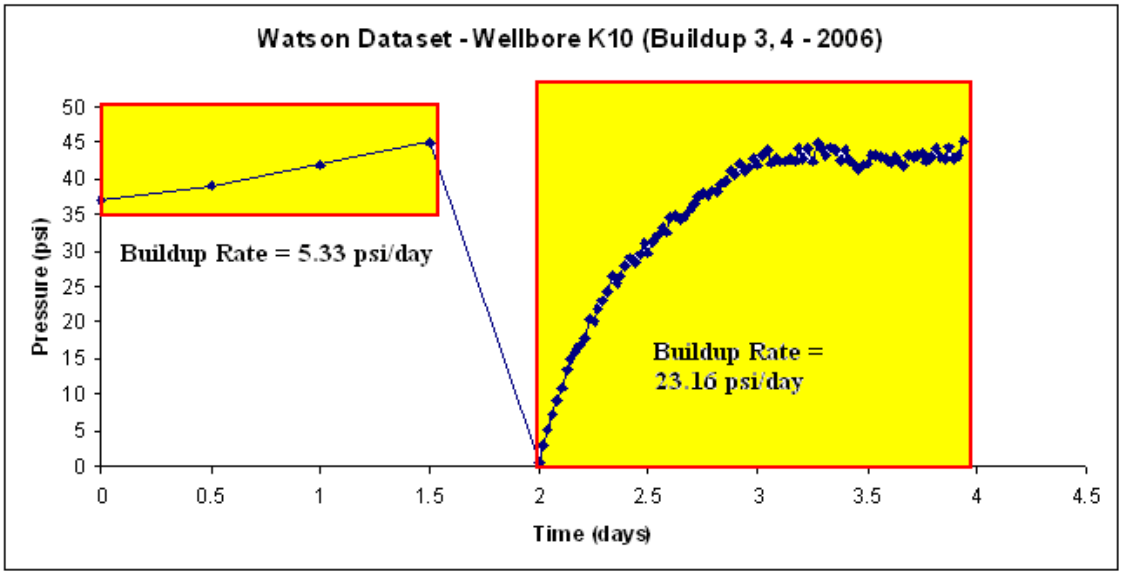

Figure 4.4.1c – Pressure buildup no.3, no.4 of Wellbore K10.

Wellbore M8

For wellbore M8, the chemical gas analysis indicated that the leakage depth was located between a range of 328 ft and 426 ft. The 7.0'' intermediate casing was set to a depth of 1305 ft for a hole-size of 9.9''. The 10.75'' surface casing string was set to a depth of 354 ft. Thus only leakage depths lower than 354 ft depth were considered. The mud length was 146 ft and the total length of cement was 1159 ft. The mud density was unknown, but assumed to range between 8.8 ppg and 14.3 ppg. No flow rate was recorded. Wellbore K10 had recorded 2 separate pressure buildups (Fig. 4.4.2a,b) from years 2004 and 2005. The pressure buildups reached different asymptotic pressure values.

Picture 4.4.2 - Surface wellhead of wellbore M8 (Watson, 2004).

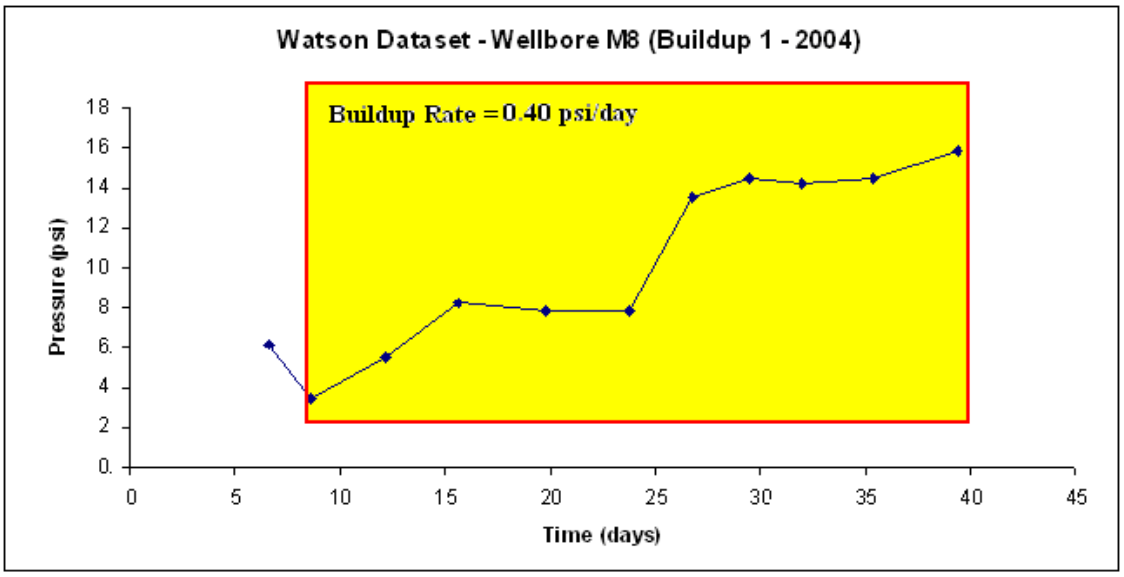

Figure 4.4.2a – Pressure buildup no.1 of Wellbore M8.

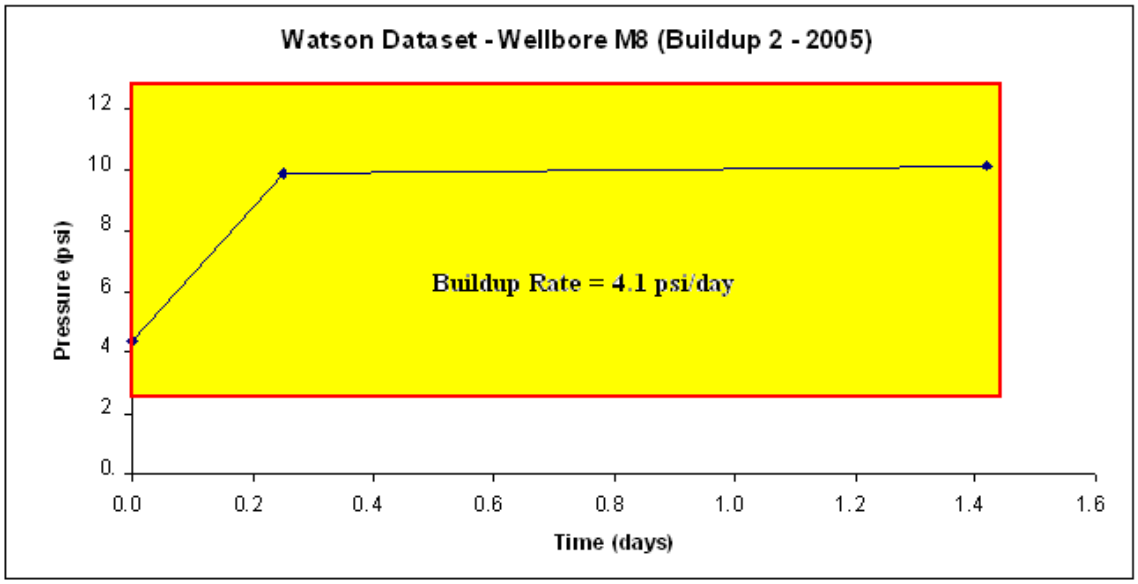

Figure 4.4.2b – Pressure buildup no.2 of wellbore M8.

Wellbore P9

For wellbore P9, the chemical gas analysis indicated that the leakage depth was located at a depth between 328 ft and 426 ft. The 7.0'' intermediate casing was set to a depth of 1601 ft for a hole-size of 9.9''. The 10.75'' surface casing string was set to a depth of 417 ft. Leakage depths below 417ft should only be considered, as it would be impossible to migrate up the intermediate casing string otherwise. The mud length was 417 ft and the total length of cement was 1184 ft. The mud density was unknown, but assumed to range between 8.8 ppg and 14.3 ppg. When the valve was opened, a flow rate of 0.29 m^3/day was recorded. Wellbore P9 had recorded 3 separate pressure buildups (Fig. 4.4.3a,b,c) from years 2005 and 2006. The pressure buildups reached different asymptotic pressure values.

Picture 4.4.3 - Surface wellhead of wellbore P9 (Watson, 2004).

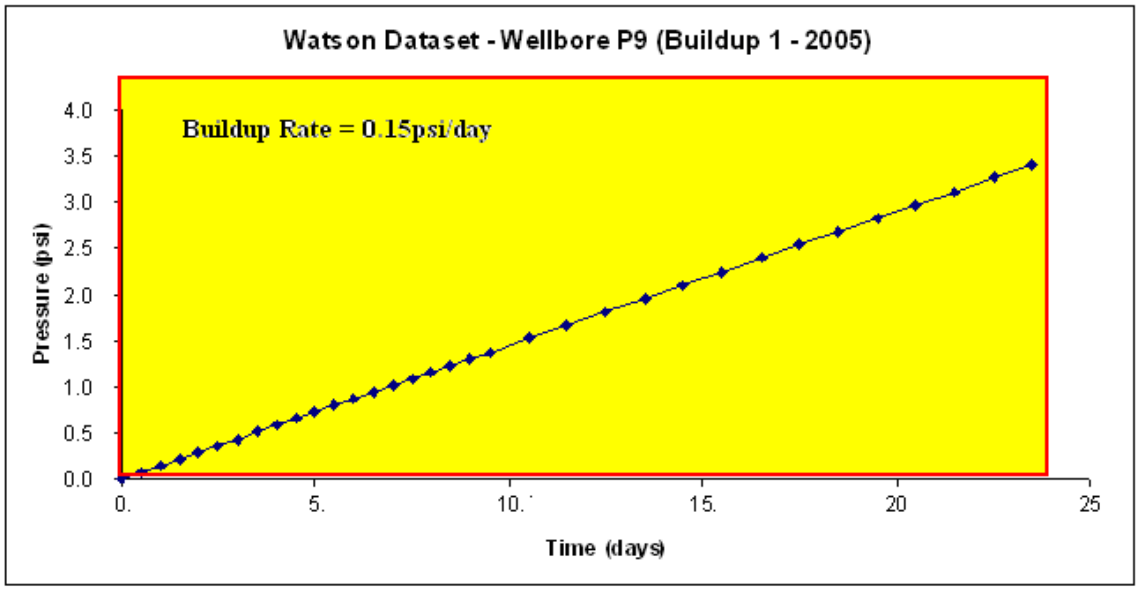

Figure 4.4.3a – Pressure buildup no.1 of Wellbore P9.

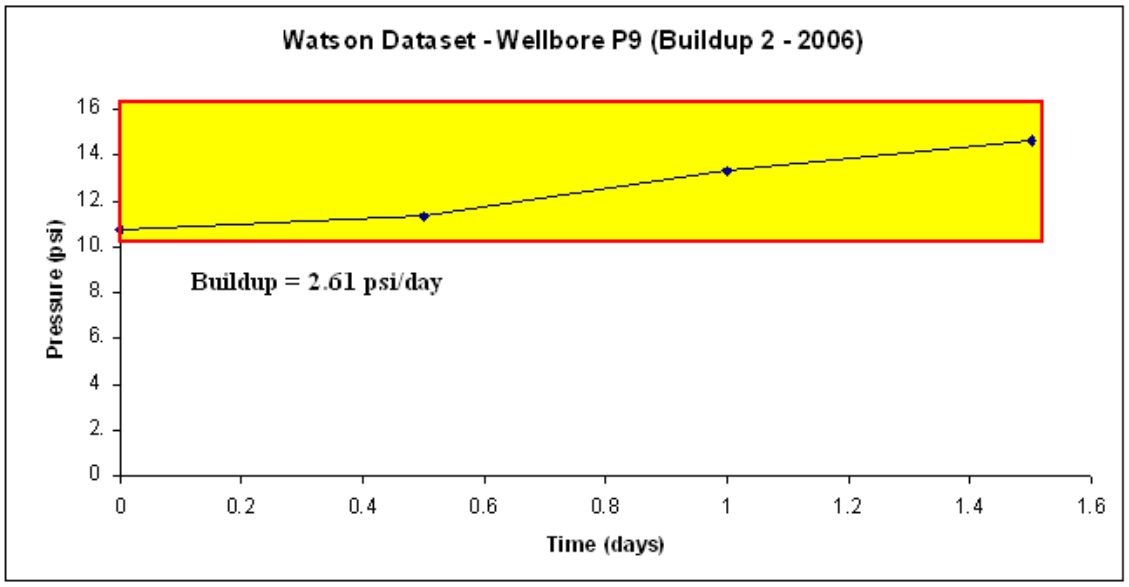

Figure 4.4.3b – Pressure buildup no.2 of Wellbore P9.

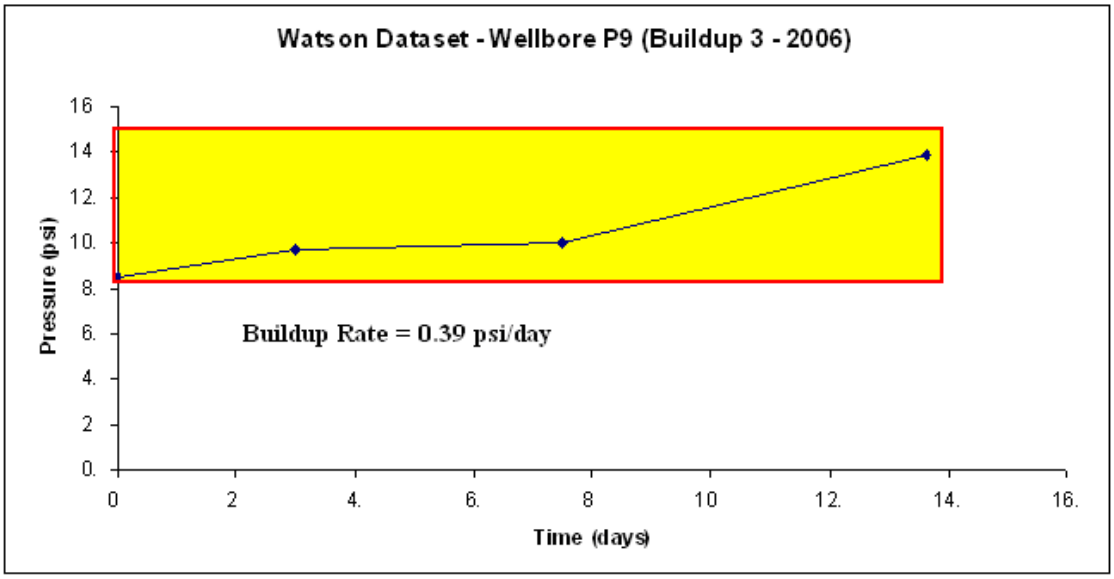

Figure 4.4.3c – Pressure buildup no.3 of Wellbore P9.

Wellbore J9

For wellbore J9, the chemical gas analysis indicated that the known leakage depth was located between a depth of 1299 ft and 1319 ft. For modeling purposes, the leakage depth was averaged to be 1309 ft. The lower 7.0'' casing string was set to a depth of 1853 ft. The upper 10.75'' casing string was set to a depth of 488 ft. The completion mud density was an unknown, but was assumed to range from 8.3 ppg and 14 ppg. The length of mud was unknown, but was assumed to range from 10 ft to 488 ft. A flow rate of 0.29 m^3/day was recorded during bleed down. After closing the valve on the surface annular space, pressure built up to 20 psi (0.28 psi/day).

Picture 4.4.4 – Surface wellhead of wellbore J9 (Watson, 2004).

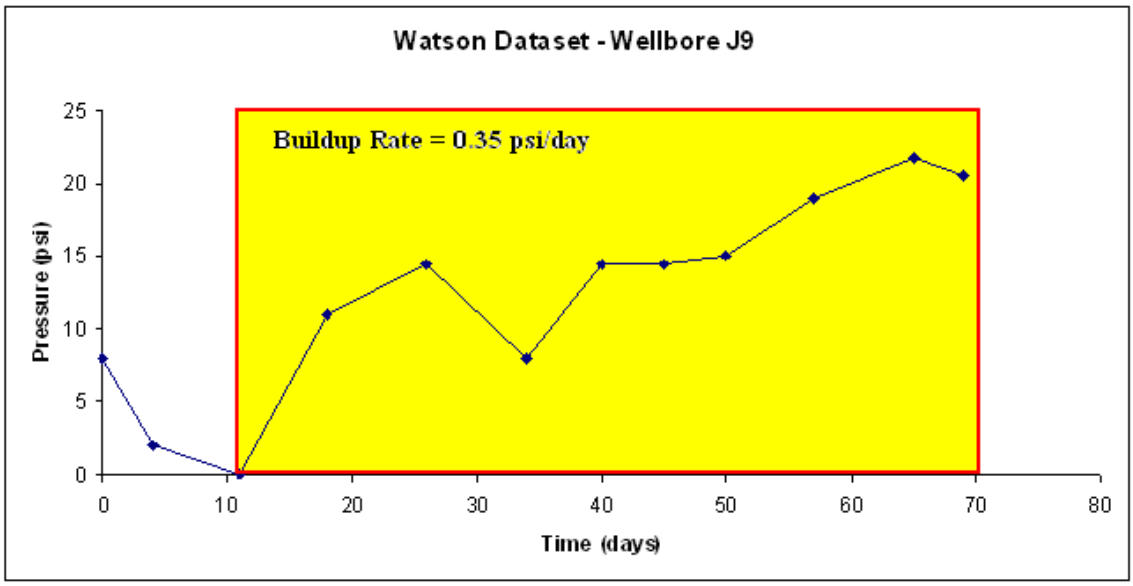

Figure 4.4.4 – Pressure buildup of wellbore J9.

Wellbore J10

For wellbore J10, the well pressure built up and was not stabilized at the end of the test period. The chemical gas analysis indicated that a leakage depth was 623 ft. Since no information was provided about the sizes of the upper and lower casing strings and the leaky wellbores are all located in the same field, it was assumed that the casing sizes were the same as wellbores J9, K10, M8. The 7.0'' lower casing string was set to a depth of 1778 ft. The 10.75'' upper casing string was set to a depth of 524 ft. The mud density was unknown, but was assumed to range between 8.3 ppg and 14 ppg. The length of mud was unknown, but was assumed to range between 10 ft and 524 ft (largest mud length corresponds to the depth of the upper casing string). A flow rate of 0.55 m^3/day was recorded during bleed down. When the valve was shut in, pressure built up (Fig. 4.4.2) and reached a final asymptotic pressure of 200 psi (1.92 psi/day).

Picture 4.4.5 – Surface wellhead of wellbore J10 (Watson, 2004).

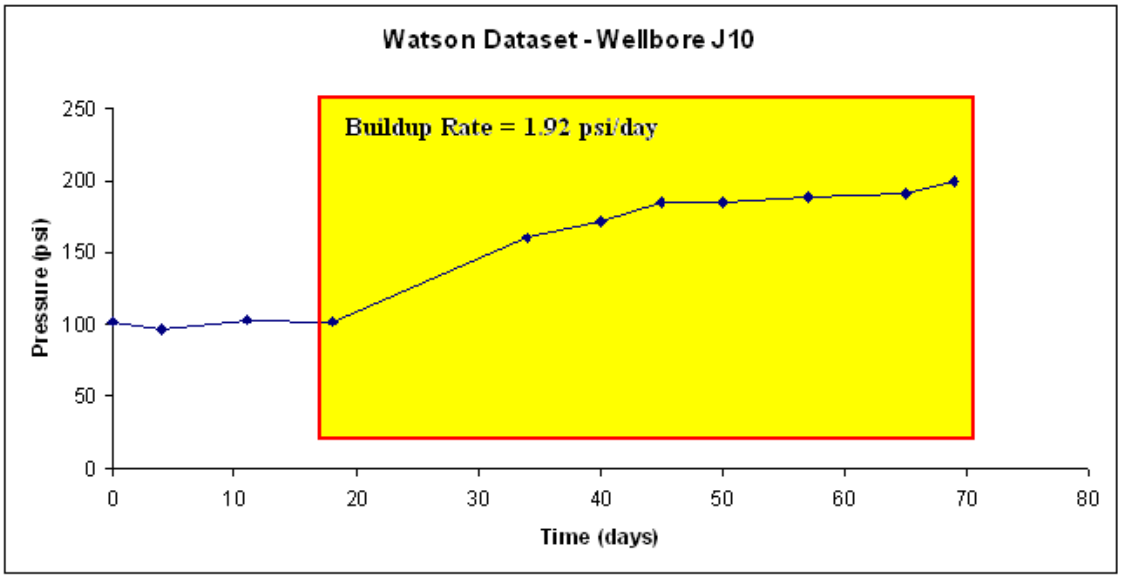

Figure 4.4.5 – Pressure buildup of wellbore J9.

Wellbore N8

For wellbore N8, the chemical gas analysis indicated that the leakage depth was located between a depth of 328 ft and 426 ft. An average leakage depth of 377 ft was used. No information was provided about the sizes of the upper and lower casing strings, therefore it is assumed that the casing sizes were the same as wellbores J9, K10, M8. The 7.0'' lower casing string was set to a depth of 1374 ft. The 10.75'' upper casing shoe was set to a depth of 374 ft. The mud density was unknown, but was assumed to range between 8.3 ppg and 14 ppg. The length of mud was unknown, but was assumed to range between 10 ft and 328 ft. A flow rate of 0.28 m^3/day was recorded during bleed down. When the valve was shut in, pressure built up (Fig. 4.4.3) and reached a final asymptotic pressure of 73.0 psi (0.66 psi/day).

Picture 4.4.6 - Surface wellhead of wellbore N8 (Watson, 2004).

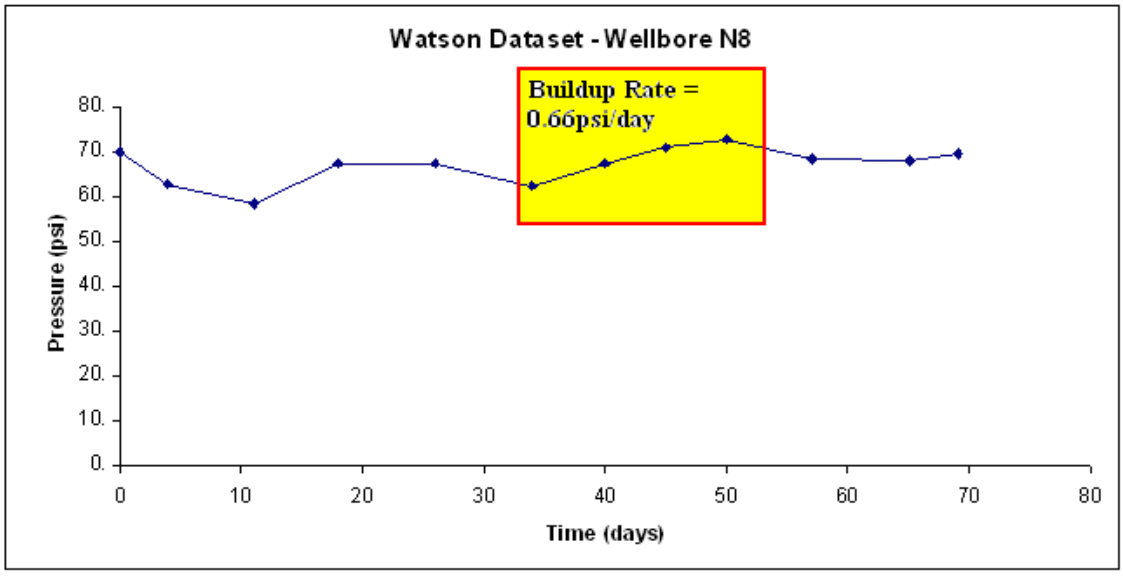

Figure 4.4.6 – Pressure buildup of wellbore N8.

Wellbore N9

For wellbore N9, the original chemical gas analysis had indicated that the leakage depth was at 590 ft. However, based on recorded pressure buildup levels of 518 psi, this leakage depth is impossible. At a pressure gradient of 0.465 psi/ft, the formation leakage pressure would be 255 psi. Physically it is obvious that the asymptotic pressure cannot build up to a value exceeding the leakage pressure. Since the final asymptotic pressure is 518 psi, this indicates that the leakage source is deeper than 590 ft. Using a normal pressure gradient of 0.465 psi/ft, the leakage depth would then be (518 psi / 0.465 psi/ft) = 1114 ft, which is between the upper (377 ft) and lower (1325 ft) casing seat depth.

No information was provided about the sizes of the upper and lower casing strings, however since the wells were drilled in the same field, it was assumed that the casing sizes were the same as wellbores J9, K10, M8. The 7.0'' lower casing string was therefore set to a depth of 1325 ft. The 10.75'' upper casing string was set to a depth of 377 ft. The mud density was unknown, but was assumed to range between 8.3 ppg and 14 ppg. The length of mud was unknown, but was assumed to range between 10 ft and 377 ft. No flow rate was recorded during bleed down. When the valve was shut in, pressure built up (Fig. 4.4.4) and reached a final asymptotic pressure of 518 psi.

Picture 4.4.7 - Surface wellhead of wellbore N9 (Watson, 2004).

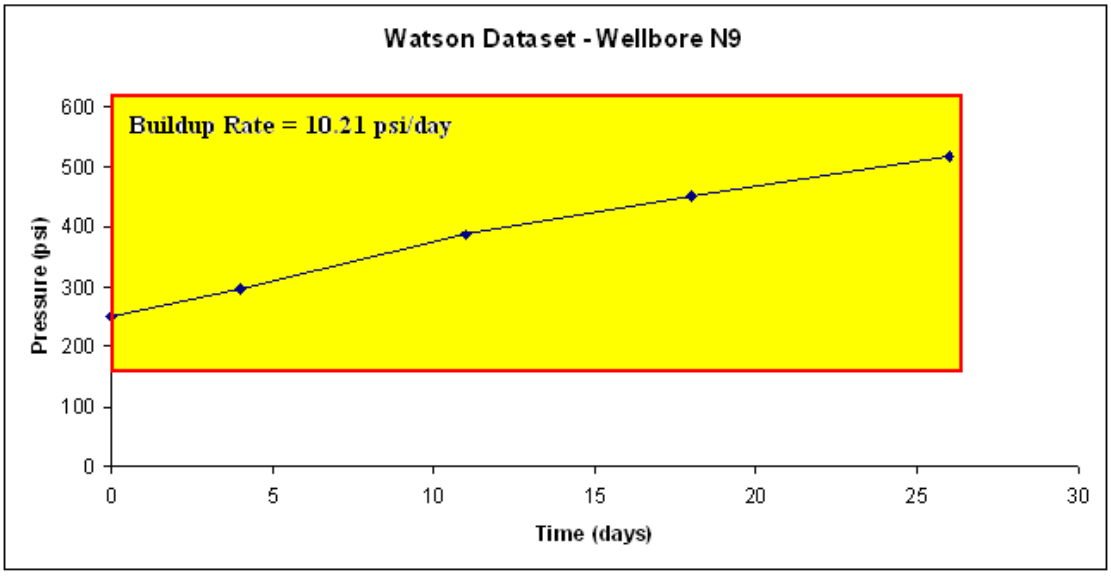

Figure 4.4.7 - Pressure buildup of wellbore N9.

Wellbore Q7

For wellbore Q7, the chemical gas analysis indicated that the leakage depth was located between 328 ft and 426 ft. Since the surface casing pressure built up to an asymptotic value of 523 psi, the leakage depth cannot be located at this depth. The gas formation pressure would be, at most 198 psi (0.465 psi/ft @ 426 ft). There is not enough driving force to cause a buildup to pressures greater than the leakage source pressure. Since this leakage depth is too shallow to be consistent with the asymptotic casing pressure, an assumption is made that the leakage depth occurred between the upper 10.75'' casing string depth at 508 ft and the lower 8.625'' casing string depth at 2047 ft. Using a pressure gradient of 0.465 psi/ft, the leakage depth = 523 psi / 0.465 psi/ft = 1125 ft.

The mud density was unknown, but was assumed to range between 8.3 ppg and 14 ppg. The length of mud was unknown, but was assumed to range between 10 ft and 508 ft. A flow rate of 10.58 m^3/day was recorded during bleed down. When the valve was shut in/closed, pressure built up (Fig. 4.4.5) and reached a final asymptotic pressure of 523 psi (42.9 psi/day).

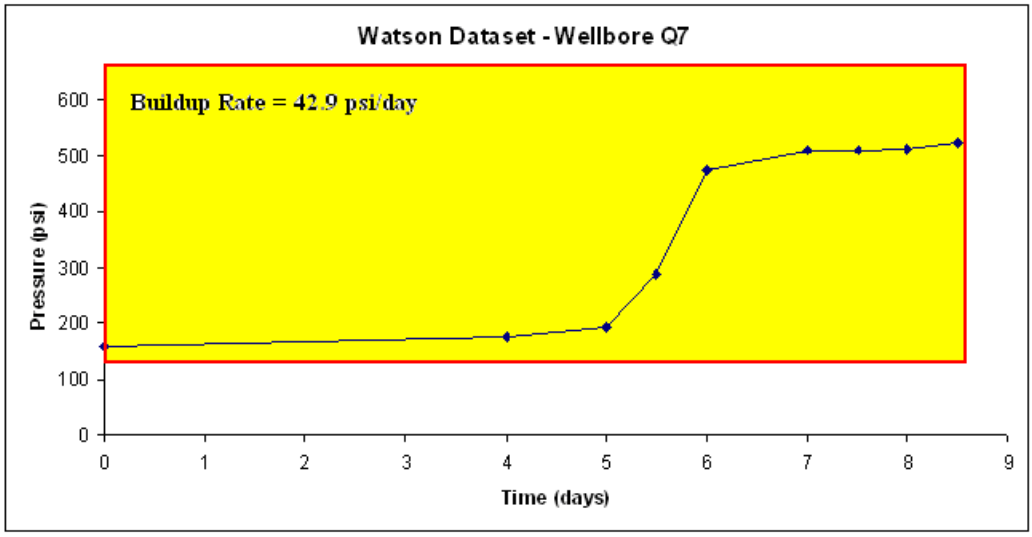

Figure 4.4.8 - Pressure buildup of wellbore Q7.

Wellbore Q9

For wellbore Q9, the chemical gas analysis indicated that the leakage source depth was located between 328 ft and 426 ft. The components of the gas collected at surface matched the components of the formation gas at this depth. However, if the leakage depth is located at a depth of 492 ft, the leakage pressure would, at most be 229 psi. This is not enough source pressure for the wellbore surface casing to reach the observed asymptotic pressure of 446 psi. Using a normal pressure gradient of 0.465 psi/ft, the leakage depth = 446 psi / (0.465 psi / ft) = 1125ft.

The upper casing size is 10.75'' at a depth of 508 ft and the lower casing size is 8.625'' at a depth of 2047 ft. The mud density was unknown, but was assumed to range between 8.3 ppg and 14 ppg. The length of mud was also unknown, but was assumed to range between 10 ft and 492 ft. A flow rate of 10.58 m^3/day was recorded during bleed down. On June 10, 2004, a flow rate of 2.25 m^3/day was recorded. On May 11, 2004, a flow rate of 0.32 m^3/day was recorded (these values are used in the SCVF Model). When

the valve was shut in, the pressure built up (Fig. 4.4.6) to a final asymptotic pressure of 446 psi (rate of 12.7 psi/day).

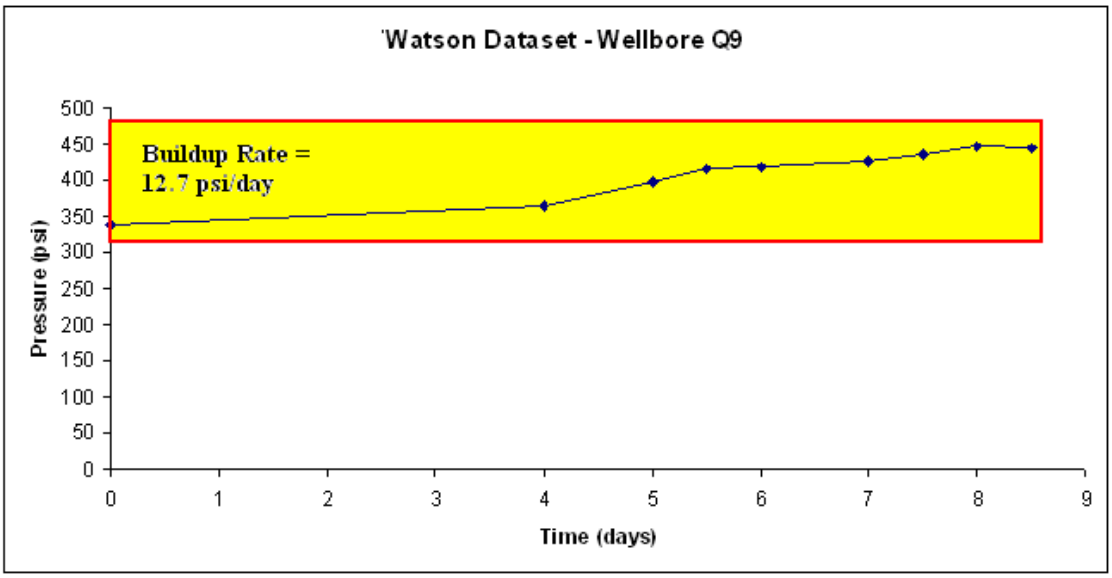

Figure 4.4.9 - Pressure buildup of wellbore Q9.

Wellbore O8

For wellbore O8, the gas analysis provided inconclusive results, so the leakage depth was not identified through these means. If the leakage depth was calculated using the asymptotic pressure of 15 psi, it would be too close to shallow for reasonable gas sources (normal pressure gradient of 0.465 psi/ft, the leakage depth = 15 psi / (0.465 psi/ft) = 32 ft). Therefore, it was assumed that the leakage depth was located halfway (1278 ft) between the lower casing 7.0'' at 508 ft, and the upper casing 10.75'' at 2047 ft. The mud density was unknown, but was assumed to range between 8.8 ppg and 14.3 ppg. The length of mud was unknown, but was assumed to range between 10 ft and 508 ft. The pressure in the surface casing - formation annulus space built up to a maximum level of 15 psi (0.45 psi/day).

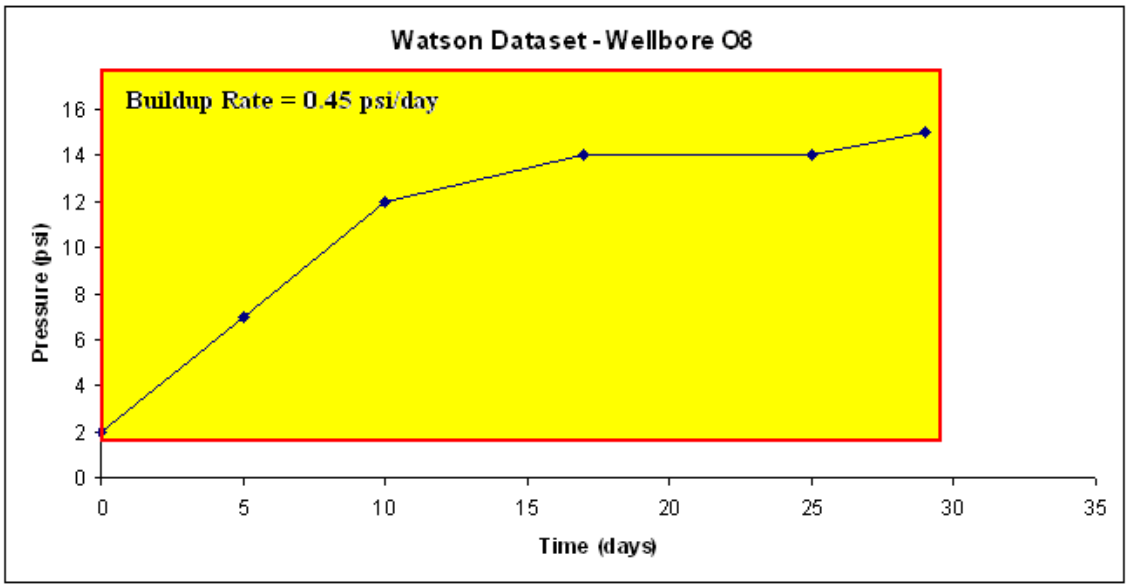

Figure 4.4.10 - Pressure buildup of wellbore O8.

4.5 HUERTA WELLBORES

Huerta analyzed an onshore wellbore (Case Study 1) and generated leakage path permeability based on changing the unknown leakage depths. To provide additional leaky wellbore results for research needs, this example wellbore generated a range of leakage path permeability values, one for each pressure buildup interval recorded.

Wellbore Case Study 1 was described as a gas well in an over pressured reservoir (0.92 psi/ft) (Huerta, 2009). The intermediate annulus space filled with cement demonstrated several high pressure buildup rates (4000-5000 psi/day), soon after cementing the production casing. Similar remediation work was performed on the wells, as described by the wellbore Case History 2 in the Bourgoyne dataset, (pumping in high density mud to increase weight on cement and to plug the crack).

The operator was unsuccessful at solving the casing vent flow problem, and later had to perform a more invasive cement squeeze job. After each remedial cement

injection period, the operator recorded the sustained casing pressure buildup data that followed.

Huerta further analyzed the well design and pressure buildup data to estimate plausible ranges of leakage depths. Huerta assigned different leakage depths, based on the model's ability to history match the pressure buildup data. The pressure buildup data was measured by a surface gauge that recorded data from the intermediate annulus space. These pressure buildup rates were some of the highest recorded of all the datasets that were analyzed (several 1000 psi/day).

The details of the wellbore construction information and the leakage depths are schematically displayed in Figure 4.5.1. The intermediate annulus consisted of a 4.5'', 15.1 lb/ft P-100 steel production casing set to a lower bound depth of 13,171 ft and a 7'', 29 lb/ft P-100 intermediate steel casing set to a upper bound depth of 10,607 ft. The length of completion mud was measured at 8700 ft, from the top of cement to surface. The total length of cement was estimated to be 4471 ft. The completion mud density was reported as 17.39 ppg. (Huerta, 2009).

Huerta Case Study 1

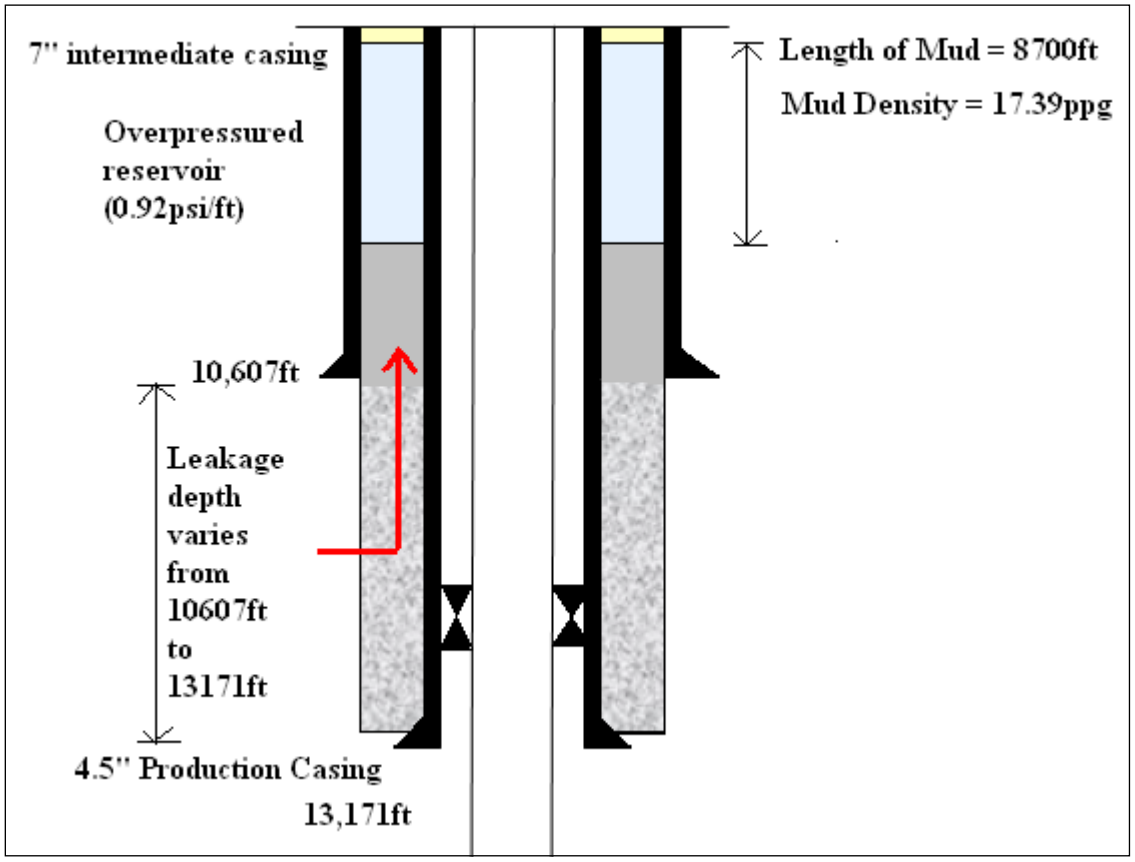

Figure 4.5.1 - Schematic of wellbore Case Study 1 and leakage scenario (Huerta, 2009).

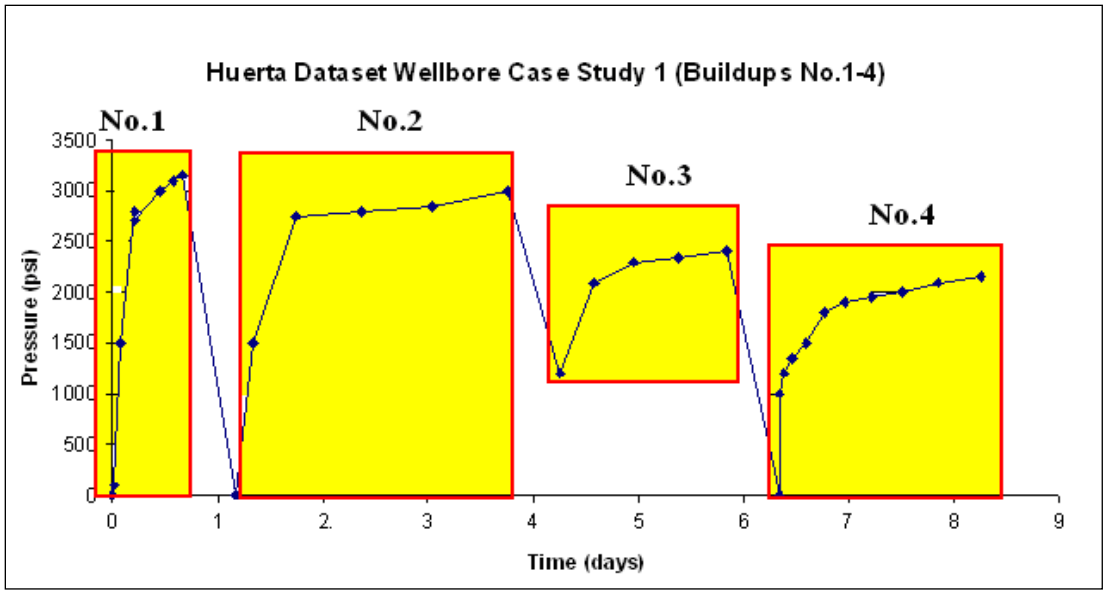

Figure 4.5.2 - Pressure buildups for wellbore Case Study 1 (Huerta, 2009).

4.6 British Columbia Oil and Gas Commission Wellbore Dataset

A leaky wellbore dataset from the British Columbia Oil and Gas Commission (Parsonage K. Personal Communication 2011) consisted of a large number wellbores (350+) that demonstrated recorded SCVF. The leaky wellbores have been classified into different subsets by their flow rates (m^3/day) (Fig. 4.6.1). There were a significant number of wellbores (100+) that demonstrated low flow rates, between a range of 0.1 m^3/day and 1.0 m^3/day. Fewer wellbores (50+) demonstrated moderate flow rates, between a range of 1.0 m^3/day and 2.0 m^3/day. A large number of wellbores demonstrated high flow rates (200+), between a range of 2.0 m^3/day and 1500 m^3/day.

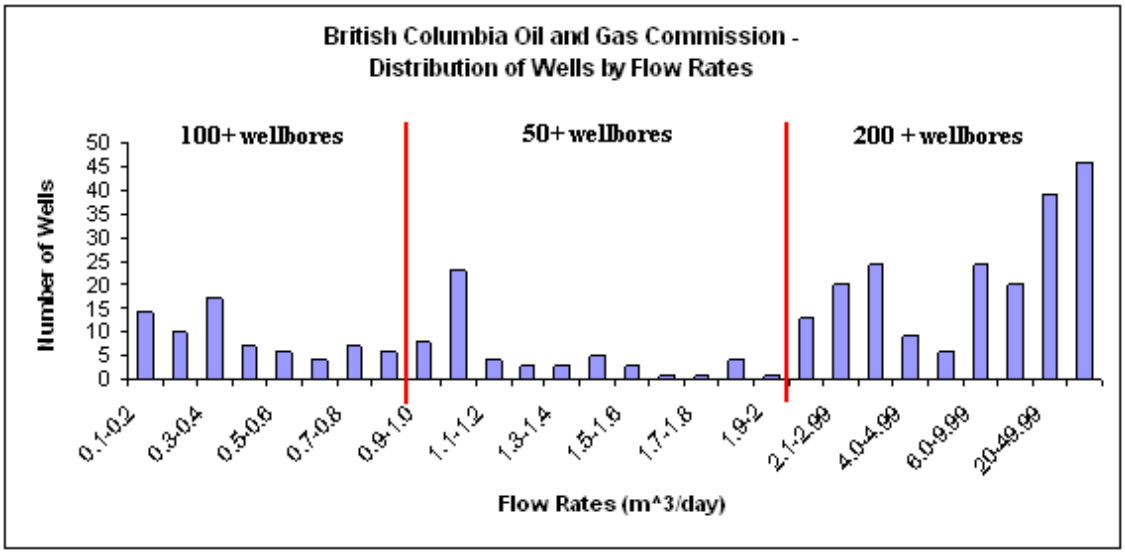

Figure 4.6.1 – Distribution of Wells by Flow Rates

Due to the large number of wellbores in the dataset, individual raw wellbore construction information was not provided in this chapter, however it was included in the appendix (A.02). The original BC Oil and Gas Commission dataset provided detailed wellbore construction information (casing sizes, depths, hole sizes, cement volume, etc), pressure on annulus (not pressure vs. time), and flow rates. From the original 350+ wellbores, the number of wellbores that could be analyzed was reduced to a total of 210+ wellbores. For these wellbores, the leakage depth was assigned at two depths (upper casing string depth and lower casing string depth) and the flow rate information was compiled to generate leakage path permeability distribution from the (SCVF) model, as described in Chapter 6.

Chapter 5: Methods to Reduce Uncertainty

CHAPTER 5 OVERVIEW

The six leaky wellbore datasets, consisting of 238 wellbores described in Chapter 4 provided various amounts of detailed information that could be used as inputs to the SCP model or SCVF model to estimate the effective permeability of the leakage pathway. The quality and amount of information that was provided varied from wellbore to wellbore, within the specific dataset. When the wellbore parameter value was clearly defined in the original dataset, this value was used. The unknown parameter values were bound by a range usually on physical grounds (range of leakage depths, range of mud densities, etc.) or described by a frequency distribution based on estimates for which the parameter value was most likely and least likely to be. The existence of unknown parameters meant that a single value of effective permeability could not be estimated from the pressure buildup. Instead a range of effective permeability was obtained, depending on the range within which the unknown parameters varied.

It is of interest to determine whether the uncertainty in the estimate of effective permeability can be reduced. In Chapter 4, the wellbore information in each of the datasets was provided. Different types of data were used to reduce uncertainty. For example, maximum buildup pressure levels identified possible leakage source depths and mud lengths. Wellbore construction information about cement slurry volume also provided an alternative for estimates of leakage source depths. For a given wellbore, different methods were applied to produce a series of comparable ranges of effective permeability. The goal of applying the different methods to the datasets was to reduce uncertainty in leakage path permeability. The following methods have been developed and applied to the datasets:

(1) **Maximum Pressure Method** – For each individual pressure buildup dataset, the highest pressure value (maximum pressure) recorded was assumed to be the asymptotic pressure. That is, the leakage was assumed to have stopped when the annulus reached that pressure. This reduces uncertainty in two unknown parameter values; length of mud, and leakage depth by imposing a relationship between mud density and leakage depth, as seen in Eq. 5.1.1. For an assigned mud length, the leakage depth will increase to compensate for the additional pressure (hydrostatic gradient of the mud density). The new parameter values, used to describe the leakage scenarios, are used as inputs to the SCP model when generating leakage path permeability values.

Maximum and minimum permeability values were only generated by changing two unknown variables, leakage depth and mud length, across their range of plausible values. As demonstrated in Chapter 4, the leakage depths ranged from the upper casing string to the lower casing string. In most cases, the maximum pressure level recorded in the pressure buildup plus the hydrostatic pressure due to completion mud corresponded to a appropriate leakage depth within these values. There were a few cases of high pressure levels and shallow casing depth intervals where using Eq. 5.1.1 generated a leakage depth beneath the lower casing string. However, for the majority of the wellbores, the maximum pressures corresponded to leakage sources within the appropriate casing depth interval provided.

(2) **Cement Slurry Method** – Wellbore construction information compared the annular space to the amount of cement slurry volume pumped into this space. The length of the cement column was calculated directly from this data, and the remainder of annulus was assumed filled with completion mud. This eliminates uncertainty in two key model inputs, the length of mud column in the annulus and the location of the top of cement. The latter determines the length of the leakage path, given the depth of the

leakage source. Maximum and minimum permeability values were generated by changing the leakage depth (1 unknown variable) across a range of plausible values.

(3) **Monte Carlo Method** – For unknown parameter values, an uniform probability distribution was assigned for each of the parameters. When using the Monte Carlo Script, a parameter within the range of values was selected and then combined with the other selected wellbore parameter values to produce an output of leakage path permeability. This selection process was repeated for 10,000 runs in order to generate a distribution of leakage path permeability. This does not reduce uncertainty but does quantify it and enable the user to estimate an expected value of leakage path permeability. The expected values are used to generate an effective permeability distribution that is compared with the permeability distribution of Celia et al. in Chapter 6.

5.1 Summary of the Maximum Pressure Method

The Maximum Pressure Method focused on each pressure buildup data interval to determine the leakage depth / entry point to the system. This method was applied to the all of the wellbore datasets that contained sustained casing pressure buildup data. For each pressure buildup interval, the measured asymptotic or maximum pressure level was used to create different leakage scenarios. The maximum and minimum leakage path permeability values correspond to different lengths of mud used. As can be observed from the raw pressure buildup data intervals in Chapter 4, not every buildup exhibited a well defined asymptotic pressure value. Frequently the operator vented the surface wellhead of the intermediate annulus space, while the pressure was still increasing. The maximum pressure method makes the assumption that the largest pressure recorded

during a buildup would be the asymptotic pressure, had the buildup been allowed to continue.

When the intermediate annulus space reaches an asymptotic pressure value during a buildup, this is a good indication that leakage has stopped. The pressure at the top of cement (due to the hydrostatic head of completion fluid plus the gas cap) has equaled the pressure at the leakage depth. Since the pressures have equalized, the potential gradient between the leakage source and the top of the leakage path through the cement has declined to zero. The following pressure balance equation expresses this condition, relating the asymptotic pressure level to the system's parameter values:

$$p_{\max} + 0.052\rho_{mud} \bullet l_{mud} = \qquad (5.1.1)$$

$$0.445d_{water} + 0.052\rho_{mud1}\ d_{cas1} + 0.052\rho_{mud2}(d_{leak} - d_{cas1})$$

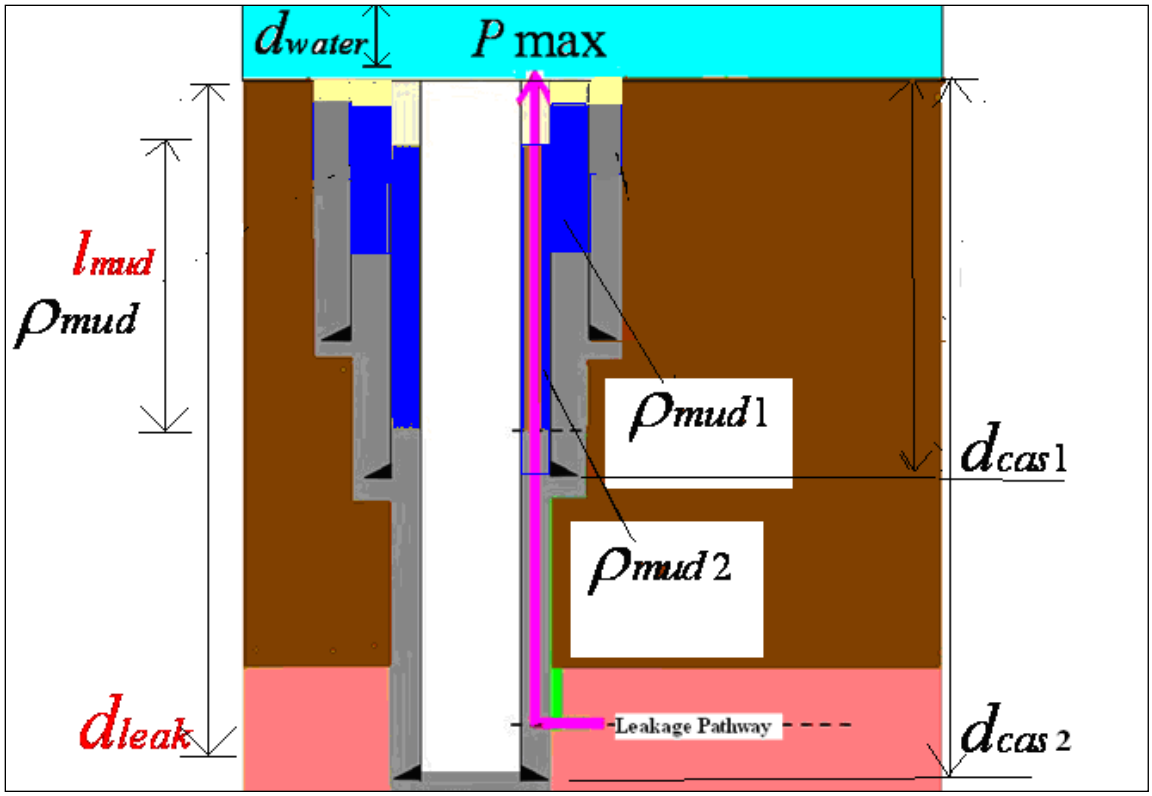

Figure 5.1.1 – Schematic of the equation Eq. 5.1.1 with defined variables

Eq. 5.1.1 is a pressure balance equation of the intermediate annular space. For most wellbores, the two unknown variables (highlighted in red) are length of mud, l_{mud} and leakage depth, d_{leak}. The leakage depth variable, d_{leak} (units of ft) was set to minimum and maximum feasible depths to solve for maximum or minimum leakage path permeability values.

The left hand side of Eq. 5.1.1 describes the fluid pressure at the top of the cement column in the annulus at the end of the buildup interval. Maximum pressure, P_{max} is the highest recorded pressure level (psi) of the buildup interval. The mud density ρ_{mud} was provided in the drilling/completion report, given in units of pounds per gallon (ppg). To convert this value to units of psi/ft, a conversion factor of 0.052 was used. Length of

mud, l_{mud}, given in units of ft, was either solved for, given the leakage depth, or it was fixed to prescribed value. This depended on whether the objective was to solve for maximum permeability or minimum permeability.

The right hand side of Eq. 5.1.1 represents the pressure at the leakage source. The water depth for the offshore dataset, d_{water} was provided at 350 ft, the average water depth of production activity. For onshore datasets the water depth, d_{water} is set to zero. The seawater pressure gradient is 0.445 psi/ft. The mud density that was used to drill the upper portion of the hole, ρ_{mud1} reached the depth of the upper casing shoe, d_{cas1}. The mud density was given in units of ppg, so it was multiplied by 0.052 in order to convert pound per gallon (ppg) to a pressure gradient in units of psi/ft. The mud density that was used to drill the lower portion of the hole, ρ_{mud2} reached the depth of the lower casing shoe, d_{cas2}. However, since mud density is used as a proxy for pore pressure, the mud density, ρ_{mud2} would only extend from the depth of the upper casing shoe, d_{cas1} to the leakage depth, d_{leak}, hence using the length measurement, $(d_{leak} - d_{cas1})$ instead.

The drilling report for each wellbore contained detailed information about the mud densities used to drill each hole section of the completed well. Usually, deeper wells require several different completed sections to compensate for higher pore pressures and adequate drilling mud density to prevent from taking "kicks" and to avoid fracturing the formation. Most of the Offshore wellbores were drilled with one surface hole size and several intermediate hole sizes, therefore the right hand side of Eq. 5.1.1 changed. There would instead be several different mud densities and casing string depths.

The operator also recorded the casing shoe depths, TMD and TVD in units of ft. and the angle of deviation from vertical. As discussed previously, the difference in mud weight used for setting casing depths served as a proxy for pore pressure. Because the

pore pressure gradient can vary with depth, this information gives a better estimate of maximum pore pressure in a formation than the standard assumption of 0.465 psi/ft. This estimate gives a maximum value of pore pressure because conventional drilling is conducted in an overbalanced state, i.e. the mud weight exceeds the pore pressure of the formation being drilled.

Equality between left hand and right hand sides of Eq. 5.1.1 represents a balance between pressures at the inlet and outlet of the leakage path through the cement, under the assumption that the density of the gas phase filling the leakage path is negligible. The Maximum Pressure Method provided minimum and maximum leakage path permeability values, depending on the choices made for unknown parameters. The utility of Eq. 5.1.1 is that it provides a relationship between the (unknown) leakage depth, d_{leak} and the (unknown) length of the mud column, l_{mud} in the annulus. This method reduces the range of uncertainty in the permeability, since the mud length and leakage depth cannot be varied independently across their ranges.

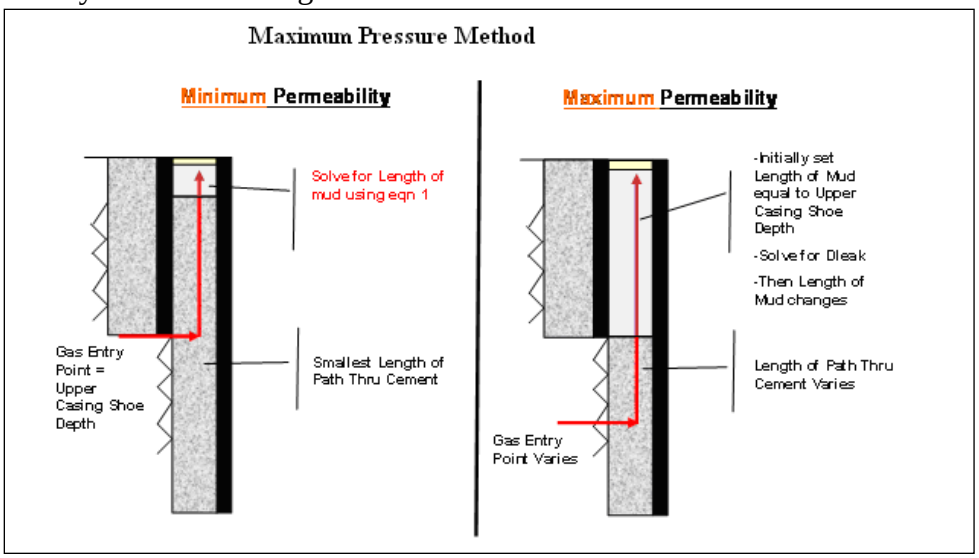

Figure 5.1.2 – Schematic of Maximum Pressure Method Leakage Scenarios. Left side is for determining minimum permeability. Right side is for determining maximum permeability.

For the maximum permeability value calculation, the largest length of mud possible (upper casing shoe depth) was used, right panel of Fig. 5.1.2. The corresponding leakage depth computed from Eq. 5.1.1 is generally located at or near the bottom casing depth, where the formation pressures are very high. To calculate the minimum permeability value, the gas entry point is set at the upper casing shoe depth and then length of mud is solved using Eq. 5.1.1. The hydrostatic head of the completion fluid plus the pressure of the gas cap are balanced by the formation fluid pressure at the entry point to the system. When the formation pressure exceeds the pressure of the hydrostatic fluid head, formation fluids will enter the system and migrate to surface.

This approach was only used for the offshore wellbore dataset, since complete drilling mud information was provided. For the other datasets, different pressure balance equation was used (5.1.2). If mud density was not provided in the dataset, a mud density, ρ_{mud} of 11.6 ppg was assumed.

$$p_{\max} + 0.052\rho_{mud} \bullet l_{mud} = 0.465 d_{leak} \qquad (5.1.2)$$

In order to generate maximum and minimum permeability values, the same process described above for offshore wells was followed. The length of mud was fixed, and then the leakage depth was solved from Eq. 5.1.2. Or the leakage depth was fixed, and the length of mud was determined. The combination of these values created a leakage scenario, which was run using the SCP buildup model.

5.2 Summary of the Cement Slurry Method

The Cement Slurry Method was applied to a total of 17 wellbores (Offshore dataset, Xu dataset, Huerta dataset) that contained annular cement slurry volume and

wellbore construction information. The length of cement was a fixed input parameter value in the SCP model for generated outputs of leakage path permeability. The results from the Cement Slurry Method were compared to previously generated permeability results that were generated from the Maximum Pressure Method. One of the important differences between the two methods was that the length of mud and length of cement were both fixed values for the Cement Slurry Method. The Maximum Pressure Method, in contrast, relates the two values by Eq. 5.2.1 but does not fix either value. .

The mechanics of the Cement Slurry Method was to compare the volume of pumped cement slurry to the available open intermediate annular space (between the formation and steel casing string). For most wellbores, the cement slurry volume was provided in units of raw sacks of cement. The number of sacks was multiplied by the yield factor (ft^3/sacks) to generate the cement slurry volume (ft^3). As can be observed in Figure 5.2.1, the top of cement was calculated by first subtracting the cement slurry volume (ft^3) by the annular space above the lower casing shoe (ft^3). The remaining volume is then divided by the area (ft^2) between the upper casing string (outer diameter) and the lower casing string (inner diameter). This length of cement is subtracted from the depth of the upper casing string. The top of cement is measured relative to sea level.

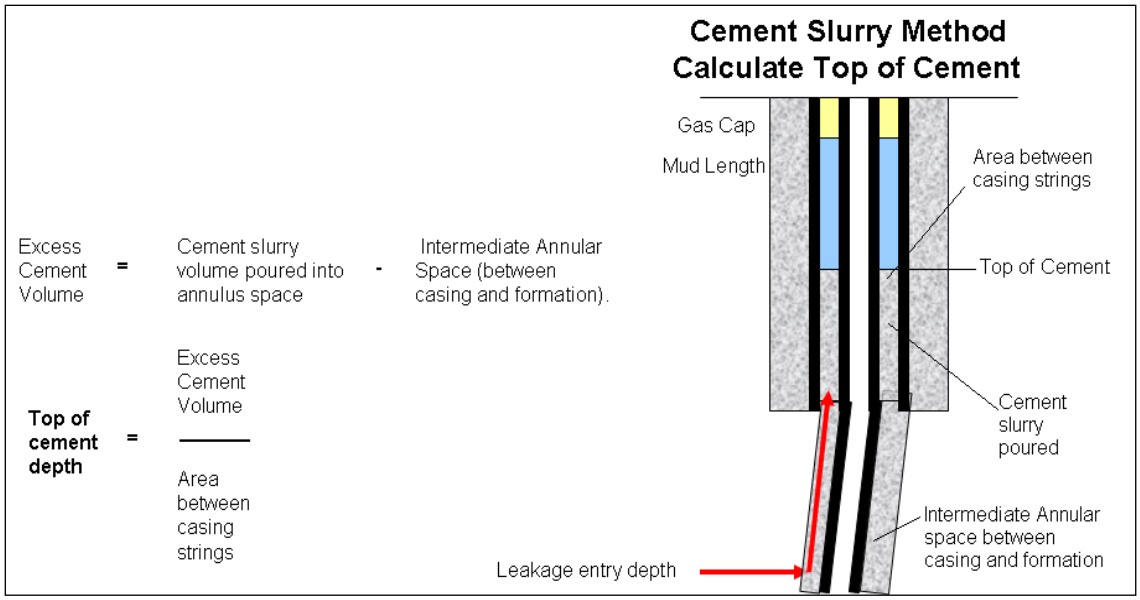

Figure 5.2.1 – Schematic of calculating top of cement, relative to sea level, for example wellbore.

During well completion (post-cementing), completion mud (density in ppg) remained in the annulus space, located above the top of cement. The length of cement and the length of completion mud are key input parameter values for the SCP model

Since little to no data was made available identifying the leakage depth/ entry points to the annulus space, this parameter was the unknown value in the application of the SCP model to estimate leakage path permeability. Therefore, to generate a range of leakage path permeability, the leakage depths were varied within a defined range, namely between upper and lower casing shoe depths. When generating a minimum permeability value, (left panel of Fig. 5.2.2), the leakage depth was fixed to the lower casing string depth. The gas entered the system at the deepest depth possible, and migrated over a large length of cement, before reaching the mud column and accumulating in the surface gas cap. At the appropriate permeability value, the SCP model output matched the raw pressure data set with minimum errors.

When generating a maximum permeability value (right panel of Fig. 5.2.2), the leakage depth was set to the upper casing string depth. The gas entered the system at the shallowest point possible, and migrated over a small length of cement before reaching the mud column, and accumulating in the surface gas cap. The SCP Model produced an appropriate leakage path permeability value.

In rare cases, the cement slurry volume exceeded the annulus space which limited the mud column height to near zero lengths. However previous research findings showed that during drilling operations, drilling mud that contacts the formation rock can cause the hole to enlarge due to washout (Nelson, 1990). Hole enlargement can be as much as 10 to 15% larger than the bit size, depending on the interaction between the formation and the drilling mud (Chenevert, 1986). In these rare cases, enlarging the hole-size/annular space provided sufficient volume to accommodate the pumped cement slurry volume.

As an example calculation, the following is the Cement Slurry Method applied to an example wellbore.

<u>Given data (example wellbore):</u>
Number of cement sacks = 791
Yield Factor = 1.6
Upper casing depth = 2000ft TVD, 2002 ft TMD.
Upper casing depth deviation from vertical = 2.5 degrees
Annular area between upper, lower casings = 0.56 ft^2
Lower casing depth = 4202ft TVD, 4255 ft TMD.
Lower casing depth deviation from vertical = 9 degrees
Annular area between formation and lower casing = 0.76 ft^2

Step (1) Calculate cement slurry volume by multiplying the number of sacks of cement by the yield factor per sack.

Cement slurry volume = (791sacks)(1.6 ft^3/sack) = 1266 ft^3

Step (2) Calculate the height of the top of cement which has filled the annular space between the outer diameter of the steel casing and the formation.

Annular Space Available = 1266 ft^3 - [(4255ft – 2002 ft) (0.76 ft^2)] = 446 ft^3
Length of Space Available = 446 ft^3 / 0.76 ft^2 = 587 ft
Length of Cement = 2253 ft – 587ft = 1666 ft TMD.
Length of Mud = 2002 ft + 587 ft = 2589 ft TMD.
Length of Cement = 1666 ft cos (9°) = 1645 ft TVD
Top of Cement = 2000 ft TVD + 587 ft cos (9°) = 2580 ft TVD

Step (3) Calculate the length of completion mud located above the top of cement.

Length of Mud = 2580 ft TVD

Step (4) Since length of mud does not reach the upper casing string depth, assign leakage depths at either 10 ft below TOC or at the lower casing string seat depth.

Therefore, leakage depths range from 2590 ft TVD to 4202 ft TVD.

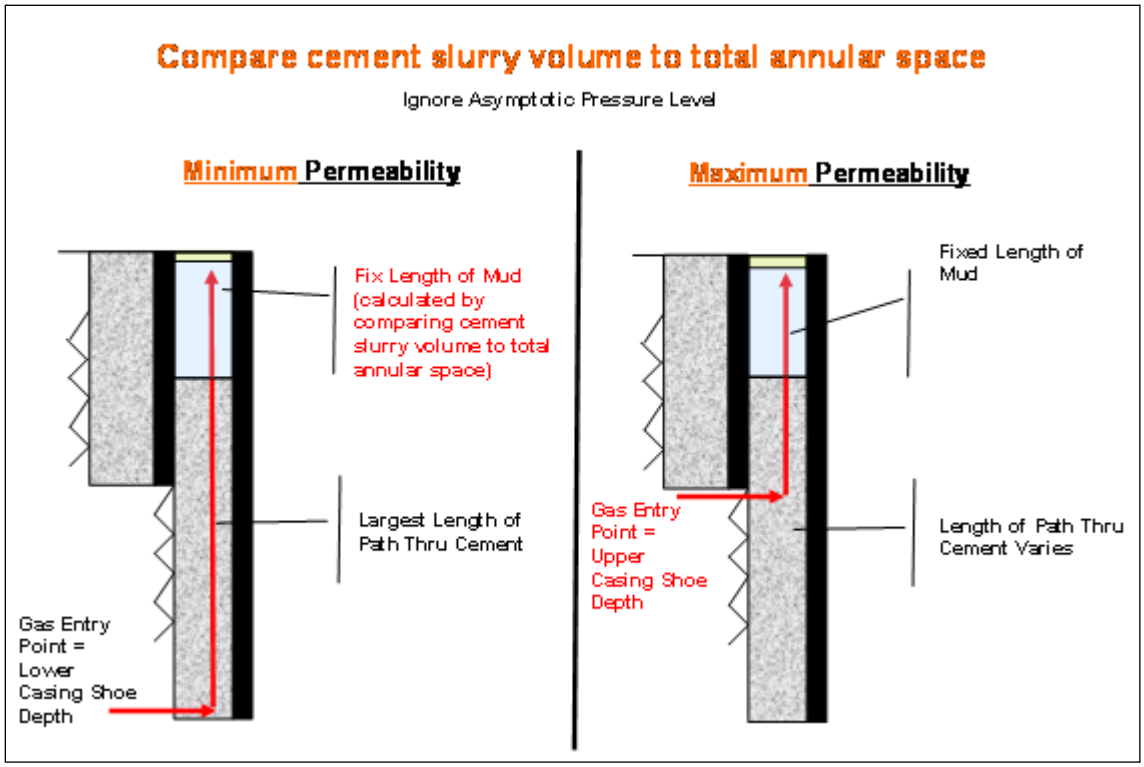

Figure 5.2.2 - Cement Slurry Method leakage scenarios. Boundary conditions for selection of the gas entry at the two casing shoes provided a means to estimate the maximum and minimum permeability, respectively.

The Cement Slurry Method was applied to all of the datasets; however, not all of the wellbores in the datasets contained cement slurry volume information. Therefore, the length of mud could not be determined and assigned a fixed value in these cases. The wellbores and datasets that were omitted include the following: From Watson dataset, wellbores O8, J9, Q7, Q9, J10, N8; from the Xu dataset, wellbores 19, 23, 23; from Bourgoyne's dataset, wellbores case history 1, 2, 3.

5.3 SUMMARY OF THE MONTE CARLO METHOD

The Monte Carlo Method was applied to all the wellbore datasets in order to generate maximum, most probable/expected, and minimum permeability values for each pressure buildup interval. The Monte Carlo Method results are used for comparison with the results from the Maximum Pressure Method and Cement Slurry Method. Rather than assign values to unknown wellbore characteristics, a probability distribution described the frequency and range of possible values. Within this range, different parameter values were selected based on the uniform probability distribution used to describe different unknown parameter values (i.e. gas cap length, mud density, etc.) The Monte Carlo script/code iteratively ran through numerous loops (10,000) in order to obtain representative samples from the assumed distributions of parameters. This results in a frequency distribution of leakage path permeability values that fit the measured pressure buildup (Fig. 5.3.1).

For each wellbore, the parameter values describing the characteristics of the wellbore were identified as either being a known value or an unknown value. The following were unknown parameter values:

(1) Leakage depth

(2) Mud length

(3) Mud density

A three digit combination, (1 = parameter value was provided, 0 = parameter value was not provided) was assigned to each leaky wellbore. This combination corresponded to 1 out of 8 different Monte Carlo scripts that could be applied to the leaky wellbore dataset.

For example, wellbore 1 from the Cement Slurry Section (5.2) the leakage depth was not provided, but mud length was calculated, and mud density was provided, then three digit combination was (0,1,1). The leakage depth was assigned a uniform distribution ranging from X590 ft TVD to X202 ft TVD. Mud length was fixed at X580 ft TVD. Mud density was described as having a uniform distribution, ranging from 8.9 ppg to 14.3 ppg.

Although one leaky wellbore could have multiple pressure buildups, the same 3 digit combination/ script was used to describe the leakage scenarios for all pressure buildups. The Monte Carlo Method script generated a range of permeability values for each pressure buildup. The range of permeability values does not vary widely from the most probable, mean value. The typical permeability value distribution could be described as a log normal frequency distribution skewed towards the maximum possible value. The expected value of permeability is the most probable value in the distribution. The confidence interval (low, high permeability values) is defined as a statistical method used to estimate the population parameters.

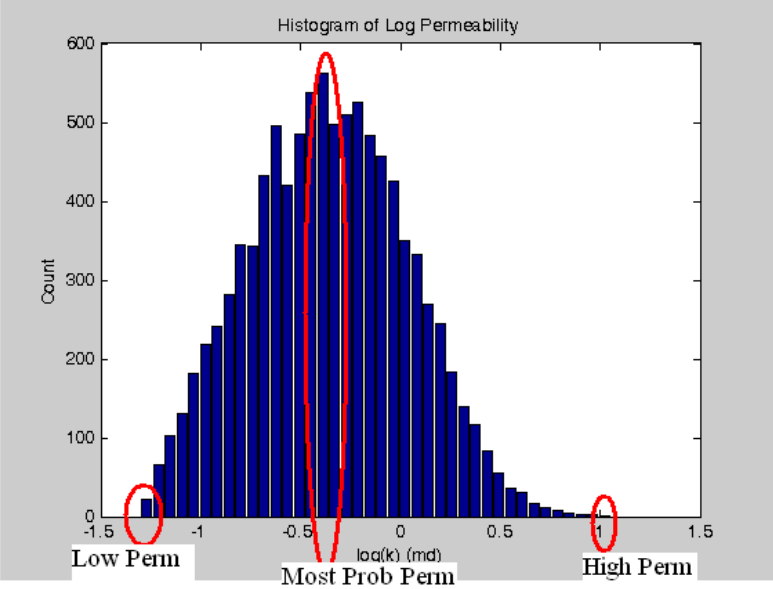

Figure 5.3.1 – Permeability Frequency Distribution from the Monte Carlo Script.

For this example output from the Monte Carlo Method, the frequency distribution of permeability values closely matched a normal frequency distribution. Therefore, the most probable/expected permeability value (0.398 md) is the mean value. Since the x-axis is reported in log scale, the value taken from the axis should be raised to the power of 10. For example, the following permeability values were calculated from the range in figure 5.3.1:

(1) Low permeability, log(k) = -1.25 md, or $10^{-1.25}$ md = 0.056md.

(2) Most probable permeability, log(k) = -0.40 md, or $10^{-0.40}$ md = 0.398 md.

(3) High permeability, log(k) = 1.05 md, or $10^{1.05}$ md = 11.22 md.

The calculated range of permeability used for comparison purposes is 0.056 md to 11.22 md, covering three orders of magnitude. For each pressure buildup, a new permeability distribution was generated. In these cases, the permeability distribution may not closely match a normal distribution. Therefore, the most probable or expected

permeability value and mean values are different. When applied to each wellbore in the entire dataset, a frequency distribution of leakage path permeability is generated.

5.4 Conclusion: Utility of Applying Three Different Methods to the Datasets

The purpose of applying the three different methods to all the wellbore datasets was to leverage the known wellbore data to reduce the uncertainty of unknown values. For each leakage scenario, a robust range of leakage path permeability values was generated. It was instructive to then compare the permeability results from the different datasets analyzed. Since the complete set of information was rarely provided, assumptions had to be made in order to generate comparable results between the datasets. The differences in permeability were due to the assumptions made to characterize unknown parameter values. The application of each of the methods described provided results in Chapter 6, for the selected pressure buildup intervals.

Chapter 6: Leakage Path Permeability Distribution Results

CHAPTER 6 OVERVIEW

The effective permeability values for the wellbore pressure buildups in all the dataset are displayed and analyzed in this chapter. Data interpretation provides answers to the research questions for this thesis: how can analyzing characteristics of leaky wellbore conduits provide evidence supporting the development of carbon sequestration projects in the long term?

This chapter is broken into the following 4 sections:

(1) The first section discusses the effective permeability results of applying the Cement Slurry Method and the Maximum Pressure Method to all the leaky wellbore datasets. By comparing the effective permeability results, a distinction can be made between these two methods. Overall, the Maximum Pressure Method yields larger values of leakage path permeability, as compared to the Cement Slurry Method.

(2) The second section summarizes the effective permeability results from the Monte Carlo Method, which provides a detailed distribution of effective permeability for all wellbore datasets. The Monte Carlo Method assigned probability distributions to unknown parameter values, and the script ran through 10,000 iterations to select combinations of inputs to produce a distribution of permeability. The analysis of these results helps identify trends in data.

(3) The third section provides a summary of the results of conducting a sensitivity analysis on certain parameters. By changing these input parameter values in the model, and holding all other parameter values constant, trends in leakage path permeability are identified. For example, increasing gas cap length (from 0 ft to 10 ft) had a large effect

on increasing permeability values. Other changes to input parameter values had less of an influence on altering the leakage path permeability outputs.

(4) The final section demonstrates the usefulness of applying known leakage path permeability values to plausible carbon sequestration projects. For example, when analyzing the leakage risk associated with CO_2 sequestration, a migrating CO_2 plume from an injection well may reach a crack/conduit in the cement-filled intermediate annulus of an existing wellbore. Because bulk phase CO_2 is non-wetting phase, it will not enter the crack unless the capillary pressure of the plume exceeds the entry pressure of the crack. Thus the properties of the crack and the height of the gas plume determine whether migration will occur, and if so, at which rate. This type of analysis provides regulators with the ability to forecast CO_2 leakage fluxes for such wellbores.

6.1 MAXIMUM PRESSURE METHOD RESULTS VS. CEMENT SLURRY METHOD RESULTS

The application of the Maximum Pressure Method and the Cement Slurry Method to the leaky wellbore datasets was to narrow the range of possible leakage depths/sources from different sets of information/data provided. Since the leakage source depth was rarely identified and incomplete wellbore construction information was often provided, the utility of these methods was to reduce the range of permeability values. These results between the two methods were used for comparison purposes.

First, the leakage path permeability values for all the datasets are analyzed in detail. The permeability results of the Offshore dataset span five orders of magnitude (Fig. 6.1.1), from 0.0001 md to 10 md. Due to the magnitude of the range in values, the leakage path permeability (md) is plotted in log-scale on the y-axis. For each wellbore, in the dataset, the permeability values are grouped together in a grey-red colored box,

which displays the range of permeability values generated. The boxed-in region and ovals do not represent values. These shapes are used to identify the permeability values between the two different methods for each wellbore (Fig. 6.1.1).

The first oval (yellow) contains the maximum permeability (magenta colored point) and minimum permeability (blue colored point) generated from the Maximum Pressure Method. The second oval (light blue) contains the maximum permeability (magenta colored point) and minimum permeability (blue colored point) generated from the Cement Slurry Method. The two consecutive ovals connected by a straight vertical line represent the permeability values from the same pressure buildup interval. The grey color within the boxed-in region represents permeability ranges greater than the upper level of intact cement (0.020 md). The dark red color within the boxed-in region represents the upper range of cement permeability (0.020 md - 0.001 md). The light red color within the boxed-in region represents the lower range of cement permeability (less than 0.001 md).

In some cases, there is only one permeability value data point within the respective oval. This is a situation in which the SCP Model was unable to generate a close fit to the field data, so the permeability value was not reported. In a few cases, the maximum and minimum permeability values nearly coincide, making the appearance that there is only one point, when there is actually two values, a maximum and minimum permeability.

It is instructive to compare the leakage path permeability values between the Maximum Pressure Method (yellow) and the Cement Slurry Method (blue) in order to identify trends in data (Fig. 6.1.1). For the Offshore dataset wellbores 1,2,3,4,5, the Maximum Pressure Method (yellow) generated larger leakage path permeability than the Cement Slurry Method (blue). For wellbores 8 and 9, the Maximum Pressure Method

(yellow) generated smaller permeability values than the Cement Slurry Method (blue). For wellbores 6 and 7, there are mixed results.

There is little correlation between permeability and time, and this will be discussed further in Section 6.2.4 – Changes in Permeability Over Time. Originally, it had been hypothesized that the leakage path permeability values would increase over time due to gas entering the conduit and increasing the size of the aperture. When the leakage conduit increased in diameter, there would be higher permeability values for the same amount of gas entering. However, the data did not support this hypothesis.

As can be observed in Fig. 6.1.1, for wellbore 1, the permeability values increased slightly over time. For wellbore 2, the permeability values decreased, and then increased over time. For wellbore 5, the permeability values increased over time. For 6, the permeability values decreased, then increased, and then decreased over time. For wellbore 7, the perm values decreased over time. For wellbore 9, the permeability values decreased over time. Therefore, the results are inconclusive and the hypothesis cannot be proven true.

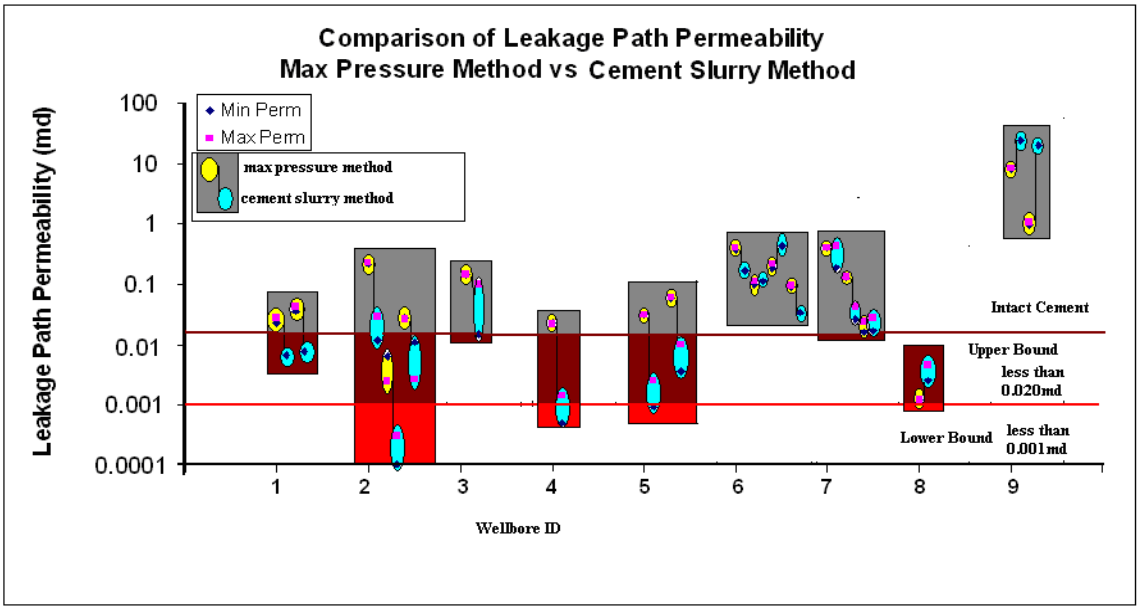

Figure 6.1.1– Leakage path permeability distribution for Offshore dataset. Comparison of permeability values between Maximum Pressure Method (yellow) and Cement Slurry Method (blue).

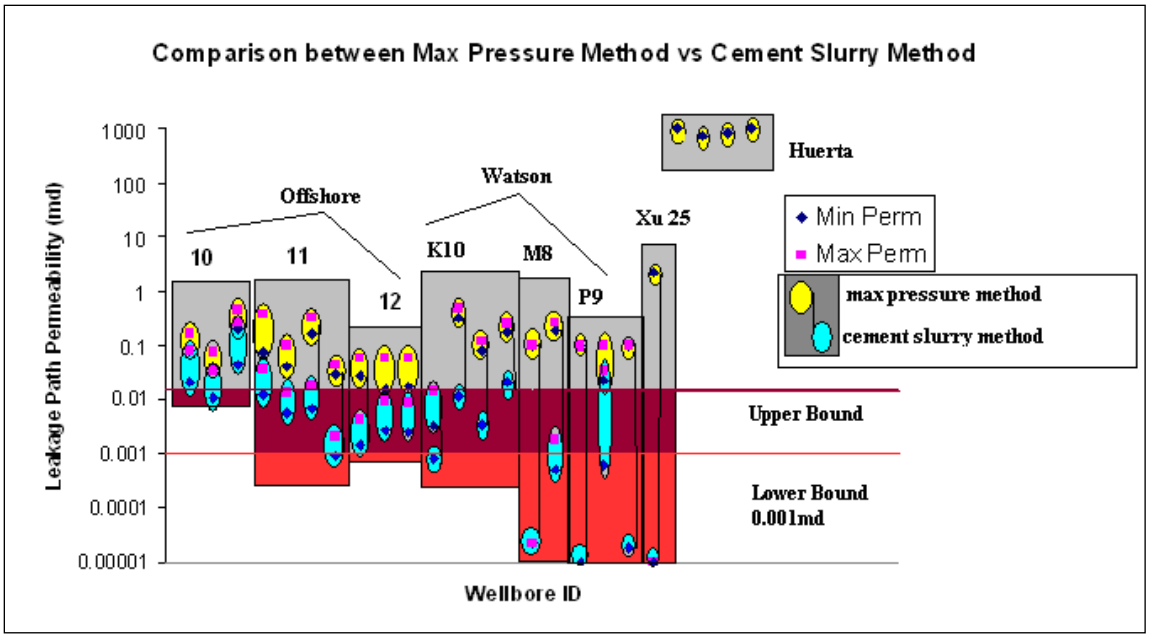

Figure 6.1.2– Leakage path permeability distribution for Offshore, Watson, Xu, and Huerta datasets. Comparison of permeability values between Maximum Pressure Method (yellow) and Cement Slurry Method (blue).

For Fig. 6.1.2, the permeability values for the other datasets (Watson, Xu, and Huerta) are plotted. The same color scheme/shapes are used to identify maximum, minimum permeability values for the two methods, and clarify the bounds of intact cement. The first three wellbores (10, 11, and 12) are from an original subset of the Offshore wellbore dataset. These results are a comparable range (0.001 md to 1 md) to the results of Fig. 6.1.1, and are generally larger than intact cement.

The next three wellbores in Fig. 6.1.2 (K10, M8, P9) are from the Watson dataset. Not all of the wellbores could be used due to insufficient cement slurry information. Therefore, the length of mud, length of cement could not be fixed. In general, the results of the Watson dataset demonstrate a larger difference in permeability values between the Maximum Pressure Method and the Cement Slurry Method. The lower range of

permeability values (Cement Slurry Method) is between 0.001 md to 0.00001 md (Fig. 6.1.2), which is within levels of intact cement.

The next wellbore permeability result in Fig. 6.1.2 is from Xu's dataset (wellbore 25). There is also a very wide range of permeability values between the methods (5 md to 0.00001 md). The final wellbore result is from Huerta's dataset. The Cement Slurry Method was not applied to this dataset. This wellbore had very high pressure buildup rates (several 1000's psi/day). The permeability values are at the very highest end of the range (near 1000 md), several magnitudes greater than any other dataset results.

In aggregate, most of the leakage path permeability values ranged from 0.0001 – 10 md (5 orders of magnitude). In Fig. 6.1.1, there are four pressure buildups from four different wellbores where the permeability value was smaller than the lower bound of intact cement, highlighted with a red line (wellbore 2, buildup No.2 Cement Slurry Method; wellbore 4, buildup No.1 Cement Slurry Method; wellbore 3, buildup No.1 Cement Slurry Method; wellbore 8, buildup No.1 Maximum Pressure Method). In Fig. 6.1.2, there are eight pressure buildups from five different wellbores where the permeability value of the Cement Slurry Method was smaller than the lower bound of intact cement (wellbore 11, buildup No.4; K10, buildup No.1; M8, buildup No.1, No.2; P9, buildup No.1,2,3; Xu 25, buildup No.1).

As has been discussed in Chapter 2, it is impossible that the gas flowed through intact cement; these small values of effective permeability correspond to very small defects in the cement. As can be observed in Fig. 6.1.1 and Fig 6.1.2, most pressure buildups yielded permeability values (grey colored region), ranging from 0.001 md – 1 md, higher than intact cement. Permeability values within this range indicate the presence of defects such as micro-fractures of various aperture widths where gas

migrated to the surface. The sizes of these defects will be analyzed in Section 6.4 of this chapter.

Gas migrates through porous media when permeability is large enough to support movement of gas from zones of high pressure to zones of low pressures. When water is present, the pressure difference must also be large enough to overcome capillary forces in the pathway that prevent movement of a gas/water interface. In these wellbores, the high formation gas pressure forced gas to migrate through highly permeable channels, or fractures. These pathways are conduits for the gas to reach the annulus in the intermediate casing. Without these channels, the gas would not be able to migrate. As seen in Fig. 6.1.1 and Fig. 6.1.2, most leakage pathways are higher permeability than intact cement (0.001 md). This result supports the hypothesis that a properly sealed, cement filled annulus (no cracks) prevents gas from migrating to surface.

6.1.1 Permeability Differences between Maximum Pressure Method and Cement Slurry Method

The permeability values obtained from the Maximum Pressure Method and the Cement Slurry Method generally range between 1-2 orders of magnitude. However, in most cases, the Cement Slurry Method consistently produced significantly lower permeability values than the Maximum Pressure Method, for the same wellbore and same pressure buildup (Fig. 6.1.1 and Fig. 6.1.2). Also, there was a greater range of permeability uncertainty for the Maximum Pressure Method results.

The range in permeability values for a given method was a result of changing mud lengths and leakage depths for a given pressure buildup and wellbore (Table 6.1.1). For example, with the Cement Slurry Method, the mud length was a fixed value (Fig. 5.2.2). The leakage depths varied from the upper casing shoe depth to the lower casing shoe

depth. With the Maximum Pressure Method, the mud length varied and the cement length also varied (Fig. 5.1.2), though it was related linearly to the mud length by Eqn. 5.1.1.

Comparison of Methods

		Leakage Depth	Mud Length	Cement Length
Min Perm	Max Pressure Method	Upper Casing Shoe	Solve using Eqn 5.1.1	Solve using Eqn 5.1.1
Min Perm	Cement Slurry Method	Lower Casing Shoe	fixed	fixed
Max Perm	Max Pressure Method	Solve using Eqn 5.1.1	Solve using Eqn 5.1.1	Solve using Eqn 5.1.1
Max Perm	Cement Slurry Method	Upper Casing Shoe	fixed	fixed

Table 6.1.1 – Comparison of input parameter values for methods.

As a comparison between the two methods, when generating maximum permeability values, the mud length from the Maximum Pressure Method was generally longer than the mud length from the Cement Slurry Method. The leakage depth from the Maximum Pressure Method was generally deeper than the leakage depth from the Cement Slurry Method.

When generating minimum permeability values for the Maximum Pressure Method, the leakage depth was set at the upper casing string depth. For the Cement Slurry Method, the leakage depth was set at the lower casing string depth. Clearly, the leakage depth from the Maximum Pressure Method was shallower than the leakage depth from the Cement Slurry Method. The mud length from the Maximum Pressure Method was generally shorter than the mud length from the Cement Slurry Method. A more detailed discussion of the sensitivity analysis of such parameter values is presented in Section 6.3 – Sensitivity Analysis of Wellbore Parameters.

In summary, for cases in which the permeability values varied significantly between the two methods, the mud lengths and leakage depths were much different. By focusing on different portions of the dataset for each method, it was possible to provide

significantly different inputs to the SCP Model. Therefore, in order for permeability values to be more consistent, these mud lengths and leakage depths would have to be similar. Future work should focus on reconciling the differences in permeability between the two models.

6.2 Monte Carlo Method - SCP Model & SCVF Model Permeability Distribution Results

The Monte Carlo Method that was applied to all of the six datasets generated a range (minimum permeability, most probable permeability, and maximum permeability) of leakage path permeability results. For each leaky wellbore analyzed, a set of input parameter values were entered to the SCP Model or SCVF Model. The unknown parameter values were bound within a range of upper and lower values, described by a probability distribution. For example, the gas cap length was unknown, and a uniform probability distribution described the likelihood of selecting a value between 0 ft and 10 ft. The Monte Carlo script ran for 10,000 iterations, selecting a gas cap length within the given range, each time permeability was generated. Rather than provide a single value of permeability, a frequency distribution of leakage path permeability was generated. Thus, the permeability output was more robust than the results from the Maximum Pressure Method and Cement Slurry Method. Results were generated using wellbores that contained either SCVF data, SCP data, or both. The Monte Carlo Method results were converted to a final permeability distribution that was compared to a previously published permeability distribution by Celia *et al.,* 2008.

6.2.1 Monte Carlo Method - SCP Model Results

At the XIX Computational Water Resources Management Conference, Celia acknowledged that one of the largest degrees of uncertainty of the input parameter values to the leakage model was the distribution of leakage path permeability (Celia, 2012). In his presentation entitled, *"Practical Models for Large-Scale CO_2 Sequestration,'* he stated that it was imperative to model leakage scenarios using an accurate distribution of leakage path permeability based on field measured leaky wellbore data. Celia emphasized that a smaller range of permeability would reduce the uncertainty of fluxes.

Due to the effectiveness of generating robust results, the Monte Carlo Method was applied to all of the wellbores and pressure buildups in each of the six different datasets. The effective permeability results are plotted and grouped together in Fig. 6.2.1.1 by individual wellbore datasets (labels, red boxes). As discussed in Section 5.3 – Summary of the Monte Carlo Method, there were three uncertain parameter values that were assigned uniform probability distributions. Mud density values ranged from 8.9 ppg to 14.3 ppg. Mud length values ranged from 10 ft to several 1000 ft, depending on the wellbore characteristics. Leakage depth values ranged from several 100 ft to several 1000 ft, depending on the wellbore.

By applying the Monte Carlo Method to wellbores with SCP buildup data, permeability distributions with smaller ranges of uncertainty were generated. As can be observed in Fig. 6.2.1.1, the permeability values are located within a medium range (several orders of magnitude) of leakage path permeability (green bar) for wells demonstrating SCP buildups. The most probable/expected permeability values (magenta color) are significantly greater than intact cement (horizontal red line at 0.001 md). The range of most probable permeability spans four orders of magnitude. The minimum permeability values (blue color) are sometimes located lower than that of intact cement.

The most probable/ expected values (magenta color) are located at the upper range of permeability, near the maximum permeability values (yellow color).

The average pressure buildup rates varied from wellbore to wellbore in each dataset. However, as can be observed in Fig. 6.2.1.2, there is a relationship between increasing effective permeability vs. increasing pressure buildup rates. On average, the Offshore dataset had the slowest average buildup rate, followed by increasing buildup rates in the Watson, Xu, Bourgoyne, and Huerta datasets. Effective permeability increased along with buildup rate for each of the datasets.

For each wellbore, multiple pressure buildups were recorded, and each pressure buildup data interval generated a range of permeability values (Fig. 6.2.1.1 - green bar). The minimum (blue dot), maximum (yellow dot), and most probable (magenta dot) permeability values are highlighted for comparison purposes. For the SCP Model generated results, the most probable permeability value is generally located at the upper end of the range of permeability values (green bar) due to the skewed distribution of model generated output permeability, as discussed in Section 5.3 (Fig. 5.3.1).

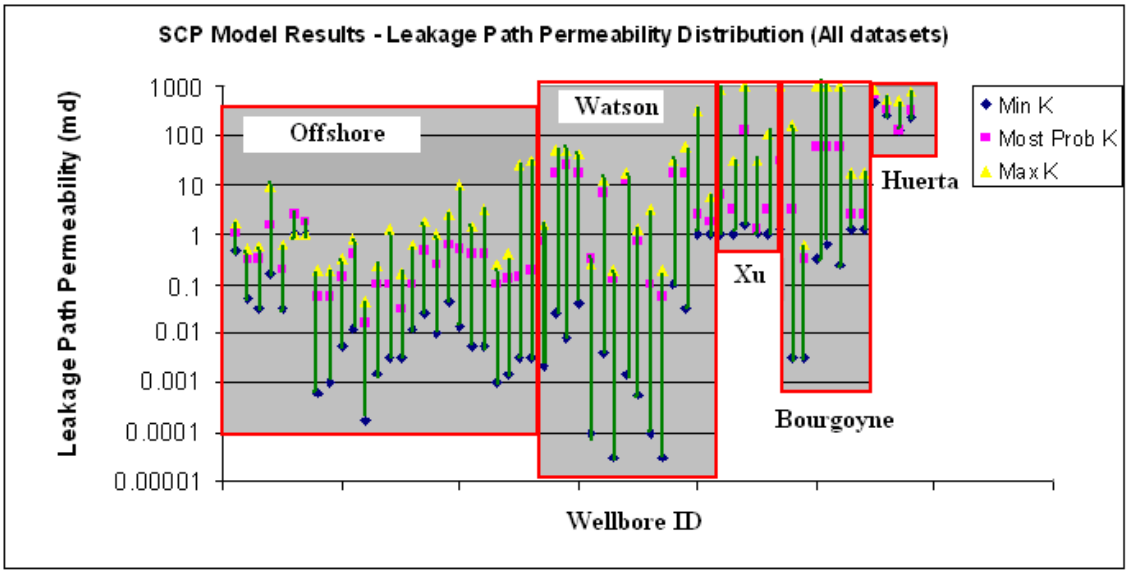

Figure 6.2.1.1 – Leakage path permeability for all wellbore datasets using Monte Carlo Method for the following uncertain input parameters, ranges: mud density [8.9 ppg, 14.3 ppg], length of mud [10 ft, several 1000 ft], leakage depth [upper casing depth, lower casing depth]. The probability distribution for each input parameter was uniformly distributed.

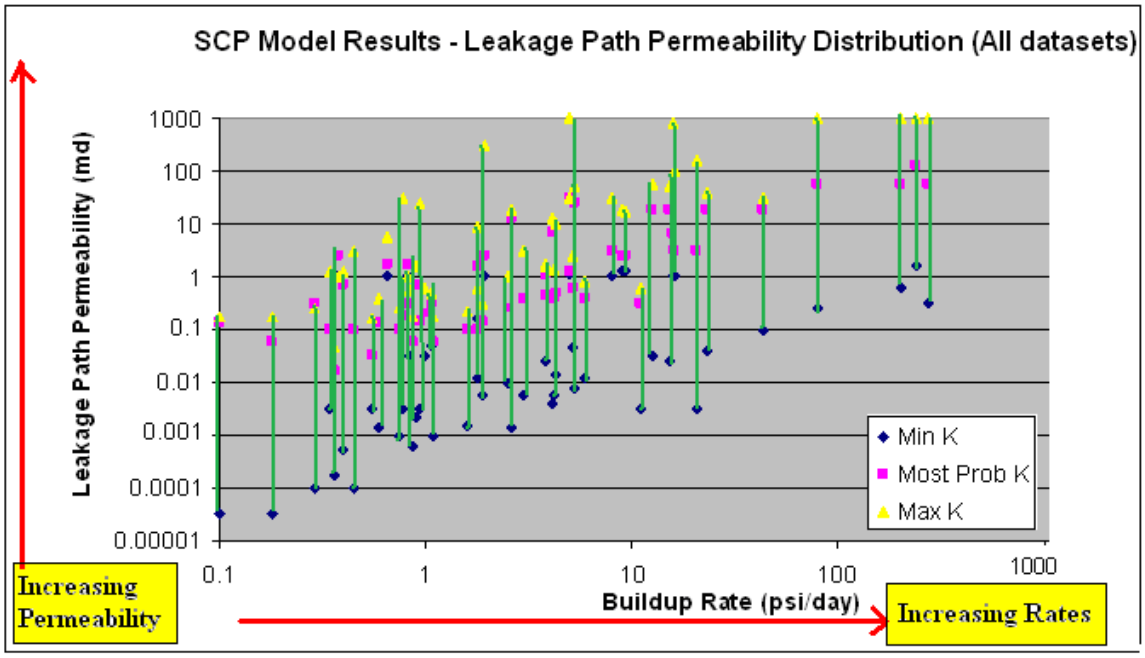

Figure 6.2.1.2 – Leakage path permeability (log-scale) vs. buildup rate (log-scale) for all wellbore datasets, analyzed using Monte Carlo Method (same as Fig 6.2.1.1). Wellbores are not grouped by specific datasets. Increasing trend can be identified, for increasing pressure buildup rates; there are larger leakage path permeability values.

Further analysis of the Monte Carlo Method results for each of the datasets helps to identify trends in permeability. The permeability results of the pressure buildups for individual wellbores are extracted from Figure 6.2.1.1.

For the Offshore dataset, the range of leakage path permeability values for each pressure buildup ranges from one to three orders of magnitude. Figure 6.2.1.3 displays the leakage path permeability distribution for the Offshore dataset. The most probable/expected permeability values (magenta colored dots, light green band) range across two orders of magnitude, between 0.01 md and 5 md.

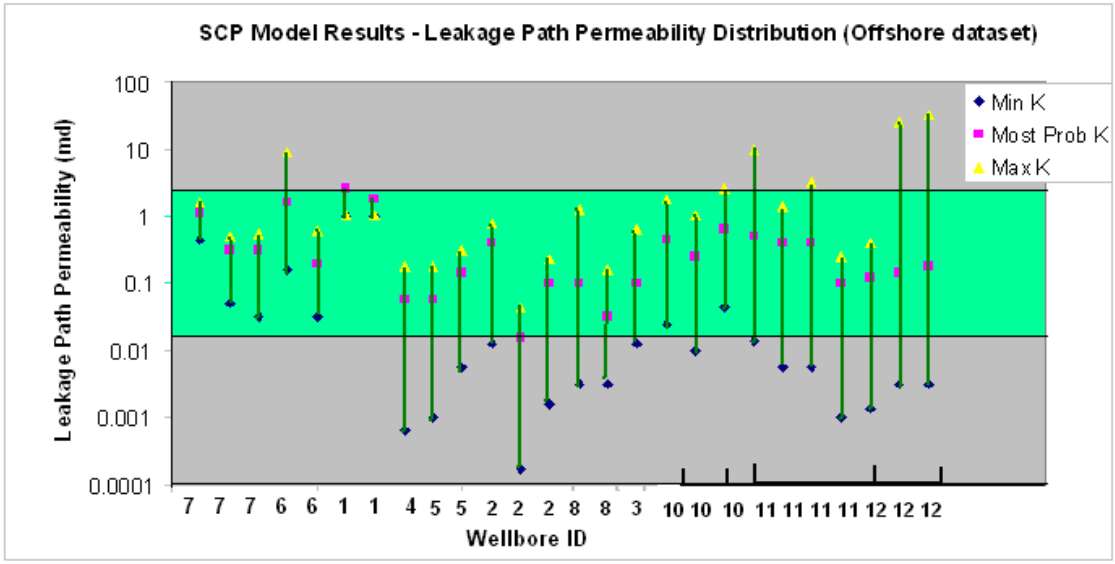

Figure 6.2.1.3 – Leakage path permeability for the Offshore dataset, analyzed with Monte Carlo Method for uncertain input parameters to the SCP Model.

For leakage path permeability results of the Watson dataset, Fig. 6.2.1.1, these results are generally one to two orders of magnitude higher than the results of the Offshore dataset. This can be attributed to the increase in pressure buildup rates. As can be observed in Fig. 6.2.1.4, the most probable/expected permeability values range across less than three orders of magnitude, from 0.05 md to 50 md (light green band), which is higher than the permeability values range from the Offshore dataset (0.01 md to 5 md).

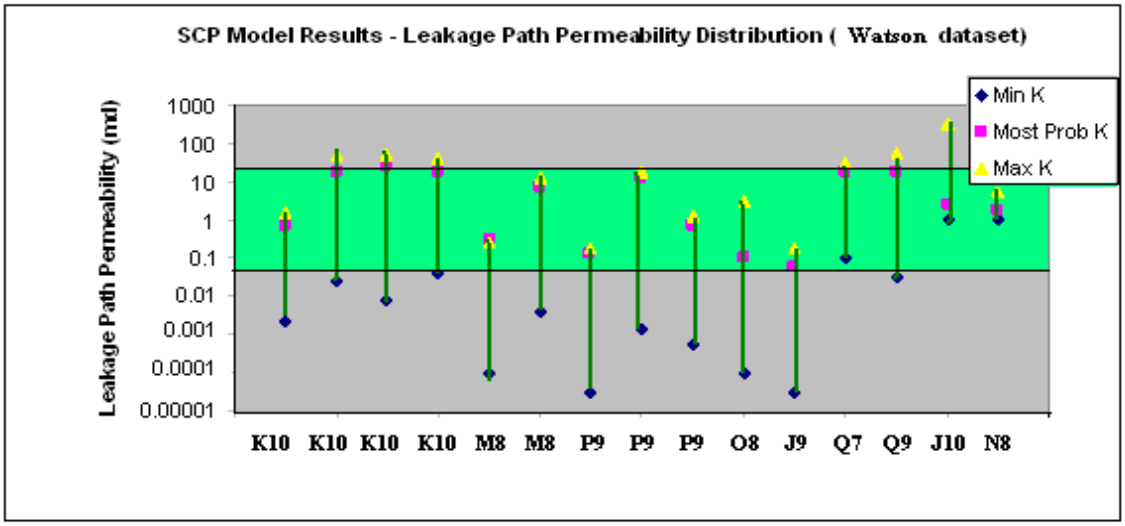

Figure 6.2.1.4 – Leakage path permeability for Watson dataset.

For the wellbores in the Xu dataset, there were fewer wellbores and pressure buildups to analyze (four wellbores) as compared to the Offshore dataset (eleven wellbores) and Watson dataset (nine wellbores). The average pressure buildup rate for this dataset also increased, as compared to the previous two datasets. The resulting permeability values range from 1 md to 1000 md (Fig. 6.2.1.5), which is a higher range of values, than had been observed from the previous two datasets. The upper end of permeability is 1 Darcy. The most probable/expected permeability values range between 1 md and 100 md (light green band).

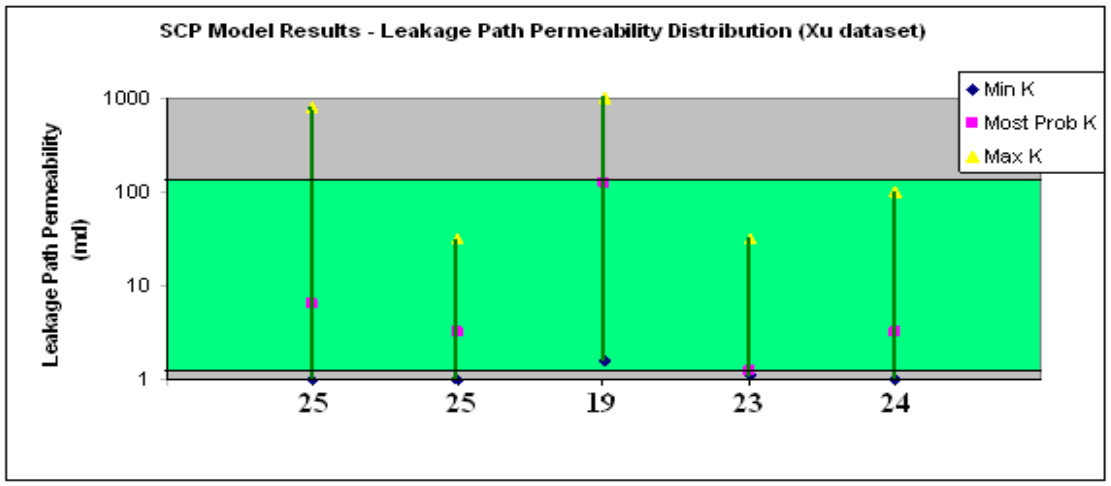

Figure 6.2.1.5 – Leakage path permeability for Xu dataset.

Bourgoyne's dataset contained three wellbores, each with multiple pressure buildups. The range of permeability value range (0.001 md to 1 Darcy) covers 4-5 orders of magnitude (Fig. 6.2.1.6). The most probable/expected permeability values (light green band) range across two orders of magnitude, from 0.50 md to 90 md.

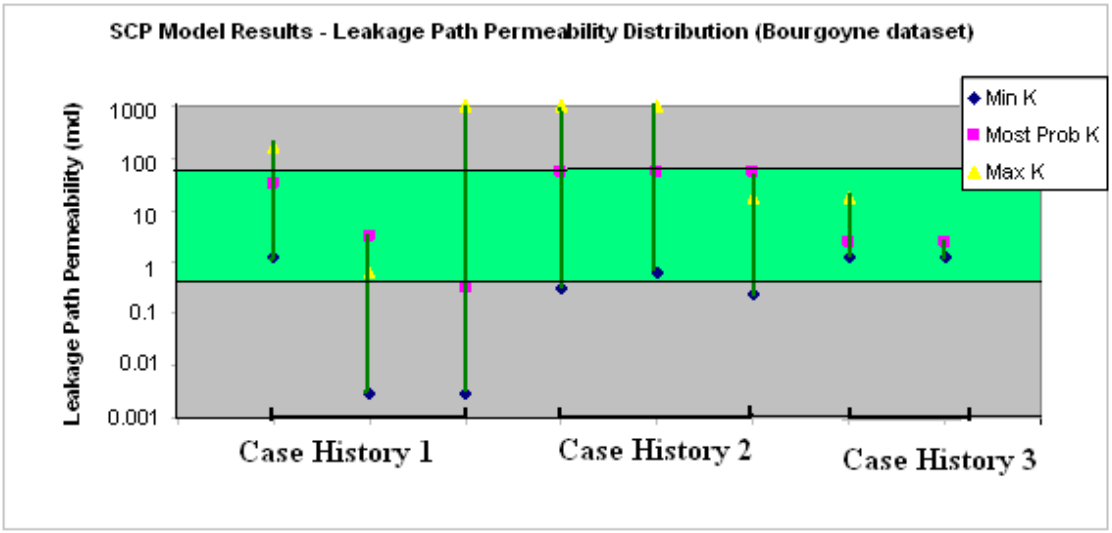

Figure 6.2.1.6 – Leakage path permeability for the Bourgoyne dataset.

Lastly, the Huerta dataset contained wellbores with the highest pressure buildup rates (several 1000 psi/day), as compared to all the other datasets (Fig. 6.2.1.7). Due to this, the resulting permeability range is within upper levels (100 md to 1 Darcy). The most probable/expected permeability values are between 300 md and 800 md (light green band), higher than what was demonstrated from all previous datasets.

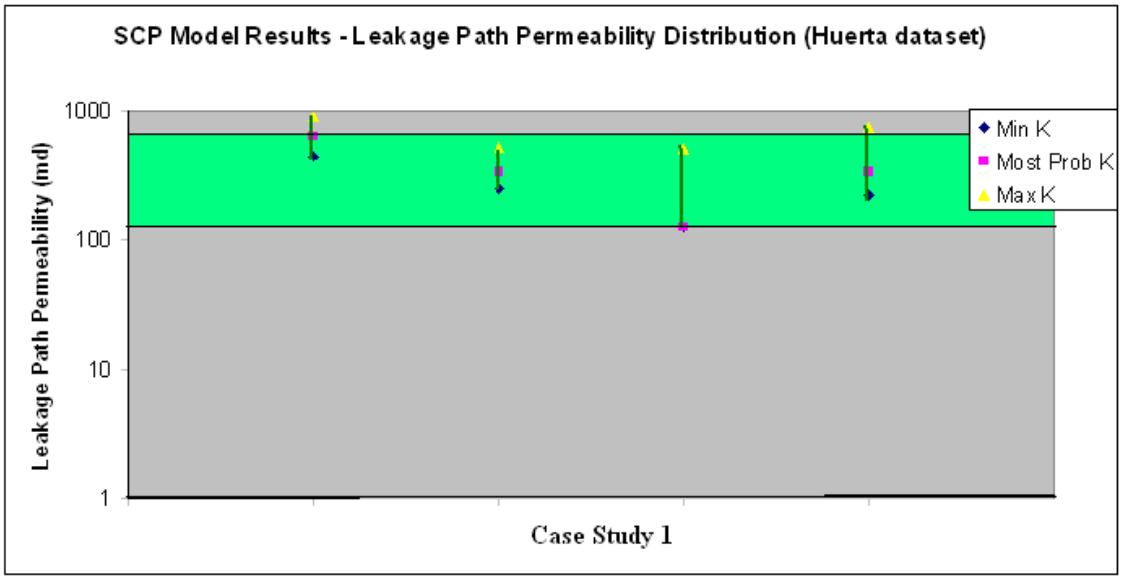

Figure 6.2.1.7 – Leakage path permeability for Huerta dataset.

In summary, the most probable/expected permeability values of the Monte Carlo Method SCP Model show the relationship between pressure buildup rates and leakage path permeability. As was demonstrated from the results of the previous datasets, the range of permeability generally increases for higher pressure buildup rates. The most probable permeability values (light green bands) are a useful indicator of this trend, which clearly demonstrates an increasing order of magnitude change for increasing pressure buildup rates. This trend is unsurprising, but no other trend with independent wellbore parameters has been identified.

Lastly, the most probable or expected values for permeability (Fig. 6.2.1.1-magenta points) were used to create a frequency distribution, to compare with previously published results by Celia *et al.* (2008). The latter permeability distributions were used to model gas leakage pathways, by assuming a leakage path permeability distribution based on the characteristics of the wellbore. For a set of wellbores presumed to have a ratio of one well with intact cement to four wells with degraded cement, the permeability values ranged 10 orders of magnitude, from 10^{-6} md to 10^{4} md (Fig. 6.2.1.8).

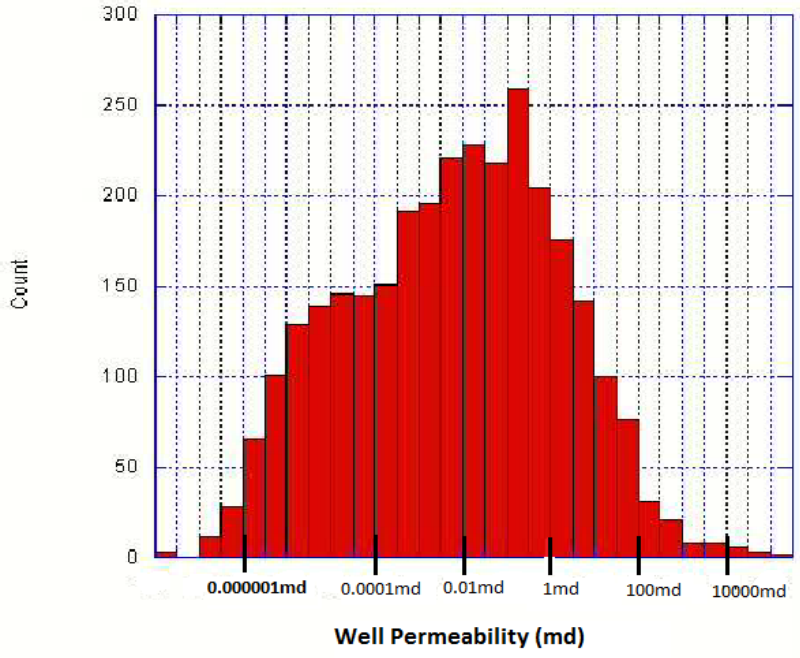

Figure 6.2.1.8 – Leakage path permeability distribution for set of wellbores with intact and degraded cement (Celia *et al.*, 2008).

There is a strong correlation between leakage flux and permeability of the leakage pathway. Since this permeability range spans ten orders of magnitude, there are correspondingly high degrees of uncertainty when predicting sizeable leakage fluxes reaching the surface.

In order to compare with the assumed permeability distribution published by Celia *et al*. (Fig. 6.2.1.8), the frequency distribution of most probable/expected values for all the pressure buildups and wellbores in Fig. 6.2.1.1 is shown in Fig. 6.2.1.9 (y-axis is "count", x-axis is "permeability") and overlaid on the Celia et al. distribution in the inset.

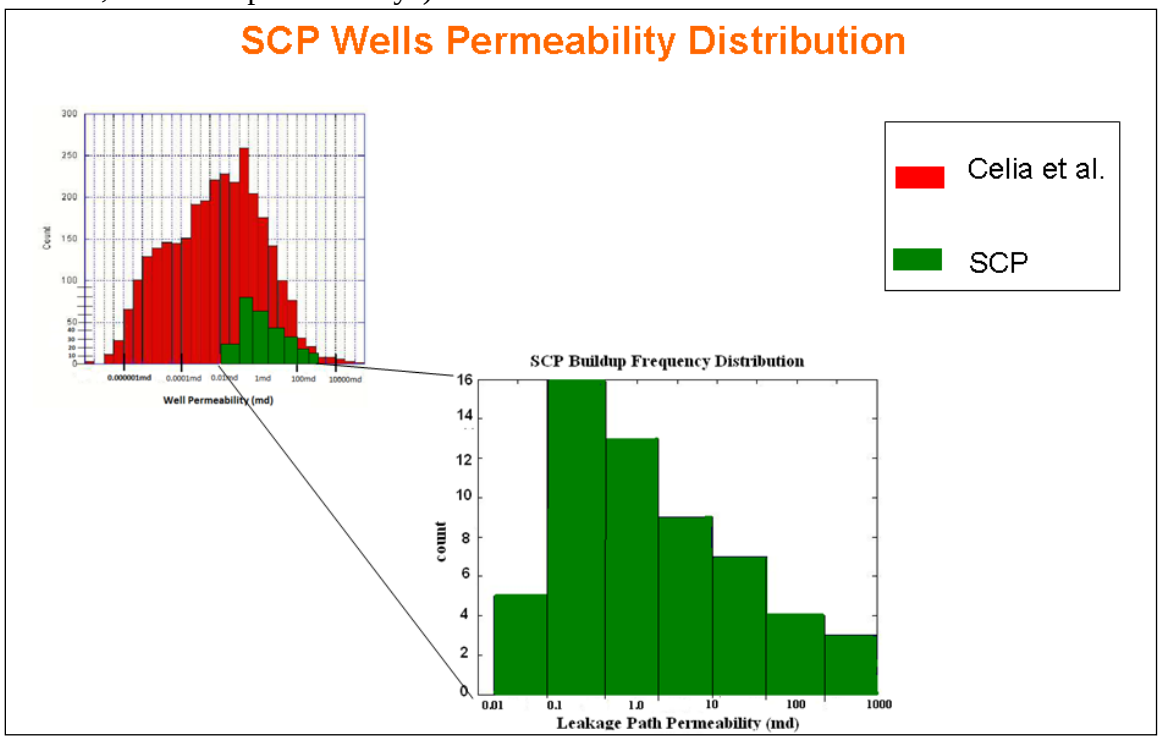

Figure 6.2.1.9 – Distribution of expected values of leakage path permeability for SCP wells. Inset compares distribution with one used by Celia et al (2008).

In Figure 6.2.1.9, the comparison between permeability distributions is highlighted in the upper left-hand corner. The SCP Model permeability range was divided into separate intervals (i.e.: 0.1 md to 1.0 md). If the most probable/expected values were between these two values, then the frequency distribution would add "one" to the count of leakage path permeability (Fig. 6.2.1.9). One "count" represents a one "expected value". For example, between the range 0.01 md and 0.1 md, the count is "5", meaning that five wellbores had expected permeability values between these ranges. In

aggregate, the new permeability distribution range covers five orders of magnitude, which is smaller than Celia *et al*. permeability range (10 orders of magnitude).

6.2.2 Monte Carlo Method - SCVF Model Results

For the SCVF Model, the wellbores in each dataset were chosen based on identifying known and unknown parameter values. A different combination value identified a different script to be used when generating results. For known parameter values, a value "1" was assigned. For unknown parameter values, a value "0" was assigned. The parameters of interest were the following: mud density, length of mud, and leakage depth. There were a total of eight possible combinations, (000, 001, 011, 111, 100, 101, 010, 110), however the two combinations (1,0,0 and 1,1,0) represented approximately 95% of all the wellbores that were modeled.

The permeability results for wellbores with known mud density, unknown length of mud, and unknown leakage depth (1,0,0) are plotted vs. flow rate in Fig. 6.2.2.1. The permeability results for wellbores with known mud density, known length of mud, and unknown leakage depth (1,1,0) are plotted vs. flow rate in Fig. 6.2.2.2. The y-axis is log-scaled leakage path permeability (units of md). The x-axis is log-scaled flow rate (units of m^3/day). The minimum permeability value (blue diamond), most probable/expected permeability (magenta square), and maximum permeability (yellow triangle) compose a range of permeability (vertical blue bar).

As can be observed in Fig. 6.2.2.1 and Fig. 6.2.2.2, there is a relationship between permeability vs. flow rates. For greater flow rates, there are increases in leakage path permeability. The most probable/expected values (magenta color squares) are generally

located near the minimum permeability values (dark blue color), at the lower end of the permeability range, closer to intact cement (0.001 md).

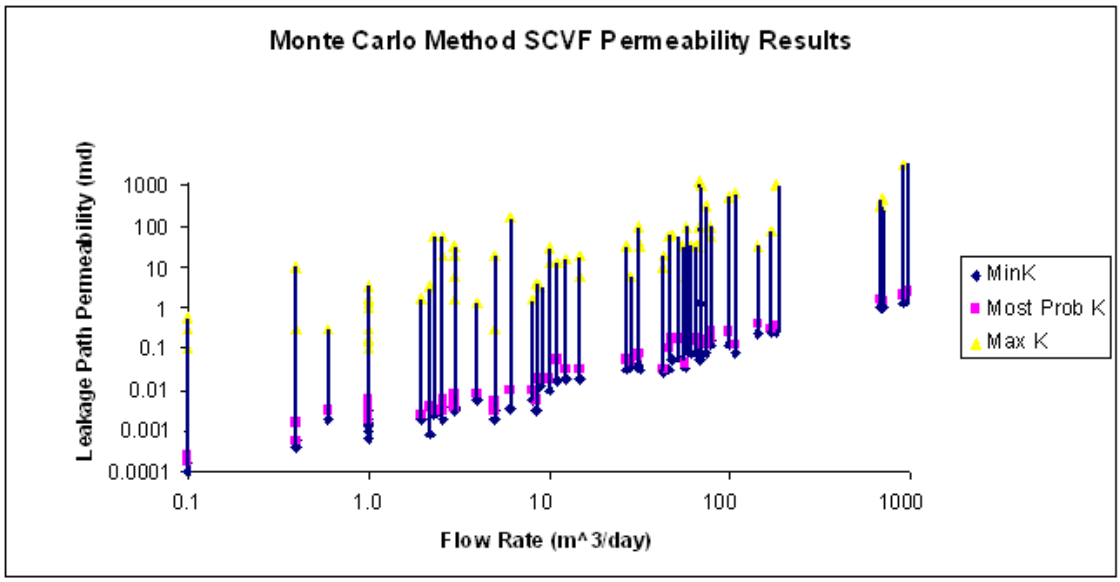

Figure 6.2.2.1 –Monte Carlo Method - SCVF Model Leakage path permeability vs. flow rate for wellbores with known mud density, unknown mud length, and unknown leakage depth. (British Columbia Oil and Gas Commission dataset).

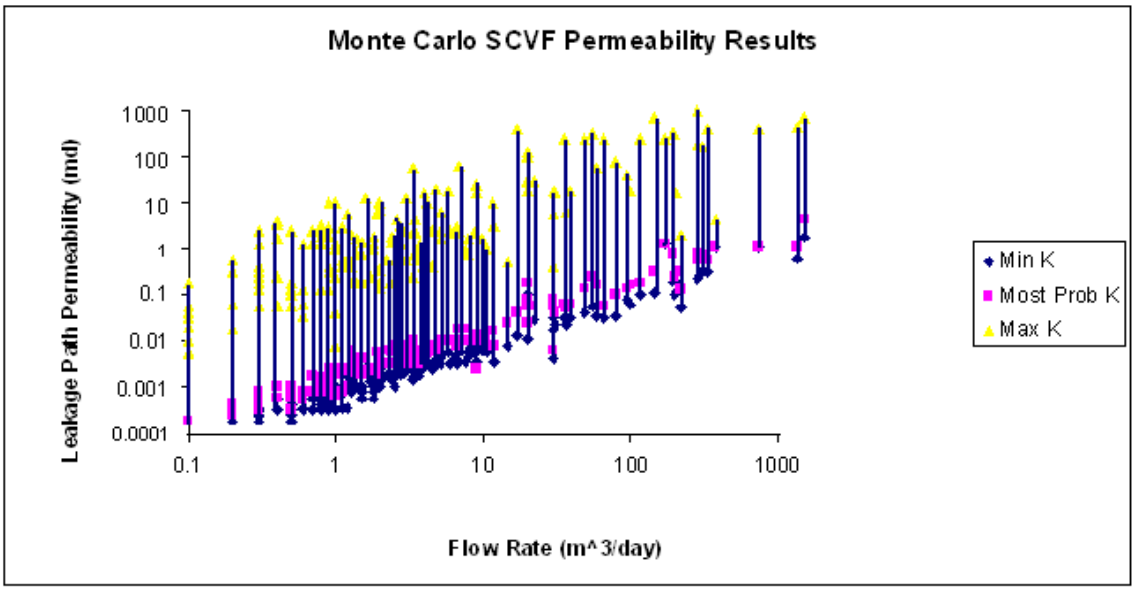

Figure 6.2.2.2 – Monte Carlo Method – SCVF Model Leakage path permeability vs. flow rate for wellbores with known mud density, known mud length, and unknown leakage depth (British Columbia Oil and Gas Commission dataset).

As was completed for the SCP Model results, the most probable/ expected values (magenta color) were extracted from the permeability ranges in Fig. 6.2.2.1 and Fig. 6.2.2.2 and used to populate a permeability frequency distribution used for comparison with Celia *et al*. (Fig. 6.2.2.3).

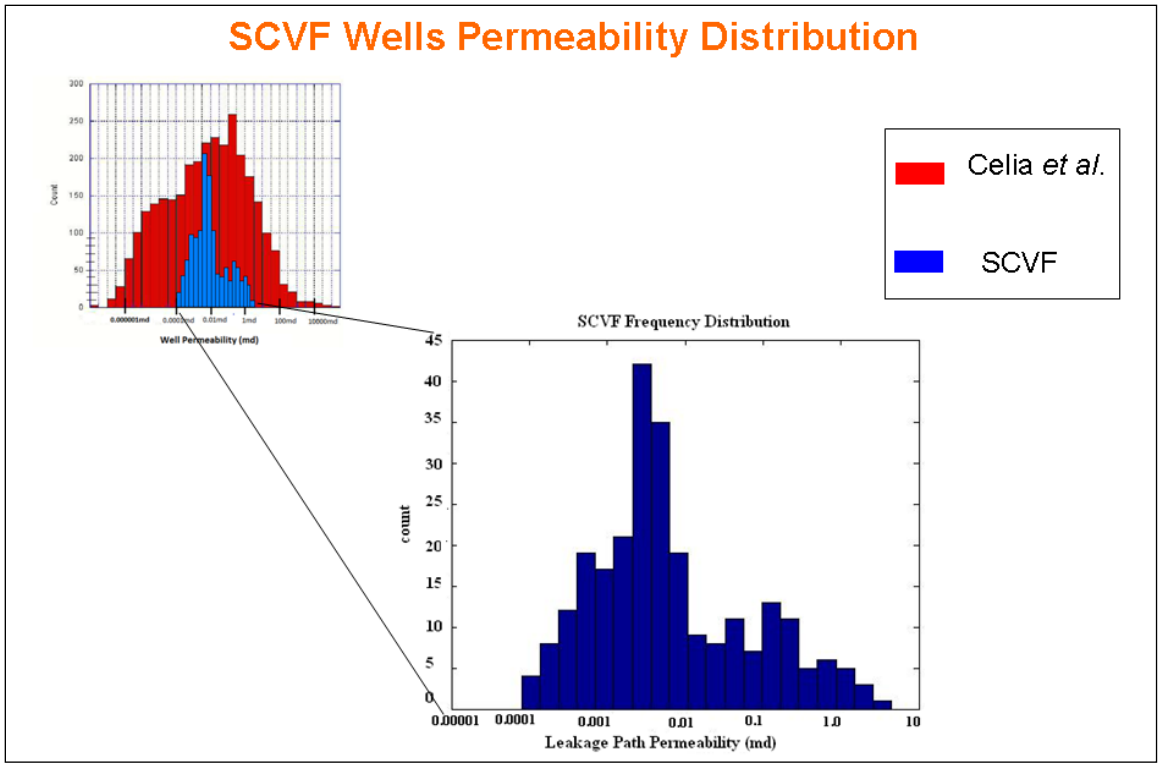

Figure 6.2.2.3 – Comparison of leakage path permeability for SCVF Model results.

The upper left-hand is the permeability comparison between the Celia *et al* and the SCVF Model results. As can be observed, there is a smaller range of permeability covering 4 orders of magnitude (0.0001 md to 5.0 md), as compared to 10 orders of magnitude by Celia *et al*. Also, the permeability range is one to two orders of magnitude lower than the SCP Model range, as will be discussed in Section 6.2.3.

6.2.3 Comparison between Monte Carlo Method SCVF Model and SCP Model Results

As discussed, there were two applications of the Monte Carlo Method; one that used the pressure buildup data (SCP Model), the other that used the flow rate bleed down information (SCVF Model). The goal of Section 6.2.3 is to compare the permeability

results between the SCVF Model and the SCP Model. However, the SCVF Model was primarily used for the British Columbia Oil and Gas Commission dataset, since this data did not contain any pressure buildup information. This dataset was not used in the Monte Carlo Method SCP Model.

Since flow rate was used as inputs to the SCVF Model, and pressure buildup data was used as inputs to the SCP Model, only wellbores with both types of information could be used for comparison purposes. The following two datasets provided both flow rates and pressure buildup data: Watson dataset and Bourgoyne dataset. Therefore, it was only possible to compare results between the SCP Model and SCVF Model for these wellbores.

The first dataset results comparison is from the Monte Carlo Method SCP Model permeability results for the Watson dataset (Fig. 6.2.3.1). These wellbores had parameter values with (1) known leakage depth, (0) unknown length of mud, and (0) unknown mud density.

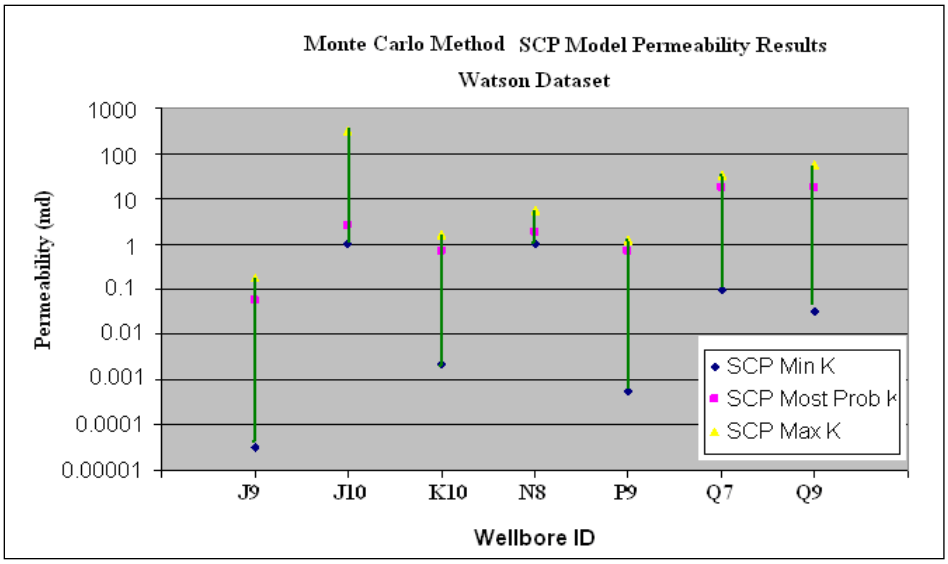

Figure 6.2.3.1 – SCP Model Outputs – Leakage Path Permeability (md) for selected buildups from the Watson dataset.

The range of leakage path permeability is identified by green bars (between maximum (yellow) and minimum (blue) values) and covers 1-4 orders of magnitude, depending on the wellbore. The most probable permeability value is highlighted in magenta color, and this tends to be at or near the upper end of the permeability range.

The Watson wellbores also contained gas vent flow rate data, so they could be used as inputs to the Monte Carlo Method SCVF Model. The leakage path permeability results from the SCVF Model are shown in Fig. 6.2.3.2.

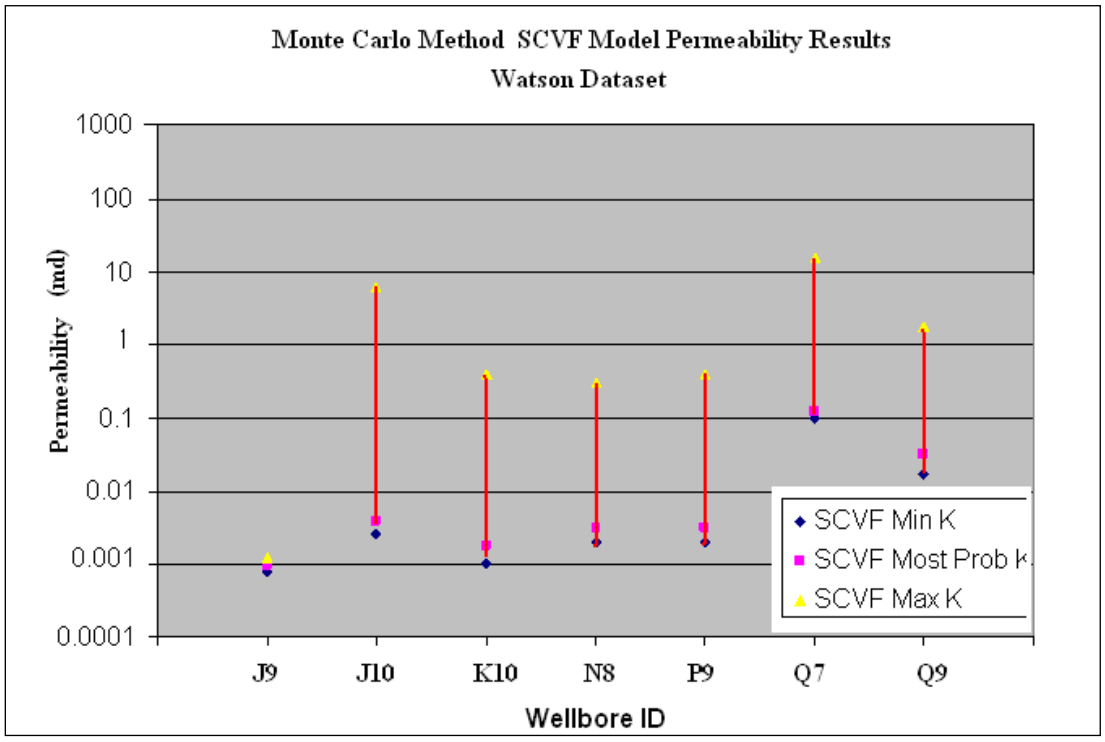

Figure 6.2.3.2 – SCVF Model Outputs – Leakage Path Permeability (md) for same wellbores as Fig. 6.2.3.1.

As can be observed in Fig. 6.2.3.2, the range of leakage path permeability output for the SCVF model is identified by red bars (between maximum (yellow) and minimum

(blue) values) and covers 1-4 orders of magnitude, depending on the wellbore. The most probable permeability value is highlighted in magenta color, and this tends to be at or near the lower end of the permeability range.

Having run the SCP Model and SCVF Model on the same wellbores, it is insightful to compare the permeability results (Fig. 6.2.3.3). The permeability values are plotted next to each other, for the same wellbore.

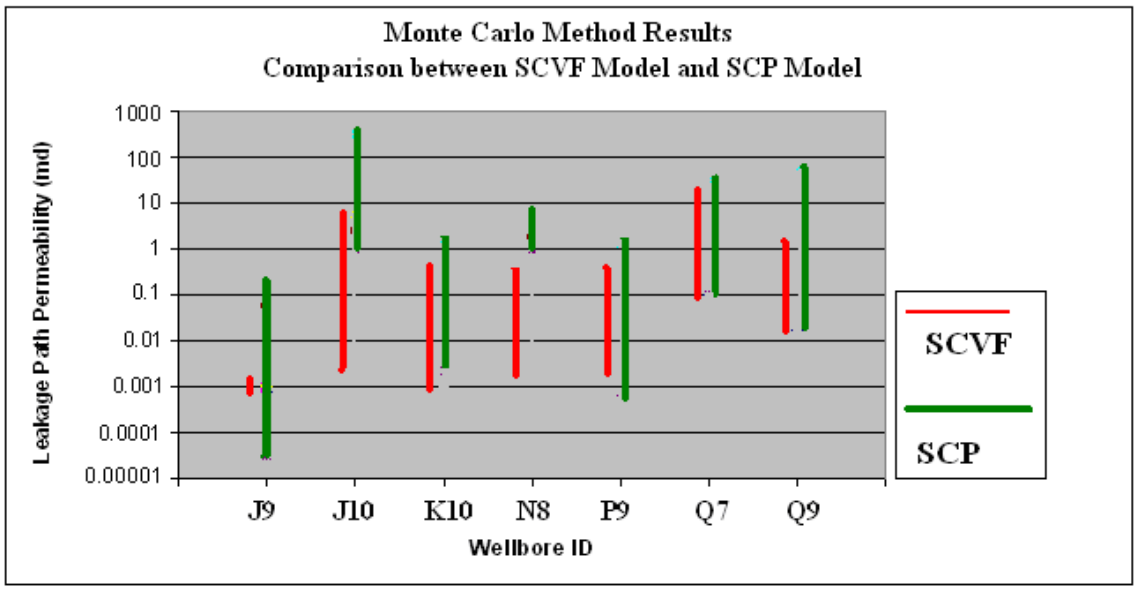

Figure 6.2.3.3 – Comparison of leakage path permeability for wellbores in Watson dataset that have both buildup and flow rate data obtained with the Monte Carlo SCP Model and the SCVF Model.

As can be observed in Fig. 6.2.3.3, there is some overlap between the results from each wellbore, except for wellbore N8. In general, the SCP Model results (green bar) tend to be greater than the SCVF Model results (red). Also, the range of the SCVF Model permeability covers a wider range of magnitude (3-4 orders) than the range of the SCP Model (2-3 orders). This comparison is important, because it shows that

overlapping results can be obtained by applying the two different models to the same dataset of leaky wellbores.

The only other wellbore that can be used as a comparison is from Bourgoyne (Fig. 6.2.3.4) wellbore case history 1. This wellbore contained vent flow information and pressure buildup data, so it could also be run using each model.

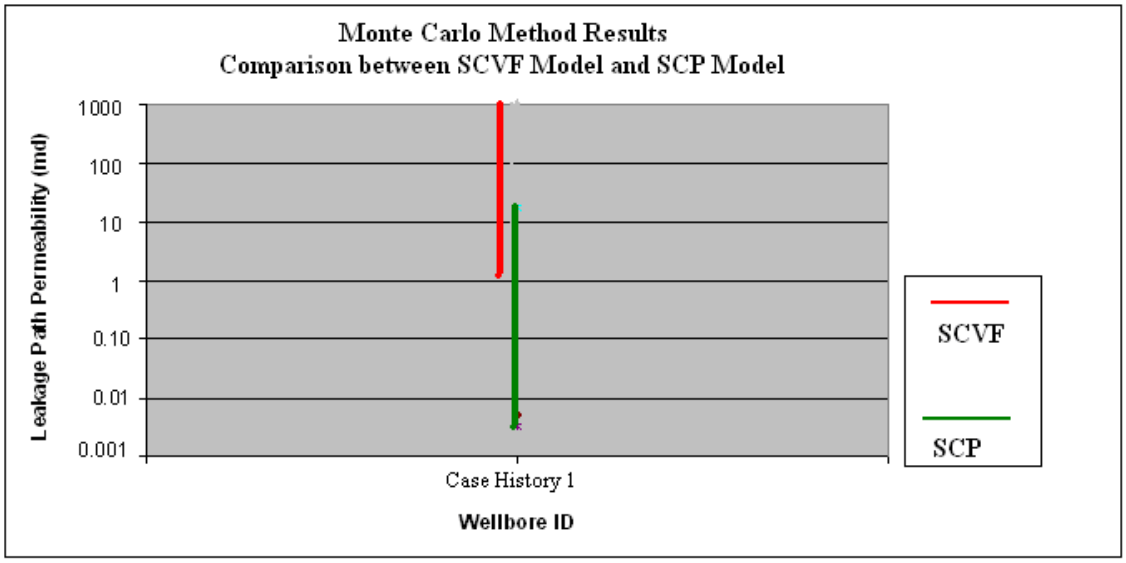

Figure 6.2.3.4 – Comparison of leakage path permeability results for Bourgoyne dataset, between the Monte Carlo SCP Model and the SCVF Model.

For wellbore Case History 1, the SCVF Model results (red color bar) are a few orders of magnitude greater than the SCP Model results (green color bar). This result indicates the same leakage conduit may have different characteristics at different times. As discussed in Chapter 3, wellbore Case History 1 demonstrated periodic pressure buildups and bleed downs. The gas flow rate was measured during a 24 hour period and leveled out at 5 m^3/day. The pressure buildup occurred during an earlier time period, when the leakage conduit may have had smaller permeability. Cycling of the

intermediate annulus system, by opening and closing the surface valve, could have removed obstructions within the leakage path..

Having obtained results from two different datasets, the distribution of permeability for the SCVF wells and the SCP wells can be combined and compared with the distribution assumed by Celia *et al* (see Fig. 6.2.3.5). There is overlap between the results of the two models between 0.01 md and 1 md. However, the extended range of estimated permeability (6 orders of magnitude) between the two models is considerably narrower than the range from Celia *et al.*, (10 orders of magnitude). Thus, the SCVF Model and SCP Model provided quantitative estimates of leakage path permeability for existing wellbores.

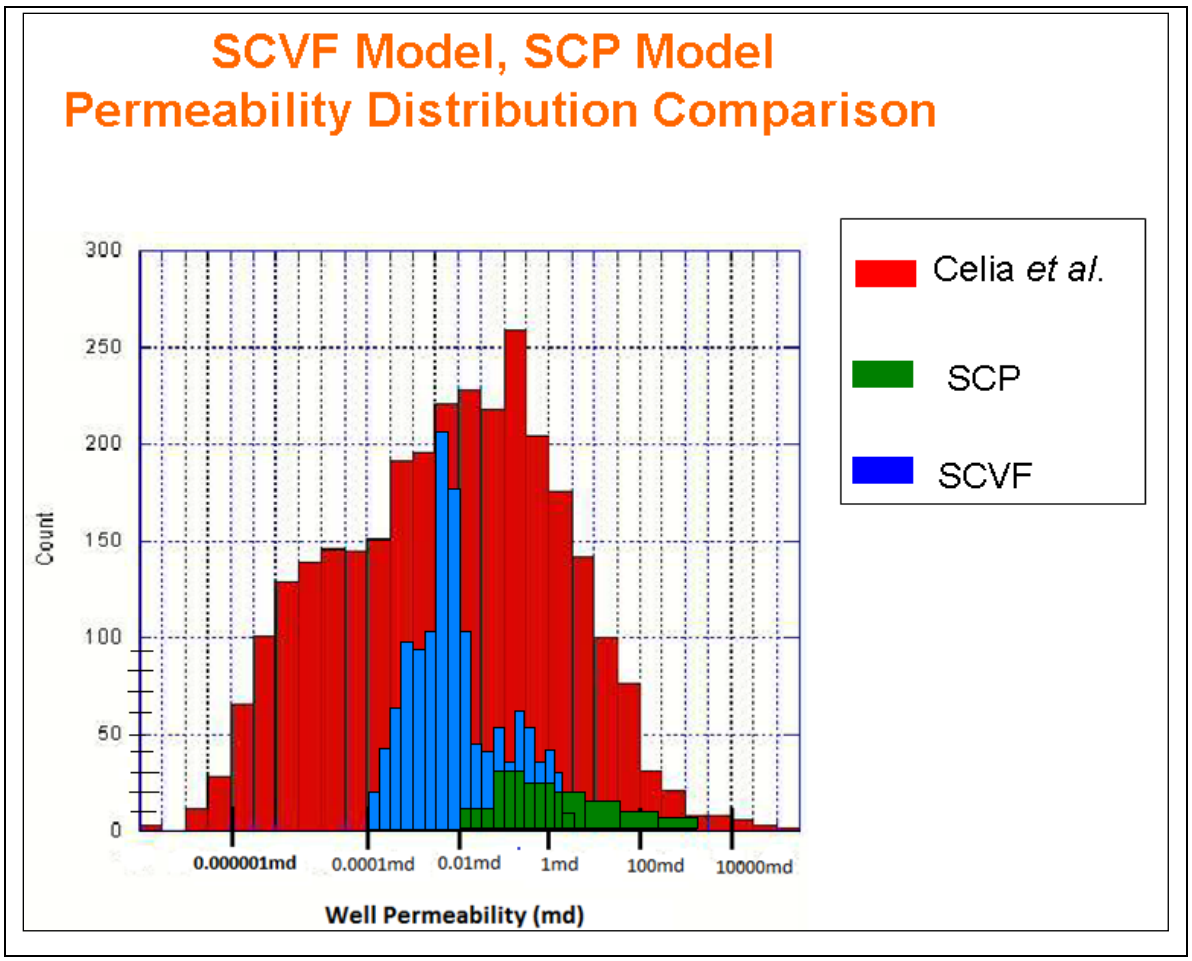

Figure 6.2.3.5 – Comparison of leakage path permeability (expected values obtained for each wellbore from Monte Carlo Method) between the SCP wells (green) and the SCVF wells (blue). Red bars are an example hypothetical distribution used by Celia et al (2008).

Lower Perm Range md	Upper Perm Range md	Percent
0.0001	0.001	14%
0.001	0.01	37%
0.01	**0.1**	16%
0.1	**0.5**	12%
0.5	**1**	9%
1.0	**10**	8%
10	50	2%
50	100	1%
100	1000	1%

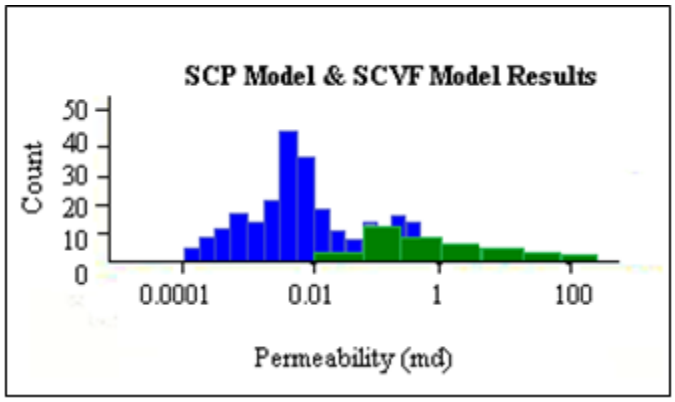

Figure 6.2.3.6 – (a) Statistics of Permeability Ranges (b) SCP wells (green) vs. SCVF wells (blue) Permeability Distributions.

The range of the combined permeability distribution covered 6 orders of magnitude (0.0001 md to 100 md). However, a closer evaluation of the final results breakdown provided a better estimation of the most probable ranges. For example, 14% of the total permeability values were between 0.0001 md and 0.001 md. 37% of values were between 0.001 md and 0.01 md. Two thirds of the values are less than 0.1 md, and 80% of the permeability values were within 3 orders of magnitude (0.0001 md to 0.5 md). This is considerably smaller range of uncertainty than used by Celia et al (2008).

In summary, the SCVF dataset (blue color) contains a larger number of wellbores (210 wellbores) than what was analyzed using the SCP Model (green color) (28 wellbores). Therefore, in each interval of effective permeability, the count of the SCVF Model is higher than the count of the SCP Model. As stated, the SCVF Model results produced a lower range of permeability values than the permeability values of the SCP Model results. These combined permeability results are compared to the assumed permeability distribution by Celia *et al.*,(red color). It is recommended that the

combination of the SCVF and SCP Model permeability distributions be used for future leakage modeling purposes since they are generated from leaky field data.

6.2.4 Changes in Permeability Over Time

One of the underlying questions about the permeability results and the comparison of these values was the relationship between time and permeability. For example, if the same wellbore was tested for gas flow issues at multiple points in time, how much did the permeability value change? Did the interval of time between testing dates increase, decrease, or keep permeability the same? To answer these questions, the permeability results vs. time of the Offshore dataset are first discussed, followed by the permeability results vs. time of the Watson dataset. Different conclusions are made for each dataset.

For the Offshore wellbore dataset, the same wellbores and the permeability values listed are grouped together according to each wellbore (grey boxes). The relationship between permeability vs. time is identified by the black trend line. The results are inconclusive. As can be observed, for wellbore 2, permeability decreases over time. For wellbore 5, permeability increases over time. For wellbores 6 and 7, permeability decreases over time.

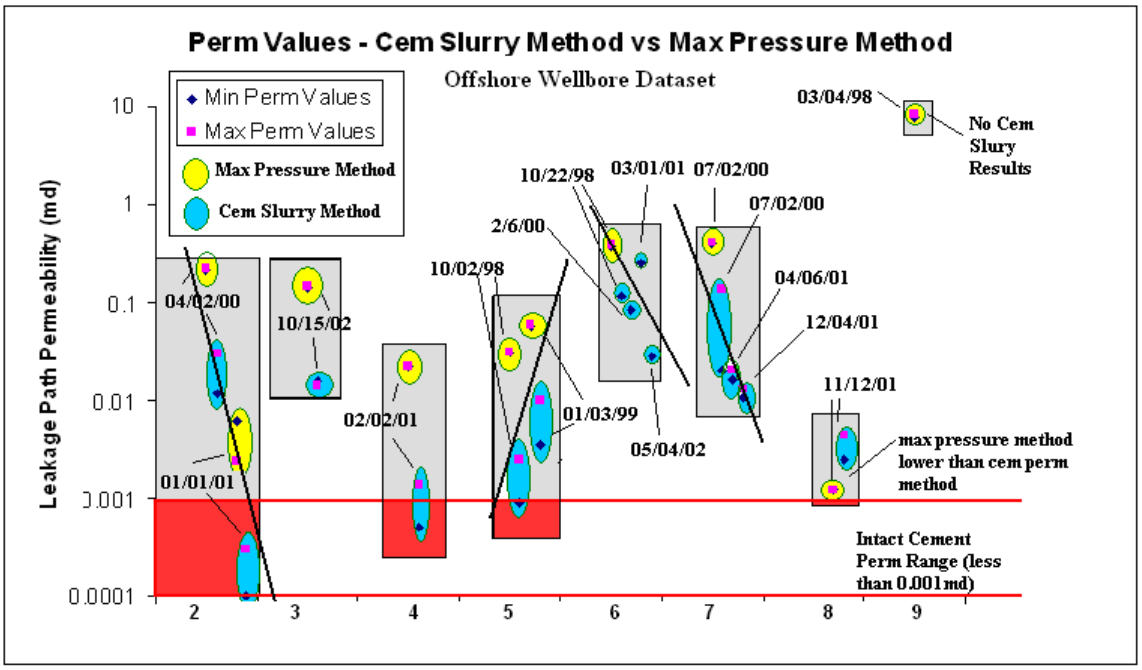

Figure 6.2.4.1 – Leakage path permeability vs. time for the offshore wellbore dataset.

For the Watson wellbore dataset, however, a different trend was identified. A measurement of sustained casing vent flow (SCVF) was generally taken before a measurement of sustained casing pressure (SCP) was taken. This timeline of "measurements taken" provides evidence to support the theory that gas flow during SCVF testing changed the characteristics of the leakage pathway. Over time, the leakage pathway permeability increased.

The results from the Monte Carlo Method showed that the SCP Model permeability values (green color) were generally greater than the SCVF Model permeability values (red color) (Fig. 6.2.4.4). The timeline of "measurements taken" show that SCVF testing occurred before the SCP testing (Fig. 6.2.4.2). The top horizontal line of the figure "SCP" indicates when such work was measured on the well.

The second horizontal line “SCVF” and third horizontal line “Remediation” indicate when this work was performed. The x-axis is a timeline of events (dates).

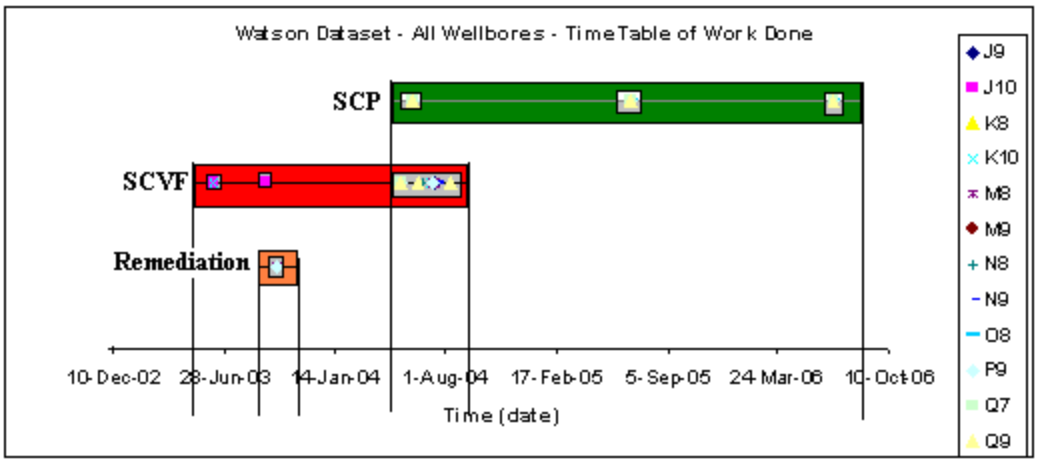

Figure 6.2.4.2 – Watson wellbores. Timeline and type of work performed.

As can be observed in Fig. 6.2.4.2, the SCVF measurements (red color) were taken from June 28, 2003 to August 1, 2004. The SCP measurements were taken from August 1, 2004 to October 10, 2006. Thus, the SCVF measurements were taken several years earlier than when the SCP measurements were taken. It is also important to point out that remediation work on a few wellbores occurred before August 1, 2004. This also must have had significant effects of changing the characteristics of the leakage pathway.

For a closer evaluation of the timeline of “measurements taken” the results from one example wellbore are displayed in Fig. 6.2.4.3.

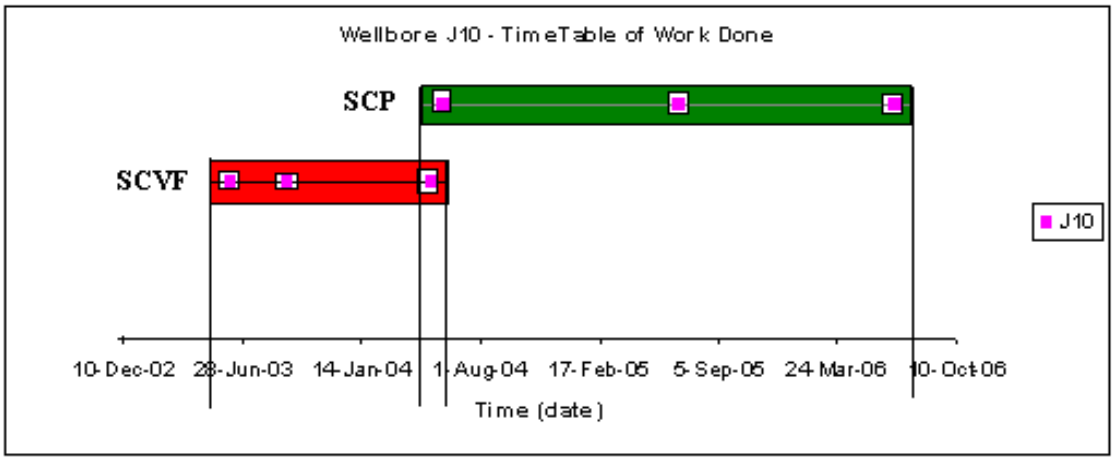

Figure 6.2.4.3 – Watson wellbores, J10. Timeline and type of work performed.

For this example wellbore, the SCVF (red color) was measured at three early points in time (June 10, 2003; September 11, 2003; May 04, 2004). The SCP (green color) was then measured at three later points in time (June 01, 2004; July 01, 2005; July 01, 2006). No remediation was performed. By focusing on the permeability results of this wellbore (Fig. 6.2.4.4), it can be observed that there is an increase in permeability values when SCP is measured (green bar) vs. when SCVF was measured (red bar). This indicates an increase in permeability over time.

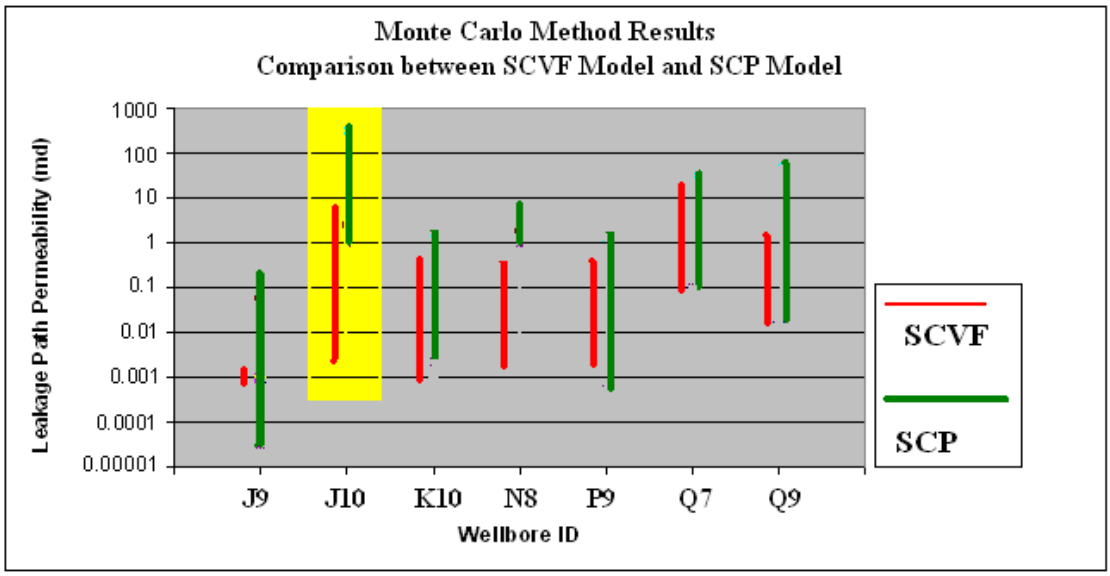

Figure 6.2.4.4 – Watson wellbores, highlighted wellbore J10.

6.3 Sensitivity Analysis of Certain Wellbore Parameters

Sensitivity studies were performed to better understand how leakage path permeability was affected by changes in different parameter values. Huerta (2009) and Xu (2001) performed sensitivity studies for different wellbore parameter values in order to determine how these changes affected the SCP Model's ability to match raw pressure buildup data. The purpose of a sensitivity analysis is to identify the controlling factors for pressure bleed-down and buildup (Xu, 2001). It was instructive to show, to what extent changing different unknown parameter values had on the leakage path permeability values. When performing a sensitivity analysis, all parameter values were kept constant, except for the parameter value of interest. This value was incrementally increased or decreased, depending on the analysis performed. Once completed and the results were recorded, a sensitivity analysis was extended to the other parameter values. In other cases, the permeability results are plotted versus the change in the designated parameter value to identify trends in data.

As the sensitivity analysis showed, there can be a large degree of uncertainty when describing the unknown characteristics of a leaky wellbore system. For unknown wellbore parameters, the values were limited within an established range. Model output permeability values were generated when the targeted parameter values changed. This process was repeated until the parameter value reached the end values of the range and all results were recorded. The movement of the permeability value depended on the parameter value that was changing and was confirmed mathematically with Eqn. 3.3.3. The sensitivity of the change in permeability was quantified by the change in pressure buildup data matching capability. A sensitivity analysis was performed on the following parameter values: gas cap length, mud density, leakage depth, mud length, mud compressibility, and gas flow rate.

6.3.1 Gas Cap Length Sensitivity Analysis

A gas chamber was formed instantaneously after the surface valve was closed and the well was shut-in. This created a "closed" system. The gas chamber was the void space between the top of the completion mud column to the closed surface wellhead valve. This space was normally composed of gas or gas-cut mud with high gas concentrations. Sensitivity analysis showed that the size of the gas cap had a significant effect on the matching capability of the model generated pressure buildup curve to the field data.

Xu modeled the gas migration in a series of cells, where the gas migrated upward from cell to cell, increasing the volume size of the final cell (gas chamber) (Xu, 2001). At each time step, the volume of the gas cap increased in size. Xu initially filled the annular space with completion mud (0 ft gas cap length). A gas cap volume sensitivity

analysis was then performed by increasing the initial gas volume in stages, (0 ft^3, 37 ft^3, 75 ft^3, 188 ft^3). Results from the model showed that the larger volume of the gas chamber acted as a "stabilizer" (Xu, 2001). The larger the gas cap volume chamber, the slower the pressure built up, and the longer the time was needed to reach higher stable asymptotic pressure levels (Xu, 2001). A larger gas cap reduced the hydrostatic pressure of mud. More gas then migrated upward after the bleed-off.

As Xu had recommended, by setting the initial default length of gas column length to 0 ft, the smallest permeability values (lower bound) were generated. Results from a gas cap sensitivity analysis performed on the Offshore dataset, also showed that larger gas cap lengths (5 ft to 10 ft) increased the leakage path permeability values. Keeping all other parameter values the same, the larger initial gas cap lengths (red and blue points outside the ovals in Fig 6.3.1.1) increased the leakage path permeability values by a factor of between 2 and 20, as compared to the 0 ft gas cap length used for the original Cement Slurry Method (points inside cyan ovals in Fig 6.3.1.1). For a given pressure vs. time data interval, non-zero gas cap lengths required higher permeability values in order to match the data, as compared to a 0 ft gas cap length for the offshore dataset (Fig. 6.3.1.1).

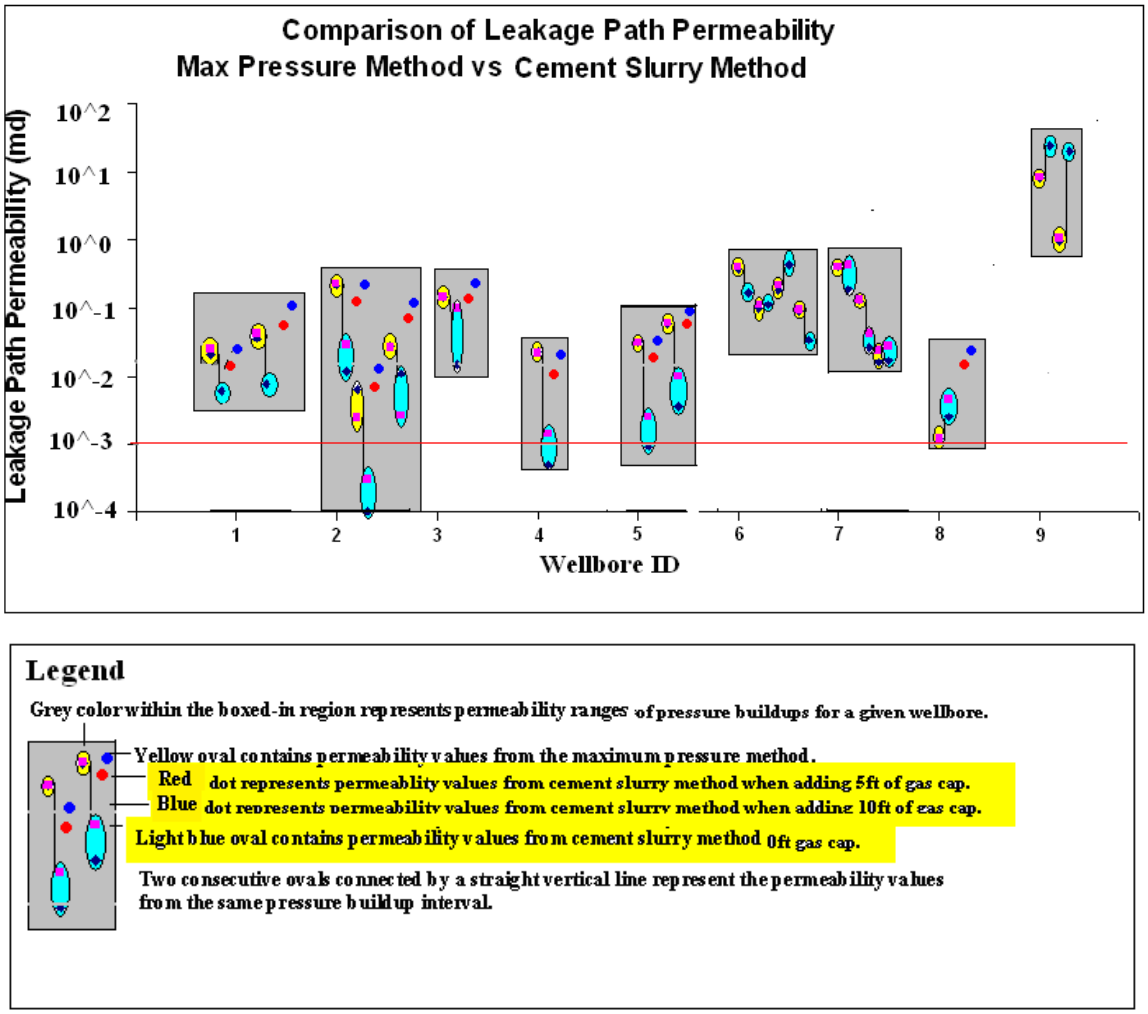

Figure 6.3.1.1 – Effect of initial gas cap length. For a larger gas cap length (symbols inside ovals: 0 ft; red symbols: 5 ft; blue symbols: 10 ft) the leakage pathway permeability increase by one to two orders of magnitude, as compared to 0 ft initial gas cap for the Offshore wellbore dataset

Furthermore, a closer evaluation of the effect of gas cap can be observed with wellbore 1 and wellbore 2 of the offshore dataset. For these wellbore examples, the same pressure buildup data and leakage scenarios were created. The only parameter value that was changing was the "length of gas cap" (from 0 ft to 10 ft). The resulting plot (Fig. 6.3.1.2) demonstrate that leakage pathway permeability increases linearly with increasing

lengths of gas cap, keeping the other parameter values constant. These effects clearly demonstrate the significant impact that changing the gas cap length has on leakage path permeability and agree with Xu's findings.

For example, there are higher degrees of leakage path permeability, as the gas cap length increased from 1 ft to 10 ft for Buildup 1 (0.60 psi/day) (blue colored line) and buildup 2 (0.64 psi/day) (magenta colored line) in Fig. 6.3.1.2.

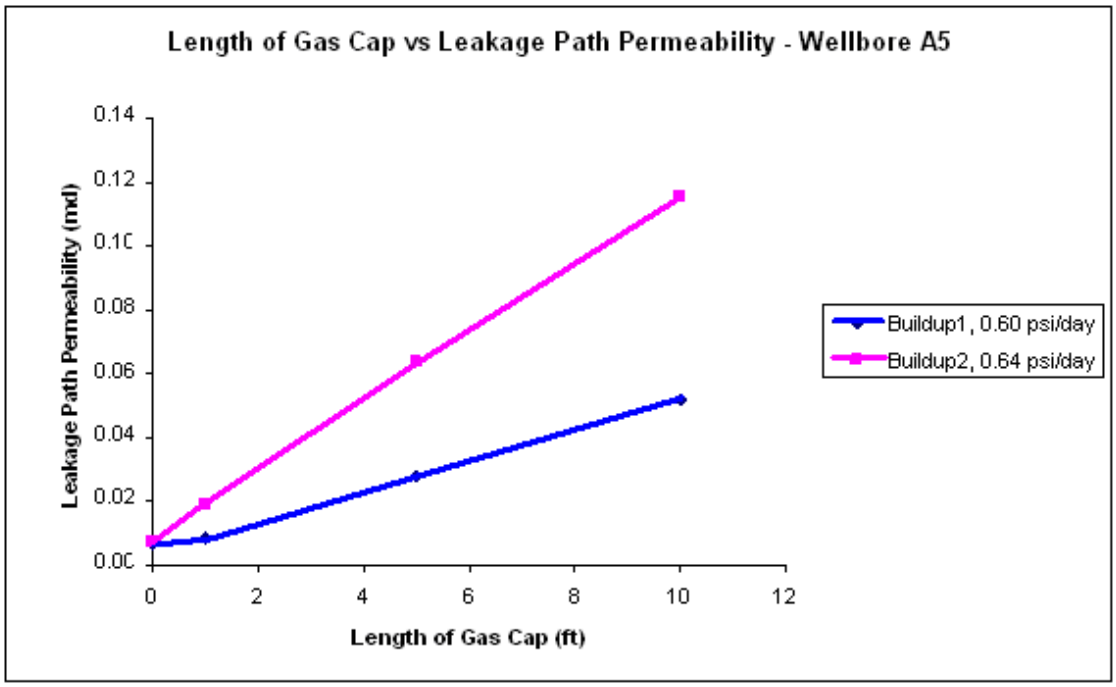

Figure 6.3.1.2 – Closer evaluation of the effects of changing gas cap length vs. leakage path permeability for wellbore 1 (two buildups, 0.60 psi/day and 0.64 psi/day).

As can be observed in Fig. 6.3.1.2, for a ten-fold increase in gas cap length (to 10 ft from 1 ft), there is a five to eightfold increase in permeability values (to 0.05 md from 0.007 md or to 0.12 md from 0.02 md, depending on buildup rate), everything else kept

the same. This is also demonstrated with the results from wellbore 2 in Fig. 6.3.1.3. Therefore, it can be concluded that there is a strong relationship between gas cap length and permeability inferred from a given buildup.

Furthermore, this relationship seems to hold for larger pressure buildup rates. As can be observed, in Fig. 6.3.1.3, a pressure buildup of 4.4 psi/day (blue line) generated greater permeability values than a pressure buildup of 1.6 psi/day (green line) and a pressure buildup of 0.35 psi/day (magenta line). The ratio of permeability, k(10 ft) / k(1 ft), between a gas cap length of 10ft and a gas cap length of 1 ft for each of the buildup rates is the following:

(1) For 4.4 psi/day, k(10 ft) / k (1 ft) = 6.5

(2) For 1.6 psi/day, k(10 ft) / k (1 ft) = 5.1

(3) For 0.35 psi/day, k(10 ft) / k (1 ft) = 3.3

Since the ratios are different, the buildup rate influences the sensitivity of the effective permeability to the initial gas cap length. For greater buildup rates, increasing the initial gas cap length yields greater increases in the estimated permeability value.

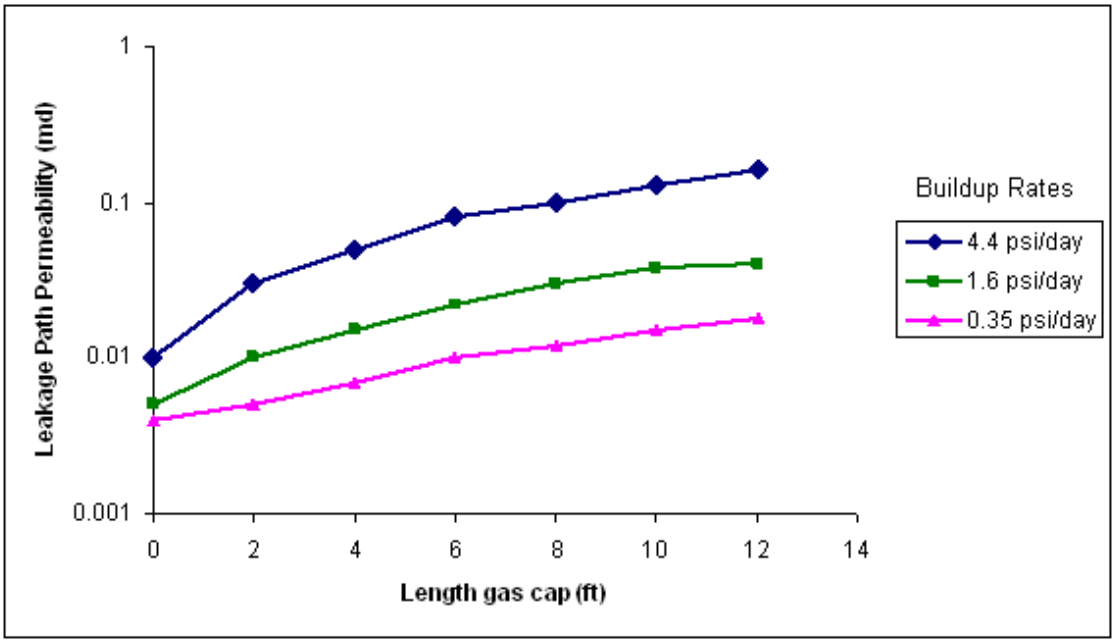

Figure 6.3.1.3 – Closer evaluation of the effects of changing gas cap length vs. leakage path permeability for wellbore 2.

6.3.2 Mud Density Sensitivity Analysis

A mud density sensitivity analysis was performed to compare what effects that changing mud density had on leakage path permeability for the Offshore dataset. Keeping all other parameters constant, mud density was decreased. The smaller value of mud density used in the analysis was based on the assumption that the completion mud was a two phase gas/liquid mixture with a density of 4.15 ppg. This completion mud density a factor of two smaller than that of a one phase incompressible completion mud used before (8.9 ppg).

To compare the permeability results between larger and smaller mud density, the Maximum Pressure Method and was applied to several of the wellbores from the

Offshore dataset in Fig. 6.3.2.1 These wellbores (highlighted in grey boxes) had originally demonstrated large differences in permeability between the Maximum Pressure Method (yellow ovals) and the Cement Slurry Method (blue ovals). With the reduced mud density, the Maximum Pressure Method yielded leakage path permeability (green oval) to closer to the results from the Cement Slurry Method.

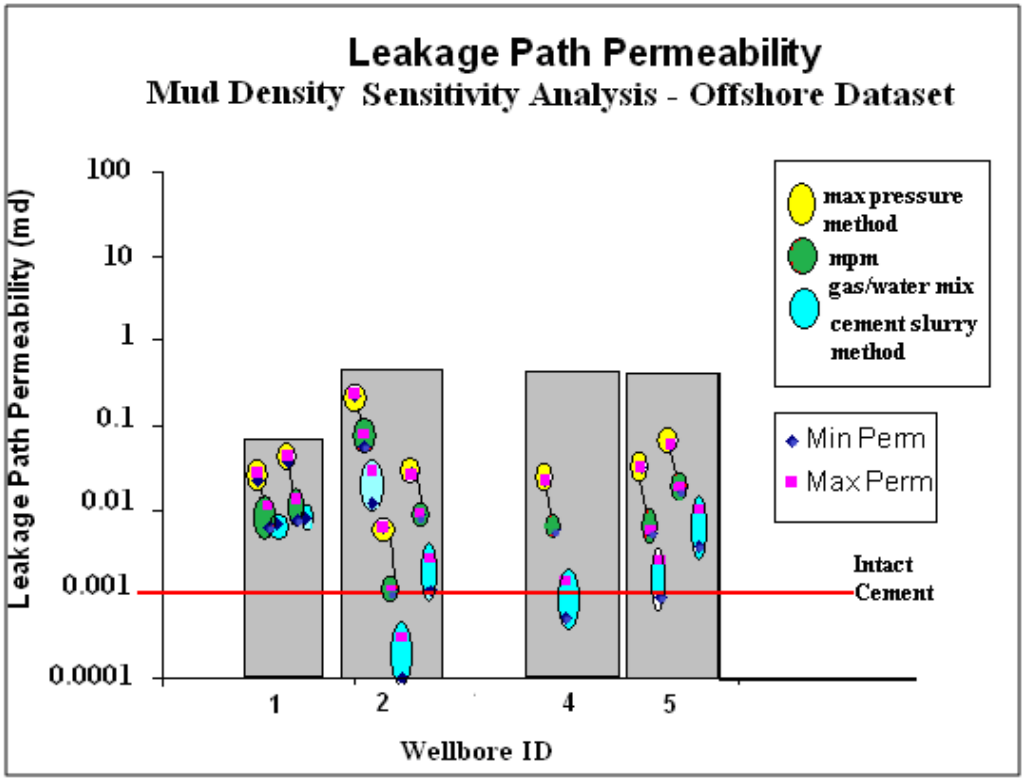

Figure 6.3.2.1 – Completion mud sensitivity analysis. In the grey boxes, notice a decrease in permeability between the Maximum Pressure Method (yellow) and the Cement Slurry Method (blue) when the assumed mud density for the Maximum Pressure Method is reduced by a factor of two (green).

Using the reduced mud density, there was a smaller difference between the permeability values between the two methods. Smaller mud density values lowered the leakage path permeability. Therefore, having assumed a less dense fluid occupies the leakage pathway; the results between the two methods became considerably closer than

when a liquid-only completion mud was used. This method was not applied to the other wellbores within this offshore dataset, because the permeability values between the methods were already close together.

6.3.3 Leakage Depth Sensitivity Analysis

The leakage depth sensitivity analysis was conducted differently than the sensitivity analysis described in the previous two sections. In order to identify the relationship between leakage depth and permeability, the SCP Model results (Cement Slurry Method) from wellbores 10, 11, 12 (Offshore dataset) and wellbore M8 (Watson dataset) were plotted vs. leakage depth (Fig. 6.3.3.1). Additional Offshore wellbores were plotted in Fig. 6.3.3.2.

Each data point represents a permeability value obtained from the SCP Model – Cement Slurry Method for each pressure buildup. The lines connect pairs of points for which the same pressure buildup data were used to generate permeability but with different leakage depths. Each well has two or more buildups, so two or more pairs of points are plotted for each well. As explained above, the two leakage depths correspond to the minimum and maximum reasonable depths, which depend on the well construction details.

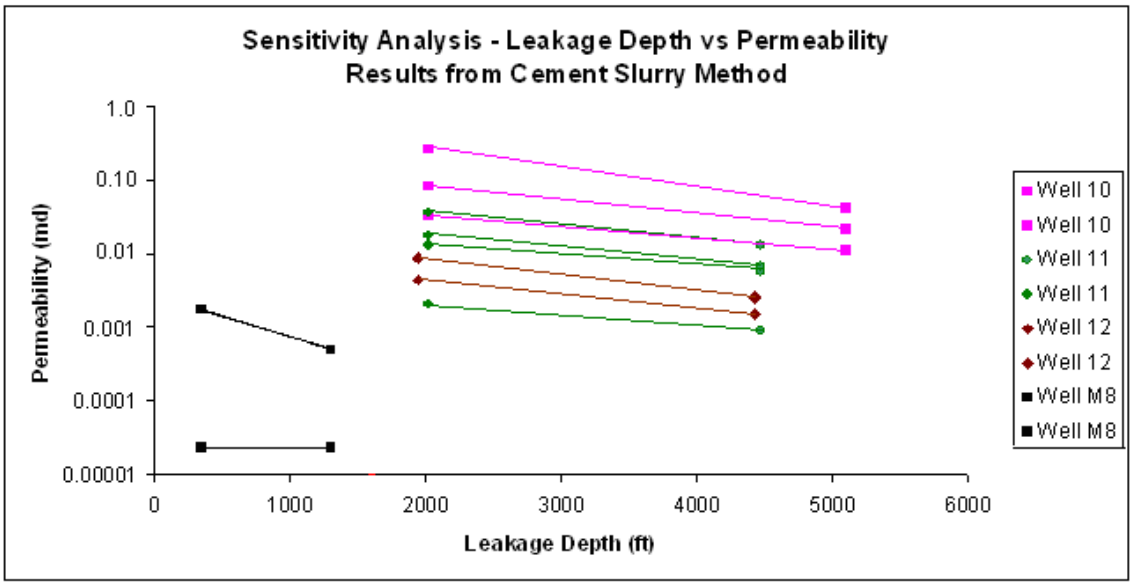

Figure 6.3.3.1 – Leakage depth sensitivity analysis. For these wellbores, all other parameter values have remained constant, but leakage depth is changing. All else being equal, deeper leakage depths yield smaller values of effective permeability.

For example, with wellbore 10, the shallow leakage depth was fixed at 2028 ft. There were three pressure buildups that generated three permeability values (0.03 md, 0.08 md, 0.10 md). Then, the leakage depth was set to its maximum value of 5093 ft. Using this depth, the three pressure buildups generated three lower permeability values (0.01 md, 0.02 md, 0.04 md).

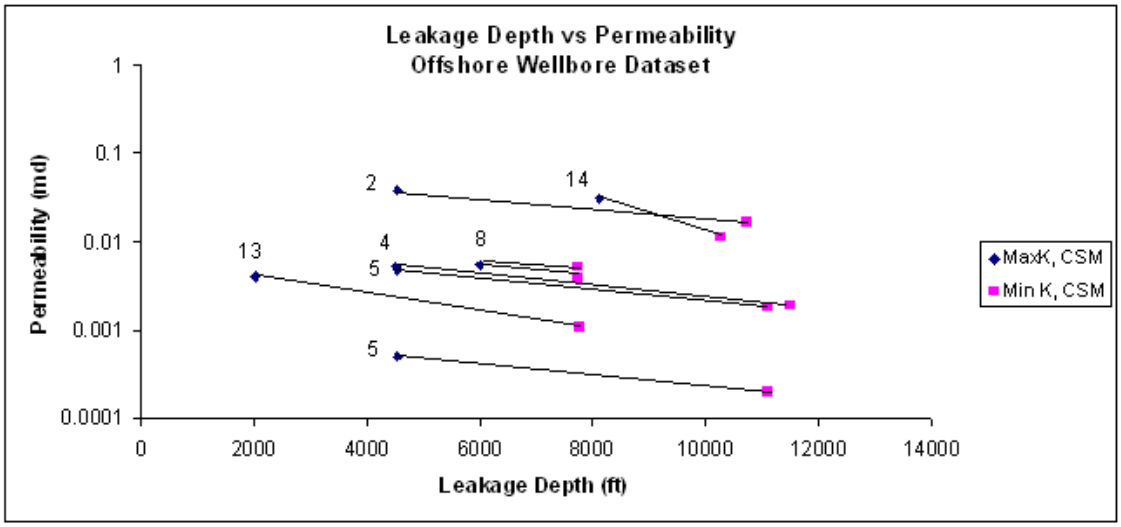

Figure 6.3.3.2 – Leakage depth sensitivity analysis. For these wellbores, all other parameter values have remained constant, but leakage depth is changing. All else being equal, deeper leakage depths yield smaller values of effective permeability.

Extending this same analysis to all example wellbores, a clear decreasing trend can be identified. The length of the leakage path along the cement also increases with depth, but this value is embedded in the script and is accounted for when leakage depth is changed. Therefore, it can be concluded that holding all parameter values constant, for deeper leakage depths, permeability decreases.

Referring to Eqn. 3.3.3, from Chapter 3, one would generally assume that this relationship between leakage depth and permeability is the same for all other wellbores. At deeper leakage depths, this would increase the length travelled by the gas to reach the surface, L_c and increase the pressure at the leakage depth, P_f. Since the pressure, P_f is squared in the numerator, the permeability value, k would have to decrease for larger pressures, P_f to keep the same flow rate, q_c and therefore the same rate of pressure buildup in the annulus.

$$q_c^n = \frac{0.00316kT_{sc}A}{p_{sc}TL_c\mu\, Z}\left[\, p_f^2 - \left(p_c^n\right)^2 \,\right] \tag{3.3.3}$$

6.3.4 Mud Length Sensitivity Analysis

Focusing on eqn. 3.3.3, the mud length sensitivity analysis can be explained mathematically. In eqn, 3.3.3, there is not a length of mud term. However, due to a hydrostatic gradient, the length of mud increases the pressure at the top of cement, P_c. For larger lengths of mud, there are greater pressures at the bottom of the mud column. However, in eqn. 3.3.3, P_c is subtracted from the formation pressure term, P_f to provide the driving force for gas flow. Therefore, in order to keep the same flow rate, q_c and thus achieve the same rate of pressure buildup, the effective permeability, *k* must increase to compensate for the smaller value of the pressure difference, $[p_f^2 - \left(p_c^n\right)^2]$. All other variables held constant, for longer mud lengths, there are increasing permeability values.

6.3.5 Gas Flow Rate Sensitivity Analysis

Since gas flow rate was generally not recorded for most of the datasets, the gas flow sensitivity analysis was performed by plotting the SCVF model results of the British Columbia Oil and Gas Commission dataset (Fig. 6.3.5.1). This plot contains flow rates (m^3/day) on the x-axis and leakage path permeability on the y-axis. The results show that for increasing flow rates, there are increasing permeability values. This relationship is confirmed in Eqn. 3.3.3 and also makes physical sense. A larger flow rate requires either a larger pressure gradient or a larger permeability, *k*. Since the pressure gradient is approximately constant in this data set (we assume 0.465 psi/ft), a larger flow rate, q_t corresponds to larger leakage path permeability, *k*.

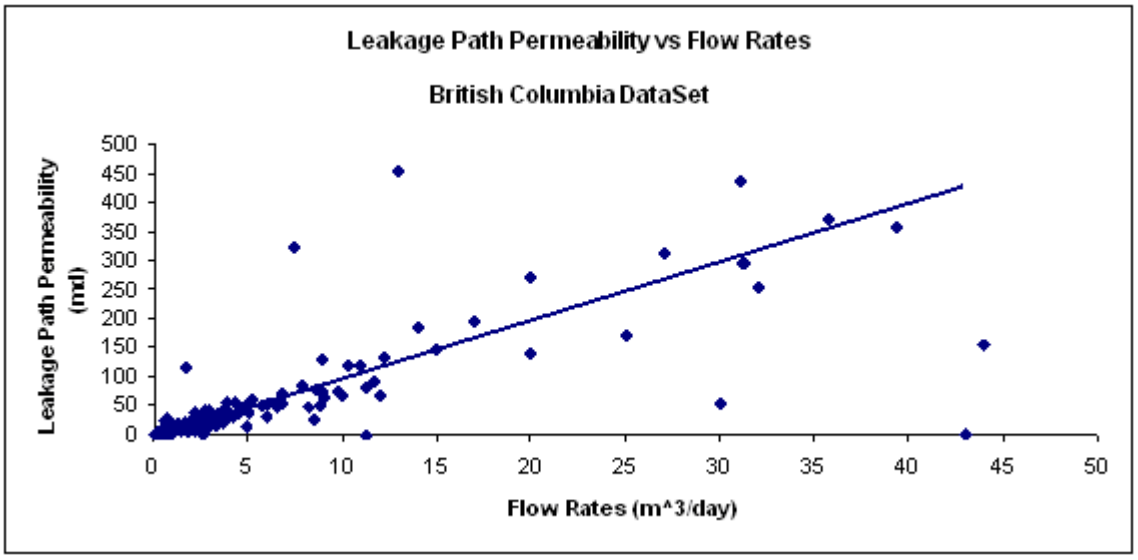

Figure 6.3.5.1 – Gas flow rate sensitivity analysis. For larger flow rates, there is an increase in leakage path permeability.

6.3.6 Mud Compressibility Sensitivity Analysis

Mud compressibility was taken to be single value (3.3×10^{-6} $psig^{-1}$,as described by Kutasov (1988). Xu performed a sensitivity analysis to compare the permeability results of slightly compressible mud to that of incompressible mud. In her conclusions, Xu acknowledged that the effect of mud compressibility would be negligible during bleed-down, since the system was open to the atmosphere (Xu, 2001). However, during pressure buildup, the valve was closed, creating a closed system. Mud compressibility then becomes an important factor in controlling the buildup rate. Xu showed that a smaller compressible mud would allow for faster buildups, but the asymptotic pressure would be the same. Since Kutasov had published findings validating that mud compressibility of WBM is 3.3×10^{-6}, $psig^{-1}$(Kutasov, 1988) this value was used for baseline results. Rather than vary the mud compressibility within a specified range (as

was done in previous sensitivity studies), mud compressibility remained at this constant value for all analysis in this work.

6.4 Application of Leakage Path Permeability to CO_2 Plume Migration

The SCP and SCVF models treat the leakage pathway as an equivalent permeable medium that fills the annular space and has an effective permeability to gas. The actual leakage path way is a discrete defect such as a crack or channel that extends between the leakage source and the top of cement. Flow within the crack or channel is a function of the geometry of the crack. It is instructive to evaluate the crack geometry that gives the same flow as the equivalent permeable medium. Leakage path permeability is used as input parameter values when converting to geometries of cracks in cement, such as the average aperture of a micro-annulus. Huerta first demonstrated this technique by converting leakage path permeability into the geometry of a slit (Huerta, 2009). Using Hagen-Poiseuille's Eqn. 6.4.1 for flow through a micro-fracture, the leakage path permeability is an input when generating different sizes and shapes of micro-fractures in the cement.

Assuming that the micro-fracture was a narrow, rectangular slit bordered by the casing boundaries (inner diameter and outer diameter), an aperture size of the slit was determined for each wellbore leakage scenario. Plotting the leakage path permeability values together generated a distribution of permeability. The permeability values, used as an input to Eqn. 6.4.1, were determined using different methods for each dataset. For example, permeability was generated by applying the Maximum Pressure Method and the Cement Slurry Method to the Offshore dataset. Most probable permeability was generated using the Monte Carlo Method for the other datasets. The wellbore

characteristics (measurement of width, etc) were known values (Fig. 6.4.1). The relationship between well characteristics (annulus cross section, A), leakage path geometry (width *W* and micro-fracture aperture *B*) and permeability is given by Eq. (6.4.1).

$$kA = \frac{WB^3}{12} \tag{6.4.1}$$

where

k = Leakage path permeability.

A = Area between the inner casing string and the outer casing string.

W = Distance between the casings.

B = Aperture size.

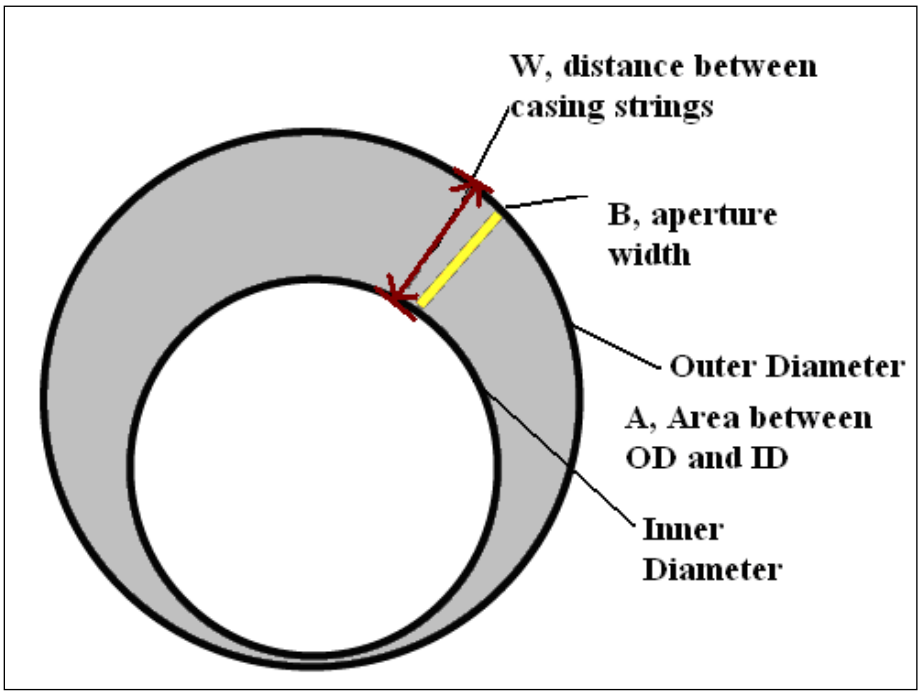

Figure 6.4.1 – Plan view of a leakage aperture through a cement filled intermediate annular space. (Huerta, 2009).

For different input parameter values, the Hagen-Poiseuille Eqn. 6.4.1 generated a distribution plot of different aperture sizes for all the dataset (Fig. 6.4.2). For the Offshore dataset, the aperture sizes range from 0.001 mm to 0.035 mm. For the Watson dataset, the aperture sizes range from 0.006 mm to 0.042 mm. For the Bourgoyne dataset, the aperture sizes are approximately 0.05 mm. For the Huerta dataset, the aperture sizes are approximately 0.12 mm. Overall, approximately 85% of all the aperture sizes range in value from 0.005 mm to 0.10 mm.

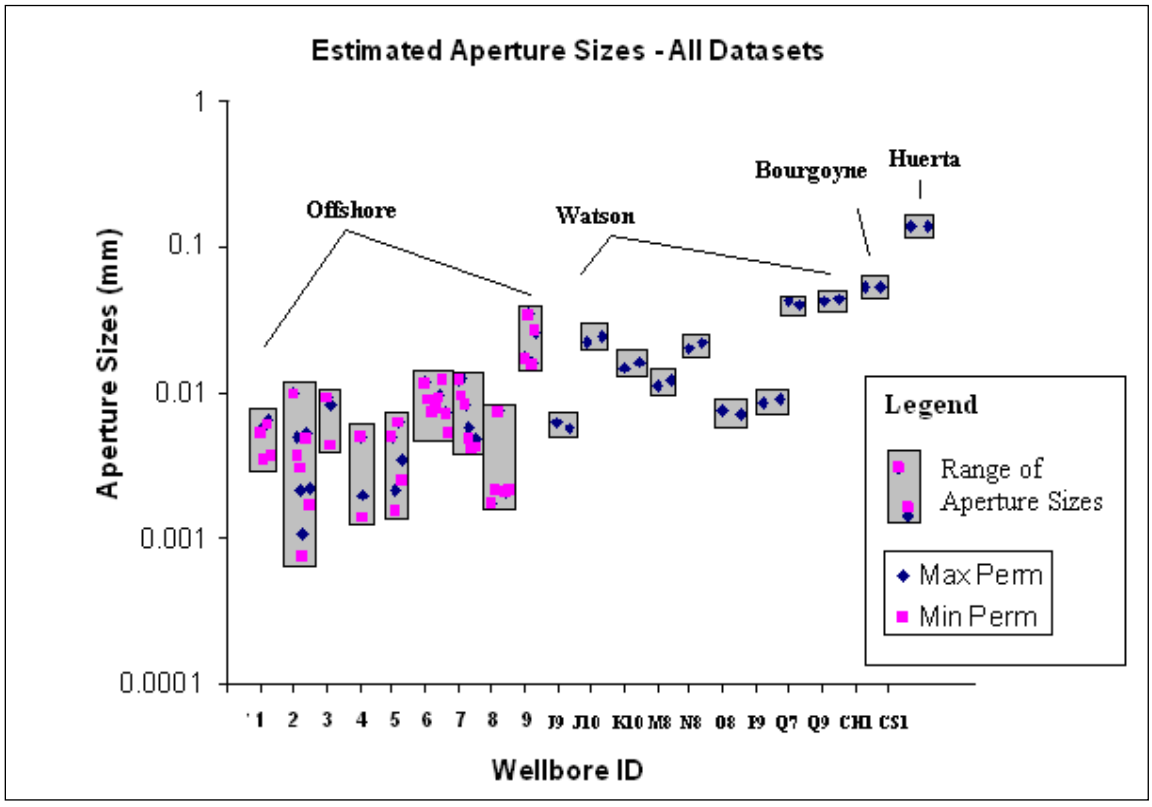

Figure 6.4.2 - Distribution of aperture sizes (mm) for all SCP datasets.

6.4.1 Comparison of Heights of CO_2 Plumes and Leakage Rates of CO_2

The wellbore leakage pathway permeability can be used as input parameter values to describe characteristics of a migrating CO_2 plume that contacts an existing wellbore. The composition of the gas that flowed through the wellbore leakage pathway was methane (CH_4). In order to apply this to CO_2 sequestration reservoirs, it was assumed that there were analogous pathways, along which CO_2 plumes would migrate towards the surface, through existing wellbores. In CO_2 sequestration projects, a plume of CO_2 can migrate after injection into highly permeable storage layers, from an injection well to an existing wellbore. As shown in Fig. 6.4.1.1, if the existing wellbore has cracks in the portion of the cement filled annulus that penetrates the storage layer, this acts as a primary leakage pathway in the steel/cement/earth system for buoyant CO_2 to migrate out of the storage layer, potentially to the surface (Tao *et al.*, 2010).

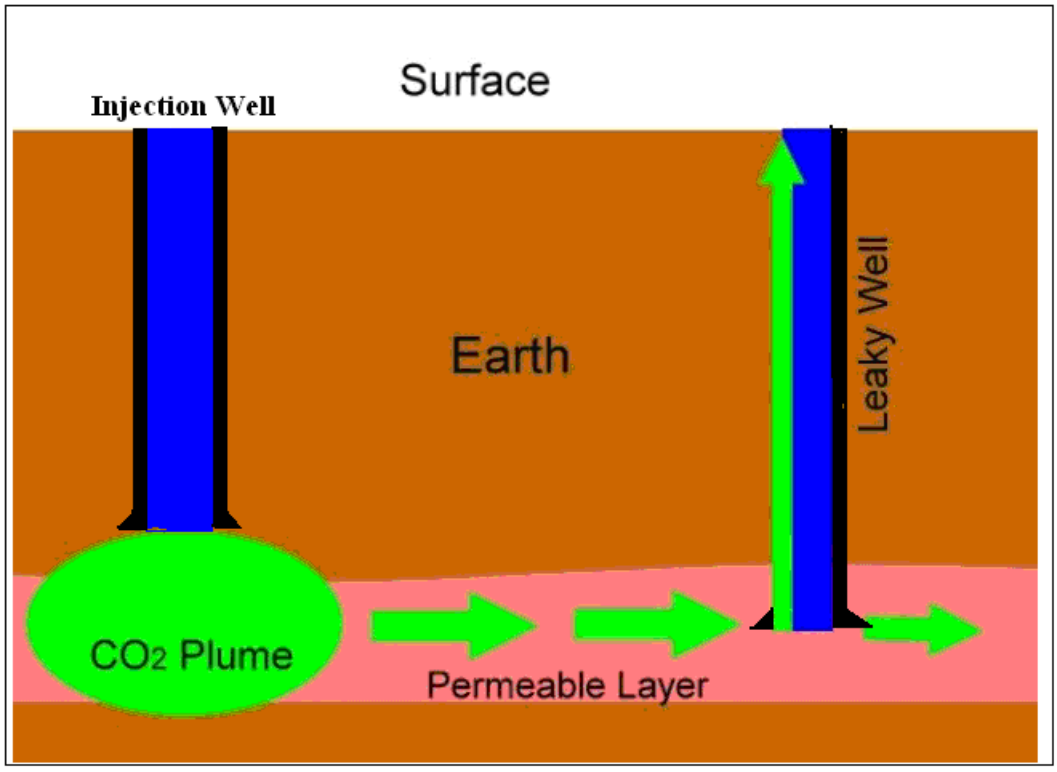

Figure 6.4.1.1 Schematic of stored CO2 plume migrating through a permeable layer, from an injection source to an existing leaky wellbore, up the crack in the cement filled annulus space (Tao *et al..*, 2010).

In order to estimate the amount of CO_2 that would leak out over time, the field measured sustained casing pressure (SCP) buildup are used as inputs to the SCP Model. The gas source is assumed to be CO_2 rather than CH_4. The unknown parameters values are the following:

(1) Leakage path permeability.

(2) Leakage source depth.

A nonwetting phase such as methane gas or bulk CO_2 cannot enter a microfracture, crack, channel, or pore throat unless the capillary pressure (the difference between nonwetting phase pressure and aqueous phase pressure) exceeds the entry pressure for that microfracture, crack, etc. Far from an injection well, the capillary

pressure, p_c in a CO_2 plume will be a function of the height, h of the plume: $p_c = (\rho_{brine} - \rho_{CO_2})gh$. When modeling the migration of CO_2, the height of the plume, h is therefore an important characteristic that dictates whether the plume can enter a leakage conduit and subsequently migrate towards the surface. Therefore, the distributions of the heights of CO_2 that are needed to overcome capillary entry pressures are calculated. The heights are then used as inputs to determine the distribution of the flow rates of CO_2 reaching the surface.

For example, with CO_2 sequestration projects, a heightened pressure level forces the migration of a plume to travel away from the injection wellbore (high pressure) through a highly permeable layer to an existing wellbore (low pressure). This wellbore may have cracks in the cement filled annular space between the formation and the steel casing. The cracks act as permeable conduits that allow gas to travel up through the annulus space. Due to the difference in density between the pore filling formation brine and the CO_2 plume, the height of the plume generates a buoyant force that can be greater than the conduit capillary entry pressure. When this criterion is satisfied, flow occurs. CO_2 enters the crack, and travels the length of the conduit to the surface, compromising the security of a carbon sequestration project.

The minimum height of CO_2 that was needed to overcome the capillary entry pressure was calculated by first estimating the density of CO_2 at a given leakage entry point into the system. For a given leakage depth, there is a corresponding leakage pressure and leakage temperature, calculated from the pressure gradient and temperature gradient. The leakage pressure was calculated using the pressure gradient Eqn. 6.4.2 and the leakage temperature was calculated using the geo-thermal temperature gradient Eqn. 6.4.3.

$$p_{leak} = 14.7 + 0.465D \tag{6.4.2}$$

$$T_{leak} = 60 + 0.015D \tag{6.4.3}$$

where

p_{leak} = leakage pressure [psi]

D = depth [ft]

T_{leak} = leakage temperature [F]

For different subsurface temperatures, T_i and pressures, P_i the CO_2 density was calculated from using Eqn. 6.4.4

$$\rho_i = \frac{4400 P_i}{ZRT_i} \tag{6.4.4}$$

The constant, 4400 is used as a conversion factor to obtain the correct units for density $\frac{kg}{m^3}$ when P_i, T_i and R have units of *atm, Kelvin,* $\frac{Jmol}{K}$, respectively. The value, Z is obtained from the roots of the Peng Robinson Equation of State.

The density of water changed at different pressures, temperatures at depths, according to a density diagram (see Fig. 6.4.1.2). On the left hand side of the phase diagram, the density of water (kg/m^3) is plotted against temperature (Celsius). On the right hand side of the plot, the density of water (kg/m^3) is plotted against pressure (MPa). For these leakage scenarios, (temperatures and pressures) the density of water did not vary significantly from 1100 kg/m^3 (green line, left/right panel of Fig. 6.4.1.2). The difference between the density of CO_2 and the density of water, $\Delta\rho$ was then calculated for each leakage scenario.

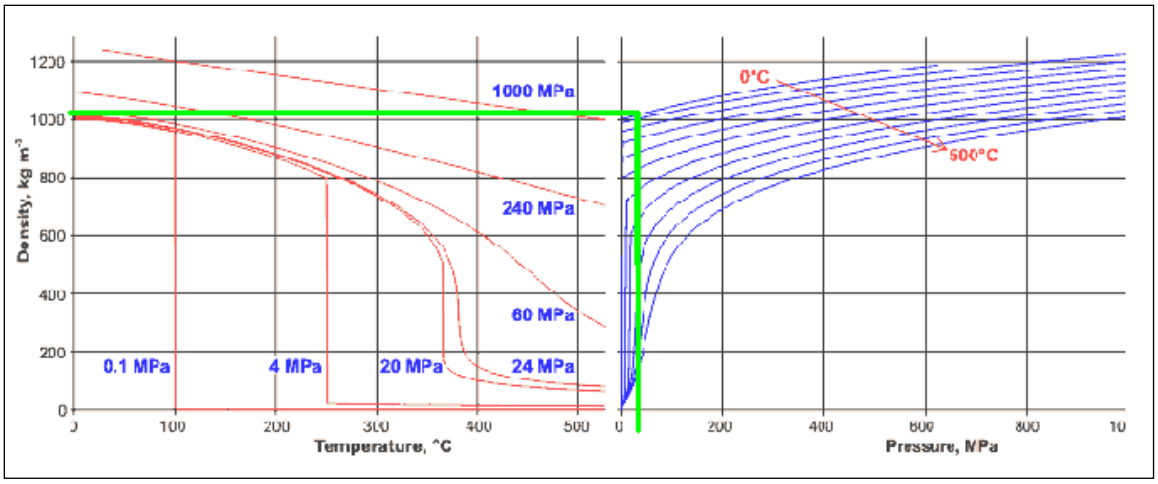

Figure 6.4.1.2– Change in water density diagram for different pressures, temperatures.

At the contact point between the CO_2 plume and the crack in cement, there is interfacial contact between the CO_2 phase and brine. The interfacial tension between these two fluids at leakage depth (pressures, temperatures) is taken as $23\ \frac{\text{mN}}{\text{m}}$ (Chiquet *et al.*, 2006). The capillary entry pressure was calculated using Eqn. 6.4.5,

$$Pc = \frac{2 * \lambda \cos\theta}{B} \tag{6.4.5}$$

where

P_c = capillary entry pressure [Pa]

λ = interfacial tension between CO_2 and water [$23\frac{mN}{m}$]

θ = contact angle [0 degrees]

B = aperture size [m]

Aperture sizes *B* were calculated previously by using Eqn. 6.4.1 and the leakage path permeability, *k* and other wellbore characteristics. Capillary entry pressures, P_c were determined for the different aperture sizes, *B*. Using the different values for capillary entry pressure, P_c, the corresponding heights of CO_2 needed to enable the CO_2 to enter the aperture were calculated, using Eqn. 6.4.6:

$$h = \frac{P_c}{9.81\Delta\rho} \tag{6.4.6}$$

where

h = height [m]

P_c = capillary entry pressure [Pa]

$\Delta\rho$ = difference in density between CO_2 and water [$\frac{kg}{m^3}$]

The results of the distribution of the estimated heights of CO_2 plumes for all the datasets are plotted in Fig. 6.4.1.3. As can be observed, smaller aperture widths require larger capillary entry pressures. In order to overcome this gas entry requirement, larger heights of CO_2 plumes were needed. Therefore, the largest height of CO_2 (18 m) was required for the smallest aperture width (Offshore - wellbore 2) to allow the plume to enter the crack/conduit. The smallest height of CO_2 (0.09 m) was needed for the largest aperture width (Huerta-Case Study 1). In general, for the Watson, Bourgoyne, and Huerta datasets, the aperture widths were much larger than what were observed in the Offshore dataset. Therefore, much smaller heights of CO_2 (0.1 m to 1.0 m) were required (Fig. 6.4.1.3).

This raises concern that only a minimal amount of CO_2 that is pumped into the subsurface would provide sufficient driving force to overcome capillary entry pressures

of such large aperture widths. However, it is important to note that this set of wellbore data contained some of the highest pressure buildup rates recorded (several 1000's psi/day). Focusing on the range of CO_2 plume heights that includes most of the results from all the datasets, the range would be between 10m and 0.5m.

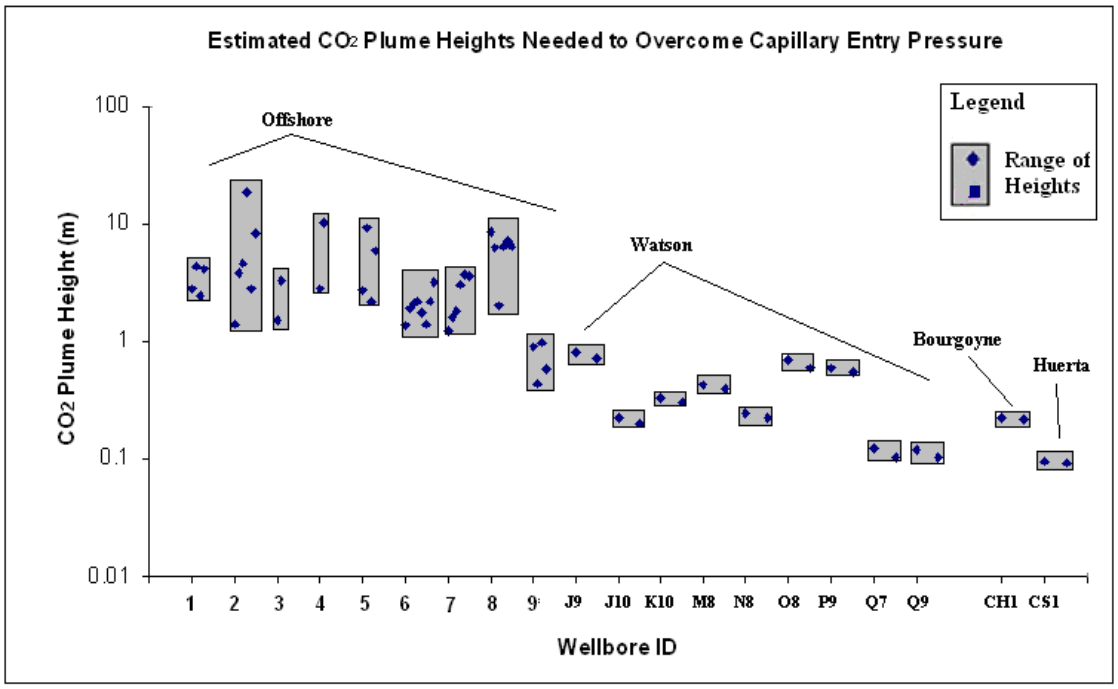

Figure 6.4.1.3 - Distribution of heights of CO_2 plume needed in order for the CO_2 plume to enter wellbore leakage path for SCP wellbores. The CO_2 plume height that is necessary to enter the leakage conduit varies from 1 meter to 18 meter.

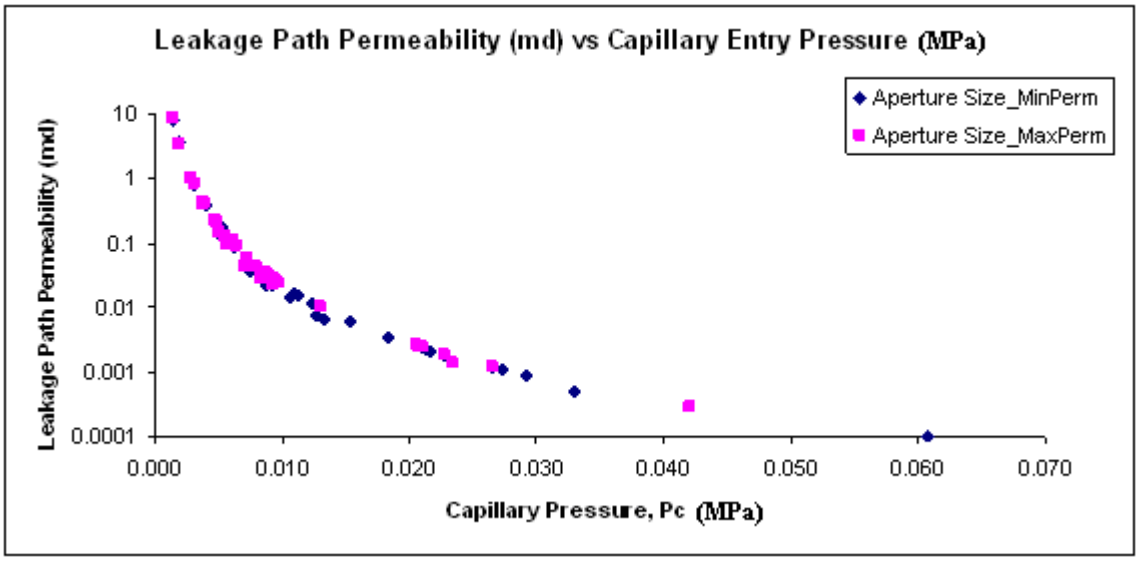

Figure 6.4.1.4 – Leakage path permeability vs. capillary entry pressure for CO_2/brine, assuming interfacial tension of 23 mN/m and zero contact angle.

There is an inverse relationship between leakage path permeability and capillary pressure. For larger leakage path permeability, there is a much smaller capillary entry pressure. As leakage path permeability decreases by a magnitude of 10 (y-axis is log scaled), capillary entry pressure increases proportionately. Very small orders of magnitude of leakage path permeability (0.0001 md) correspond to the highest capillary entry pressures (0.065 MPa), converting this to psi, 0.065 MPa = 9.4 psi

There is also an inverse relationship between aperture sizes and capillary entry pressures (Fig. 6.4.1.5). For larger aperture widths, there is decrease in capillary entry pressures required for formation fluid/ gas to enter the leakage pathway (notice: the y-axis is not log-scaled). Initially, for large changes in aperture width, there are small differences in capillary entry pressure. This relationship is consistent until the aperture widths are around or below 0.005 mm, and then this trend is no longer applicable. For small changes in aperture width, there are large differences in capillary entry pressure. For very small aperture widths (less than 0.005 mm), a very large capillary entry pressure

exists (greater than 0.020 MPa). High capillary entry pressures require large heights of CO_2 gas to enter the conduit. Therefore, only a large volume of pumped CO_2 would generate plume height of the necessary characteristics to enter the leakage pathway and migrate to surface.

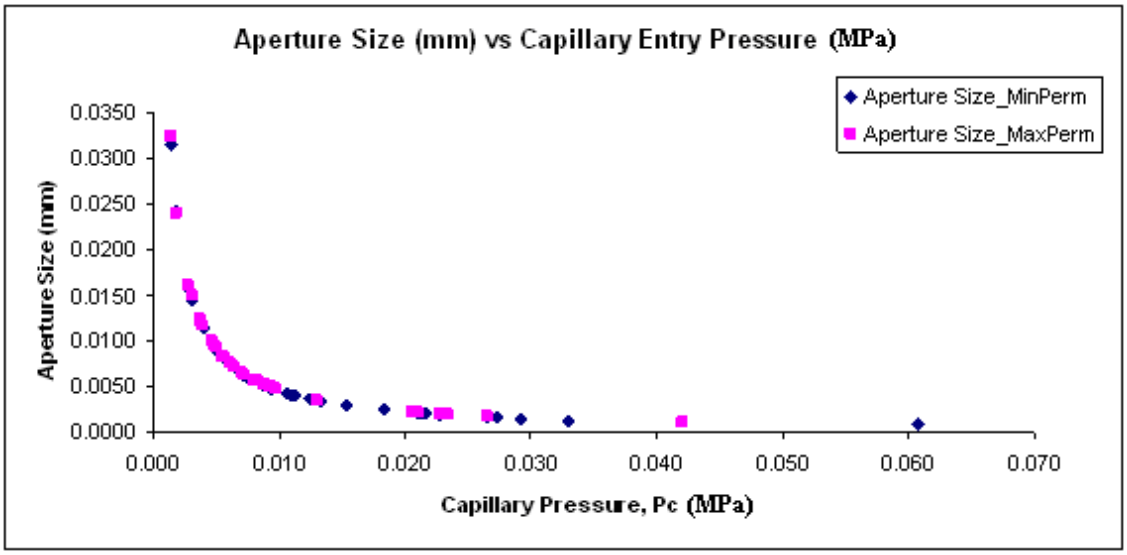

Figure 6.4.1.5 - Aperture size vs. capillary entry pressure.

The final application of using the SCP and SCVF Model outputs (permeability) and wellbore parameters was to determine the range of fluxes of a CO_2 plume (tons/year) that would migrate from the storage reservoir (at depth) up the leakage pathway/conduit, to the surface. For this purpose the model described in Tao *et al.* (2010) was used. As can be observed in Fig. 6.1.4.6, the larger the permeability, the greater the CO_2 flux. Since the relationship is linear, CO_2 flow rates are directly proportional to permeability, which are directly proportional to aperture sizes. A distribution of permeability would therefore be similar to a distribution of CO_2 leakage fluxes.

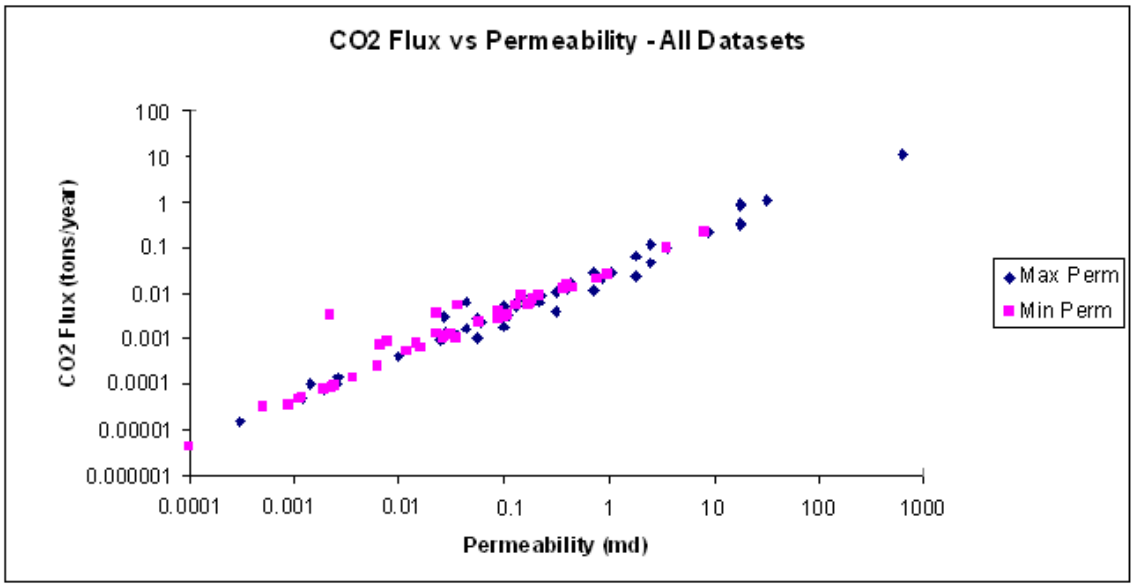

Figure 6.4.1.6 – CO_2 flux vs. permeability (for all datasets). Linear relationship observed.

A closer analysis of the estimated CO_2 fluxes for all the datasets can be observed in Fig. 6.4.1.7. For the Offshore dataset, the fluxes range from 1 ton/year to 0.00001 ton/year. For the Watson dataset wellbores, the fluxes range from 0.001 ton/year to 0.5 ton/year. For the Bourgoyne dataset, the fluxes are about 1 ton/year. For the Huerta dataset, the fluxes are about 11 ton/year.

The distribution of fluxes is very similar to the distribution of permeability values (Fig. 6.2.1.1) For example, wellbore 9 had the largest permeability values for the Offshore dataset, and the highest flux. The same is true for the other datasets; therefore there is a strong relationship between flux and permeability.

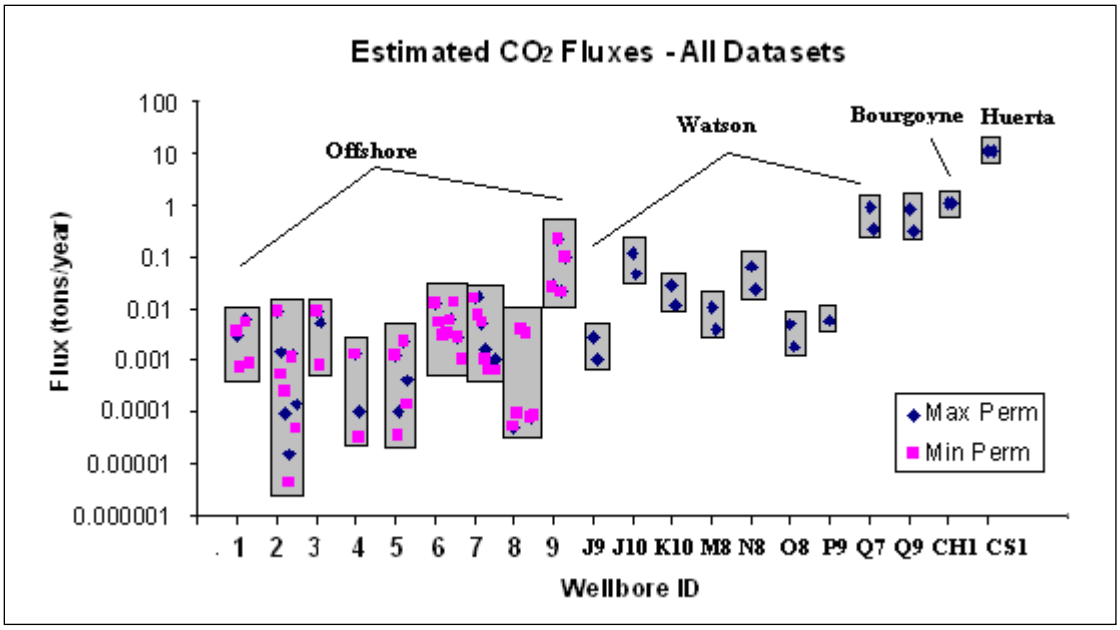

Figure 6.4.1.7 – Distribution of CO_2 fluxes (tons/year) for given wellbores, if plume encountered analogous conduits along wellbores penetrating storage formation.

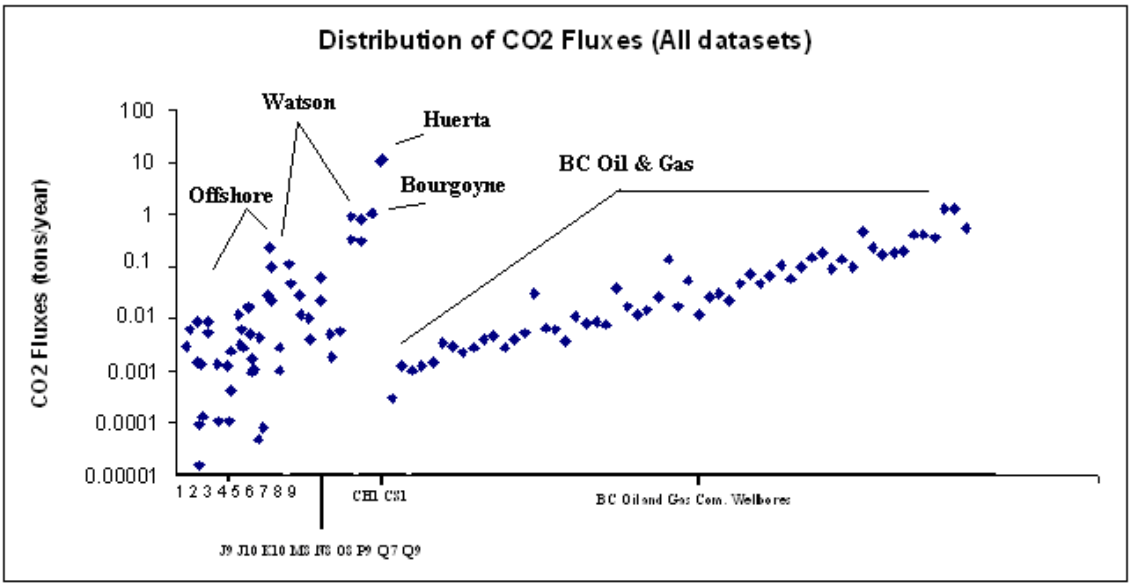

Figure 6.4.1.8 – Comparison of CO_2 fluxes (tons/year) between wellbores analyzed by SCP Model and SCVF Model.

Given that typical CO_2 sequestration projects would be injecting around 1,000-10,000 ton/year of CO_2 into a target reservoir, such low leakage fluxes are further evidence to support such projects. Even at the higher range of leakage fluxes between 1 tons/year to 10 tons/year, this would only be 0.1% to 1% of the volume injected per leaky wellbore over time. In order to provide a comprehensive site leakage assessment, all the existing wellbores in contact with the reservoir would have to be accounted for.

This concludes the section describing the application of effective permeability. Future sequestration reservoir projects that depend on modeling leakage through existing wellbores should be able to use these results in order to assess the risk of gas leakage. The leakage flux depends on the leakage path permeability and the size of the gas plume that contacts the entry point into the annulus. The number of wells analyzed (238) and the corresponding effective permeability distributions provide robust input parameter values for leakage models.

Chapter 7: Conclusion

7.1 Leakage Path Permeability Distributions - SCP Model and SCVF Model

The important contribution of this research, which can be used for future CO_2 leakage modeling, is the leakage path permeability distribution from the SCP Model and the SCVF Model, applied to oil and gas well data. These two final distributions were generated by analyzing field datasets for leaky wells, using the Monte Carlo Method. The distributions are believed to be the most comprehensive compiled to date, with 39 pressure buildups chosen from a total of 17 offshore wells and 19 pressure buildups chosen from a total of 10 wells onshore. 210 wellbores were chosen from an original 350 wellbores that demonstrated SCVF. The pressure buildups and vent flows were screened to ensure they were due to gas migrating from an earth formation along the casing/cement/earth interface into the annulus so that they could be used for modeling purposes.

Making the assumption that these leakage paths are analogous to those along existing wellbores that could be encountered by CO_2 plumes, readers are encouraged to use these permeability distributions when modeling leakage pathways and generating gas leakage fluxes. The distribution of expected values of provide a smaller range of uncertainty (3 orders of magnitude, from 0.001 md to 1 md) for leakage path permeability compared with the range used by Celia *et al.* (10 orders of magnitude) for risk assessment. The Celia *et al.* leakage permeability distribution is based on an assumption of wellbore characteristics, rather than leaky wellbore field data. Therefore, if these measurements are representative of existing wells likely to be encountered by CO_2 plumes, this reduction of uncertainty narrows the range of fluxes that would escape from the storage formation for a given sequestration project.

7.2 METHODS TO REDUCE UNCERTAINTY

Since the leaky wellbore datasets provided little information about the leakage depth into the intermediate annulus space, three different methods were used to reduce uncertainty of this parameter value. The three methods (Cement Slurry Method, Maximum Pressure Method and Monte Carlo Method) used different known wellbore information to bind the unknown leakage depth parameter values. By doing so, the SCP Model and the SCVF Model produced comparable leakage path permeability ranges, populated by the results from each pressure buildup.

The comparison of the results for the same pressure buildup interval should be nearly identical for the methods. However, the Maximum Pressure Method permeability results were generally higher than the Cement Slurry Method, for the same pressure buildup. The Monte Carlo Method generally provides the widest range of permeability values, and the results from the other two methods are located within this wide range of values. The more useful comparison is therefore between the Cement Slurry Method and the Maximum Pressure Method.

7.3 RANGE OF CO_2 FLUXES FOR THESE WELLBORE DATASETS

As discussed in Chapter 6, the flux of CO_2 is a function of leakage path permeability. Holding all other variables constant, the greater the permeability, the larger the flux. As has been demonstrated, permeability is used as an input to calculating crack aperture widths. Holding all other variables constant, the greater the permeability, the larger the crack aperture widths.

One measurement used by regulatory agencies to access the risk of a CO_2 sequestration project is the amount of measurable CO_2 that would migrate to surface over time. Having obtained effective permeability, the migrating amount (flux) can be estimated from the wellbores in the Offshore dataset. The fluxes of CO_2 were generated, assuming buoyancy driven upward force.

In conclusion, the overall range of CO_2 fluxes varied from 0.0001 tons/year to 10 tons/year for individual wells. However, 9/10 of the fluxes are within a range of 0.001 tons/year to 1 ton/year. These rates are not considered to be serious threat to sensitive areas/depths. The leakage fluxes are relatively small, as compared to the large injection well rates (several 1000 tons/year) of CO_2. Large gas volumes would be pumped into the storage reservoir during the lifetime of the sequestration operations. At the upper end of the range, only 1% of the injected amount would have leaked to surface from this existing wellbore. Therefore, it would be recommended that sequestration projects in contact with wellbores examined in this thesis would provide sufficient seals to prevent significant leakage to surface.

7.4 FUTURE WORK

There remains much work to be done in analyzing new leaky wellbore datasets and comparing results with existing findings. Additional wellbores would provide data to compare results between the Cement Slurry Method and the Maximum Pressure Method, to have closer overlaps. One possible source of additional leaky wellbore dataset information is from wellbores that are in communication with CO_2 Enhanced Oil Recovery (EOR) projects.

At a March, 2012 CO_2 EOR Conference sponsored by the Permian Technology Transfer Council (PTTC), engineers discussed the use of CO_2 for tertiary recovery in developed fields of the Permian Basin region. Operators of existing injection and producing wells mentioned recording sustained casing pressure buildups and vent flows on intermediate annulus. The Texas Railroad Commission requires reporting on such issues from the operators. It is recommended that future investigative work would involve collaboration with these operators.

Existing data would be located within the company, and may require additional searching in-house. Gas leakage rates and pressure buildup data on existing producing and injection wellbores should be reported. Other fields outside the Lubbock-Midland, TX area may be investigated additionally. Non EOR fields would also be worth investigating and some information may be available at the Texas Railroad Commission, which requires that operators install surface leakage monitoring devices collect existing leaky wellbore data. Once analyzed, the additional permeability values could be compared to the current SCVF and SCP distributions. Contact information for these operators is listed in the appendix.

Last, as mentioned in Chapter 6, future work on comparing the permeability values between the Cement Slurry Method and the Maximum Pressure Method would be very beneficial. If new leaky wellbores can be obtained with several pressure buildups, a series of permeability values can be generated using the SCP Model or SCVF Model. The comparison between these permeability values would provide a useful analysis between the two methods.

Appendix

A.01 - SCVF Model Derivation (Tao, 2012)

We assume that gas establishes a steady saturation in the pathway. The pathway is treated as an equivalent Darcy continuum, consistent with the assumptions in the SCP model used to estimate the permeability. The mass flow of gas is given by

$$m = -\rho \frac{k_{eff} A}{\mu} \nabla \Phi , \tag{1}$$

where m is mass flow rate, ρ is density, k_{eff} is effective permeability of leakage pathway, A is cross-sectional area, μ is viscosity and Φ is potential of gas.

The potential of gas is given by

$$\Phi = p - \rho g z , \tag{2}$$

where p is pressure, z is depth and g is gravitational constant.

The density of gas varies along the pathway. The Peng-Robinson equation of state (Sandler, 2006) is used, given by

$$P = \frac{RT}{\underline{V} - b} - \frac{a(T)}{\underline{V}(\underline{V} + b) + b(\underline{V} - b)}, \tag{3}$$

with

$$a(T) = 0.45724 \frac{R^2 T_c^2}{P_c} \alpha(T) , \tag{4}$$

$$b = 0.07780 \frac{RT_c}{P_c} , \tag{5}$$

$$\sqrt{\alpha} = 1 + \kappa \left(1 - \sqrt{\frac{T}{T_c}} \right), \tag{6}$$

$$\kappa = 0.37464 + 1.54226\omega - 0.26992\omega^2, \quad (7)$$

where T_c and P_c are critical temperature and pressure, and ω is the acentric factor. For methane, they are given by (Sandler, 2006)

$$T_c = 190.45 \text{ K}, \; P_c = 45.96 \text{ MPa}, \; \omega = 0.008, \quad (8)$$

Solving Eq. (3) to (8) enables us to compute the gas density. The viscosity is assumed to be constant as 0.02 cP. The temperature along the pathway simply follows the geothermal gradient.

We solve in discretized form the flow equation Eq. (1) and (2), together with steady state mass balance equation given by

$$m_{i,in} = m_{i,out}, \quad (9)$$

where *i* denotes spatial grid block. Eq. (9) indicates that there is no accumulation and gas has established steady saturation along the pathway.

It yields the pressure profile of gas along the pathway. The solution is iterative with the density of gas estimated from the pressure profile using the methods described above. The property profiles are then used to update the gas flux.

Reference:

Sandler, S.I., 2006. Chemical, Biochemical and Engineering Thermodynamics. John Wiley & Sons, Inc. 4th Edition, 6 (4), p. 208-210.

Figure A1 – Derivation of SCVF Model Equation (Tao, 2012).

A.02 - SCVF WELLBORE DATABASE (BC OIL AND GAS COMMISSION WELLBORES)

Area Name	WA #	Analysis Date	Build Up Pressure kPa	Flow Rate m^3/day	Casing Size mm	Casing Type	Cement Vol Tons	Casing Size mm	Casing Type	Cement Vol Tons	Len_cem m	Len_mud m	TOC m	Upper Casing Depth m	Lower Casing Depth m
RING	5242	23-Feb-10	86	0.1	244.5	SFC		114.3	PROD	36.5	319	2197	2197	466	2516
BLUEBERRY	6672	30-Mar-10	327	0.1	339.7	SFC		177.8	INT	32.5	158	1920	1920	331	2078
GUNNELL	11670	5-Aug-10	30	0.1	244.5	SFC		177.8	INT		0	1580	1580	215	1580
SIERRA	12275	18-Sep-09	247	0.1	244.5	SFC		177.8	PROD		0	1506	1506	230	1506
BLUEBERRY	13933	20-Dec-08	650	0.1	244.5	SFC		177.8	INT		0	1747	1747	282	1747
CUTBANK	16952	18-Nov-09	1	0.1	244.5	SFC	31	177.8	INT	26	377	2156	2156	370	2533
CUTBANK	18240	4-Nov-09	212	0.1	244.5	SFC	22	177.8	INT	25	362	2081	2081	362	2443
HIDING	19477	7-Aug-09	626	0.1	244.5	SFC	37	139.7	PROD	73	740	2792	2792	481	3532
SUNDOWN	21138	20-Oct-09	258	0.1	219.1	SFC	19.5	114.3	PROD	37	432	1549	1549	360	1981
CLARKE	22601	27-Feb-08	474	0.1	244.5	SFC	22.5	177.8	INT	34.8	504	1594	1594	453	2098
SIERRA	24050	28-May-09	44	0.1	244.5	SFC	19.5	177.8	INT	26	377	1120	1120	278	1497
SIERRA	24125	5-Jul-10	718	0.1	244.5	SFC	17.7	177.8	INT						
KOMIE	24219	15-Dec-08	3975	0.1											
HERITAGE	24359	23-Jul-10	1983	0.1	244.5	SFC	33	177.8	INT	46.9	679	2433	2433	540	3112
KYKLO	25337	20-Sep-09	448	0.1	244.5	SFC	18.7	177.8	INT	22	319	1193	1193	277	1512
AIRPORT	7434	22-Mar-10	64	0.2	219.1	SFC	25	139.7	PROD	109.2	1564	604	604	343	2169
ALTARES	20757	2-Dec-07	265	0.2	219.1	SFC	25	139.7	INT	65.6	940	1073	1073	310	2013
CARIBOU	25296	21-Aug-09	105	0.2	244.5	SFC	24	177.8	PROD	31	449	1721	1721	371	2170
CUTBANK	20723	29-Oct-09	25	0.2	244.5	SFC	18	177.8	INT	25	362	2093	2093	347	2455
FIREWEED	16569	21-Jun-09	79	0.2	219.1	SFC	23	139.7	PROD	32	458	1272	1272	265	1730
GUNNELL	21461	26-Jul-10	5	0.2	244.5	SFC	21								
HELMET	11969	26-Jul-10	33	0.2	219.1	SFC		139.7	INT						
HERITAGE	24361	25-Aug-09	277	0.2	244.5	SFC	28.2	177.8	INT	34.9	506	1944	1944	443	2450
KOMIE	24577	21-Jan-10	1355	0.2			10.5								
KYKLO	25659	12-Jul-10	90	0.2	244.5	SFC	18	177.8	INT	26.4	382	1146	1146	276	1528
SIERRA	24125	28-May-09	443	0.2											
ALTARES	20757	7-Sep-07	2800	0.3	219.1	SFC	25	139.7	INT	65.6	940	1073	1073	310	2013
CUTBANK	22903	4-Nov-09	132	0.3	244.5	SFC	25	177.8	INT	30.5	442	2064	2064	368	2506
FIREWEED	20945	21-Jun-09	106	0.3	219.1	SFC	17	114.3	PROD	33	385	1431	1431	308	1817
GUNNELL	17417	27-Jul-10	18	0.3	244.5	SFC	22	177.8	INT	31	449	1141	1141	267	1590
GUNNELL	17421	6-Aug-10	232	0.3	244.5	SFC	21	177.8	INT	28.4	411	1232	1232	265	1643
HELMET	19818	26-Jul-10	4	0.3	244.5	SFC	21.4	177.8	INT	25.1	364	808	808	289	1172
NOEL	16732	29-Oct-09	42	0.3	244.5	SFC	22.1	177.8	INT	29	420	2048	2048	367	2468
NOEL	16852	20-Oct-09	490	0.3	244.5	SFC	20	177.8	INT	38	551	1849	1849	406	2400
OAK	8154	25-Oct-09	589	0.3	219.1	SFC	16	139.7	PROD	21	301	948	948	199	1249
SAHTANEH	19118	5-Aug-10	1	0.3	244.5	SFC	20.3	177.8	INT	38	551	1068	1068	264	1619
SAHTANEH	23079	15-Jul-10	10	0.3	244.5	SFC	19	177.8	INT	28.3	410	1171	1171	281	1581
SAHTANEH	24945	5-Aug-10	9	0.3	244.5	SFC	17.7	177.8	INT	31	449	1138	1138	283	1587
SUNDOWN	19415	20-Oct-09	85	0.3	244.5	SFC	20	177.8	INT	36	522	1976	1976	372	2498
TUPPER	14249	20-Oct-09	54	0.3	219.1	SFC		139.7	PROD						
TUPPER	16328	14-Oct-10	263	0.3	177.8	SFC	16.4	114.3	PROD	23.5	517	1051	1051	253	1568
TUPPER	19681	18-Nov-09	111	0.3	219.1	SFC	10.2	114.3	PROD	37	432	1799	1799	361	2231
TWO RIVERS	9991	3-Jun-09	673	0.3	219.1	SFC	10	139.7	PROD	18	258	884	884	157	1142
WALRUS	14750	26-Jul-10	60	0.3	244.5	SFC		177.8	INT						
ALTARES	20757	7-Sep-06	2800	0.4	219.1	SFC	0	139.7	PROD	11.9	171	1030	1030	174	1201
BULLMOOSE	21737	21-Jan-07	1000	0.4	244.5	SFC	0	114.3	PROD	12.7	111	1167	1167	162	1278
FIREWEED	19373	21-Jun-09	364	0.4	219.1	SFC	19	114.3	PROD	42	491	1378	1378	306	1869
NOEL	16051	20-Oct-09	115	0.4	244.5	SFC	28	177.8	INT	35	507	2001	2001	376	2508
SIERRA	11976	8-Jul-10	61	0.4	244.5	SFC		177.8	PROD						
SUNDOWN	21312	8-May-09	919	0.4	244.5	SFC	21	177.8	INT	31	449	1986	1986	357	2435
SUNDOWN	21768	20-Oct-09	1070	0.4	244.5	SFC	25	177.8	INT	29	420	1876	1876	344	2296
W GUNDY	4965	10-Mar-09	2275	0.4	244.5	SFC	39.7	139.7	PROD	82.9	840	1050	1050	378	1890
BRASSEY	19833	20-Oct-09	290	0.5	244.5	SFC	23	177.8	INT	27	391	1987	1987	375	2378
HELMET	18250	26-Jul-10	73	0.5	244.5	SFC	20	177.8	INT	29	420	919	919	277	1339
JACKPINE	17698	14-Oct-09	249	0.5	244.5	SFC	35	139.7	PROD	92.5	938	2972	2972	611	3910
NOEL	18550	20-Oct-09	88	0.5	244.5	SFC	26	177.8	INT	24	348	2034	2034	346	2382
SUNDOWN	19131	17-Sep-10	260	0.5	219.1	SFC	21	114.3	PROD	44	514	2071	2071	397	2585
SUNDOWN	20984	29-Sep-09	797	0.5	244.5	SFC	20.5	177.8	INT	24	348	2053	2053	347	2401
SUNSET	25773	31-Mar-10	1226	0.5	219.1	SFC	45	114.3	PROD	102.4	1196	3097	3097	650	4293
NOEL	18910	29-Oct-09	340	0.6	244.5	SFC	28.5	177.8	INT	24.5	355	2091	2091	367	2446
NOEL	20102	18-Nov-09	2950	0.6	244.5	SFC	28	177.8	INT	29	420	2076	2076	372	2496
S THETLAANI	3481	29-Jul-10	143	0.6	219.1	SFC	0	114.3	PROD	19.1	223	304	304	160	526
SIERRA	25481	12-Jul-10	173	0.6	244.5	SFC	18	177.8	INT	22.7	329	1216	1216	281	1545
SUNDOWN	19805	5-Oct-09	759	0.6	244.5	SFC	29	177.8	INT	30.5	442	2158	2158	373	2600
CUTBANK	17048	18-Nov-09	156	0.7	219.1	SFC	22	114.3	PROD	45.5	531	1803	1803	361	2334
CUTBANK	20983	8-Mar-09	461	0.7	244.5	SFC	21	177.8	INT	33	478	2022	2022	361	2500
FIREWEED	20068	21-Jun-09	242	0.7	219.1	SFC	19	114.3	PROD	33.5	391	1437	1437	268	1828
HELMET	11709	28-Nov-09	341	0.7	244.5	SFC		177.8	PROD						

HERITAGE	24361	25-Aug-09	277	0.2	244.5 SFC	28.2	177.8 INT	34.9	506	1944	1944	443	2450
KOMIE	24577	21-Jan-10	1355	0.2		10.5							
KYKLO	25659	12-Jul-10	90	0.2	244.5 SFC	18	177.8 INT	26.4	382	1146	1146	276	1528
SIERRA	24125	28-May-09	443	0.2									
ALTARES	20757	7-Sep-07	2800	0.3	219.1 SFC	25	139.7 INT	65.6	940	1073	1073	310	2013
CUTBANK	22903	4-Nov-09	132	0.3	244.5 SFC	25	177.8 INT	30.5	442	2064	2064	368	2506
FIREWEED	20945	21-Jun-09	106	0.3	219.1 SFC	17	114.3 PROD	33	385	1431	1431	308	1817
GUNNELL	17417	27-Jul-10	18	0.3	244.5 SFC	22	177.8 INT	31	449	1141	1141	267	1590
GUNNELL	17421	6-Aug-10	232	0.3	244.5 SFC	21	177.8 INT	28.4	411	1232	1232	265	1643
HELMET	19818	26-Jul-10	4	0.3	244.5 SFC	21.4	177.8 INT	25.1	364	808	808	289	1172
NOEL	16732	29-Oct-09	42	0.3	244.5 SFC	22.1	177.8 INT	29	420	2048	2048	367	2468
NOEL	16852	20-Oct-09	490	0.3	244.5 SFC	20	177.8 INT	38	551	1849	1849	406	2400
OAK	8154	25-Oct-09	589	0.3	219.1 SFC	16	139.7 PROD	21	301	948	948	199	1249
SAHTANEH	19118	5-Aug-10	1	0.3	244.5 SFC	20.3	177.8 INT	38	551	1068	1068	264	1619
SAHTANEH	23079	15-Jul-10	10	0.3	244.5 SFC	19	177.8 INT	28.3	410	1171	1171	281	1581
SAHTANEH	24945	5-Aug-10	9	0.3	244.5 SFC	17.7	177.8 INT	31	449	1138	1138	283	1587
SUNDOWN	19415	20-Oct-09	85	0.3	244.5 SFC	20	177.8 INT	36	522	1976	1976	372	2498
TUPPER	14249	20-Oct-09	54	0.3	219.1 SFC		139.7 PROD						
TUPPER	16328	14-Oct-10	263	0.3	177.8 SFC	16.4	114.3 PROD	23.5	517	1051	1051	253	1568
TUPPER	19681	18-Nov-09	111	0.3	219.1 SFC	10.2	114.3 PROD	37	432	1799	1799	361	2231
TWO RIVERS	9991	3-Jun-09	673	0.3	219.1 SFC	10	139.7 PROD	18	258	884	884	157	1142
WALRUS	14750	26-Jul-10	60	0.3	244.5 SFC		177.8 INT						
ALTARES	20757	7-Sep-06	2800	0.4	219.1 SFC	0	139.7 PROD	11.9	171	1030	1030	174	1201
BULLMOOSE	21737	21-Jan-07	1000	0.4	244.5 SFC	0	114.3 PROD	12.7	111	1167	1167	162	1278
FIREWEED	19373	21-Jun-09	364	0.4	219.1 SFC	19	114.3 PROD	42	491	1378	1378	306	1869
NOEL	16051	20-Oct-09	115	0.4	244.5 SFC	28	177.8 INT	35	507	2001	2001	376	2508
SIERRA	11976	8-Jul-10	61	0.4	244.5 SFC		177.8 PROD						
SUNDOWN	21312	8-May-09	919	0.4	244.5 SFC	21	177.8 INT	31	449	1986	1986	357	2435
SUNDOWN	21768	20-Oct-09	1070	0.4	244.5 SFC	25	177.8 INT	29	420	1876	1876	344	2296
W GUNDY	4965	10-Mar-09	2275	0.4	244.5 SFC	39.7	139.7 PROD	82.9	840	1050	1050	378	1890
BRASSEY	19833	20-Oct-09	290	0.5	244.5 SFC	23	177.8 INT	27	391	1987	1987	375	2378
HELMET	18250	26-Jul-10	73	0.5	244.5 SFC	20	177.8 INT	29	420	919	919	277	1339
JACKPINE	17698	14-Oct-09	249	0.5	244.5 SFC	35	139.7 PROD	92.5	938	2972	2972	611	3910
NOEL	18550	20-Oct-09	88	0.5	244.5 SFC	26	177.8 INT	24	348	2034	2034	346	2382
SUNDOWN	19131	17-Sep-10	260	0.5	219.1 SFC	21	114.3 PROD	44	514	2071	2071	397	2585
SUNDOWN	20984	29-Sep-09	797	0.5	244.5 SFC	20.5	177.8 INT	24	348	2053	2053	347	2401
SUNSET	25773	31-Mar-10	1226	0.5	219.1 SFC	45	114.3 PROD	102.4	1196	3097	3097	650	4293
NOEL	18910	29-Oct-09	340	0.6	244.5 SFC	28.5	177.8 INT	24.5	355	2091	2091	367	2446
NOEL	20102	18-Nov-09	2950	0.6	244.5 SFC	28	177.8 INT	29	420	2076	2076	372	2496
S THETLAANI	3481	29-Jul-10	143	0.6	219.1 SFC	0	114.3 PROD	19.1	223	304	304	160	526
SIERRA	25481	12-Jul-10	173	0.6	244.5 SFC	18	177.8 INT	22.7	329	1216	1216	281	1545
SUNDOWN	19805	5-Oct-09	759	0.6	244.5 SFC	29	177.8 INT	30.5	442	2158	2158	373	2600
CUTBANK	17048	18-Nov-09	156	0.7	219.1 SFC	22	114.3 PROD	45.5	531	1803	1803	361	2334
CUTBANK	20983	8-Mar-09	461	0.7	244.5 SFC	21	177.8 INT	33	478	2022	2022	361	2500
FIREWEED	20068	21-Jun-09	242	0.7	219.1 SFC	19	114.3 PROD	33.5	391	1437	1437	268	1828

HELMET	11709	28-Nov-09	341	0.7	244.5 SFC		177.8 PROD							
KYKLO	11782	12-Jul-10	315	0.7	244.5 SFC		177.8 PROD							
NOEL	16668	29-Oct-09	402	0.7	244.5 SFC	58	177.8 INT							
SUNDOWN	21645	14-Oct-09	2965	0.7	244.5 SFC	27	177.8 INT	29.5	427	1989	1989	349	2416	
SUNSET	24694	21-Dec-09		0.7	219.1 SFC	38.5	114.3 PROD	133	1553	2785	2785	569	4338	
ELLEH	24276	5-Jul-10	290	0.8	244.5 SFC	19	177.8 INT	27.5	398	1227	1227	276	1625	
FIREWEED	16430	21-Jun-09	1352	0.8	219.1 SFC	26	139.7 PROD	41.5	594	1126	1126	260	1720	
KELLY	22905	18-Nov-09	69	0.8	244.5 SFC	22.5	177.8 INT	36	522	2236	2236	403	2758	
PETITOT	14866	27-Jul-10	58	0.8	244.5 SFC									
SUNDOWN	15491	17-Sep-10	795.4	0.8	219.1 SFC									
SUNSET	24700	22-Dec-09	317	0.8	219.1 SFC	38.5	114.3 PROD	112.5	1314	2949	2949	566	4263	
TUPPER	19809	20-Oct-09	464	0.8	219.1 SFC	18	114.3 PROD	47	549	1997	1997	388	2546	
BRASSEY	19529	8-Sep-10	840	0.9	219.1 SFC	19	114.3 PROD	37.2	434	1953	1953	367	2387	
CUTBANK	16961	18-Nov-09	100	0.9	244.5 SFC	24.5	177.8 INT	32	464	1972	1972	370	2436	
ELLEH	25250	12-Aug-10	4	0.9	244.5 SFC	18.5	177.8 INT	24.5	355	1260	1260	276	1615	
GUNNELL	13241	6-Aug-10	253	0.9	244.5 SFC	1551 INT								
SIERRA	23189	5-Jul-10	0	0.9	244.5 SFC	21	177.8 INT	27	391	1080	1080	270	1471	
SUNDOWN	17742	20-Oct-09	28	0.9	244.5 SFC	20	177.8 INT	41	594	2084	2084	396	2678	
SUNSET	25667	3-Sep-10	2240	0.9	219.1 SFC	35	114.3 PROD	114	1331	2973	2973	518	4304	
SUNSET	25925	7-Oct-10	174	0.9	219.1 SFC	34.6	114.3 PROD	97	1133	2782	2782	519	3915	
TOWN	19744	30-Jun-09	2950	0.9	244.5 SFC	17	139.7 PROD	54	547	1009	1009	255	1556	
BIRCH	8216	1-Sep-01	12	1.0										
BUICK	1508	1-Nov-00	74	1.0	273 SFC	0	177.8 PROD	4.6	43	1021	1021	156	1065	
BUICK	1508	30-Sep-01	26	1.0	273 SFC	0	177.8 PROD	4.6	43	1021	1021	156	1065	
CACHE	9014	4-Oct-10		1.0	219.1 SFC				0	140	140	221	140	
CUTBANK	17913	4-Nov-09	30	1.0	244.5 SFC	21	177.8 INT	35.8	519	1912	1912	362	2431	
FIREWEED	4146	13-Oct-00	65	1.0	219.1 SFC	0	114.3 PROD	43.3	506	1152	1152	259	1658	
INGA	2720	27-Oct-96	116	1.0	219.1 SFC	0	114.3 PROD	21.9	255	1379	1379	184	1635	
INGA	8033	13-Oct-00	28	1.0	244.5 SFC	39.2	139.7 PROD	80.3	814	1216	1216	320	2030	
INGA	8033	1-Sep-01	29	1.0	244.5 SFC	39.2	139.7 PROD	80.3	814	1216	1216	320	2030	
MILO	25346	19-Jan-10	180	1.0										
MONIAS	2242	24-Mar-10	263	1.0	339.7 SFC	0	244.5 INT	0	0	1449	1449	188	1449	
N BOUNDARY	16098	11-Oct-07	635	1.0	219.1 SFC	23	139.7 PROD	1.11	16	1422	1422	233	1438	
NOEL	13121	29-Oct-09	96	1.0	244.5 SFC	2425 PROD								
PEEJAY	588	26-Oct-00	54	1.0	219.1 SFC	0	114.3 PROD	10.9	128	1056	1056	162	1184	
PEEJAY	588	13-Sep-01	47	1.0	219.1 SFC	0	114.3 PROD	10.9	128	1056	1056	162	1184	
PEEJAY	2219	12-Sep-01	397	1.0	219.1 SFC	0	114.3 PROD	10.9	128	1076	1076	158	1204	
RIGEL	5406	27-Sep-01	37	1.0	219.1 SFC	17.4	114.3 PROD	5.1	60	1060	1060	182	1120	
SATURN	9822	27-Oct-98	120	1.0	219.1 SFC	27	139.7 PROD	52	745	1008	1008	277	1753	
SUNDOWN	18503	6-Oct-09	914	1.0	244.5 SFC	19	177.8 INT	41	594	2116	2116	399	2710	
SUNRISE	21073	14-Aug-07	193	1.0	219.1 SFC	26	139.7 PROD	76.5	1096	1106	1106	303	2202	
SWAN	23830	21-Nov-08	500	1.0	219.1 SFC	33	114.3 PROD	69.5	812	3688	3688	433	4500	
W BEG	9659	30-Sep-01	30	1.0	244.5 SFC	32	177.8 PROD	21.5	311	1174	1174	250	1485	
WEASEL	1531	20-Oct-00	31	1.0	219.1 SFC	0	114.3 PROD	9.9	116	1054	1054	152	1170	
WEASEL	1531	12-Sep-01	39	1.0	219.1 SFC	0	114.3 PROD	9.9	116	1054	1054	152	1170	
BRASSEY	19833	26-Sep-07	694	1.1	244.5 SFC	23	177.8 INT	27	391	1987	1987	375	2378	
GROUNDBIR(	25644	4-Apr-10	440	1.1	244.5 SFC	16.7	177.8 INT	24.3	352	1263	1263	279	1615	
GROUNDBIR(	25644	2-Jul-10	641	1.1	244.5 SFC	16.7	177.8 INT	24.3	352	1263	1263	279	1615	
SUNDOWN	25739	10-May-10	2976	1.1	219.1 SFC	44	114.3 PROD	146.4	1710	3596	3596	648	5306	
SWAT	15906	5-Jul-10	571	1.1	244.5 SFC	1717								
CUTBANK	16013	8-May-09	1535	1.2	244.5 SFC	18.5	177.8 INT	36	522	1938	1938	397	2460	
NOEL	18370	20-Oct-09	241	1.2	244.5 SFC	28	177.8 INT	28.5	413	2107	2107	361	2520	
SUNDOWN	21089	6-Oct-09	909	1.2	244.5 SFC	40.6	139.7 PROD	70	709	3011	3011	602	3720	
GUNNELL	24021	15-Jul-10	5	1.3	244.5 SFC	18	177.8 INT	26.5	384	1227	1227	279	1611	
SIERRA	25313	8-Jul-10	370	1.3	244.5 SFC	17.3	177.8 INT	25.5	369	1092	1092	281	1461	
SUNDOWN	20969	29-Oct-09	412	1.3	244.5 SFC	20.5	177.8 INT	25	362	2033	2033	347	2395	
BEG	13503	1-Mar-10	54	1.4	219.1 SFC	1826 INT								
CHOWADE	25970	20-Oct-10	1192	1.4										
GUNNELL	11669	5-Aug-10	48	1.4	244.5 SFC		177.8 PROD							
GUNNELL	16288	19-Jul-10	0	1.4	244.5 SFC	23	177.8 INT	32	464	1098	1098	260	1562	
NOEL	19085	29-Oct-09	249	1.4	244.5 SFC	21.5	177.8 INT	24.5	355	2123	2123	361	2478	
SIERRA	26091	5-Jul-10	313	1.4	244.5 SFC	22.7	177.8 INT	20.7	300	1156	1156	281	1456	
FIREWEED	19619	21-Jun-09	327	1.5	219.1 SFC	19.4	114.3 PROD	46.4	542	1322	1322	277	1864	
SUNDOWN	20906	30-Jan-08	781	1.5	244.5 SFC	25	177.8 INT	27	391	1927	1927	361	2318	
SUNDOWN	23132	25-Aug-09	170	1.5	244.5 SFC	22.5	139.7 PROD	65	659	2191	2191	422	2850	
TUPPER	19703	20-Oct-09	230	1.5	219.1 SFC	17.5	114.3 INT	48.8	570	1992	1992	375	2562	
SUNDOWN	16243	1-Oct-10	505	1.6	219.1 SFC	32	139.7 PROD	43	616	1869	1869	376	2485	
FIREWEED	4146	31-Aug-01	83	1.7	219.1 SFC	0	114.3 PROD	43.3						
NOEL	20153	18-Nov-09	1626	1.7	244.5 SFC	30	177.8 INT	29.5	427	2102	2102	365	2529	
BLAIR	19746	30-Jun-09	3343	1.8	244.5 SFC	17	177.8 INT	31	449	765	765	252	1214	
SUNDOWN	19190	29-Sep-09	132	1.8	244.5 SFC	22	177.8 PROD	28	406	2029	2029	352	2435	
SUNDOWN	19190	1-Oct-09	132	1.8	244.5 SFC	22	177.8 PROD	28	406	2029	2029	352	2435	
SUNDOWN	20722	19-Feb-08	855	1.8	244.5 SFC	19.6	177.8 INT	26.7	387	1808	1808	335	2195	

SUNDOWN	21279	8-May-08	-2	1.8	244.5 SFC	31	139.7 PROD	80	811	2447	2447	479	3258
GUNNELL	13272	6-Aug-10	50	1.9	244.5 SFC		177.8 INT						
SUNSET	24707	15-Dec-09	1068	1.9	219.1 SFC	38.9	114.3 PROD	117.5	1372	3058	3058	561	4430
BLUEBERRY	24249	1-Sep-10	549	2.0	244.5 SFC	39	114.3 PROD	81	708	1559	1559	610	2267
BUICK	3927	1-Nov-00	104	2.0	219.1 SFC	0	114.3 PROD	6.95					
BUICK	3927	30-Aug-01	36	2.0	219.1 SFC	0	114.3 PROD	6.95					
BUICK	9898	1-Jan-07	2	2.0	244.5 SFC	25	177.8 INT	37	536	929	929	211	1465
BUICK	15125	30-Nov-06	-6	2.0	244.5 SFC		177.8 INT						
CLARKE	2540	25-Mar-01	1200	2.0	339.7 SFC	0	244.5 INT	17.7					
DAHL	8340	28-Feb-08	70	2.0	219.1 SFC	14	114.3 PROD	16.1	188	1001	1001	183	1189
KELLY	21298	26-Sep-10	64	2.0	219.1 SFC	23	114.3 PROD	56	654	2087	2087	411	2741
N BUBBLES	10536	5-Aug-10	556	2.0	339.7 SFC	MN80	4 jts 43.2 kg/m to 47 m, 166 jts 38.7 kg/m to 2169 m, 76 jts 43.2 kg/m to 3145 m						
NIG	5251	6-Oct-00	74	2.0	219.1 SFC	18.5							
NIG	5251	30-Sep-01	47	2.0	114.3 PROD	35							
S JULIENNE	4060	2-Oct-09	175	2.0	244.5 SFC	0	139.7 INT	19.9	201	1554	1554	381	1755
SUNDOWN	19456	17-Mar-09	1070	2.0	244.5 SFC	21.5	177.8 INT	28.3	410	2139	2139	371	2549
SUNDOWN	24253	29-Sep-09	665	2.0	244.5 SFC	35	177.8 INT	44	637	2829	2829	543	3466
SPRUCE	13566	26-Jul-10	5	2.1	244.5 SFC		177.8 PROD						
SUNDOWN	21644	29-Sep-09	235	2.1	244.5 SFC	22	177.8 INT	28.5	413	2019	2019	357	2432
SUNDOWN	22094	3-Nov-09	264	2.1									
N BUBBLES	7411	5-Aug-10	1356	2.2	244.5 SFC	32	177.8 INT	35	507	753	753	226	1260
SUNDOWN	3231	5-Oct-09	1485	2.2	339.7 INT	0	244.5 INT	82.25	604	2795	2795	728	3398
JULIENNE	23040	10-Feb-09	206.5	2.3	219.1 SFC	17	114.3 PROD	48.6	568	890	890	221	1458
N JULIENNE	4618	7-Aug-09	310	2.3	177.8 INT	0	114.3 LINR	15.89	350	2349	2349	1959	2699
KYKLO	25487	15-Jul-10	186	2.4									
SUNDOWN	19457	17-Mar-09	598	2.4	244.5 SFC	23	177.8 INT	27.5	398	2207	2207	370	2605
SUNDOWN	22321	7-Aug-09	212	2.4	244.5 SFC	23.5	177.8 INT	27.5	398	1781	1781	367	2179
BRASSEY	19453	21-Sep-10	962	2.5	219.1 SFC	19	114.3 PROD	48.3	564	1967	1967	359	2531
BEG	1095	8-Jan-10	68	2.6	177.8 INT	0	114.3 LINR	6.36	140	1469	1469	1243	1609
GUNNELL	13275	6-Aug-10	309	2.6	244.5 SFC		177.8 INT						
SUNDOWN	19418	6-Oct-09	298	2.6	244.5 SFC	20	177.8 INT	29.5	427	2071	2071	370	2498
SUNDOWN	21262	9-Sep-10	1254	2.6	244.5 SFC	43	139.7 PROD		0	1876	1876	647	1876
DOE	25785	10-Jun-10	950	2.7	244.5 SFC	18	114.3 PROD	35	306	3380	3380	298	3686
SUNDOWN	21592	29-Sep-09	437	2.7	244.5 SFC	27	177.8 INT	28	406	2008	2008	357	2414
ESKAI	24568	6-Aug-10	26	2.8	244.5 SFC	18.7	177.8 INT	32.1	465	1486	1486	321	1951
GUNNELL	21151	29-Jul-10	1120	2.8	244.5 SFC	17	177.8 INT	25.7	372	1259	1259	263	1631
KYKLO	13382	12-Jul-10	24	2.8	244.5 SFC		177.8 INT						
SUNDOWN	17690	14-Oct-09	396	2.8	219.1 SFC	28.5	139.7 PROD	40.5	580	2025	2025	401	2605
BERNADET	22969	14-Sep-08	1700	3	244.5 SFC	17.5	177.8 PROD	41	594	1121	1121	261	1715
BIRCH	8216	13-Oct-00	14	3									
N BUICK	3756	30-Oct-00	90	3	219.1 SFC	0	114.3 PROD	11.9	139	1072	1072	162	1212
N JULIENNE	4618	4-Sep-08	410	3	177.8 INT	0	114.3 LINR	15.9	350	2349	2349	1959	2699
N NIG	7571	30-Sep-01	71	3	339.7 SFC	42	244.5 INT	94	690	861	861	250	1551
NOEL	19132	18-Nov-09	3405	3	244.5 SFC	28.5	177.8 INT	26	377	2155	2155	369	2532
PEEJAY	1851	15-Dec-00	68	3	219.1 SFC	0	114.3 PROD	11.13	130	1053	1053	160	1183
SILVERBERR	7051	11-Jan-07	60	3	219.1 SFC	17	139.7 PROD	31	444	1131	1131	31	1575
TOWN	20904	19-Feb-09	276	3	219.1 SFC	19	114.3 PROD	55	642	835	835	229	1477
W EAGLE	4631	2-Oct-08	480	3	219.1 SFC	21.8	139.7 PROD	38	544	1349	1349	289	1893
WEASEL	1713	11-Sep-01	219	3	219.1 SFC	0	114.3 PROD	9.9	116	1057	1057	161	1174
CUTBANK	21427	18-Nov-09	707	3.3	244.5 SFC	24	177.8 INT	31	449	2112	2112	383	2561
GROUNDBIR(	25946	11-Apr-10	1132	3.3	219.1 SFC	23	114.3 PROD	55	642	3592	3592	499	4234
MICA	4649	10-Aug-09	360	3.4	244.5 SFC	37.5	139.7 PROD	82.8	839	1724	1724	407	2563
MICA	4649	14-Aug-09	360	3.4	244.5 SFC	37.5	139.7 PROD	82.8	839	1724	1724	407	2563
MICA	4649	1-Oct-09	360	3.4	244.5 SFC	37.5	139.7 PROD	82.8	839	1724	1724	407	2563
NOEL	8078	7-Aug-02	592	3.4	219.1 SFC	18	139.7 PROD	21.7	311	1663	1663	301	1974
SUNDOWN	22975	5-Oct-09	1229	3.4	244.5 SFC	24	177.8 INT	30.5	442	2099	2099	374	2541
ETSHO	25198	19-Nov-09	2222.3	3.6									
SUNDOWN	23544	15-Dec-08	16	3.6	244.5 SFC	23.5	177.8 INT	34	493	2019	2019	374	2512
BLUEBERRY	24149	1-Sep-10	299	3.7	244.5 SFC	40	114.3 PROD	50	437	1382	1382	614	1819
GRAHAM	25738	10-Apr-10	3600	3.7									
SUNDOWN	23544	5-Oct-09	1485	3.7	244.5 SFC	23.5	177.8 INT	34	493	2019	2019	374	2512
HELMET	23569	26-Jul-10	271	3.8	244.5 SFC	21	177.8 INT	24.5	355	1024	1024	268	1379
SUNDOWN	21591	8-May-09	1601	3.9	244.5 SFC	27	177.8 INT	26	377	2047	2047	363	2424
BRASSEY	6888	19-Aug-07	1542	4	244.5 SFC	44	177.8 PROD	102.8	1489	1673	1673	607	3162
N BUICK	3756	1-Nov-00	91	4	219.1 SFC	0	114.3 PROD	11.92	139	1072	1072	162	1212
BEG	11489	21-Feb-10	873	4.1	219.1 SFC		139.7 PROD						
W BEG	21383	9-Oct-09	207	4.2	219.1 SFC	21	114.3 PROD	65	759	963	963	268	1722
SUNDOWN	21159	29-Sep-09	1530	4.3	244.5 SFC	22	177.8 INT	28	406	2017	2017	345	2423
CUTBANK	16759	29-Oct-09	988	4.5	244.5 SFC	21	177.8 INT	25	362	2120	2120	361	2482
SUNDOWN	21607	29-Sep-09	541	4.5	244.5 SFC	27	177.8 INT	30	435	2038	2038	366	2473
GUNNELL	11127	6-Aug-10	466	4.7	244.5 SFC		177.8 PROD						
RING	12325	11-Oct-00	180	4.7	177.8 SFC		114.3 PROD						
BEG	5138	4-Mar-10	799	4.8	219.1 SFC	31	139.7 PROD	51	731	1068	1068	267	1799

ADSETT	20706	29-Sep-06	1000	5	177.8 INT		177.8 INT	20						
OSBORN	322	17-Nov-00	137	5	339.7 SFC	0	139.7 PROD	18.9	80	1548	1548	184	1628	
SIERRA	25298	12-Jul-10	50	5.1	244.5 SFC	17.7	177.8 INT	24	348	1165	1165	279	1513	
SUNDOWN	15955	10-Jun-09	2819	5.1	219.1 SFC	17	139.7 PROD	23.5	337	1534	1534	342	1871	
SUNDOWN	21131	29-Sep-09	38	5.1	244.5 SFC	30	177.8 INT	27	391	2031	2031	360	2422	
CUTBANK	20998	4-Nov-09	1414	5.3	244.5 SFC	23	177.8 INT	30.5	442	2116	2116	373	2558	
RING	12086	11-Oct-00	110	5.6	177.8 SFC		114.3 PROD							
SUNSET	9410	27-Oct-98	190	5.8	219.1 SFC	17	139.7 PROD	40.2	576	1159	1159	267	1735	
RING	12098	11-Oct-00	120	5.9	177.8 SFC		114.3 PROD							
NOEL	23434	14-May-08	12	6	219.1 SFC	17.5	114.3 PROD	43.6	509	2064	2064	371	2573	
TOWN	315	16-Sep-10	270	6.1	244.5 INT	0	177.8 PROD	25.6	370	1744	1744	1267	2114	
NOEL	19526	20-Oct-09	393	6.5	244.5 SFC	18	177.8 INT	29.5	427	1929	1929	350	2356	
BRASSEY	19473	1-Oct-09	384	6.6	244.5 SFC	38.5	177.8 INT	37	536	2461	2461	586	2997	
ADSETT	22247	30-May-08	1016	6.8	244.5 SFC	48.9	177.8 INT	38.9	564	1964	1964	752	2528	
CUTBANK	18328	4-Nov-09	1198	6.9	244.5 SFC	25	177.8 INT	29.5	427	2135	2135	370	2562	
W STODDAR	5449	14-Jun-10	216	6.9	219.1 SFC	22.8	139.7 PROD	35.4	507	1414	1414	300	1921	
W BLUEBERF	15024	22-Sep-09	403	7.1	244.5 SFC		177.8 PROD							
SIERRA	12275	12-Jul-10	4.1	7.2	244.5 SFC		177.8 INT							
BLUEBERRY	25673	27-Jun-10	2390	7.5										
NOEL	25571	24-Jan-10	3503	7.5	219.1 SFC	26	114.3 PROD	40	467	1921	1921	426	2388	
GUNNELL	14204	6-Aug-10	600	7.7	244.5 SFC		177.8 INT							
KOMIE	24577	24-Aug-10	705	7.8										
ALTARES	24098	19-Jan-10	730	7.9	244.5 SFC	24	177.8 INT	33	478	1364	1364	309	1842	
GUNNELL	13251	6-Aug-10	33	7.9	244.5 SFC		177.8 INT							
TSEA	23899	3-May-08	4570	8	244.5 SFC	22.8	177.8 INT	26.8	388	1292	1292	262	1680	
N JULIENNE	4618	22-Aug-10	280	8.2	273 SFC	21.7	177.8 INT	83.4	793	1166	1166	307	1959	
SIERRA	8933	9-Jul-10	70	8.5	339.7 SFC	57	177.8 PROD							
OJAY	3976	6-Oct-02	85	8.6	339.7 SFC	0	244.5 INT	41.7	306	2578	2578	602	2884	
SUNDOWN	21608	29-Sep-09	780	8.7	244.5 SFC	27	177.8 INT	31	449	1978	1978	355	2427	
GROUNDBIR	25946	16-May-10	1605	8.9	219.1 SFC	23	114.3 PROD	55	642	3592	3592	499	4234	
KYKLO	25337	12-Jul-10	893	9	244.5 SFC	18.7	177.8 INT	22	319	1193	1193	277	1512	
OAK	3269	7-Jun-10	81	9	219.1 SFC	0	114.3 PROD	16.1	188	1089	1089	156	1277	
BLUEBERRY	24149	5-Oct-08	1233	9.1	244.5 SFC	40	114.3 PROD	50	437	1382	1382	614	1819	
SUNDOWN	22974	5-Oct-09	305	9.8	244.5 SFC	24	177.8 INT	31	449	2104	2104	375	2553	
INGA	3156	11-Oct-06	229	10	244.5 SFC	0	139.7 PROD	34.9	354	1253	1253	232	1607	
INGA	3156	11-Oct-06	229	10	244.5 SFC	0	139.7 PROD	34.9	354	1253	1253	232	1607	
BRIAR RIDGE	25778	10-Sep-10	2352	10.4	219.1 SFC	36	114.3 PROD	41	479	2016	2016	491	2495	
SUNDOWN	23543	5-Oct-09	1438	11	244.5 SFC	24	177.8 INT	34.5	500	2025	2025	375	2525	
BEG	1154	25-Jan-10	120	11.3	244.5 SFC	0	177.8 PROD	0	0	1315	1315	80	1315	
CACHE	19301	4-Oct-10	1160	11.3	244.5 SFC	26	139.7 PROD	70	709	1185	1185	287	1894	
CUTBANK	17918	4-Nov-09	239	11.7	244.5 SFC	22	177.8 INT	31	449	1959	1959	360	2409	
GUNNELL	16114	19-Jul-10	111	11.9	244.5 SFC		177.8 INT							
SUNDOWN	25258	20-Jul-10	4478	12	244.5 SFC	44	114.3 PROD	140	1223	3589	3589	708	4812	
W STODDAR	4112	2-Sep-10	758	12.3	219.1 SFC	0	114.3 PROD	22.3	260	1141	1141	220	1401	
ETSHO	24961	8-Oct-09	6058	12.8										
ETSHO	25941	29-May-10	5460	12.9										
BUICK	9391	14-Aug-09	3265	13	244.5 SFC	28	177.8 INT	35.4	513	964	964	275	1477	
NOEL	25651	18-Dec-09	2141	14.1	219.1 SFC	25	114.3 PROD	35	409	1934	1934	479	2343	
BEATTON	393	5-Aug-09	4551	14.4	273 SFC	0	139.7 PROD							
TOWN	19294	30-Jun-09	3230	14.8	244.5 SFC	16	114.3 LINR	28	245	1241	1241	254	1486	
TOWN	3753	1-Jul-10	310	15	244.5 SFC	0	177.8 PROD	34	489	1338	1338	186	1827	
TOWN	3753	19-Jul-10	310	15	244.5 SFC	0	177.8 PROD	34	489	1338	1338	186	1827	
BEG	11488	25-Sep-09	336	15.7	219.1 SFC		139.7 PROD							
ALTARES	9417	2-Dec-07	1265	17	244.5 SFC	17.6	177.8 INT	36	522	1481	1481	310	2003	
N JULIENNE	2574	21-Aug-10	896	18.8	244.5 SFC	0	114.3 PROD							
KYKLO	14545	12-Jul-10	2055	19.8	244.5 SFC		139.7 LINR	4	41	1974	1974	289	2014	
BLUEBERRY	8179	30-Jul-00	758	20	219.1 SFC	20	139.7 INT	38	544	682	682	208	1226	
JEDNEY	8183	23-Apr-08	712	20	244.5 INT	80	177.8 PROD	64	927	2578	2578	1922	3505	
SHEKILIE	20082	30-Dec-08	216	20	177.8 SFC	10.5	114.3 PROD	14.5	319	135	135	156	454	
ETSHO	25205	19-Nov-09	4058	20.5										
BIRCH	6136	13-Nov-00	1331	22	219.1 SFC	18	114.3 PROD	14.6	171	1135	1135	204	1305	
SUNRISE	20801	26-Jul-07	1130	25	219.1 SFC	28	114.3 PROD	91	1063	1114	1114	311	2177	
PEEJAY	2219	24-Oct-00	667	27	219.1 SFC	0	114.3 PROD	10.9	128	1076	1076	158	1204	
SUNSET	9734	27-Oct-98	1800	27.1	219.1 SFC	27	139.7 PROD	63.2	905	804	804	271	1710	
KYKLO	14545	4-May-10	2840	27.2	244.5 SFC		139.7 LINR	4	41	1974	1974	289	2014	
ETSHO	23881	8-Oct-09	6422	27.4										
ADSETT	12863	10-Mar-10	4805	27.8	244.5 SFC									
KOMIE	24220	30-Oct-08	8600	28										
BLAIR	8477	6-Oct-10	1434	28.3	244.5 SFC	14	139.7 PROD	23	233	1312	1312	224	1545	
BEG	806	19-Feb-10	730	28.6	244.5 SFC	0	177.8 INT	10.7	155	1263	1263	161	1419	
BUICK	9412	2-Nov-09	2677	29.7	244.5 SFC	22	177.8 SFC	52.1	755	782	782	228	1537	
ADSETT	22253	25-Jan-07	5145	30	244.5 SFC	53.3	177.8 INT	36.2	524	1961	1961	749	2485	
OJAY	5184	21-Feb-08	3	30	339.7 SFC	80	177.8 PROD	30	146	3381	3381	453	3527	

GUNNELL	16109	19-Jul-10	265	30.9	244.5 SFC	1615 INT								
ADSETT	5926	12-Sep-09	2937	31.1	244.5 SFC	42	177.8 INT	50	724	1677	1677	360	2401
RIGEL	2707	16-Apr-10	61.7	31.2	219.1 SFC	0	114.3 PROD	9.9	116	971	971	152	1087
RIGEL	2707	4-May-10	60	31.3	219.1 SFC	0	114.3 PROD	9.9	116	971	971	152	1087
PARADISE	4164	21-Sep-08	316	32	219.1 SFC	0	114.3 PROD	29.0	339	1164	1164	232	1503
HALFWAY	11521	30-Mar-01	1278	35	244.5 SFC		177.8 INT						
GUNNELL	21685	19-Jul-10	82	35.7	244.5 SFC	23	177.8 INT	29	420	1166	1166	268	1586
NOEL	25669	24-Feb-10	4263	36.8	244.5 SFC	30	177.8 INT	59.5	862	2528	2528	534	3390
TOWN	21425	8-Feb-09	1379	39.3	244.5 SFC	28	114.3 PROD	53	463	927	927	258	1390
DAHL	15900	27-Sep-09	1550	43	244.5 SFC		139.7 PROD		0	2743	2743	410	2743
OJAY	3511	4-Sep-01	241	44	339.7 SFC	0	244.5 INT	39.7	292	2089	2089	262	2380
N JULIENNE	2574	4-Sep-08	1350	46	244.5 SFC	0	114.3 PROD	32.2	281	1375	1375	204	1657
WEASEL	1713	20-Oct-00	579	48	219.1 SFC	0	114.3 PROD	9.9	116	1057	1057	161	1174
RIGEL	6770	27-Sep-01	101	49	219.1 SFC	20	139.7 PROD	34	487	835	835	203	1322
INGA	12305	22-Sep-10	125	54.6	219.1 SFC		139.7 PROD		0	1645	1645	251	1645
RIGEL	6770	17-Oct-00	1344	56	219.1 SFC	20	139.7 PROD	34	487	835	835	203	1322
N JULIENNE	4017	27-Mar-10	110	57	244.5 SFC	0	139.7 PROD	0	0	2348	2348	391	2348
RING	12099	11-Oct-00	150	57.7	177.8 SFC		114.3 PROD		0	916	916	159	916
ALTARES	9417	10-Aug-06	923	59	244.5 SFC	17.6	177.8 INT	36	522	1481	1481	310	2003
RIGEL	1163	10-Jun-10	456	62.3	219.1 SFC	0	114.3 PROD	4.4	51	1024	1024	163	1075
PEEJAY	1736	26-Oct-00	108	66	219.1 SFC	0	114.3 PROD	9.9	116	1086	1086	155	1202
NOEL	5389	4-Aug-99	420	66.2	339.7 SFC	65	244.5 INT	86	631	1311	1311	387	1942
PEEJAY	1736	12-Sep-01	137	67	219.1 SFC	0	114.3 PROD	9.9	116	1086	1086	155	1202
NOEL	4275	4-Aug-99	1925	68.6	244.5 SFC	0	177.8 PROD	28.8	417	2258	2258	487	2675
LAPRISE	1852	28-Feb-09	1289	69.5	219.1 SFC	0	114.3 PROD	6.0	70	1303	1303	152	1373
EKWAN	13178	18-Jul-07	2800	74	244.5 SFC		177.8 PROD		0	1665	1665	310	1665
INGA	7206	27-Oct-96	1356	80	244.5 SFC	32	139.7 PROD	30	304	1497	1497	301	1802
NIG	12111	28-Jun-00	984	80	219.1 SFC		139.7 PROD		0	1273	1273	218	1273
NIG	12111	30-Jun-00	984	80	219.1 SFC		139.7 PROD		0	1273	1273	218	1273
ALTARES	22912	11-Oct-07		84	219.1 SFC	35	139.7 LINR	51	731	1119	1119	359	1850
EAGLE	3202	5-Oct-08	1269	96	219.1 SFC	0	139.7 PROD	36	516	1164	1164	209	1680
GUNNELL	9269	6-Aug-10	686	99.5	219.1 SFC		139.7 PROD		0	1536	1536	147	1536
BLUEBERRY	9376	8-Feb-08	3137	100	219.1 SFC	28	139.7 PROD	39	559	1527	1527	314	2086
N JULIENNE	2574	11-Sep-09	1490	109.1	244.5 SFC	0	114.3 PROD	32.2	281	1375	1375	204	1657
HALFWAY	11521	3-Oct-00	1856	111	244.5 SFC		177.8 INT						
SUNSET	8230	27-Oct-98	640	118	219.1 SFC	17.5	139.7 PROD	48.8	699	1155	1155	283	1854
SUNSET	8356	27-Oct-98	970	124.8	219.1 SFC		139.7 PROD						
HELMET	12549	5-Apr-09	3500	130	177.8 SFC		114.3 PROD						
JEDNEY	1082	16-Nov-01	65.5	144	244.5 SFC	0	177.8 INT	5.96047	86	1228	1228	83	1315
W STODDAR	5745	12-Mar-08	640	146.4	219.1 SFC	22.8	139.7 PROD	48	688	1325	1325	304	2013
HELMET	5966	12-Nov-99	3515	169	244.5 SFC	41	177.8 PROD	38.1	552	971	971	304	1523
SHEKILIE	2038	7-Feb-07	2043	170	177.8 INT	0	114.3 LINR	2.11	46	1582	1582	1580	1628
BEG	1268	18-Dec-09	1175	182.4	250.8 SFC	0	177.8 INT	8.74	114	1289	1289	237	1404
BUICK	21538	7-Oct-10	1238	195	219.1 SFC	12.4	139.7 PROD	47.5	680	735	735	204	1415
INGA	8033	5-Aug-99	1700	200	244.5 SFC	39.2	139.7 PROD	80.3	814	1216	1216	320	2030
VELMA	8610	31-May-00	68	206.3	219.1 SFC	14	114.3 PROD	13.5	158	1052	1052	182	1210
KLUA	7553	9-Apr-07	665	220	339.7 SFC	55	177.8 INT	36.1	176	1898	1898	350	2074
BLAIR	8477	9-Mar-09	3033	283.3	244.5 SFC	14	139.7 PROD	23	233	1312	1312	224	1545
SUNSET	8162	27-Oct-98	3400	284.2	219.1 SFC	19	139.7 PROD	47	673	1184	1184	288	1857
HELMET	5966	9-Apr-10	1797	305	244.5 SFC	41	177.8 PROD	38.1	552	971	971	304	1523
SQUIRREL	12990	17-Sep-10	1314	336.8	219.1 SFC		139.7 PROD	32	458	1002	1002	227	1460
BOUNDARY	4279	5-Aug-10	476	374	219.1 SFC	17	139.7 PROD	21.6	309	1173	1173	233	1482
JEDNEY	460	23-Apr-08	1700	381	139.7 PROD	0							
SILVER	4294	8-Mar-07	341	692	219.1 SFC	0	114.3 PROD	5.96	70	1080	1080	180	1150
SILVER	4294	4-Mar-08	339	700	219.1 SFC	0	114.3 PROD	5.96	70	1080	1080	180	1150
OJAY	22041	12-Sep-07	1496	741	244.5 SFC	20	177.8 INT	34	493	2377	2377	308	2870
FIREBIRD	4354	4-Mar-08	1169	915	219.1 SFC	0	114.3 PROD	0	0	1200	1200	184	1200
N BUICK	3756	31-Aug-01	145	970	219.1 SFC	0	114.3 PROD	0	0	1212	1212	162	1212
HIDING	13908	9-Oct-08	625	1351.8	219.1 SFC		139.7 PROD	36.3	520	2162	2162	400	2682
EKWAN	9610	11-Oct-02	4200	1500	244.5 SFC		177.8 INT	28.5	413	885	885	204	1298

Figure A2 – British Columbia Oil and Gas Commission Wellbore Data.

A.03 - SCP MODEL RESULTS

The following are the results from running the SCP Model for the Maximum Pressure Method and the Cement Slurry Method. Starting at the upper left-hand corner of Figure A3, (No.1) the wellbore number (1), and the pressure buildup rate interval (0.60 psi/day) are listed. Moving right to this panel, (No.2), the pressure buildup data (red dots) are compared to the model generated buildup (blue fitting curve). The input parameter values (leakage depth, mud length, etc) are provided. The output parameter values (permeability) are given. The minimum permeability output is displayed in the

panel No.2, the maximum permeability output is displayed in the panel No.3. The pressure buildup for maximum permeability is also provided.

In the panel labeled No.4, the same wellbore (1) and pressure buildup (0.60 psi/day) was evaluated using the Cement Slurry Method. The results are displayed in panel No.5 and panel No.6. For panel No.5, the leakage depth, mud length, gas cap, etc. are provided. The minimum permeability value is given and matching pressure buildup data/ model results are compared. For panel No.6, the maximum permeability values are provided. The same numbering is applied to all subsequent figures.

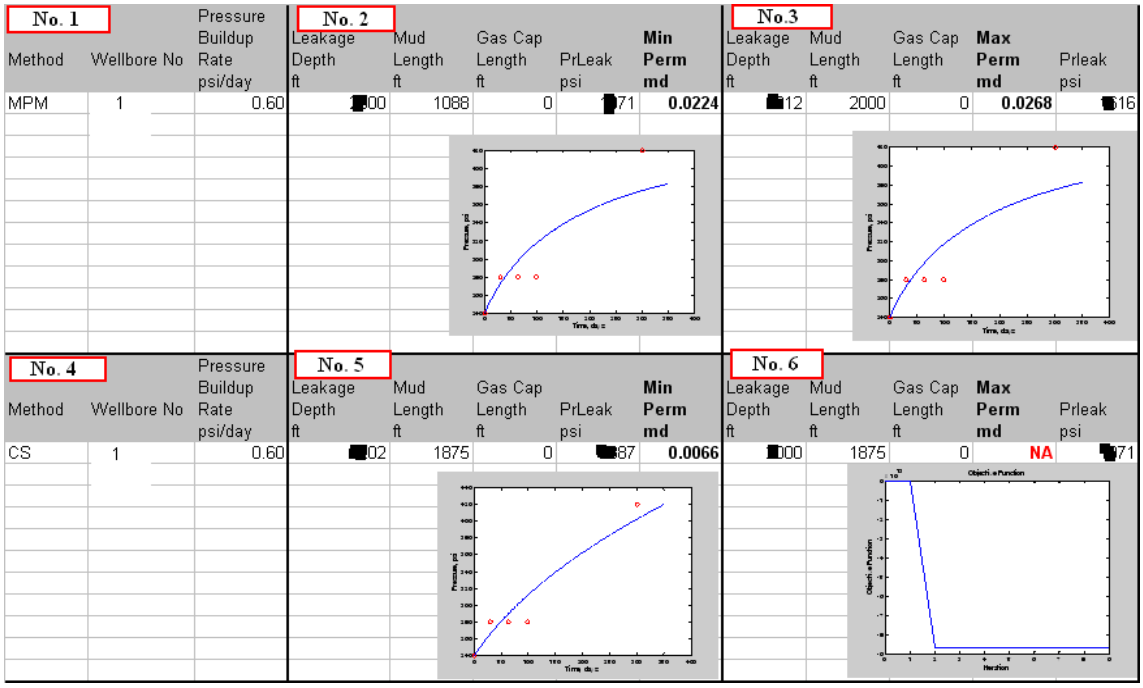

Figure A3 - Wellbore 1 - Best-fit SCP curve matching field pressure data #1.

Wellbore No	Pressure Buildup Rate psi/day	Leakage Depth ft	Mud Length ft	Gas Cap Length ft	PrLeak psi	**Min Perm md**	Leakage Depth ft	Mud Length ft	Gas Cap Length ft	**Max Perm md**	Prleak psi
1	0.64	[redacted]00	1088	0	[redacted]71	**0.0358**	[redacted]12	1088	0	0.0431	[redacted]16
Wellbore No	Pressure Buildup Rate psi/day	Leakage Depth ft	Mud Length ft	Gas Cap Length ft	PrLeak psi	**Min Perm md**	Leakage Depth ft	Mud Length ft	Gas Cap Length ft	**Max Perm md**	Prleak psi
1	0.64	[redacted]02	1875	0	[redacted]87	0.0076	[redacted]00	1875	0	**NA**	[redacted]71

Figure A4 - Wellbore 1 - Best-fit SCP curve matching field pressure data #2.

Method	Wellbore No	Pressure Buildup Rate psi/day	Leakage Depth ft	Mud Length ft	Gas Cap Length ft	PrLeak psi	**Min Perm md**	Leakage Depth ft	Mud Length ft	Gas Cap Length ft	**Max Perm md**	Prleak psi
MPM	2	4.4	[redacted]81	3382	0	[redacted]33	0.2186	[redacted]80	4281	0	0.2258	[redacted]32
CS	2	4.4	[redacted]071	788	0	[redacted]54	**0.0117**	[redacted]81	788	0	**0.0282**	[redacted]33

Figure A5 - Wellbore 2 - Best-fit SCP curve matching field pressure data #1.

Method	Wellbore No	Pressure Buildup Rate psi/day	Leakage Depth ft	Mud Length ft	Gas Cap Length ft	PrLeak psi	**Min Perm md**	Leakage Depth ft	Mud Length ft	Gas Cap Length ft	**Max Perm md**	Prleak psi
MPM	2	0.35	[redacted]281	3895	0	[redacted]32	**0.0062**	[redacted]67	4281	0	**0.0024**	[redacted]94
CS	2	0.35	[redacted]071	788	0	[redacted]55	**0.0001**	[redacted]81	**788**	0	**0.0003**	[redacted]33

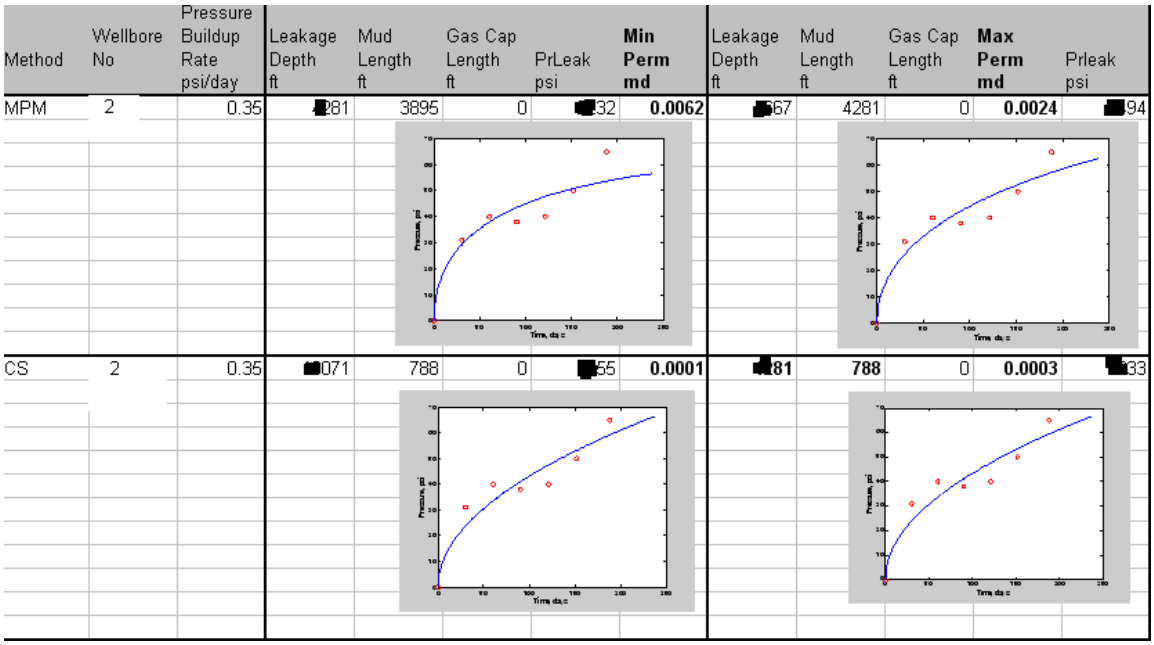

Figure A6 - Wellbore 2 - Best-fit SCP curve matching field pressure data #2.

Method	Wellbore No	Pressure Buildup Rate psi/day	Leakage Depth ft	Mud Length ft	Gas Cap Length ft	PrLeak psi	**Min Perm md**	Leakage Depth ft	Mud Length ft	Gas Cap Length ft	**Max Perm md**	Prleak psi
MPM	2	1.6	[redacted]81	3783	0	[redacted]55	**0.0271**	[redacted]88	4281	0	**0.0339**	[redacted]98
CS	2	1.6	[redacted]071	788	0	[redacted]55	**0.0011**	[redacted]81	**788**	0	**0.0026**	[redacted]33

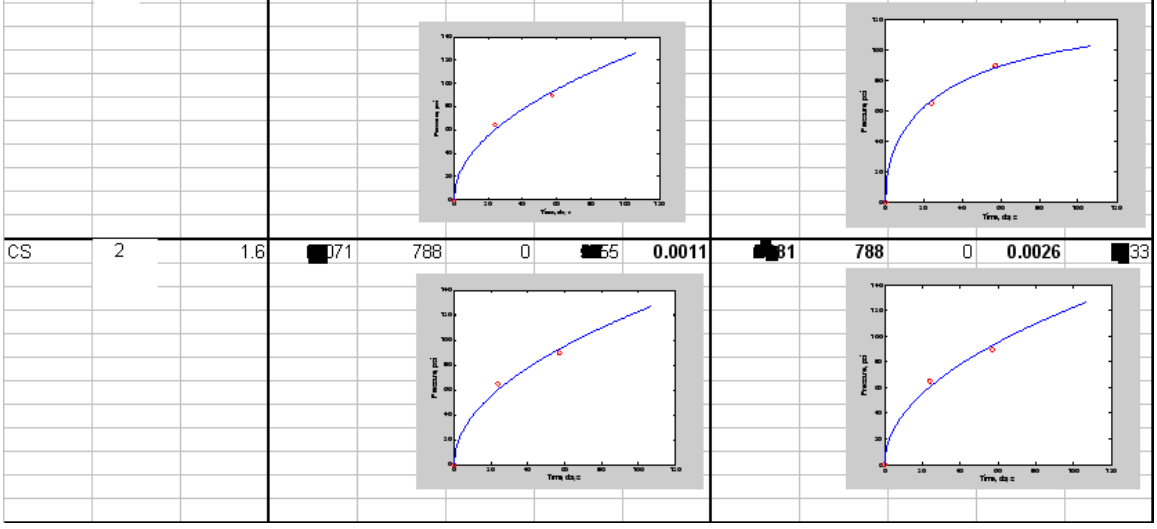

Figure A7 - Wellbore 2 - Best-fit SCP curve matching field pressure data #3.

Method	Wellbore No	Pressure Buildup Rate psi/day	Leakage Depth ft	Mud Length ft	Gas Cap Length ft	PrLeak psi	**Min Perm md**	Leakage Depth ft	Mud Length ft	Gas Cap Length ft	**Max Perm md**	Prleak psi
MPM	3	1.23	[redacted]090	3420	0	[redacted]56	**0.1442**	[redacted]60	4090	0	**0.1463**	[redacted]39
CS	3	1.23	[redacted]923	5693	0	[redacted]021	**0.0147**	[redacted]93	5693	0	**0.1000**	[redacted]73

Figure A8 – Wellbore 3 – Best-fit SCP curve matching field pressure data.

Method	Wellbore No	Pressure Buildup Rate psi/day	Leakage Depth ft	Mud Length ft	Gas Cap Length ft	PrLeak psi	**Min Perm md**	Leakage Depth ft	Mud Length ft	Gas Cap Length ft	**Max Perm md**	Prleak psi
MPM	4	0.87	[redacted]00	3882	0	[redacted]55	0.0223	[redacted]18	4500	0	**0.0222**	[redacted]06
CS	4	0.87	[redacted]172	556	0	[redacted]37	0.0005	[redacted]00	556	0	**0.0014**	[redacted]55

Figure A9 – Wellbore 4 – Best-fit SCP Curve matching field pressure data.

Method	Wellbore No	Pressure Buildup Rate psi/day	Leakage Depth ft	Mud Length ft	Gas Cap Length ft	PrLeak psi	**Min Perm md**	Leakage Depth ft	Mud Length ft	Gas Cap Length ft	**Max Perm md**	Prleak psi
MPM	5	1.1	[redacted]40	3857	0	[redacted]51	0.0308	[redacted]23	4540	0	0.0307	[redacted]56
CS	5	1.1	[redacted]105	2369	0	[redacted]43	0.0009	[redacted]40	2369	0	0.0025	[redacted]51

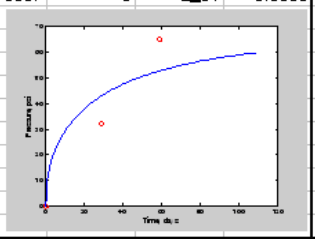
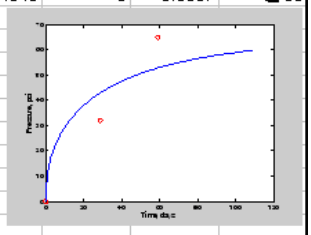
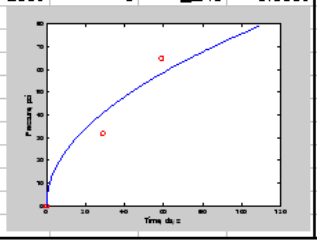
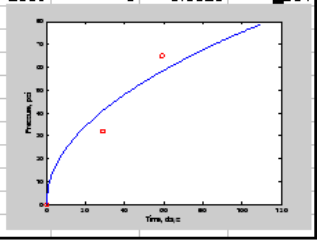

Figure A10 – Wellbore 5 – Best-fit SCP Curve matching field pressure data #1

Method	Wellbore No	Pressure Buildup Rate psi/day	Leakage Depth ft	Mud Length ft	Gas Cap Length ft	PrLeak psi	**Min Perm md**	Leakage Depth ft	Mud Length ft	Gas Cap Length ft	**Max Perm md**	Prleak psi
MPM	5	2.49	[redacted]540	3693	0	[redacted]51	0.0584	[redacted]87	4540	0	0.0590	[redacted]53
CS	5	2.49	[redacted]105	2369	0	[redacted]43	0.0036	[redacted]40	2369	0	0.0100	[redacted]51

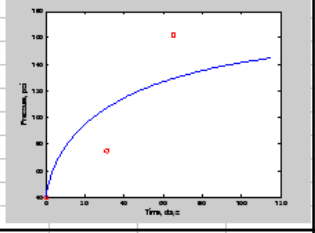
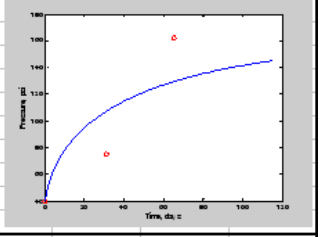
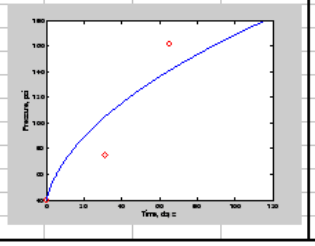
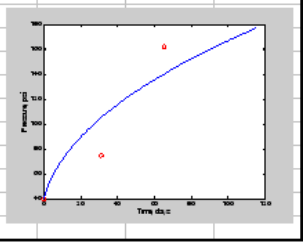

Figure A11 – Wellbore 5 – Best-fit SCP Curve matching field pressure data #2

Method	Wellbore No	Pressure Buildup Rate psi/day	Leakage Depth ft	Mud Length ft	Gas Cap Length ft	PrLeak psi	**Min Perm md**	Leakage Depth ft	Mud Length ft	Gas Cap Length ft	**Max Perm md**	Prleak psi
MPM	6	1.82	[redacted]88	2696	0	[redacted]44	**0.373**	[redacted]12	4188	0	**0.3961**	[redacted].38
CS	6	1.82	[redacted]12	3702	0	[redacted]38	**0.1687**	[redacted]88	3702		**NA**	[redacted]44

Figure A12 – Wellbore 6 – Best-fit SCP Curve matching field pressure data #1

Method	Wellbore No	Pressure Buildup Rate psi/day	Leakage Depth ft	Mud Length ft	Gas Cap Length ft	PrLeak psi	**Min Perm md**	Leakage Depth ft	Mud Length ft	Gas Cap Length ft	**Max Perm md**	Prleak psi
MPM	6	2.31	[redacted]88	2455	0	[redacted]44	**0.0974**	[redacted]20	4188	0	**0.1101**	[redacted]97
CS	6	2.31	[redacted]12	3702	0	[redacted]38	**0.1112**	[redacted]88	3702	0	**NA**	[redacted]44

Figure A13 – Wellbore 6 – Best-fit SCP Curve matching field pressure data #2

Method	Wellbore No	Pressure Buildup Rate psi/day	Leakage Depth ft	Mud Length ft	Gas Cap Length ft	PrLeak psi	**Min Perm md**	Leakage Depth ft	Mud Length ft	Gas Cap Length ft	**Max Perm md**	Prleak psi
MPM	6	1.96	[redacted]88	2170	0	[redacted]44	**0.1798**	[redacted]06	4188	0	**0.2184**	[redacted]88
CS	6	1.96	[redacted]12	3702	0	[redacted]38	**0.4391**	[redacted]88	3702	0	**NA**	[redacted]44

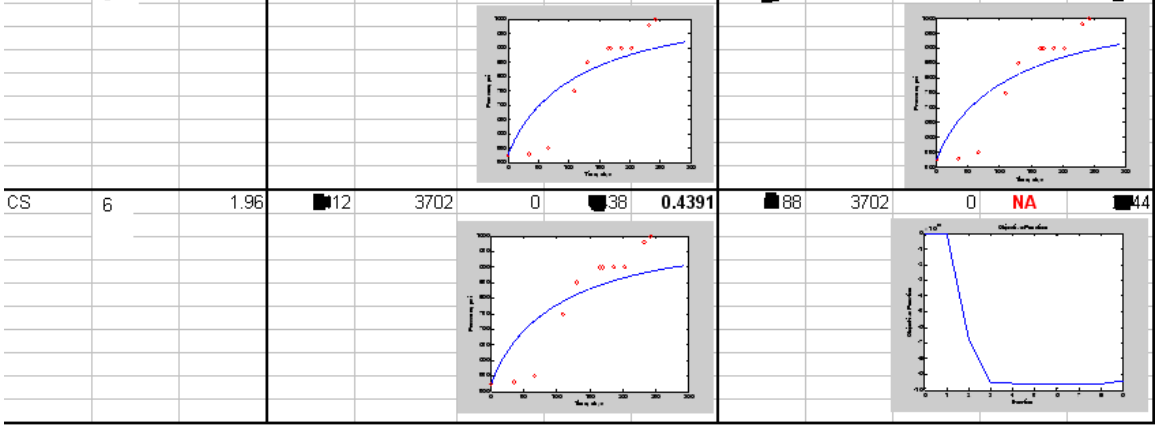

Figure A14 – Wellbore 6 – Best-fit SCP Curve matching field pressure data #3

Method	Wellbore No	Pressure Buildup Rate psi/day	Leakage Depth ft	Mud Length ft	Gas Cap Length ft	PrLeak psi	**Min Perm md**	Leakage Depth ft	Mud Length ft	Gas Cap Length ft	**Max Perm md**	Prleak psi
MPM	6	1.05	[redacted]88	2921	0	[redacted]44	0.0898	[redacted]60	4188	0	0.0945	[redacted]91
CS	6	1.05	[redacted]12	3702	0	[redacted]38	0.0344	[redacted]88	3702	0	NA	[redacted]44

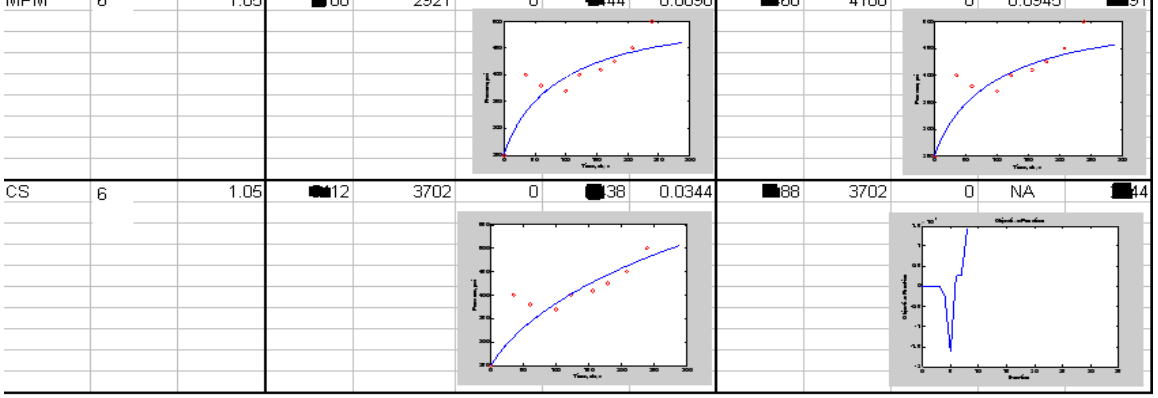

Figure A15 – Wellbore 6 – Best-fit SCP Curve matching field pressure data #4

Method	Wellbore No	Pressure Buildup Rate psi/day	Leakage Depth ft	Mud Length ft	Gas Cap Length ft	PrLeak psi	**Min Perm md**	Leakage Depth ft	Mud Length ft	Gas Cap Length ft	**Max Perm md**	Prleak psi
MPM	7	3.8	[redacted]707	3715	0	[redacted]34	**0.3980**	[redacted]78	4386	0	**0.4103**	[redacted]77
CS	7	3.8	[redacted]78	3749	0	[redacted]77	**0.1869**	[redacted]07	3749	0	**0.4298**	[redacted]34

Figure A16 – Wellbore 7 - Best-fit SCP Curve matching field pressure data #1

Method	Wellbore No	Pressure Buildup Rate psi/day	Leakage Depth ft	Mud Length ft	Gas Cap Length ft	PrLeak psi	**Min Perm md**	Leakage Depth ft	Mud Length ft	Gas Cap Length ft	**Max Perm md**	Prleak psi
MPM	7	1.08	[redacted]07	4215	0	[redacted]34	**0.1292**	[redacted]78	4886	0	**0.1313**	[redacted]77
CS	7	1.08	[redacted]78	4215	0	[redacted]77	**0.0263**	[redacted]07	3749	0	**0.043**	[redacted]34

Figure A17 – Wellbore 7- Best-fit SCP Curve matching field pressure data #2

Method	Wellbore No	Pressure Buildup Rate psi/day	Leakage Depth ft	Mud Length ft	Gas Cap Length ft	PrLeak psi	**Min Perm md**	Leakage Depth ft	Mud Length ft	Gas Cap Length ft	**Max Perm md**	Prleak psi
MPM	7	0.83	[redacted]78	3655	0	[redacted]77	**0.0158**	[redacted]07	3655	0	**0.0241**	[redacted]34
CS	7	0.83	[redacted]78	3749	0	[redacted]77	**0.0166**	[redacted]07	3749	0	**0.0267**	[redacted]34

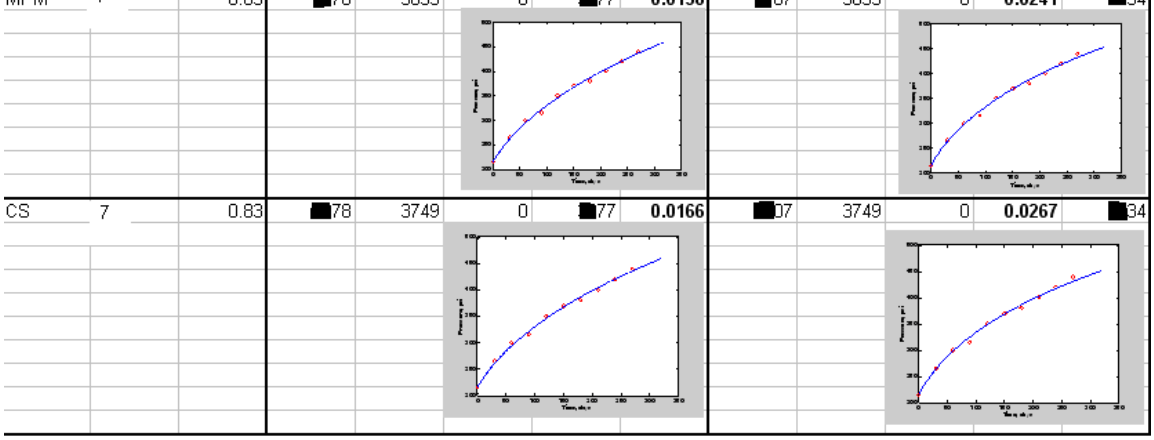

Figure A18 – Wellbore 7- Best-fit SCP Curve matching field pressure data #3

Method	Wellbore No	Pressure Buildup Rate psi/day	Leakage Depth ft	Mud Length ft	Gas Cap Length ft	PrLeak psi	**Min Perm md**	Leakage Depth ft	Mud Length ft	Gas Cap Length ft	**Max Perm md**	Prleak psi
MPM	8	0.55	[redacted]40	3087		1723	**0.0012**	[redacted]93	3140	0	**0.0012**	[redacted]50
CS	8	0.55	[redacted]65	4035		4080	**0.0024**	[redacted]35	4035		**0.1**	[redacted]79

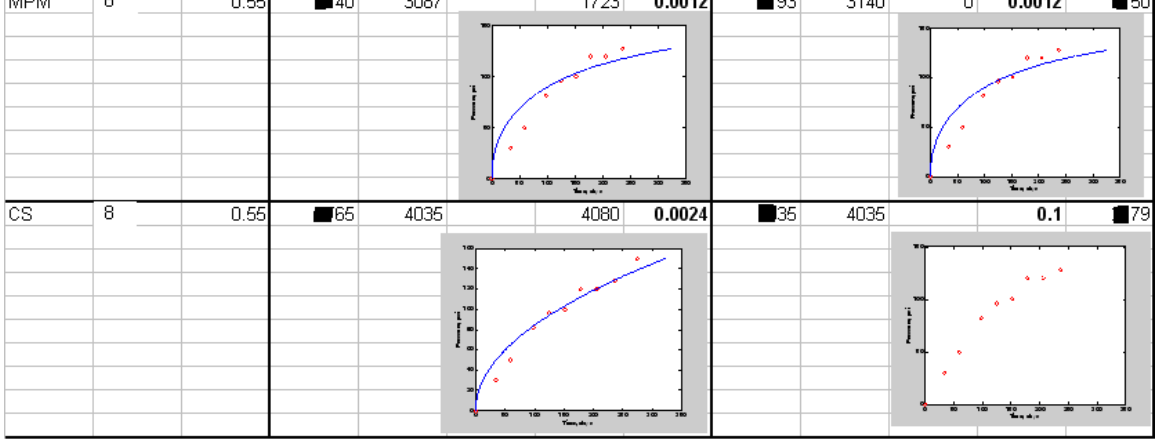

Figure A19 – Wellbore 8 – Best-fit SCP curve matching field pressure data #1

Method	Wellbore No	Pressure Buildup Rate psi/day	Leakage Depth ft	Mud Length ft	Gas Cap Length ft	PrLeak psi	**Min Perm md**	Leakage Depth ft	Mud Length ft	Gas Cap Length ft	**Max Perm md**	Prleak psi
MPM	8	0.34	[redacted]40	3068		[redacted]23	**0.0878**	[redacted]12	3140		**0.1**	[redacted]63
CS	8	0.34	[redacted]65	4035		[redacted]80	**0.0022**	[redacted]35	4035		**0.1**	[redacted]79

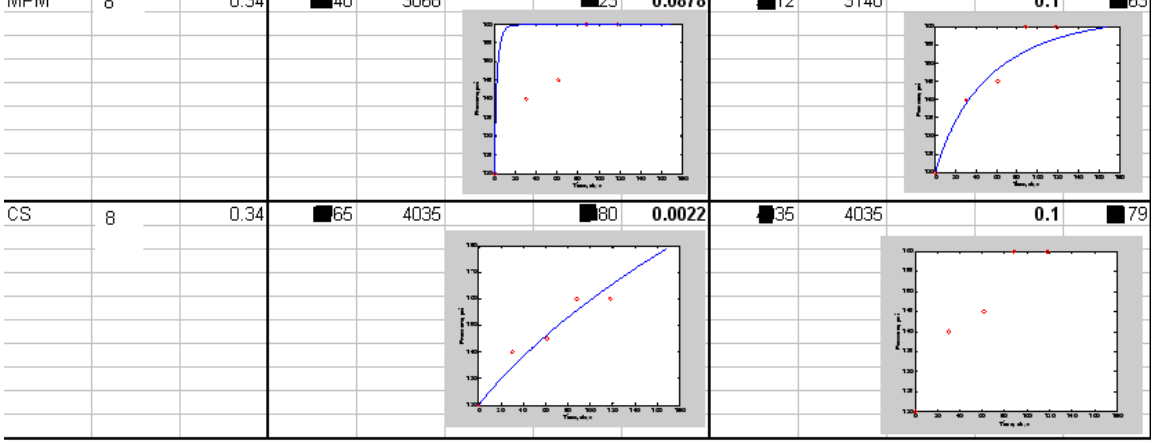

Figure A20 – Wellbore 8 – Best-fit SCP curve matching field pressure data #2

Method	Wellbore No	Pressure Buildup Rate psi/day	Leakage Depth ft	Mud Length ft	Gas Cap Length ft	PrLeak psi	**Min Perm md**	Leakage Depth ft	Mud Length ft	Gas Cap Length ft	**Max Perm md**	Prleak psi
MPM	9	8.85	[redacted]500	5689	0	[redacted]96	**0.9742**	[redacted]662	7811		**1.05**	[redacted]30
CS	9	8.85	[redacted]662	9923		[redacted]30	**16.49**	[redacted]662	9923		**16.49**	[redacted]30

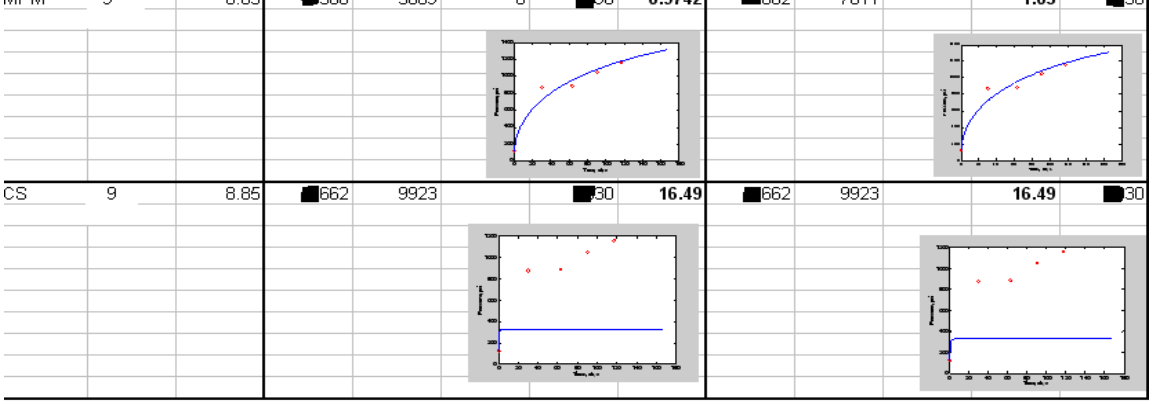

Figure A21 – Wellbore 9 – Best-fit SCP curve matching field pressure data #1. Notice: the cement slurry method results will not be used due to poor matching.

Method	Wellbore No	Pressure Buildup Rate psi/day	Leakage Depth ft	Mud Length ft	Gas Cap Length ft	PrLeak psi	**Min Perm md**	Leakage Depth ft	Mud Length ft	Gas Cap Length ft	**Max Perm md**	Prleak psi
MPM	9	22.3	[redacted]500	5689	0	[redacted]96	**8.03**	[redacted]662	7811	0	**8.63**	[redacted]30
CS	9	22.3	[redacted]662	9923	0	[redacted]30	**10.05**	[redacted]500	9923	0	**NA**	[redacted]96

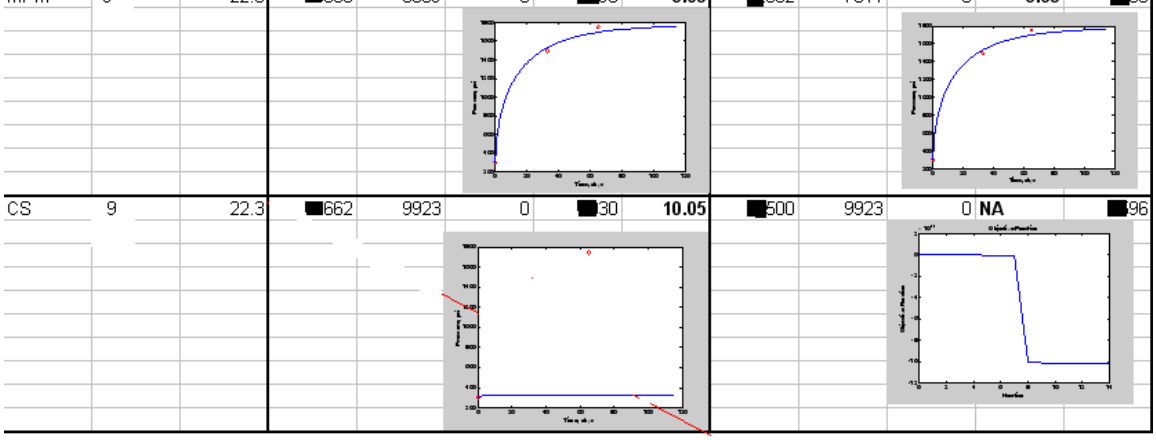

Figure A22 – Wellbore 9 – Best-fit SCP curve matching field pressure data #2. Notice: the cement slurry method results will not be used due to poor matching.

Method	Wellbore No	Pressure Buildup Rate psi/day	Leakage Depth ft	Mud Length ft	Gas Cap Length ft	PrLeak psi	**Min Perm md**	Leakage Depth ft	Mud Length ft	Gas Cap Length ft	**Max Perm md**	Prleak psi
MPM	9	6.5	[redacted]500	6562		[redacted]596	**0.7700**	[redacted]662	8724	0	**0.84**	[redacted]030
CS	9	6.5	[redacted]662	9923		[redacted]030	**1.69**	[redacted]500	9923	0	**NA**	[redacted]596

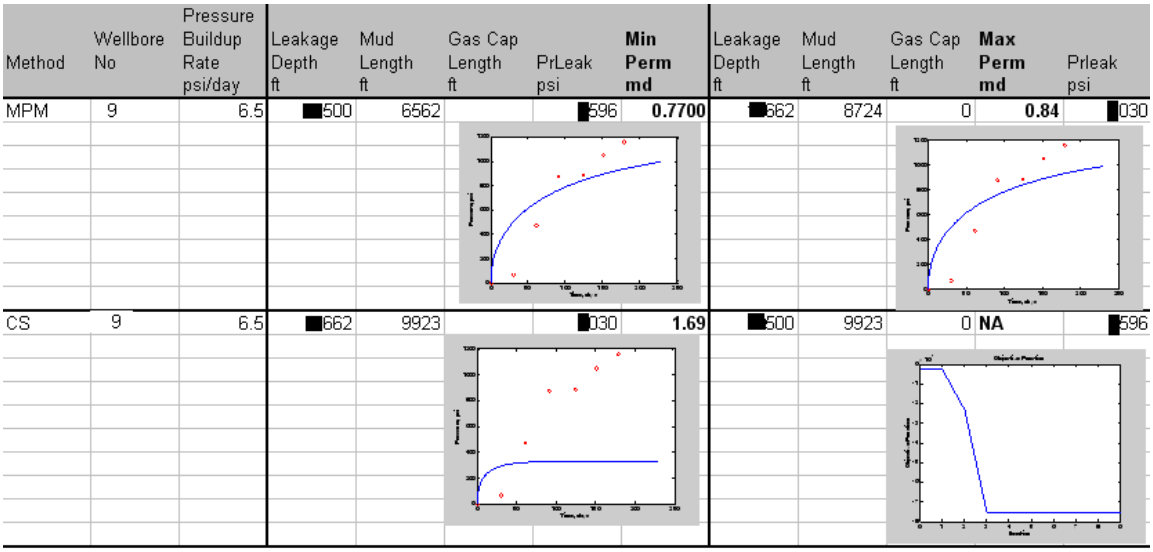

Figure A23 – Wellbore 9 – Best-fit SCP curve matching smoothed pressure data #1. Notice: there is poor fits for the cement slurry method.

Method	Wellbore No	Pressure Buildup Rate psi/day	Leakage Depth ft	Mud Length ft	Gas Cap Length ft	PrLeak psi	**Min Perm md**	Leakage Depth ft	Mud Length ft	Gas Cap Length ft	**Max Perm md**	Prleak psi
MPM	9	14	[redacted]500	5689		[redacted]96	**3.3100**	[redacted]662	7851	0	**3.54**	[redacted]30
CS	9	14	[redacted]662	9923		[redacted]30	**28.9**	[redacted]500	9923	0	**NA**	[redacted]96

Figure A24 – Wellbore 9 – Best-fit SCP curve matching smoothed field pressure data #2.

A.04 - SCP MODEL SCRIPT WRITTEN IN MATLAB WHICH WAS USED TO GENERATE PERMEABILITY RESULTS.

```
%Remember to change values in this code to run model.
function misfit = objfun(Para)

convertTime=1; %for months2day '1*30', for hour2day '1/24'
% *Pressure in units of psi

data = load('W7.dat');
n_d = length(data);
Data_time = data(1:n_d,1);
Data_time = Data_time.*convertTime;
Data_press = data(1:n_d,2);

% fileName = 'MMS_LSU_pressureData_well23n24.xls';
% sheetName = 'Well24_1';
% range = [1 25];
% timeCol = 'A';
% pressCol = 'B';
% Data_time=xlsread(fileName,sheetName,[timeCol num2str(range(1))
':' timeCol num2str(range(2))]);
% Data_time=Data_time.*convertTime;
% Data_press=xlsread(fileName,sheetName,[pressCol
num2str(range(1)) ':' pressCol num2str(range(2))]);



%Uncomment this to look at data to make sure correct format
% figure
% plot(Data_time, Data_press,'or')
% title('Measured Casing Pressure History')
% xlabel('Time, Day')
% ylabel('Pressure, psi')
%% Parameter Initilization
%load 'Well_Parameters_081108.mat';
% Scalar variables
section***********************************************

% Cement effective permeability, md
 k = Para/1e3;
%CHANGE THIS LEAKAGE DEPTH FOR EACH NEW CASE
% Leakage depth, ft
 Dleak = 5707;
% Leak pressure, psi
 prLeak = 3234;
%CHANGE OD, ID FOR EACH NEW CASE
% Annulus OD, ft
 OD = 0.825;
% Annulus ID, ft
 ID = 0.635;
```

```
% Annulus Area, ft^2
 Area = pi/4*((OD^2)-(ID^2));
% Mud compressibility, psi^-1
 C_m   = 4.0*(10^-6);
% Gas constant
 R = 8.314;
% Reservoir condition temperature, Rankine
 T     = 626;
% Well head temperature, Rankine
 Twh   = 580;
% Average wellbore temperature
 Twb   = (T+Twh)/2;
% Temperature at standard conditions,Rankine
 Tsc = 520;
% Pressure at standard conditions, psi
 Psc   = 14.7;
% Gas law deviation factor
 Z     = 0.86;
%Gas viscosity, cp
 mu_g  = 0.02;
%Density of mud in wellbore, ppg
 rho_m = 12.7;

%True Value Depth of Len_mud(1), ft
% TVD_len_mud = 165



% Vector variables
section*********************************************
%Time, units are days - how to change to hours?
time_St = 0; %day - how to change to hours?
delTime = 1; % how to change to appropriate hours (delta)?
time_Fi = Data_time(end)+50; %day - how to change to hours?
timeV = time_St:delTime:time_Fi;

% Gas length vector, ft
Len_gas = zeros(1,size(timeV,2));
% Initial length of gas chamber, ft
Len_gas(1) = 0; %If open to the surface otherwise might need to
calculate..

% Gas volume vector, ft^3
Vol_gas = zeros(1,size(timeV,2));
% Initial Volume of gas chamber, ft^3
Vol_gas(1) = Len_gas(1) * Area;

% Mud length vector, ft
Len_mud = zeros(1,size(timeV,2));
%CHANGE LENGTH OF MUD FOR EACH NEW CASE.
% Initial length of mud column, ft
Len_mud(1)  = 3749;
```

```
% Length of cement column, ft
Len_cem = Dleak - Len_mud(1);

% Mud volume vector, ft^3
Vol_mud = zeros(1,size(timeV,2));
% Initial Volume of mud chamber, ft^3
Vol_mud(1) = Len_mud(1) * Area;

%Ratio of TVD_len_mud / Len_mud(1),
% R_TVD_TMD = 1;

% Surface pressure vector, psi
prSurfV = zeros(1,size(timeV,2));
% Initial surface pressure, psi
%CHANGE INITIAL SURFACE PRESSURE FOR EACH NEW CASE
prSurfV(1) = Data_press(1); %If reading casing pressure at start
of test put here

% Cement top pressure vector, psi
prCmtV = zeros(1,size(timeV,2));
% Initial cement top pressure, psi
prCmtV(1) = prSurfV(1) + 0.052 * rho_m * Len_mud(1); %Equivalent
to EQ B.4

% Moles of gas transported through cement
moles = zeros(1,size(timeV,2));
% Initial moles of gas at the surface
moles(1)=prCmtV(1)*Vol_gas(1)/(Z*R*Twh);
% Total moles
molesTot = moles(1);
% Flow rate vector, SCF/D
flowV= zeros(1,size(timeV,2));

%% New Implimentation of Code here

for n=2:size(timeV,2)
prCmtV(n) = prSurfV(n-1) + 0.052*rho_m*Len_mud(n-1);
flowV(n)= (0.003164 * k * Tsc * Area)/...
          (Psc * Twb *Len_cem*Z*mu_g).*...
          (prLeak^2-prCmtV(n)^2);

moles(n) = (Psc * flowV(n) * delTime); %Numerator of (B.7)

molesTot = molesTot + moles(n); %Numerator of (B.8)

prSurfV(n) = 0.5*(prSurfV(n-1)-...
             (Vol_gas(n-1)/(C_m*Vol_mud(n-1)))+...
             ((prSurfV(n-1)-(Vol_gas(n-1)/(C_m*Vol_mud(n-
1))))^2+...
              (4*Twh*molesTot/(C_m*Vol_mud(n-1)*Twb)))^(0.5)...
```

```
                    );

delV = C_m*Vol_mud(n-1)*(prSurfV(n)-prSurfV(n-1));
Vol_mud(n)=Vol_mud(n-1)-delV;
Vol_gas(n)=Vol_gas(n-1)+delV;
Len_mud(n)=Vol_mud(n)/Area;
end
% plot(timeV,prSurfV)

%% Calculate misfit
n = length(timeV);
m = length(Data_time);
k = 1;
for i=1:n
    for j=1:m
        if timeV(i)==Data_time(j)
            ind(k) = i;
            k = k+1;
        end
    end
end

n = length(ind);
for i=1:n
    j = ind(i);
    misfit_temp(i) = (Data_press(i)-prSurfV(j))^2;
end
misfit = sum(misfit_temp);

% figure
% plot(Data_time, Data_press,'or',timeV,prSurfV,'-b')
% xlabel('Time, Days')
% ylabel('Pressure, psi')

%Run this code to obtain results
clear; clc; close all;

[Para,A,b,Aeq,beq,lb,ub,nonlcon,options] = initialization();

[OptPara,OutObj] =
fmincon('objfun',Para,A,b,Aeq,beq,lb,ub,nonlcon,options);

k = OptPara/1e3;

SCP(OptPara);
```

Figure A25 – SCP Model script used to generate permeability values in MatLab.

A.05 - BEST CEMENTING PRACTICES (BOURGOYNE, 2000)

Bourgoyne emphasized that cementing practices were the main contributors to the development of sustained easing pressure (SCP). Data analysis of primary cement jobs that resulted in SCP buildups show that certain practices eventually lead to the following examples of communication: channeling, micro annuli, fractures, un-cemented zones, and poor bonding.

Listed below are the recommended "best" cementing practices that Bourgoyne compiled from discussions with various cementing companies, and a literature search through technical reports, journal articles, and proceedings from technical conferences:

1) Cement Quality and Weight - The appropriate choice of cement slurry must be designed to solve the problems specific for each string of pipe prior to cementing. Knowledge of the wellbore conditions are essential, particularly at the time of drilling, so that any problems encountered can be integrated into the cement design. Use of premium grade cements is encouraged.

2) Waiting Time - The cement slurry should be held in place and under pressure until it hardens. A cement slurry is a time-dependent liquid and must be allowed to undergo a hydration reaction in order to produce a competent cement sheath. A fresh cement slurry can be worked as long as it is plastic1 and the initial set of cement occurs during the rapid reaction stage. If the cement is not allowed to hydrate, it will be subject to changes in density, dilution, settling, water separation, and gas cutting that can lead to lack of zonal isolation with resultant bridging in the annulus.

3) Pipe Movement - This may be one of the most influential factors in hole cleaning (mud removal). Reciprocation and/or rotation with the use of wall cleaners on the casing mechanically breaks up gelled mud and constantly changes the flow patterns in the annulus for better cement bonding.

4) Mud Properties - Careful planning of mud properties such as plastic viscosity, gel strength, and filtrate loss should be done by a competent mud engineer to optimize hole cleaning and mud and filter cake removal prior to cementing.

5) Pre-Cementing Circulation - "Bottoms-up" circulation should occur twice, or until well conditioned mud is being returned to the surface. The mud return should be void of cuttings, with an optimal annular velocity of 260 feet per minute (SPE/IADC 18617), if possible.

6) Flow Rate - Turbulent flow is one of the most desirable flow regimes for mud removal. If turbulence cannot be achieved, better mud removal is found when maximum flow energy is used.

7) Hole Size - The optimum hole size recommenced for good mud removal is 1.5 inches to 2 inches larger than the casing or liner size. Hole sizes larger than 2 inches annular space can be dealt with, but those that are smaller than 1.5 inches present difficult problems.

8) Pipe Centralization - Centralizing the pipe within the well are helps to create a uniform flow area perpendicular to flow direction, and improve the chance for cement to bond to both annulus surfaces (preventing fluid migration). At least a 70 percent standoff should be achieved for centralization. This 15 particularly important in directional holes. Special centralizers are available to aid in the maintenance of turbule9t flow around the casing.

10) Rat Hole - When applicable, a weighted viscous pill in the rat hole can prevent cement from swapping with lighter weight mud when displacement stops

11) Shoe Joint - A shoe joint is recommended on all primary casings and liners. The length of the shoe joint will vary, with an accepted minimum length being one joint of pipe. If conditions exist in the well such that a bottom plug is not run in conjunction with the cement job, two joints
should be considered to be a minimum requirement.

12) Spacer - When feasible in turbulent flow, a spacer should be used to minimize contamination of the cement.

13) Plugs - Top and bottom cement plugs are recommended on every primary cementing job. The bottom plug serves to minimize contamination of the cement as it is pumped. The top plug is also used to prevent any contamination of the cement slurry by the displacement fluid. The top plug also gives a positive indication that the cement has been displaced.

14) Gas Flow - A gas flow analysis should always be used to determine the potential for gas flow on any primary cement job. While going through its gelatin phase, the cement column loses its ability to transmit hydrostatic pressure onto the formation. During this period, fluids can freely migrate into the cement and begin to form channels. Although gas flow may not be apparent at the surface, gas migration in the annuli will likely lead to problems with SCP.

Figure A26 – Best cementing techniques by Bourgoyne.

A.06 - COMPARISON OF LEAKAGE PRESSURE VS CAPILLARY ENTRY PRESSURE FOR OFFSHORE DATASET.

As described in Chapter 6, in order to determine whether there is enough driving force to allow gas leakage to occur, capillary entry pressures are compared with the leakage depth pressures for the wellbores in the Offshore dataset. The comparison shows that in almost all the leaky wellbores, the leakage source pressures are greater than the capillary entry pressures. The blue color zone is where the leakage pressures were greater than capillary entry pressures. The threshold line is where the leakage depth pressure equals the capillary entry pressure. The yellow color zone is where the leakage pressures were smaller than capillary entry pressures. Thus, this proves that there is high enough driving forces to overcome capillary pressures to allow gas to flow and migrate into the conduit/ crack.

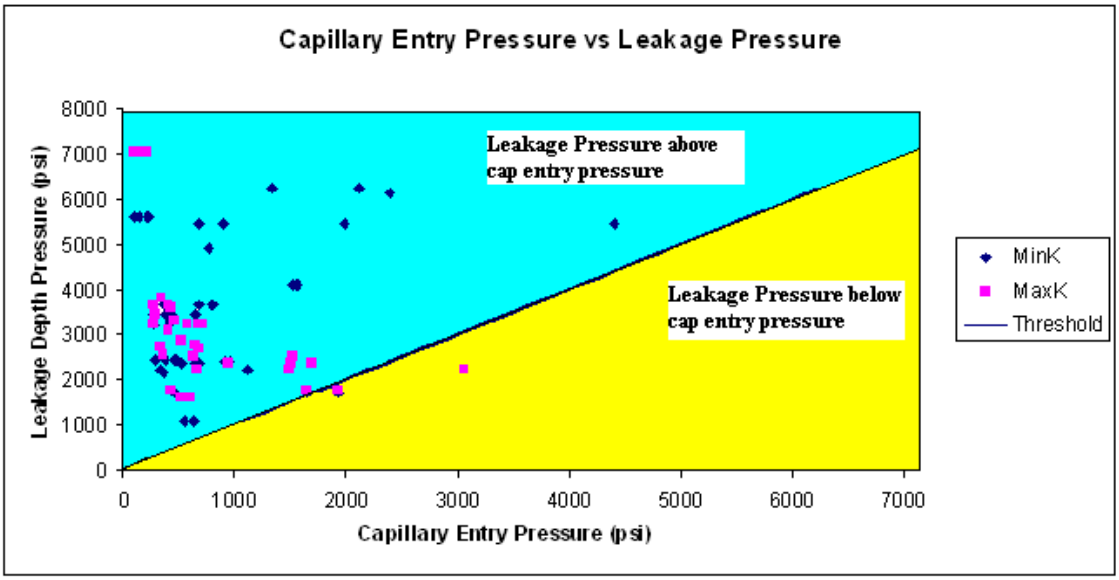

Figure A27 - Comparison of capillary entry pressures to leakage depth pressures.

A.07 - EXAMPLE PROPOSAL TO BE USED WHEN REQUESTING ACCESS TO LEAKY WELLBORE DATASETS.

Date: Monday, April 23, 2012
Outline of the Project: Collect data on existing wellbores with sustained casing pressure buildups at the Midland CO2 flooding / EOR field.
Company: _____
Research Institution: University of Texas at Austin
Location: _____
Contact Person(s): _____ (email@address.com) tel: XXX-XXX-XXX

Objective of Project: To obtain surface pressure buildup data from a pressure gauge at the wellhead or flow rate information from an open surface wellhead valve on the intermediate annular space during bleed down.

Scope of Work:
1) Perform data search internally, searching for shallow wellbores (2500' - 3500') that have cracks in cement filled annular space between the casing and formation. Formation gas enters a crack in the cement and travels to the surface, where it is measured by a pressure gauge monitoring the gas cap/ annular space pressure buildup.

2) Investigate the surface casing pressure data that has been reported during mechanical integrity (~550# hydro tests) or regulatory tests (Texas Railroad Commission - RRC H-5 and H-15) to determine what, if any pressure buildups or flow rates have recorded. Obtain the wellbore construction information pertaining to these wellbores (casing sizes, casing depth, cement slurry information, etc).

3) Obtain list of wellbore identifiers, names which can be used for searching through the Texas Railroad Commission database for information / data on regulatory testing.

4) Search for other pressure tests that were performed internally on these wells, which have been documented and stored in a database of well files. Extract all relevant pressure buildup data.

5) Once recorded, compile the dataset of leaky wellbores to determine characteristics of the leakage pathway (i.e.: permeability) and compare with other findings.

Published Results:
All published results would conceal the source of the data and not refer to the company that supplied it. There would be no liability for_____. All work would be funded by The University of Texas at Austin. A graduate student would conduct the data search and communicate with a designated person as results are used for published reports. All findings would need approval from _____upper management.

Figure A28 – Proposal letter to work with operators using CO_2 for EOR.

References

Bachu, S., Bennion D.B. "Experimental assessment of brine and/or CO_2 leakage through well cements at reservoir conditions." International Journal of Greenhouse Gas Control 3 (2009) 494-501, 2009.

Bachu, S., Watson, T. "Possible Indicators for CO_2 Leakage Along Wells" Paper submitted to GHGT, 2008.

Bourgoyne, A., Scott S., and Regg J. "Sustained Casing Pressure in Offshore Producing Wells" Offshore Technology Conference. Houston, TX 3-6 May 1999.

Bourgoyne, A., Scott S., Manowski, W. "A Review of Sustained Casing Pressure Occurring on the OCS" 2000. Study funded by MMS, US Department of Interior, Contract Number 14-35-001-30749

Castelletto, N. "CO_2 Geological Sequestration: a Numerical Study in a Real Multi-Compartment Reservoir in the Northern Adriatic Sea, Italy" XIX Conference on Computational Methods in Water Resources. University of Illinois. Champaign, Illinois. June 17-21, 2012.

Chenevert, M., Bourgoyne, A., Millheim, K., Young, F.S. "Applied Drilling Engineering" Society of Petroleum Engineers. 1986.

Cheung, P.R. and Beirute, R.M. "Gas Flow in Cements" Paper SPE 16654, 1987.

Chiquet, P., Daridon, J.L, Broseta, D. Thibeau, S. "CO_2/Water Interfacial Tensions Under Pressure and Temperature Conditions of CO_2 Geological Storage." 2006 Science Direct. Energy Conversion and Management. Elsevier.

Christopher, C. "Capillary Entry Pressure Slide" 2011. Personal Communication.

Celia, M., Nordbotten, J., Court, B Dossy, M., Bachu, S. "Field-scale application of semi-analytical model for estimation of CO_2 and brine leakage along old wells. "International Journal of Greenhouse Gas Control 5 (2011) 257-269.

Celia, M., "Practical Models for Large-Scale CO_2 Sequestration." XIX Conference on Computational Methods in Water Resources. University of Illinois. Champaign, Illinois. June 17-21, 2012

Crow, W., Williams, D.B., Carey, J.W., Celia, M., Gasda, S. "Wellbore Integrity Analysis of a Natural CO_2 Producer." 2008. Science Direct. GHGT-2009. Elsevier.

de Figueiredo, M.A. “The Liability of Carbon Dioxide Storage” Dissertation. Massachusetts Institute of Technology, 2004.

Duguid, A. “Technologies for Measuring Well Integrity in a CO_2 field” 6th Annual Conference on Carbon Capture and Sequestration. – Dept. of Energy / NETL. May 7 - 10, 2007

Elert, G. "The Physics Hypertextbook-Viscosity". 2010 Physics.info.

Evans, G.W. and Carter, L.G. “Bonding Studies of Cementing Compositions to Pipe and Formations.” API Division of Production (1962).

Goode, J. “Gas and Water Permeability Data for Some Common Oilwell Cements.” Journal of Petroleum Technology. SPE 288. August 1962

Guyvoronsky, A.A. and Farukshin, L.K. “Hydrostatic Pressure of Cement Slurry,” Neftyanik (1963). No. 10, 20-32.

Herzog, H., Golomb, D. “Carbon Capture and Storage from Fossil Fuel Use” Encyclopedia of Energy, 227 (C.J. Cleveland et al. eds, 2004).

Huerta, N. Checkai, D. Bryant, S. ““Utilizing Sustained Casing Pressure Analog to Provide Parameters to Study CO_2 Leakage Rates Along a Wellbore” SPE Paper No.126700. SPE International Conference on CO_2 Capture, Storage, Utilization. San Diego, CA 2-4 November, 2009.

Jessen, K. “Increasing CO_2 Storage in Oil Recovery,” 46 Energy Conv. Mgmt. 293, 295 (2005).

Kumar A., Ozah R., Noh M., Pope G., Bryant S., Sepehrnoori K., Lake L. “Reservoir Simulation of CO_2 Storage in Deep Saline Aquifers.” SPE No. 89343-PA. September 2005 SPE Journal.10 (3): 336-348.

Martinez, M., “Coupled Multiphase Flow and Geomechanics for Analysis of Caprock Damage during CO_2 Sequestration Operations” XIX Conference on Computational Methods in Water Resources. University of Illinois. Champaign, Illinois. June 17-21, 2012

Nelson, E. “Well Cementing” Developments in Petroleum Science. Vol 28. Schlumberger Educational Services. 1990.

National Energy Technical Laboratory (NETL), "Carbon Sequestration Atlas of the United States and Canada" 3rd Edition. 2010.

Nordbotten, J.M., Celia, M., Bachu, S., Dahle, H. "Semianalytical Solution for CO_2 Leakage through an Abandoned Well" Journal of Environmental Science & Technology. 2005. Vol 39 No(2), 602-611.

Nordbotten, J.M. "Novel Approaches for Modeling Migration and Trapping at Geological Scale" XIX Conference on Computational Methods in Water Resources. University of Illinois. Champaign, Illinois. June 17-21, 2012

Orr, F. "Distinguished Author Series: Storage of Carbon Dioxide in Geological Formations." Journal of Petroleum Technology. September, 2004.

Parsonage, K. "British Columbia SCVF Wellbores." 2011. Personal Communication.

Parcevaux, P.A. and Sault, P.H. "Cement Shrinkage and Elasticity: A New Approach for a Good Zonal Isolation." paper SPE 13176, 1984.

Pruess, K. "Numerical Simulation of CO_2 Leakage From a Geological Disposal Reservoir, Including Transitions from Super to Subcritical Conditions, and Boiling of Liquid CO_2 " SPE 86098. June 2004.

Reichle, D. "Carbon Sequestration Research and Development." U.S. DOE Report DOE/SC/FE-1, Washington DC (1999).

Stiles, D. "Challenges with Cement Evaluation. What We Know & What We Don't." Exxon Mobil Corporation. SPE Webinar. July 11, 2012.

Tao, Q. "Modeling CO2 Leakage from Geological Storage Formation and Reducing the Associated Risk." Dissertation. University of Texas at Austin Graduate School. August, 2012.

Tao, Q., Checkai, D.A., and Bryant, S.L. "Permeability Estimation for Potential CO_2 Leakage Paths in Wells Using a Sustained Casing Pressure Model." SPE No. 139576-MS 2010. Society of Petroleum Engineers. SPE International Conference on CO_2 Capture, Storage, and Utilization. New Orleans, Louisiana, USA, 10-12 November.

Tinsley, J.M., Miller, E.C., Sabins, F.L., and Sutton, D.L. "Study of Factors Causing Annular Gas Flow Following Primary Cementing." paper SPE 8257, 1979.

Wojtanowicz, A., Manowsk, W., Nishikawa, S. “Gas Flow in Wells After Cementing” Report submitted to US Department of Interior, MMS. September 2000.

Wojtanowicz, A. Nishikawa, S. and Xu R. ‘Diagnosis and Remediation of Sustained Casing Pressure in Wells.” Report submitted to US Department of Interior, MMS. July 2001.

Watson, T., Bachu, S. “Identification of Wells with High CO_2 Leakage Potential in Mature Oil Fields Developed for CO_2 Enhanced Oil Recovery.” SPE 112924. Paper for 2008 SPE/DOE Improved Oil Recovery Symposium in Tulsa, Oklahoma, USA 19-23. April 2008.

Watson, T., “Surface Casing Vent Flow Repair – A Process.” 2004. Fifth Canadian International Petroleum Conference and 55th Annual Technical Meeting of the Petroleum Society, Calgary, AB, Canada, June 8-10, 2004, 9 p. 2004

Watson, T., “Site Investigation for Gas Migration and Surface Casing Vent Flow. Pad Pressure Evaluation.” 2009. Personal Communication.

Xu, R., Wojtanowicz, A, “Diagnosis of Sustained Casing Pressure from Bleed-off/Buildup Testing Patterns.” 2001 SPE 67194. SPE Production and Operations Symposium held in Oklahoma City, Oklahoma, 24–27 March 2001.

Xu, R. “Analysis of Diagnostic Testing of Sustained Casing Pressure in Wells.” Dissertation. Louisiana State University Graduate School. 2001.

Vita

Dean Alen Checkai was born in Milwaukee, Wisconsin in January 1981. He began his studies at The University of Wisconsin-Madison in September 1999. From September 2001 to May 2002, he studied abroad in Grenoble, France as an exchange student at Ecole Nationale Supérieure de Génie Industriel (ENSGI). In May 2004, he earned a Bachelor of Science degree in Industrial Engineering from The University of Wisconsin-Madison. From January 2005 to September 2006, he worked for Accenture in Reston, VA. In October 2006, he moved to Austin, TX to work for Renewable Energy Systems until May, 2007. From July 2007 to September 2008, he worked for FirstCare Health Plans. In January 2009, he began Graduate School at The University of Texas at Austin in the Department of Petroleum and Geosystems Engineering. In October 2011, he passed the Fundamentals of Engineering (FE) Exam to become certified as an Engineer-In-Training (EIT) upon graduation.

Email address: dacheckai@gmail.com

This thesis was typed by the author.